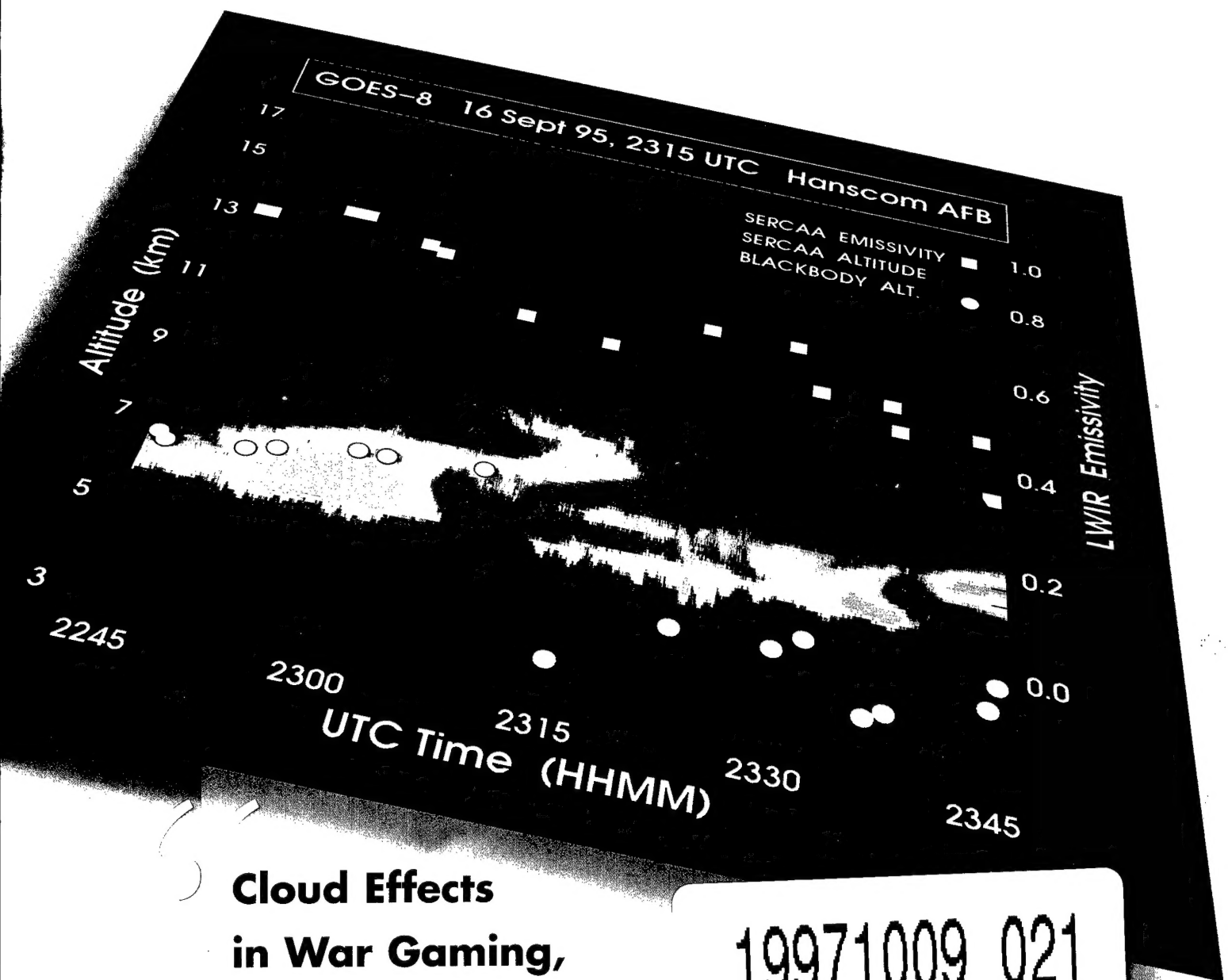


CLOUD IMPACTS ON DOD OPERATIONS AND SYSTEMS 1997 CONFERENCE

U.S. Naval War College – Sims Hall, Nott Auditorium
Newport, Rhode Island • 23-25 September 1997



**Cloud Effects
in War Gaming,
Modeling and
Simulation**

19971009 021

DISTRIBUTION STATEMENT A

Approved for public release;
Distribution Unlimited

Front Cover: Support of Environmental Requirements for Cloud Analysis and Archive (SERCAA) satellite-based cirrus altitude retrievals (red diamonds) and 10.7- μm LWIR effective emissivity retrievals (yellow squares) plotted with coincident ground-based 35-GHz radar observations of cirrus base and top. The ground-based radar data were collected as a part of a field experiment conducted over Hanscom AFB, MA during mid-September 1995. Colors are representative of the reflected power received as a function of altitude by the active 35-GHz radar, with warm colors (reds, oranges, yellows) corresponding to strong returns and cool colors (green, cyan) corresponding to weaker returns. Dark blue denotes cloud-free observations. Red diamonds denote the SERCAA 6.7-10.7- μm satellite-retrieved cirrus altitudes that correspond with their respective coincident radar observations. As can be seen, the retrievals match well with observation. Corresponding cirrus effective emissivities are plotted in yellow squares against the right-hand vertical (emissivity) axis. It is seen that the retrieved emissivities are qualitatively higher where radar returns are stronger and vice versa.

The white circles correspond to "blackbody" altitude retrievals obtained using 10.7- μm brightness temperatures that have been uncorrected for cirrus transmissive effects (i.e., assuming the cirrus is a blackbody cloud). This is the technique typically used by most cloud analysis models to compute cloud altitude for both opaque and transmissive clouds. Altitudes retrieved in this manner agree reasonably well with true cirrus altitudes wherever cirrus transmissivities are low (optically thick cirrus), as is seen on the left side of the plot. However, where cirrus is optically thin, the comparison differences are dramatic: on the right half of the plot are cirrus blackbody retrievals that differ by as much as 6 km from the true cirrus altitudes. It is important to note that the white circles denote state of the art in the current Air Force operational global cloud analysis model, the RTNEPH, as well as in the cloud altitude algorithms being implemented at AFGWC to replace the RTNEPH.

Back Cover, Top: NOAA-14 Advanced Very High Resolution Radiometer (AVHRR) raw color composite image of the northeast United States and adjacent Atlantic waters. This image is generated by using the 3.7-, 10.7-, and 11.8- μm MWIR/LWIR brightness temperatures to control the red, green, and blue intensities, respectively, of the color composite. Very little spatial variation in land-surface and sea-surface temperatures is discernible in this image.

Back Cover, Bottom: The same image scene as above, except enhanced using an automated optimal enhancement algorithm that masks out clouds and then uses the full available dynamic range of color intensities and saturations on only the remaining clear-column land- and ocean-surface pixels. The Delmarva peninsula is clearly visible in the lower left of the image. Note the detail that can be seen in the SST structure, including the Gulf Stream's North Wall and associated eddies. The pale blue tints in the lower and right sides of the image indicate the presence of very thin cirrus through which SST features are still discernible.

(Cover images provided by Robert P. d'Entremont, Atmospheric and Environmental Research, Inc., Cambridge MA 02139; and Thomas R. Caudill and James T. Bunting, Remote Sensing Applications Branch, PL/GPOR, Hanscom AFB, MA 01731. For more information on these images, please refer to articles by d'Entremont et al. in this preprint volume.)

PL-TR-97-2112

Environmental Research Papers, No. 1209

**PREPRINT OF THE CLOUD IMPACTS
ON DoD OPERATIONS AND SYSTEMS
1997 CONFERENCE (CIDOS-97)**

Editor:

Paul Tattelman

23 September 1997


Approved for Public Release; Distribution Unlimited

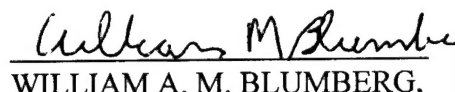


**PHILLIPS LABORATORY
Directorate of Geophysics
AIR FORCE MATERIEL COMMAND
HANSCOM AFB, MA 01731-3010**

PHILLIPS LABORATORY

This technical report has been reviewed and is approved for publication


PAUL TATTELMAN, Chief
Forecast Applications Branch


WILLIAM A. M. BLUMBERG,
Director, Optical Effects Division

This report has been reviewed by the ESC Public Affairs Office (PA) and is releasable to the National Technical Information Service (NTIS).

Qualified Requestors may obtain additional copies from the Defense Technical Information Center (DTIC). All others should apply to the National Technical Information Service (NTIS).

If your address has changed, if you wish to be removed from the mailing list, or if the addressee is no longer employed by your organization, please notify PL/IM, 29 Randolph Road, Hanscom AFB, MA 01731-3010. This will assist us in maintaining a current mailing list.

Do not return copies of this report unless contractual obligations of notices or a specific document require that it be returned.

REPORT DOCUMENTATION PAGE			Form Approved OMB No. 0704-0188	
Public reporting burden for this collection of information is estimated to average 1 hour per response, including the time for reviewing instructions, searching existing data sources, gathering and maintaining the data needed, and completing and reviewing the collection of information. Send comments regarding this burden estimate or any other aspect of this collection of information, including suggestions for reducing this burden, to Washington Headquarters Services, Directorate for Information Operations and Reports, 1215 Jefferson Davis Highway, Suite 1204, Arlington, VA 22202-4302, and to the Office of Management and Budget, Paperwork Reduction Project (0704-0188), Washington, DC 20503.				
1. AGENCY USE ONLY (Leave blank)		2. REPORT DATE 23 September 1997	3. REPORT TYPE AND DATES COVERED Scientific-Interim	
4. TITLE AND SUBTITLE PREPRINT OF THE CLOUD IMPACTS ON DoD OPERATIONS AND SYSTEMS 1997 CONFERENCE (CIDOS-97)			5. FUNDING NUMBERS PE 62101F PR 6670 TA GS WU 02	
6. AUTHOR(S) PAUL TATTELMAN, Editor				
7. PERFORMING ORGANIZATION NAME(S) AND ADDRESS(ES) Phillips Laboratory/GPOF 29 Randolph Road Hanscom AFB, MA 01731-3010			8. PERFORMING ORGANIZATION REPORT NUMBER PL-TR-97-2112 ERP, No. 1209	
9. SPONSORING/MONITORING AGENCY NAME(S) AND ADDRESS(ES) US Air Force Assistant for Battlespace Environment Office of Defense for Research and Engineering The Pentagon, Washington, DC			10. SPONSORING/MONITORING AGENCY REPORT NUMBER	
11. SUPPLEMENTARY NOTES Supported by the Air Force Phillips Laboratory, Office of the Oceanographer of the Navy, and the Army Research Laboratory				
12a. DISTRIBUTION AVAILABILITY STATEMENT Approved for public release: Distribution unlimited			12b. DISTRIBUTION CODE	
13. ABSTRACT (Maximum 200 words) The Tri-Service Cloud Modeling Program was established by OUSDR&E and is chaired by the Phillips Laboratory, Geophysics Directorate. As part of this program the CIDOS conference is held at 18 month intervals. This forum is attended by Researchers and DoD systems designers/users to exchange information on requirements and ongoing research for cloud effects on weapon, communication, and surveillance systems. The theme of CIDOS-97 is "Cloud Effects in War Gaming, Modeling and Simulation." Three days of CIDOS-97 were devoted to oral and poster presentations in seven sessions: (I) Introduction; (II) Program Reviews; (III) Cloud M&S Applications to War Gaming and Studies and Analyses; (IV) Cloud and Cloud Effects Modeling; (V) Cloud Prediction; (VI) Measurement Systems and Sensors; (VII) Cloud Datasets. Summaries of these presentations are included in this report.				
14. SUBJECT TERMS Clouds, cloud models, cloud simulation, cloud databases, cloud observing, cloud detecting, cloud retrieval, cloud effects			15. NUMBER OF PAGES	
			16. PRICE CODE	
17. SECURITY CLASSIFICATION OF REPORT Unclassified	18. SECURITY CLASSIFICATION OF THIS PAGE Unclassified	19. SECURITY CLASSIFICATION OF ABSTRACT Unclassified	20. LIMITATION OF ABSTRACT SAR	

This page was left blank intentionally.

CIDOS EXECUTIVE COMMITTEE

Col Alan R. Shaffer
U.S. Air Force Assistant for Battlespace Environment
Office of Defense Research and Engineering

Mr. Paul Tattelman, Chairman
Geophysics Directorate, Phillips Laboratory

Mr. Sam Brand
Naval Research Laboratory

CAPT Robert L. Clark
Office of the Oceanographer of the Navy

CDR George Davis
Naval War College

Mr. Raymond H. Godin
Office of the Oceanographer of the Navy

Mr. Donald D. Grantham (Ret.)
Geophysics Directorate, Phillips Laboratory

LCDR Bruce Kitchen
NTMOD Newport

Major James T. Kroll
Headquarters, U.S. Air Force

LTC Lauraleen O'Connor
NPOESS/IPO

Dr. Richard Shirkey
U.S. Army Research Laboratory

**Preprint of the Conference on
Cloud Impacts on DoD Operations and Systems
Convened at the U.S. Naval War College, Newport, Rhode Island
23-25 September 1997**

Supported by the
Phillips Laboratory, Geophysics Directorate
Office of the Oceanographer of the Navy
Army Research Laboratory

Hosted by the
U.S. Naval War College
Newport, Rhode Island

Organized and Published by
Science and Technology Corporation
Meetings Division
101 Research Drive
Hampton, VA 23666
Under ESD Contract No. F19628-95-C-005

TABLE OF CONTENTS

CIDOS Executive Committee	v
Preface	xiii

SESSION I: INTRODUCTION

Profile of Conference Welcome Speaker	3
Captain Fred G. Orchard , Director, Naval War College War Gaming Department	
Profile of Conference Introductory Speaker	4
Colonel Alan R. Shaffer , U.S. Air Force Assistant for Battlespace Environment, Office of Defense Research and Engineering	
Profile of Conference Keynote Speaker	5
Rear Admiral Paul E. Tobin, Jr. , U.S. Navy, Oceanographer of the Navy	

SESSION II: PROGRAM REVIEWS

Modeling and Simulating Clouds and Visibility: The MSEA Perspective	9
Gary B. McWilliams , Office of Executive Agent for Air and Space Natural Environment	
National Polar Orbiting Environmental Satellite System (NPOESS)	14
Col John A. Goyette , U.S. Air Force National Polar Orbiting Environmental Satellite System/IPA Deputy Director	
Integrating Weather Exploitation into Air and Space Power Doctrine Using Modeling and Simulation	15
Lt Col John M. Lanicci , Headquarters, U.S. Air Force, Directorate of Command and Control	
THE MASTER ENVIRONMENTAL LIBRARY: An Environmental Data Source for DoD Applications	16
Richard A. Siquig , Naval Research Laboratory; Steven J. Lowe, SAIC	
TAOS and High-Fidelity Virtual Environments for STOW	20
David Whitney , Robert Reynolds, Steve Olson, Peter Dailey, Dana Sherer, and Mavis Driscoll, TASC	
Environmental Representation and the Role of Clouds in Studies and Analysis Models	24
John R. Hummel and A. Peter Campbell, Argonne National Laboratory	

SESSION III: CLOUD M&S APPLICATIONS TO WAR GAMING STUDIES AND ANALYSES

The Impact of Clouds on an Engagement-Level Simulation	31
Capt Mark M. Edwards , Capt Edward E. Hume, and Lt Col Frank A. Zawada, Phillips Laboratory, Geophysics Directorate	
Cloud Transmission Effects in a Distributed Simulation	35
Joel B. Mozer , Steven M. Ayer, and Guy P. Seeley, Phillips Laboratory, Geophysics Directorate; Maureen Cianciolo, TASC	
Cloud Simulation for a Flight Mission Rehearsal System	39
Louis Hembree , Naval Research Laboratory	
Simulating Thin-Cloud Effects on Multi-Spectral Target Detection	43
Joseph G. Shanks and Frederick C. Mertz, Photon Research Associates, Inc.; William A.M. Blumberg, Phillips Laboratory, Geophysics Directorate	
Cloud Modeling and Infrared Spatial Structure	47
Robert A. McClatchey , Robert J. Jordano, and A.T. Stair, Jr., Visidyne, Inc.; Col William Smith, BMDO/TOS	

SESSION IV: CLOUD AND CLOUD EFFECTS MODELING

MODTRAN4: Simulating Atmospheric Radiation Budgets for Clouded Atmospheres	55
Gail P. Anderson and J.H. Chetwynd, Phillips Laboratory, Geophysics Directorate; A. Berk, L.S. Bernstein, and P.K. Acharya, Spectral Sciences, Inc.; H.E. Snell, Atmospheric and Environmental Research, Inc.; E.P. Shettle, Naval Research Laboratory	
Radiometric Validation of CSSM	59
Joel B. Mozer and Guy P. Seeley, Phillips Laboratory, Geophysics Directorate; Alan Wetmore, Patti Gillespie, David Ligon, and Samuel Crow, Army Research Laboratory	
Validation of Cloudscape® AF with Aircraft Data	63
Ross J. Thornburg , John G. DeVore, James H. Thompson, Robert J. Jordano, and Timothy L. Stephens, Visidyne, Inc.	
Cloud Phenomenology Relevant to Space Based Infrared Systems	67
Hsiao-hua K. Burke and J. William Snow, MIT Lincoln Laboratory; Capt David O'Donnell, United States Air Force	
Atmospheric Correction Through Transmissive Clouds	71
J. William Snow , Hsiao-hua K. Burke, Michael P. Jordan, Daniel C. Peduzzi, and Kristine E. Rhoades, MIT Lincoln Laboratory	

The Fractal Behavior of Cloud Systems	75
Kenneth E. Eis , John M. Forsythe, and Donald L. Reinke, Cooperative Institute for Research in the Atmosphere, Colorado State University	
A Method for Calculation of Near-Horizontal Cloud Free Line of Sight Probabilities	79
Eric L. Strobel and Dwayne Pribik, Schafer Corporation	
A Relocatable Climate Window for Generating Cloud Scenarios Including Structure and Physical Attributes	83
Albert R. Boehm , Hughes STX Corporation	
Dense Cloud Radiative Transfer Scenarios and Model Validation	85
David H. Tofsted , Army Research Laboratory; Sean G. O'Brien, Physical Science Laboratory	
Lattice Boltzmann Equation Models: A New Approach for Microscopic Simulation of Cloud Physics	89
Xiaowen Shan and Joel B. Mozer, Phillips Laboratory, Geophysics Directorate	
A Lattice Boltzmann Cloud Model with Moisture Parameterization	93
Susan Triantafillou , Xiaowen Shan, and Joel B. Mozer, Phillips Laboratory, Geophysics Directorate	

SESSION V: CLOUD PREDICTION

Diagnosis of Cloud Variables from Mesoscale Numerical Weather Prediction Model Forecasts	99
Donald C. Norquist , Phillips Laboratory, Geophysics Directorate	
Statistical Contrail Forecasting	103
Artie Jackson , Brian Newton, Doug Hahn, and Allan Bussey, Phillips Laboratory, Geophysics Directorate	
ADVCLD: Air Force Global Weather Center's Updated Cloud Forecast Model	107
Thomas J. Kopp , Margaret M. Wonsick, Louis E. Cantrell, and Francis D. Bieker, Headquarters, U.S. Air Force Global Weather Central	
Cloudy Regions Below the Marine Stratus Deck	111
James W. Telford , Atmospheric Concepts	
Ensemble Cloud Modeling for Mesoscale Forecast	115
Ted Yamada , Yamada Science & Art Corporation	
The Cloud Depiction and Forecast System II Nephanalysis Model	119
Gary B. Gustafson and Ronald G. Isaacs, Atmospheric and Environmental Research, Inc.; Bonnie McDonald, Sterling Software, Inc.	

SESSION VI: MEASUREMENT SYSTEMS AND SENSORS

Optimal Visualization of Multispectral and Multisensor Environmental Satellite Data	123
Robert P. d'Entremont , Joanne Zhou, and Karen Cady-Pereira, Atmospheric and Environmental Research, Inc.; James T. Bunting, Phillips Laboratory, Geophysics Directorate	
CloudSat: A Spacecraft to Measure the Vertical Structure of Clouds	127
Steven J. Walter , Deborah G. Vane, and Fuk K. Li, Jet Propulsion Laboratory, California Institute of Technology; Graeme L. Stephens, Colorado State University	
Cloud Analysis During the NPOESS ERA	131
Gary B. Gustafson , Robert P. d'Entremont, David P. Hogan, and Ronald G. Isaacs, Atmospheric and Environmental Research, Inc.	
Use of Reconnaissance Assets in Support of Theater Weather	132
Maj Michael S. Kapel , Capt John F. Polander, and Steven P. Weaver, 88th Weather Squadron; Jeffrey Pesler, Aeronautical Systems Center, Reconnaissance Program Office	
NASA DC-8 Airborne Scanning Lidar Cloud and Contrail Observations	136
Edward E. Uthe , Terje E. Oseberg, and Norman B. Nielsen, SRI International	
Cloud Database Collected in Support of the Space-Based Infrared System (SBIRS) Phenomenology Exploitation Program	140
Thomas R. Caudill , William A.M. Blumberg, and Alan Griffin, and John Wise, Phillips Laboratory; Geophysics Directorate; Capt David J. O'Donnell, Space and Missile Systems Center	
Lidar Observations Provide Information on the 3-Dimensional Structure and Optical Properties of Clouds Required for Scene Generation	144
Edwin W. Eloranta , University of Wisconsin-Madison	
Comparison of Satellite-Based Cirrus Retrievals with Coincident Ground-Based Radar and Lidar Observations	145
Robert P. d'Entremont and Gary B. Gustafson, Atmospheric and Environmental Research, Inc.; Thomas R. Caudill, Phillips Laboratory, Geophysics Directorate	
Airborne Retrieval of Cirrus Cloud Temperature and Composition Using ARES 5.1-5.3 μm and 3.7 μm Radiance Data	149
Steve C. Ou , K.N. Liou, P. Yang, and P. Polland, University of Utah; Thomas R. Caudill, Phillips Laboratory, Geophysics Directorate; J. Lisowski, SCITEC; Brian J. Morrison, Aeromet, Inc.	

SESSION VII: CLOUD DATASETS

Global Cloud Data for System Design and Simulation	155
Donald Wylie , University of Wisconsin-Madison; W. Paul Menzel, NOAA/NESDIS	

Global High-Resolution Layered Cloud Database—Research and Development at the Cooperative Institute for Research in the Atmosphere, Colorado State University	159
Donald L. Reinke , John M. Forsythe, and Thomas H. Vonder Haar, Colorado State University	
Overview and Objectives of the DoD Center for Geosciences Sponsored “Complex Layered Cloud Experiment” (CLEX)	163
Thomas H. Vonder Haar, Stephen K. Cox, Graeme L. Stephens, John M. Davis, Timothy L. Schneider, Walter A. Petersen, Arlie C. Huffman, Kenneth E. Eis, Donald L. Reinke , and John M. Forsythe, Colorado State University; Fuk K. Li, NASA Jet Propulsion Laboratory; Gregory A. Sadowy, University of Massachusetts	
Ground-Based Digital Cloud Imagery Analysis and Applications	167
Robert P. Wright, Stanley H. Grigsby , and Robert M. Holt, Planning Systems, Inc.	
Cloud Data Generation System	171
Jeffrey S. Morrison and Steven L. Rubin, TASC	

POSTER PRESENTATIONS

WWW-Based Cloud Information Reference Library and Archive (CIRLA)	177
John C. Burgeson and Paul D. Try, Science and Technology Corporation; Donald D. Grantham, Phillips Laboratory, Geophysics Directorate	
Cloud Detection/Editing Experiments on the <i>Lewis</i> and <i>Clark</i> Satellites	181
Richard E. Davis , R. Gale Wilson, and Robert L. Jones, NASA Langley Research Center	
Single-Channel Cloud Detection Using Land-Surface Bidirectional Reflectance Distribution Functions	185
Robert P. d’Entremont , Atmospheric and Environmental Research, Inc.	
A Fused Method of Determining Soil Moisture Using High Resolution Geostationary Imagery . . .	189
Kenneth E. Eis , and Andrew S. Jones, Cooperative Institute for Research in the Atmosphere, Colorado State University	
The Optical Properties of Sub-Tropical Cirrus Clouds Derived from the University of Wisconsin High Spectral Resolution Lidar	193
Edwin W. Eloranta , University of Wisconsin-Madison	
Particle Measurement and Analysis Criteria for Intercomparison with Numerical Models of Radiative Cloud Properties	197
W. Patrick Arnott, John Hallett , and Matthew Meyers, Desert Research Institute	
Post Engagement Ground Effects Model	201
Kevin W. Bruening and Jason A. Wampler, MEVATEC Corporation; Julius Q. Lilly , U.S. Army Space and Strategic Defense Command	

Time Series Cloud Forcing Study of Cloud Scene Simulation Model	205
Guy P. Seeley , Joel B. Mozer, and Erol Emre, Phillips Laboratory, Geophysics Directorate	
State of the Battlespace: Cloud and Weather Effects Visualization for the Tactical Battlefield	209
Donald Hoock, David H. Tofsted , Richard Shirkey, and Jon Martin, Army Research Laboratory; John C. Giever, Physical Science Laboratory, New Mexico State University	
Mobile Aircraft Icing Forecast System	213
Steven J. Walter and Philip I. Moyniha, Jet Propulsion Laboratory, California Institute of Technology	
One Year of World Wide Cloud Cover	217
Arnold A. Barnes, Jr. , Phillips Laboratory, Geophysics Directorate	
The Cloud-Free Line-of-Sight Aloft (CFLOSA) PC Program	220
Albert R. Boehm , Hughes STX Corporation	
Building an Improved Cirrus Model in the CSSM	222
Maureen E. Cianciolo , Mark E. Raffensberger, and Ryan B. Turkington, TASC	
Cloudscape® VR: Radiometric Visualization of Clouds for Interactive Training and Simulation	226
John G. DeVore , James H. Thompson, Ken W. Sartor, Timothy L. Stephens, and Ross J. Thornburg, Visidyne, Inc.	
Cloud Generation Using RenderWorld	230
Karl Garrison , Harry Bishop, and David A. Wasson, Areté Associates	
Visualization of Cloud Effects in Battlscene Modeling and Simulation	231
Steven M. Ayer and Joel B. Mozer, Phillips Laboratory, Geophysics Directorate	
Airborne Cloud Characterization for Radiometric Sensors	235
Brian J. Morrison, James Jung, and R. Lynn Rose , Aeromet, Inc.	
An Animated View of Global Water Vapor, 1988-1994	239
Thomas H. Vonder Haar , Mark A. Ringerud, David L. Randel, Graeme L. Stephens, and Donald L. Reinke, Science and Technology Corporation - METSAT	
Appendix A	
Agenda	243
Appendix B	
List of Registered Attendees	253
Appendix C	
Author Index	265

PREFACE

This preprint contains 60 technical papers that will be presented either orally or as posters at the Tri-Service "*Cloud Impacts on DoD Operations and Systems 1997 Conference*" (CIDOS-97) held at the U.S. Naval War College, Sims Hall, Nott Auditorium, Newport, Rhode Island.

The CIDOS-97 conference is the eleventh conference of the DoD community concerned with the impact of clouds on military systems. The first formal meeting of this community was held in 1983 under the name Tri-Service Clouds Modeling Workshop. The name was changed in 1988 to Cloud Impacts on DoD Operations and Systems (CIDOS) to reflect more accurately the intent and purpose of the CIDOS community as a resource for defense-related problems and issues of greater scope and magnitude.

The theme of the conference will be "**Cloud Effects in War Gaming, Modeling and Simulation.**" The emphasis will be on the concepts for introducing clouds with physically-based reality in emerging or developing simulations.

The three day conference format will consist of platform presentations, video and computer demonstrations, along with poster presentations. The opening session of DoD program reviews will be followed by technical sessions: Cloud M&S Applications to War Gaming and Studies and Analyses, Cloud and Cloud Effects Modeling, Cloud Prediction, Measurement Systems and Sensors, and Cloud Datasets. A full agenda of the meeting appears in Appendix A.

The CIDOS Steering Committee gratefully acknowledges direction from the CIDOS-97 sponsor, Col Alan R. Shaffer, U.S. Air Force Assistant for Battlespace Environment, Office of Defense Research and Engineering, and the financial support of the Phillips Laboratory, Geophysics Directorate, Office of the Oceanographer of the Navy, and Army Research Laboratory. The excellent cooperation and contributions of the session chairs and the presenters is also acknowledged. The conference is hosted by the U.S. Naval War College, and the administration organization was carried out by the Meetings Division of Science and Technology Corporation.

Paul Tattelman
Chairman
CIDOS Steering Committee

This page was left blank intentionally.

**SESSION I:
INTRODUCTION**

Profile of Conference Welcome Speaker

CAPTAIN FRED GREGG ORCHARD

United States Navy

CAPTAIN Fred G. Orchard, a native of Pocatello, Idaho, entered the United States Naval Academy in June 1969. He was awarded a Bachelor of Science degree in Operations Analysis and commissioned an Ensign in the US Navy in June 1973.

Following commissioning, CAPTAIN Orchard served in USS JOUETT (CG-29), homeported in San Diego, California. His first shore duty was the Naval Recruiting District, Portland, Oregon as an Officer Recruiter, and later, as Officer-in-Charge of Naval Recruiting Class "A" Station, Boise, Idaho.

In April 1980, CAPTAIN Orchard completed Surface Warfare Officer Department Head Course and was assigned as Engineer Officer in USS DECATUR (DDG-31), followed by a tour as Engineer Officer in USS ALAMO (LSD-33), both homeported in San Diego, California.

CAPTAIN Orchard graduated from the Naval Postgraduate School in Monterey, California, in 1985, earning a Master's Degree in Computer Science. Returning to sea in April 1986, he served as Executive Officer in USS JOSEPH STRAUSS (DDG-16), homeported in Pearl Harbor, Hawaii.

In February 1988, CAPTAIN Orchard was assigned to the staff of the Chief of Naval Operations (OPNAV-942), where he served as Requirements Officer for Advanced Tactical Data Link Systems.

CAPTAIN Orchard assumed command of USS ELMER MONTGOMERY (FF-1082) in January 1991, while the ship was deployed in support of Operation Desert Storm. During his command tour, the ship conducted Counter-drug operations in the Caribbean Sea and eastern Pacific Ocean. Upon completion of his command tour in July 1992, he was assigned to the staff of Commander, Battle Force Seventh Fleet as Surface Operations Officer, homeported in Yokosuka, Japan.

In September 1994, CAPTAIN Orchard reported to the Naval War College, Newport Rhode Island. He served first as Assistant Director of War Gaming and currently is the Director of War Gaming.

CAPTAIN Orchard is married to the former Karla Erickson of Pocatello, Idaho. They have a son, Nathan, and two daughters, Molly and Gwen.

CAPTAIN Orchard's personal awards include the Meritorious Service Medal (3), Navy Commendation Medal (2), and Navy Achievement Medal. In addition, he wears various campaign and unit citations. He has deployed to the Western Pacific, the Mediterranean, the Indian Ocean, and the Arabian Gulf.

Profile of Conference Introductory Speaker

COLONEL ALAN R. SHAFFER

United States Air Force

Colonel Shaffer is the Assistant for Battlespace Environments, Office of the Director, Defense Research and Engineering.

Col Shaffer was born in Dunkirk, NY, on 24 Jan 1955. He earned a B. S. in Mathematics from the University of Vermont and Air Force Commission through St. Michael's College Reserve Officer Training Commissioning Program in 1976. In 1977, he earned a B. S. in Meteorology from the University of Utah, and subsequently a M. S. (with Distinction) from the Naval Postgraduate School, Monterey, CA, and a M. S. in National Resource Management from National Defense University. In 1977, Col Shaffer was assigned to Detachment 7, 24th Weather Squadron, Mather AFB, CA, as weather forecaster, then Wing Weather Officer to both the 323d Flying Training Wing and 320th Bombardment Wing (Heavy). While supporting the 320th Bomb Wing, the unit won the Fairchild Trophy as best bomb wing in the Air Force. From Mather, Col Shaffer attended the Air Force Institute of Technology graduate education program at the Naval Postgraduate School.

Following graduation, Col Shaffer was assigned to Det 1, 2d Weather Squadron, Wright-Patterson AFB, OH as an advanced weather officer to the Air Force Foreign Technology Division, where he assessed foreign nation operational weather capabilities and the direct impact of the environment on foreign weapons systems. In 1986, Col Shaffer served an extended temporary duty as Officer in Charge, Weather Support Element, Palmerola Air Base, Honduras. While assigned to Det 1, Col Shaffer was selected as the 1986 Air Force Weather Company Grade Officer of the Year.

In 1987, he assumed command of Det 2, 7th Weather Squadron, Hanau Army Installation, Germany with concurrent duty as Weather Officer to the Commanding General, 3d Armored Division. During this tour, Det 2 was selected as the 1989 William Award winner, given to the most outstanding Air Force Weather unit. In 1990, Col Shaffer was reassigned to 5th Weather Wing, Langley Air Force Base, VA, as Chief, Operational Support Division. Upon restructure of Air Force Weather, he became Chief, Plans and Program Branch, and Deputy Chief, Weather Division, Hq Air Combat Command.

In 1993, Col Shaffer attended the Industrial College of the Armed Forces, Ft McNair, DC. Upon graduation in 1994, he was assigned to the Hq Air Force Directorate of Weather, Deputy Chief of Staff, Plans and Operations. While at Air Staff, he was Deputy Chief, Weather Plans Division; then Chief, Interagency Division; Chief, Weather Policy Division; and Chief, Weather Resources Division. He assumed his present position and rank in June 1996.

Col Shaffer's decorations include the Meritorious Service Medal with three oak leaf clusters and the Air Force Commendation Medal with one oak leaf cluster. He is married to the former Jacqueline C. Sklenar, and they have one son, Eric.

Profile of Conference Keynote Speaker

REAR ADMIRAL PAUL EDWARD TOBIN, JR.

United States Navy
The Oceanographer of the Navy

Rear Admiral Paul Edward Tobin, Jr., graduated from the Naval Academy in 1963 and reported to USS TOWERS (DDG 9) where he served as first lieutenant and main propulsion assistant. After graduating with distinction from the Naval Destroyer School in 1966, he was assigned as engineer officer in USS DAVIS (DD 937) where he was awarded a Bronze Star for operations associated with the salvage of USS LIBERTY (AGTR 5) after that ship sustained heavy combat damage in the 1967 Mideast War. In 1968, he commenced postgraduate studies at the U.S. Naval Postgraduate School which culminated in a Master of Science degree in computer systems management. In 1970, he joined the staff of Naval Destroyer School as head of the Technical Training Branch and as an engineering instructor in the department head and PCO/PXO courses.

Rear Admiral Tobin reported as aide and flag secretary to the Commander, Naval Forces Vietnam in 1971. He returned to sea duty in 1973 as executive officer in USS KOELSCH (FF 1049). Upon completing this tour, he reported as aide and flag lieutenant to the president of the Naval War College and subsequently graduated with distinction from the Naval Command and Staff course. In 1976, he reported to the office of the Chief of Naval Operations and served in the Systems Analysis Division (OP-96).

In 1979, he assumed command of USS TATTNALL (DDG 19), where he completed two Indian Ocean and Persian Gulf deployments. In 1981, he reported as chief engineer in USS FORRESTAL (CV 59) where he served for two years and participated in the 1981 Gulf of Sidra operations, two Mediterranean deployments and the initial phase of the Carrier Service Life Extension Program. In 1984, he graduated with distinction from the Industrial College of the Armed Forces in Washington, D.C.

In September 1984, he assumed command of USS FOX (CG 33) in San Diego, California. During this tour he completed a deployment to the Western Pacific and Indian Ocean. He assumed command of the Surface Warfare Officers School Command, Newport, Rhode Island, in July 1986. In October 1988, he assumed duties as Director, Department of the Navy Information Resources Management, and Director, Information Management Support Division (OP-945). He also served as Director, Naval Communication/Information Systems.

In August 1990, he assumed command of Naval Surface Group, Western Pacific; Task Force 73; and Task Force 75. In this capacity he oversaw the reorganization of naval surface forces in the Western Pacific. He then assumed the duties as Assistant Chief of Naval Personnel, Personal Readiness and Community Support (Pers-6) in September 1992. In June 1994, Rear Admiral Tobin assumed his duties as Vice Chief of Naval Education and Training. He assumed the duties of Oceanographer of the Navy in March 1996.

Rear Admiral Tobin's personal awards include: the Distinguished Service Medal, the Legion of Merit with two Gold Stars, the Bronze Star, the Meritorious Service Medal, and the Navy Commendation Medal with two Gold Stars in lieu of his second and third awards. Rear Admiral Tobin is married to Lynne Carter Tobin from Shaker Heights, Ohio, and they have two daughters: Mary Elizabeth and Patricia.

SESSION II: PROGRAM REVIEWS

References in some of the preprints had to be deleted by the editor because they referred the reader to papers with limited distribution that were not available to the public.

MODELING AND SIMULATING CLOUDS AND VISIBILITY: THE MSEA PERSPECTIVE

Gary B. McWilliams
Executive Agent for Air and Space Natural Environment
Air Force Combat Climatology Center
Scott Air Force Base, IL 62225-5116

ABSTRACT

Clouds and visibility conditions can have very significant impacts on military activities and there are several technical shortfalls in current cloud and visibility modeling and simulation capability. The Modeling and Simulation Executive Agent for the Air and Space Natural Environment (MSEA ASNE) has given a high priority to ensuring that the technical capability for realistically modeling and simulating cloud and visibility conditions in Joint Modeling and Simulation programs is available. Cloud and visibility models are required for simulations that have levels of resolution that go from engineering development to campaign level planning. The MSEA ASNE is focusing its efforts on developing those capabilities that have the potential to benefit a multitude of these simulation applications. Ongoing and planned MSEA ASNE projects will provide the modeling and simulation community with needed capabilities such as generating radiometrically validated cloud scenes and estimating visibility parameters in littoral regions using output from numerical weather prediction models.

1. INTRODUCTION

The MSEA ASNE is responsible for providing the M&S community with cost-effective capabilities to generate authoritative representations of the air and space natural environment¹. Recognizing the importance that "seeability" plays in most military situations, the MSEA ASNE has adopted a technology development strategy that gives a high priority to developing capabilities needed for generating realistic cloud impact and other visibility related parameters. We are most immediately interested in those M&S capabilities that describe atmospheric conditions affecting normal visual and Electro-Optical (EO) sensing.

2. TECHNOLOGY DEVELOPMENT STRATEGY

The MSEA ASNE technology development strategy follows the MSEA Concept of Operations (CONOPS) and supports the Defense Modeling and Simulation Office (DMSO) mission to foster the development of interoperable and re-usable M&S technology.

The CONOPS, developed jointly with our environmental MSEA counterparts for terrain and oceans, is a continuous multi-step process that begins with the identification of our customers and their requirements and ends with the delivery of products (capabilities) that satisfy their requirements. This process is depicted in Figure 1.

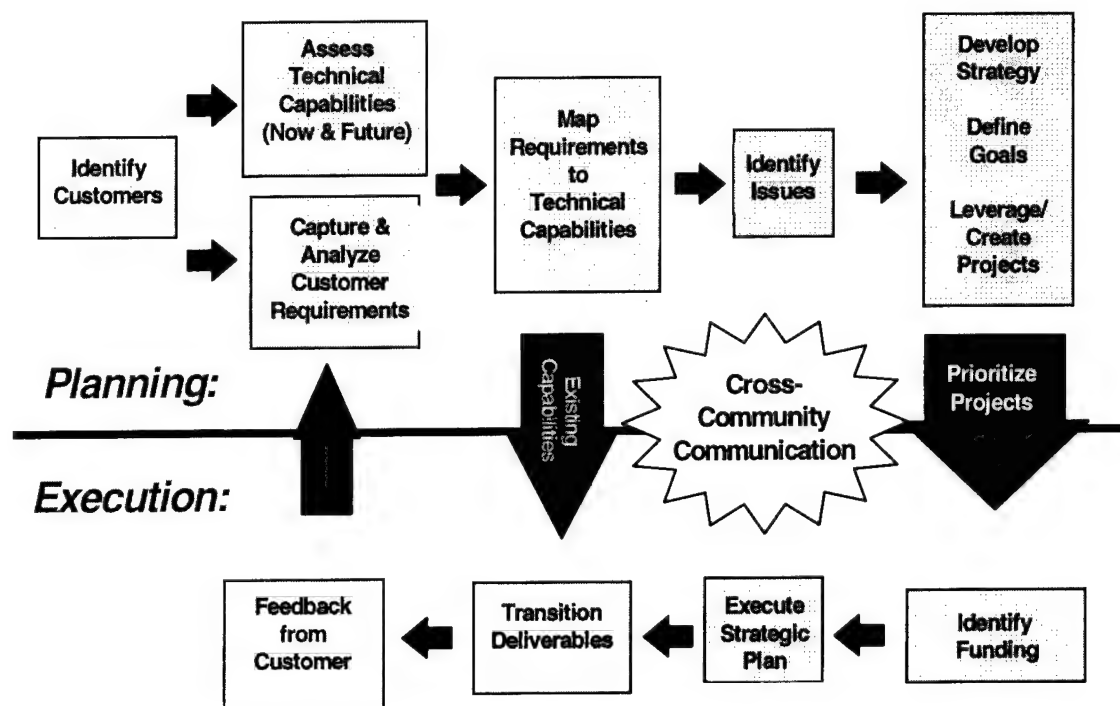


Figure 1. CONOPS for the Environmental MSEAs

As part of this process the MSEA ASNE has recently completed a baseline assessment of the air and space natural environment requirements for our three flagship M&S customers. Our flagship customers are: the Joint Simulation System (JSIMS) – a constructive simulation for training, the Joint Warfare System (JWARS) – a constructive simulation for analysis, and the Joint Modeling and Simulation System (J-MASS) – a simulation architecture for engineering and acquisition applications. The identified baseline requirements span the levels of M&S resolution shown in Figure 2. JSIMS and JWARS have requirements that range from the engagement to campaign level and J-MASS has requirements that range from the system component to engagement level. These baseline requirements are now being compared to the results of our ongoing capabilities assessment to identify areas where technical shortfalls exist. This comparison has resulted in the identification of several shortfalls in the capability to estimate cloud and visibility parameters using computer models.

Once a capability shortfall is identified, it is assigned a priority based on its potential for affecting the output generated by the simulation programs and on an assessment of whether it is feasible to develop the technology. In addressing any technical shortfall, the MSEA ASNE seeks to develop a capability that can be used by more than one of our customers, can scale with a range of available computer resources, and can be used to provide multiple levels of resolution.

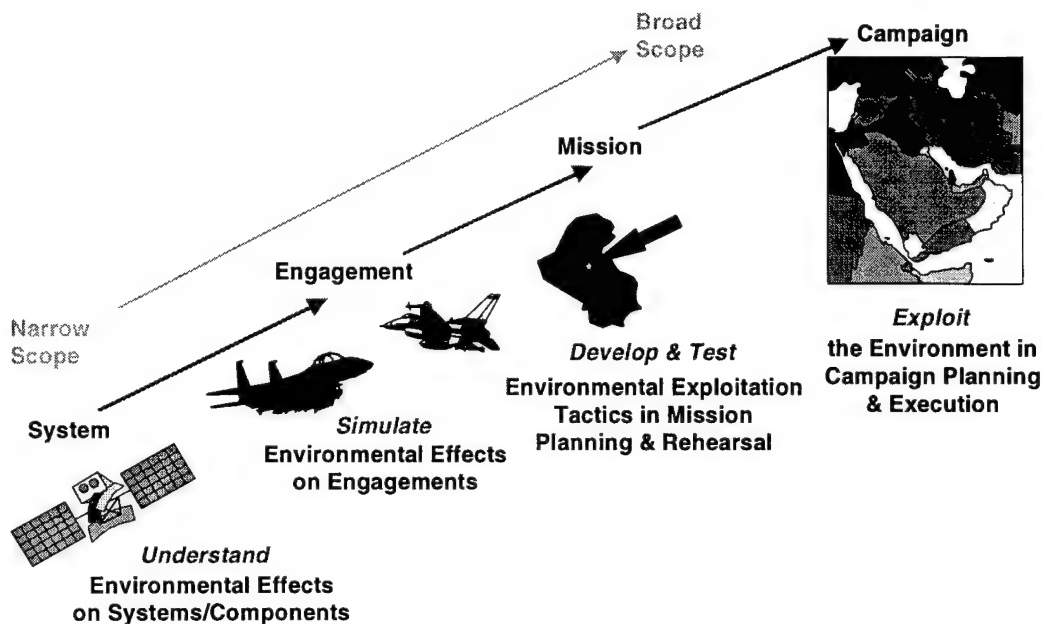


Figure 2. M&S Levels of Resolution

3. TECHNICAL SHORTFALLS

The MSEA ASNE has identified three focus areas where cloud and visibility M&S need development or significant improvement.

The first focus area involves providing an authoritative representation of cloud and visibility parameters in the littoral region. Realistically modeling this region is challenging due to the close coupling of the air, ocean, and terrain environmental processes but necessary because it is an area where many of today's conflicts occur. In more specific terms, the MSEA ASNE has identified the need for a capability to model EO visibility and cloud impact parameters using the output from numerical weather prediction models. Most importantly this new capability must be able to address the effects of marine aerosols and advection fog on visibility.

The second focus area recognizes the need to have a model that can simulate a high-resolution cloud scene that is radiometrically validated. Such a model would be particularly useful for ground target modeling and airborne target detection. Simulations that perform at the engagement level down to system component require this capability.

Our third focus area calls for the development of a capability to represent the impacts of battlespace activities on EO visibility. This capability is needed to describe how EO transmission is affected by battlespace events such as smoke obscuration, burning vehicles, and exploding artillery shells. This capability must also include the effects of the natural background conditions on EO transmission.

4. SPONSORED PROJECTS

The MSEA ASNE is sponsoring three technology development projects that address the shortfalls described above. One project began in FY 97 and the other two projects are planned as new FY 98 initiatives.

4.1 Cloud Impacts and Visibility in the Littoral Region

The Naval Research Laboratory (NRL) at Monterey is leading a cooperative project with the Air Force Research Laboratory (AFRL) at Hanscom AFB to develop capabilities that better model EO visibility and cloud impact parameters in the littoral/coastal region. This project will begin FY 98 and is expected to take three years to complete.

The EO visibility effort consists of three tasks. First, the ability of the Coupled Ocean/Atmosphere Mesoscale Prediction System (COAMPS) to forecast fog density will be improved and validated. Second, a method will be developed to use COAMPS output as input to several of the Navy's aerosol generation models. These aerosol models are needed to provide explicit predictions of aerosol size distributions. The third task involves adapting algorithms within the Electro-optical Meteorological Decision Aid (EOMDA) to provide extinction coefficient estimates in the visible and infrared based upon input from COAMPS. The extinction coefficients will then be used to provide estimates of the horizontal visibility at the surface.

The cloud parameter effort will see NRL and AFRL taking separate approaches to develop a methodology to estimate four cloud impact parameters: cloud bases, cloud tops, cloud types, and cloud amounts. NRL will be taking a physics-based perfect-prog approach for estimating cloud type and amount from COAMPS output. NRL will develop and verify algorithms that use COAMPS cloud related output parameters to estimate cloud type and amount and to refine the estimates of cloud bases and tops. The resulting estimates of the four cloud impact parameters will be used as input to AFRL's Cloud Scene Simulation Model (CSSM) to produce high-resolution cloud fields. The AFRL approach uses a statistical regression and discriminant analysis based model output statistics (MOS). The MOS methodology will use COAMPS forecasts and cloud analyses from the Air Force's Real-Time Nephelometer (RTNEPH) model. This approach will likewise provide estimates of the four cloud impact parameters that are then input to CSSM to produce high-resolution cloud fields. A determination will be made as to which approach works best and where.

4.2 Radiometrically Validated Cloud Model

AFRL and Army Research Laboratory (ARL) scientists are collaborating on a project to provide the M&S community with a radiometrically validated cloud scene model. This project will couple the CSSM that was originally developed under the Smart Weapons Operability Enhancement (SWOE) Program with ARL's radiative transfer model called Boundary Layer Illumination Radiance Model (BLIRB). Once

coupled with BLIRB, CSSM will be validated with field observation data. The validation requires developing a set of metrics for objectively comparing the observed data with the synthetic cloud data. The end product is a radiometrically validated cloud scene simulation model. This project began in FY 97 and is scheduled for completion by December 1998.

4.3 Battlefield Impacts

ARL is also undertaking an MSEA ASNE supported initiative to adapt and integrate existing models that are capable of realistically simulating battlefield impacts on atmospheric conditions. These impacts include the reduction in EO visibility caused by various battlefield-induced aerosols such as vehicular dust. Models will be needed for properly characterizing the emission source and transporting and diffusing the aerosols. These models will have to be adapted so they can dynamically respond to the battlefield events being simulated. This project will employ a neural network technique for predicting the natural background visibility. The project will start in FY 98 and is expected to be completed within three years.

5. CONCLUSIONS

The MSEA ASNE recognizes that clouds and other visibility related phenomena can have significant impacts on military operations and systems. As a result we are making a concerted effort to ensure that these phenomena can be authoritatively represented in DoD's Joint Simulation Programs. Our strategy now includes three projects that, when completed, will significantly improve the capability to more thoroughly and realistically model and simulate clouds and visibility conditions.

6. REFERENCES

1. "Air and Space Natural Environment Modeling and Simulation Execution Plan," May 1997, MSEA ASNE, AFCCC, Scott Air Force Base, IL.

NATIONAL POLAR ORBITING ENVIRONMENTAL SATELLITE SYSTEM (NPOESS)

Col John A. Goyette

U.S. Air Force National Polar Orbiting Environmental Satellite System/IPA Deputy Director

Manuscript not available at time of printing. Please contact author for further information.

INTEGRATING WEATHER EXPLOITATION INTO AIR AND SPACE POWER DOCTRINE USING MODELING AND SIMULATION

Lt Col John M. Lanicci, USAF
HQ USAF Directorate of Command and Control
1510 Air Force Pentagon
Washington, D.C. 20330-1510

A number of policy issues are “converging” today to make air and space power more sensitive to the natural environment. As new concepts such as the Air Expeditionary Force and new technologies such as Distributed Mission Training are developed, the natural environmental community cannot afford to continue in a “business as usual” mode. A smaller but lethal force is enhanced when we can make intelligent use of weather information to “exploit” the environment and “choose the weather for battle.” But how do we evolve from “cope and avoid” to “anticipate and exploit?” The answer lies in the effective translation of weather information into effects and impacts that can be incorporated into the operator’s decision cycle.

This paper outlines a strategy for development and use of sophisticated models and simulations that describe the air and space environment with a high degree of fidelity and realism, and also translate the effects of the weather into measures of performance, mission effectiveness, and outcome. The first step is to adapt physics-based environmental models to support engineering and engagement-level simulations, along with development of sophisticated weather-effects models. These effects will then be aggregated into “impacts” that can be employed in the next generation of theater and campaign-level simulations used in acquisition, analysis, training, and operations. At the campaign level, the Joint Forces Commander will be able to assimilate weather as a component of information operations to make decisions that allow air and space forces to define, direct, and dominate the battlespace of the future.

THE MASTER ENVIRONMENTAL LIBRARY:
An Environmental Data Source for DOD Applications
<http://www-mel.nrlmry.navy.mil>

Richard A. Siquig
Naval Research Laboratory
Monterey, CA 93943-5502

Steven J. Lowe
SAIC
Monterey, CA 93940

ABSTRACT

The Master Environmental Library (MEL) is a World Wide Web (WWW) based data discovery and retrieval system providing access via a consistent single interface to oceanographic, terrain, atmospheric, and near space data bases and related tools residing in geographically distributed resource sites with arbitrary data base configurations and data formats. The key features of MEL are a consistent standard for metadata contents, a common user-friendly interface, a generic order/delivery system under resource site control, and use of standard transfer formats. In the Modeling and Simulation Resource Repository (MSRR), MEL provides access to the environmental domain.

1. INTRODUCTION

1.1 BACKGROUND: *THERE IS A NEED FOR AUTHORITATIVE ENVIRONMENTAL DATA IN DOD MODELING AND SIMULATION.*

Modeling and simulation (M&S) has become increasingly important in U.S. Department of Defense (DOD) activities, such as training, analysis, acquisition, research and development (R&D), test and evaluation, and mission rehearsal, because it offers lower cost and more extensive supplemental alternatives to the more traditional approaches to these activities. However, in the simulated world the natural environment must be included in a realistic, physically consistent, correlated way to achieve the full potential of M&S. This requirement is formally included as part of the DOD M&S Master Plan¹. To help satisfy this requirement, the Defense Modeling and Simulation Office (DMSO) is funding the Master Environmental Library (MEL) Project, a joint project involving the Navy, Army, Air Force, and the National Imagery and Mapping Agency (NIMA), under the leadership of the Naval Research Laboratory.

1.2 VISION: *PROMOTE REUSE AND INTEROPERABILITY OF AUTHORITATIVE ENVIRONMENTAL DATA AND PRODUCTS FOR M&S THROUGH A ONE STOP ENVIRONMENTAL SHOP.*

MEL's vision is to enable uniform access to distributed data in arbitrary formats and to related tools to provide consistent common authoritative environmental representations and effects to various M&S users, war fighters, and other support activities. The data types can be grids, observational, raster, or vector. The environmental regimes include the atmosphere and near space, the ocean, and terrain. The data centers can be in DOD, other federal agencies, such as the National Oceanic and Atmospheric Administration (NOAA) and the National Aeronautics and Space Administration (NASA), and international sources. The data may exist "on the shelf" or may be made available through subscription when it is created. The tools include data fusion, visualization, and statistical processing. Products generated from the elemental data can be produced on a schedule, requested on demand, or produced interactively. The overall criteria for developing such a library infrastructure are to satisfy the high level DMSO goals of reuse and interoperability in the environmental domain, which are also appropriate goals for applications outside of M&S.

2. DATA DISCOVERY, RETRIEVAL, AND DELIVERY

2.1 THE PROBLEM AND A SOLUTION

When trying to locate authoritative environmental data, one finds that there is much already available and the amount is increasing rapidly, but the data are stored at various distributed data centers using different data bases and are delivered in different formats. Simply locating and retrieving the data for M&S can be a formidable problem. For geospatial data, which include data of the natural environment, such as the ocean, terrain, atmosphere, and near space, a common contents standard for *metadata* (data about data), such as the Federal Geographic Data Committee (FGDC) standard², is a powerful key to data discovery. With the rapid development of search engines and web browsers on the Internet, it became possible to create a common, consistent unified interface for parallel browsing of metadata at distributed data sites and for ordering the data itself. The actual details of data extraction, encoding in a standard delivery format, and delivery to the user, are hidden behind the user interface.

2.2 KEY COMPONENTS OF MEL'S APPROACH:

The key components of the MEL architecture are shown in Fig. 1. The user no longer has to deal with each

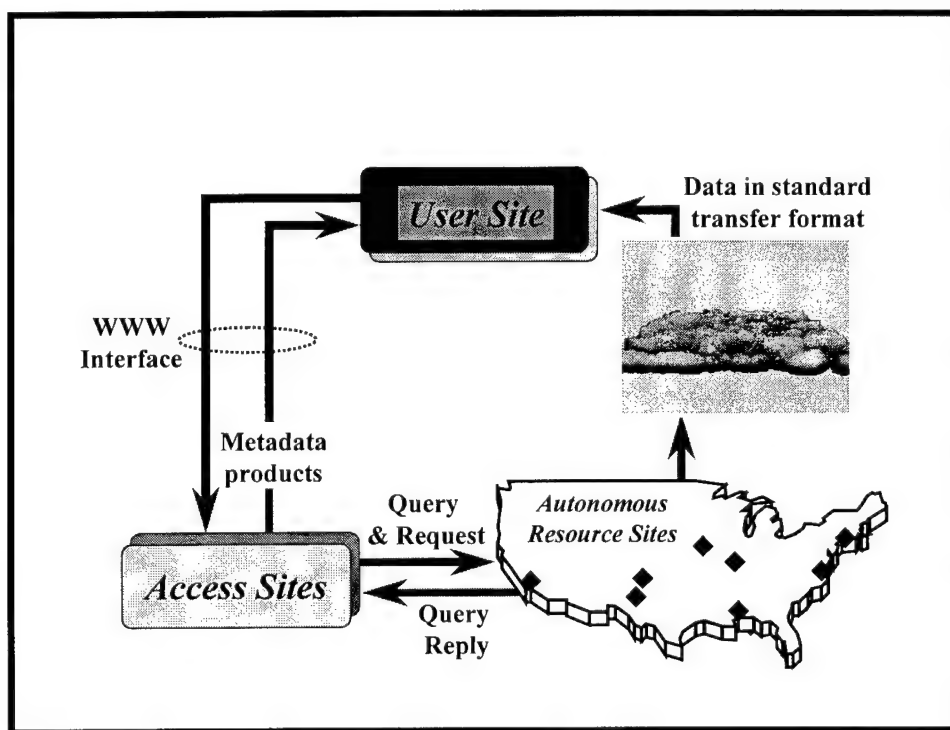


Figure 1. The different components of the MEL architecture are shown, indicating the key role of the access site as a common interface between the user and the data providers (resource sites).

provider separately, thus avoiding a variety of interfaces, methods of data querying and ordering, and different transfer formats. Such local variations are concealed behind the consistent single interface (access site). The data are left under the local control of the provider (resource site), who has only to create and maintain indexed metadata in the standard contents format for it to be searchable over the library system. The actual details of sending queries and requests from the access site, data extraction, encoding, and delivery are made generic to the greatest extent possible and customized as necessary for each resource site. Utilizing the fewest and most standard transfer formats possible and providing the corresponding decoders greatly simplifies the effort of the user to work with the data delivered. By using web technologies MEL exploits the

power of the market place for rapid technology development and de facto standards, for both unclassified and classified networks. This is consistent with the DMSO goals of reuse and interoperability of systems. As the technology evolves, it is straightforward to incorporate improvements into the basic architecture. Furthermore, the architecture is extensible to resource sites that can be processing sites for running models or tool applications. In addition to the original HyperText Markup Language (HTML) interface, a Java interface for querying the system and visualizing the results has been developed³. The current MEL sites are shown in Fig. 2.

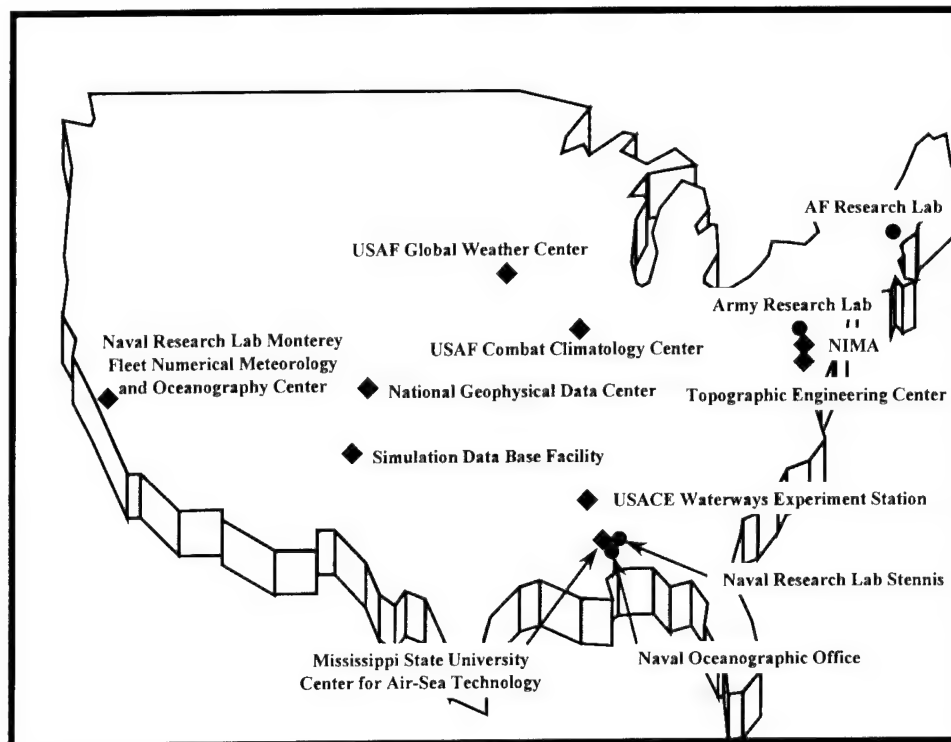


Figure 2. The current MEL sites are shown, where a diamond indicates an online site and a circle indicates a site not yet online.

3. PRODUCT GENERATION IN MEL

Most data providers in the MEL system provide basic environmental data such as winds, temperature, wave height, etc., though some offer products derived from these basic parameters. Because such products are often the information of most interest to M&S users or war fighters, the basic MEL architecture is being enhanced to provide some capability for product generation if resource sites wish to offer it. Here we describe several initial applications.

3.1 DATA ORIENTED APPLICATION

In this case, the order form for a given data set contains an additional section of possible processing options, such as creating graphics or computing statistics for every "field" selected, or a special list of "derived fields" could be presented as an option. In either case, the product involves only the selected data set, and processing occurs at the site where that data is stored.

3.2 PRODUCT ORIENTED APPLICATION

In this case the user searches for and selects a metadata record describing a field, which can be produced from one or more data sets. The data sets that can be used for generating the product are pre-determined and

the options on the order form are "input data set dependent". As a further extension, data sets can be located at one or more resource sites other than the product generator site.

3.3 INTERACTIVE APPLICATION

Here the user is connected via MEL to an "island of computation" where some interactive application is used on a selected data set. This could be generalized to include "shopping" for products. A further extension would be to allow data sets to be delivered to the interactive site prior to the user being connected there.

3.4 LOCAL APPLICATION

Developers outside of MEL could provide local applications to receive, manage, and work with data delivered from MEL. Examples of plug-in modules could be data interpolation, computation of derived fields, and data visualization. This, of course, would require strict version control on a potentially very complicated piece of software, and the user would need a machine capable of the necessary processing. It does, however, eliminate much of the load from MEL servers.

4. CONCLUSIONS

4.1 SIGNIFICANCE OF MEL

MEL is the first data discovery, retrieval, and delivery system that allows a user to query Navy, Army, Air Force, NIMA, and certain non DOD centers for the existence of geospatial data that satisfies the user's criteria, and to request either archived data or data that can be made available by subscription. The data can be from any of the natural environmental domains of terrain, ocean, atmosphere, and near space. The MEL system is also being transferred to a classified network.

4.2 FUTURE PLANS

The emphasis in FY98 will be on increased robustness of the architectural implementation and transition of independently developed tools and other applications to the system, providing enhancements for data manipulation, visualization, distributed computing, and product generators. The project expects to expand its customer base beyond M&S to include joint operational users who require access to distributed sources of geospatial data and to continue its coordination and collaboration with other library systems.

5. ACKNOWLEDGMENTS

The Defense Modeling and Simulation Office (DMSO), under the Director of Defense Research and Engineering (DDRE), funds the Master Environmental Library (MEL) project.

6. REFERENCES

1. Department of Defense, Under Secretary of Defense for Acquisition and Technology. "Modeling and Simulation (M&S) Master Plan". October 1995.
<URL:<http://www.dmsomil/docslib/mspolicy/msmp/1095msmp/>>
2. Federal Geographic Data Committee, Washington, DC. "Content standards for digital spatial metadata (June 8 draft)". 1994. <URL:<http://www.its.nbs.gov/nbs/meta/meta.htm>>
3. Alper, N. and Stein, C. "Geospatial Metadata Querying and Visualization on the WWW Using Java Applets". Proceedings, IEEE Information Visualization '96. PP 77-84, October 1996.

TAOS AND HIGH-FIDELITY VIRTUAL ENVIRONMENTS FOR STOW

David Whitney, Robert Reynolds, Steve Olson, Peter Dailey,
Dana Sherer, Mavis Driscoll

TASC
55 Walkers Brook Drive
Reading, MA 01867
dawhitney@tasc.com

ABSTRACT

One of the major technical challenges for the next generation of war gaming, analysis, and training simulations is the construction, management, and distribution of the natural atmospheric environment. This includes information necessary to generate synthetic clouds and produce their effects. As part of the Defense Advanced Research Projects Agency (DARPA) Synthetic Theatre of War (STOW) Program, the Total Atmosphere-Ocean Services (TAOS) system has been developed to provide tactically significant environmental data and effects. STOW, to occur in Fall 1997, will be the largest-scale distribution simulation event ever to make use of a physically realistic, dynamic 3-D representation of the atmosphere-ocean environment and its consistent effects on simulations. This paper describes how realistic synthetic natural entronements are being integrated by TAOS to provide a increasingly rich dynamic natural environment. The use of environmental data and effects in the STOW'97 exercise is reviewed. Data sources, integration, and distribution methods are presented. The implementation of local embedded features so as to be consistent with underlying gridded atmospheric fields, such as cloud fields, aggregate cloud information or atmospheric extinction coefficients, are discussed. Architectural alternatives available within TAOS to support the real-time distribution of data and computation of effects are discussed, including its support for the High Level Architecture and Run-time Infrastructure (HLA/RTI).

1. INTRODUCTION

1.1 NEW REALISM FOR SYNTHETIC ENVIRONMENTS

A critical objective of the next generation of simulation systems is the integration of natural or physical environment (atmosphere-ocean-space) data and effects across heterogeneous simulations to provide new levels of realism and consistency. The TAOS system, sponsored by STOW, has been developed to meet these objectives. STOW'97 is a major thrust of the DARPA initiative in Advanced Distributed Simulation (ADS). To support ADS applications ranging from individual combatants to Joint Task Force Levels, STOW seeks to develop and implement portable technologies enabling the integration of war-fighting through virtual and constructive simulations from geographically distributed locations in a common synthetic battlespace.

The STOW Program's near-term focus is on an Advanced Concept Technology Demonstration (ACTD) sponsored by DARPA with the United States Atlantic Command (USACOM). Its broader focus, and that of the TAOS Environmental Services technology, is to provide portable, high-fidelity synthetic environment technology that will support the broad range of ADS applications, such as JSIMS, JWARS, and JMASS.

2. DYNAMIC ENVIRONMENTAL DATA SERVICES SYSTEM

The TAOS system provides the fundamental environmental data needed to bring new levels of environmental realism to the virtual battlefield. TAOS provides high-fidelity, tactically significant atmosphere, ocean and surf zone data on demand to networked distributed simulations. TAOS provides key linking services between raw data sources and simulation applications. Figure 1 illustrates some of the linkage services TAOS provides.

2.1 ARCHITECTURE

A general-purpose architecture for data collection, assimilation, integration, distribution, and management that supports both the Run-time Infrastructure (RTI) and existing Distributed Interactive Simulation (DIS) protocols has been established. For example, TAOS provides the environmental data services for STOW, and drives both the Computer Generated Forces (CGF), such as ModSAF and Chemical Biological Radiation (CBR) Simulator, as well as visualization, such as ModStealth, components for the federation under HLA/RTI.

TAOS provides dynamic meteorological and oceanographic (METOC) data to the battlespace. In STOW, TAOS distributes high-fidelity, tactically significant atmosphere, ocean and surf zone data on demand to networked simulation clients including Synthetic Forces and ModStealth. TAOS has been developed within a modular architecture for collection, assimilation, integration, distribution, and management of METOC data that supports both the HLA/RTI and DIS communications protocols (1).

2.2 DATA SOURCES AND TYPES

TAOS ingests, stores and distributes gridded atmosphere-ocean-surf data which varies in three spatial dimensions and time. Authoritative gridded forecasts products, from both operational and research models, can be combined by the TAOS Integrator and stored in a database as consistent environmental data for distribution (2). Drawing largely from the Master Environmental Library (MEL), hundreds of different base gridded environmental variables from a wide range of volumetric gridded data sets are available, and others can be easily added by extending the TAOS library of data receivers. Table 1 lists some of the model/receiver pairs implemented in TAOS. For STOW'97, mesoscale meteorological data from the United Kingdom Meteorological Office for the Persian Gulf was the authoritative data source.

In addition, TAOS can link to a variety of real-time sources to collect and distribute the latest hourly field observations that are available from both public and authoritative DoD data sources. Surface, upper atmosphere, aircraft, ship, and ocean buoy observations are provided via the Automated Weather Network (AWN) of 15,000 global sites managed by the U.S. Air Force. Precipitation information in the U.S. can be derived from data collected every 15 minutes from National Weather Service weather radars, through a linkage via a commercial radar data provider (Weather Services International).

Given a database of gridded volumetric data fields, TAOS enables this database to be supplemented with localized high resolution environmental features, or more abstract aggregate features, such as the Cloud Scene Simulation Model (CSSM) for high-resolution cloud products, atmospheric extinction coefficients for specific wavebands, aggregated precipitation data to drive hydrologic models, spectral tide models, and ocean acoustic sound velocity profiles. Libraries of feature and transform objects enable such existing models to be embedded in TAOS to provide an extensible set of derived features and products (3).

TAOS provides a range of data products to meet individual user needs. For distribution of data over a simulation network, any variable can be distributed as a data object that ranges from fully-gridded to spatially uniform, depending on the resolution of data needed by the client. Specialized coordinate transforms, derived variables, and varying distribution rates are all provided by the TAOS Distributor. The TAOS Network Monitor allows this environmental network traffic to be monitored through a GUI for load and reliability analysis. TAOS also is implementing a capability to provide traditional weather graphics for human exercise players that are consistent with the environmental data being supplied to the network simulations.

2.3 TAOS FUNCTIONALITY

TAOS provides the following major functions to distributed simulations to enable the use of realistic synthetic atmosphere-ocean-surf environment data:

- High-Fidelity Dynamic 4-D Fields
- Atmosphere-Ocean-Surf Data Products
- Live Real-World Observations

- Forecasts and Analysis Products
- Environmental Features and Effects
- Live and Replay Data Modes
- Interactive Environmental Data Editing
- Dynamic Data Visualization
- Object-oriented Modeling and System Design
- Dual HLA/RTI compatibility
- Varied Output Data Products and Data Monitoring
- High-fidelity, custom environmental scenarios
- TAOS Operational METOC Chart Assistant.

3. CLOUD PRODUCTS

TAOS can provide spatially and temporally-varying cloud information, such as base, top, height and type, in two ways. It can either run a cloud simulation model that is embedded within it, such as CSSM, or drive a cloud simulation model that is distributed to a remote client, such as the ECLLOUD model running in JointSAF. In either case, TAOS uses its database of dynamic 4-D atmospheric data to provide the cloud field descriptions and base atmospheric variable profiles, such as humidity, that are used to initialize such models. Many of the gridded forecast and analysis models do not provide all the parameters needed by models such as CSSM. TAOS uses sets of empirical rules to derive required quantities, such as cloud type, top, and base. Figure 2 shows a TAOS-derived grid of cloud top information over the Persian Gulf region. Figures 3 and 4 compare a TAOS-derived IR satellite pseudo-image with an actual DMSP satellite image for the same time and place, and indicate sufficient agreement to validate the derivations used for the cloud variables.

4. SUMMARY

A critical objective of the next generation of simulation systems is the integration of natural or physical environment (atmosphere-ocean-space) data and effects across heterogeneous simulations to provide new levels of realism and consistency. This paper has described the TAOS environmental data services system, which has been designed to meet these objectives. The modular, object-based architecture of the system has been described, both in a general context and in its specific application to STOW'97, the largest-scale "environmentally-aware" entity-level simulation exercise ever conducted.

5. ACKNOWLEDGMENTS

This work is supported by DARPA, USACOM, the Defense Modeling and Simulation Office (DMSO), and the Modeling and Simulation Executive Agents (MSEA) for the Natural Environment. The U.S. Army Topographic Engineering Center (TEC) is the contract technical monitoring organization for this work.

6. REFERENCES

1. Whitney, D.A., R. Schaffer, *et al.*, "Experiences in Creating Synthetic Natural Environments and The Transition to HLA", *Proceedings of the 15th Workshop on Standards for the Interoperability of Distributed Simulations*, September 1996.
2. Whitney, D.A., *et al.*, "Developing high-fidelity, consistent environmental data products for STOW'97 and UE-98-1," *Proceedings of the Fall Simulation Interoperability Workshop*, September 1997.
3. Whitney, D.A., *et al.*, "Providing and Managing Real Natural Environments for Virtual Worlds," *Proceedings of the Fall Simulation Interoperability Workshop*, September 1997.

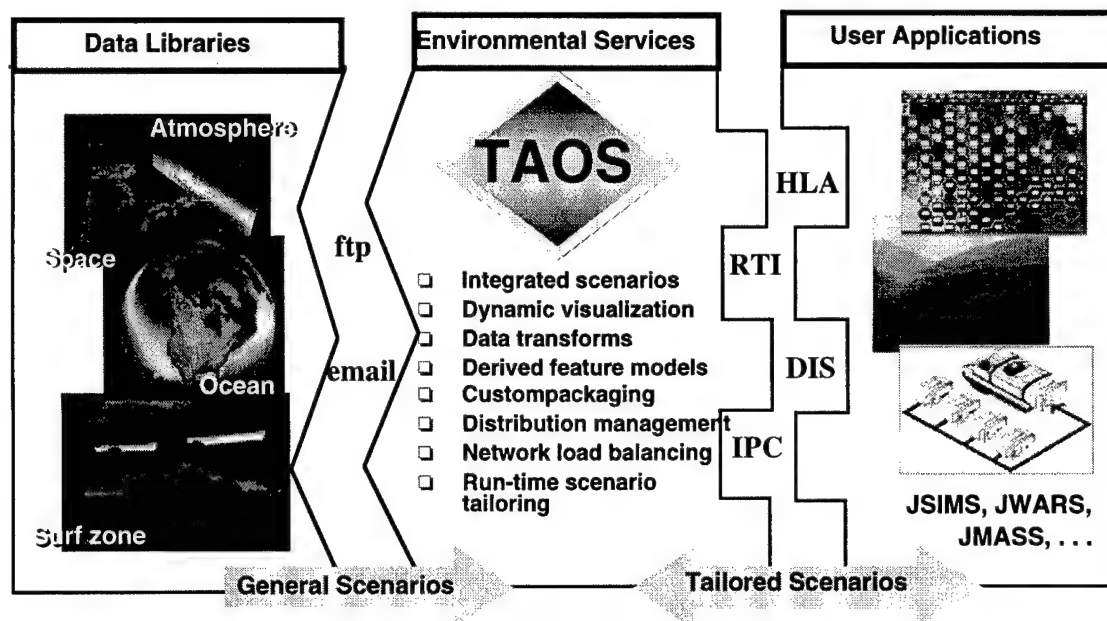


Figure 1. TAOS Provides Key Integration Links.

Table 1. Example of TAOS Data Sources.

SOURCE	DESCRIPTION
NOGAPS	Navy Operational Global Atmospheric Prediction System
NORAPS	Navy Operational Regional Atmospheric Prediction System
COAMPS	Coupled Ocean Atmosphere Mesoscale Prediction System
UKMeso	Mesoscale atmospheric forecast model from the U.K. Meteorological Office
OTIS	Optimal Thermal Interpolation System for thermal structure of the ocean
TOPS	Thermal Ocean Prediction System
WAM	Surface Ocean Wave Model
STWAVE	Stationary Wave Model that is a near-shore ocean surface spectral wave energy model
SWAFS	Princeton Oceanographic Model providing ocean volumetric data
SWAPS	A regional Wave Model that is an ocean surface spectral wave energy model
NSSM	Navy Standard Surf Zone Model for near-shore ocean features
Wx Radar	Commercial CONUS Wx radar imagery (WS-TM)
AWN	Automated Weather Network providing global observation data

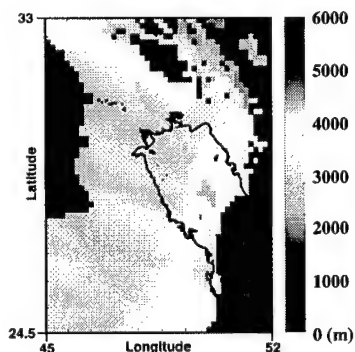


Figure 2. Derived Cloud Top.

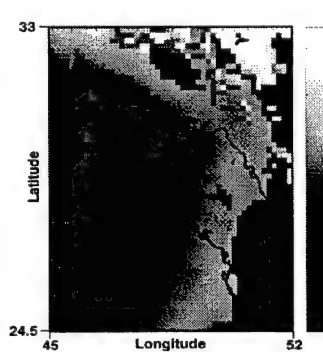


Figure 3. TAOS-Derived Satellite IR Image.



Figure 4. DMSP Satellite IR Image.

ENVIRONMENTAL REPRESENTATION AND THE ROLE OF CLOUDS IN STUDIES AND ANALYSIS MODELS

John R. Hummel and A. Peter Campbell
Argonne National Laboratory
9700 S. Cass Avenue/DIS-900
Argonne, IL 60439-4832

The submitted manuscript has been created by the University of Chicago as Operator of Argonne National Laboratory ("Argonne") under Contract No. W-31-109-ENG-38 with the U.S. Department of Energy. The U.S. Government retains for itself, and others acting on its behalf, a paid-up, non-exclusive, irrevocable worldwide license in said article to reproduce, prepare derivative works, distribute copies to the public and display publicly, by or on behalf of the Government.

ABSTRACT

The Joint Analysis community is currently making significant improvements and enhancements to its suite of modeling tools used to support studies and analyses for Joint applications. This effort is being performed under the Joint Analytic Model Improvement Program (JAMIP) that began in 1995. One part of the JAMIP effort is the development of the Joint Warfare System (JWARS). JWARS will be a state of the art closed-form, constructive simulation of multisided, joint warfare for analysis.

The environment will be a significant factor in future warfare analysis and so JWARS will include an authoritative environmental representation that can be represented at variable spatial and temporal scales. Argonne's Dynamic Environmental Effects Model (DEEM) was used to provide the environmental representation for the JWARS prototype effort. In this paper we will present an overview of JWARS and describe how the environment and environmental effects are being represented in JWARS. Specific emphasis will be given on how clouds are included in the JWARS environment and the impacts they have on the warfighting functionality included in JWARS.

1. INTRODUCTION

Existing simulations employed for analysis by the Department of Defense (DoD) are limited in the types of activities represented and in the technologies employed to represent those activities. Many important areas of warfare are treated poorly or not at all; e.g., ground maneuver, strategic air strikes, and command and control. No single simulation encompasses all joint warfare mission areas. Furthermore, the simulations systems are generally technically outmoded in design, data management, and interoperability, often rendering them difficult to use. Consequently, the simulations may provide inadequate support to senior DoD officials.

In May 1995, the Deputy Secretary of Defense (DepSecDef) approved the Joint Analytic Model Improvement Program (JAMIP) to improve the ability of the DoD to address joint operations. A major component of JAMIP is the development of JWARS, a state-of-the-art simulation of joint warfare for analysis. In November 1995, the DepSecDef established the JWARS Office to develop JWARS. Intended users of JWARS will include the Joint Staff, Services, Office of the Secretary of Defense (OSD), and other DoD organizations. JWARS applications will include the following:

- Evaluation of courses of action;
- Analysis of force sufficiency;
- Assessment of force structure alternatives;
- Joint Warfare Capability Assessments; in particular, development of joint capability issues and assessment of trade-offs;
- Determination of requirements for new war fighting capabilities;
- Analysis of weapon system alternatives, in particular, cost and operational effectiveness analyses; and
- Analysis of alternatives for program and budget reviews.

It is anticipated that the environment will have a significant impact on the kinds of simulations JWARS will perform. As a result, JWARS will have to have the ability to provide a flexible and authoritative representation of the

environment and the impacts the environment can have on JWARS applications. In the development of the JWARS prototype system, DEEM was developed by the Argonne National Laboratory was used to provide the environmental representation and environmental effects functionality.

2. OVERVIEW OF THE DYNAMIC ENVIRONMENTAL EFFECTS MODEL

DEEM is a software framework intended to facilitate holistic multidisciplinary modeling of terrestrial, aquatic, and atmospheric processes. DEEM is the first instantiation of the Dynamic Information Architecture System (DIAS), an object-oriented simulation framework. The environmental processes are modeled in DEEM as interrelated actions caused by and affecting the collection of diverse real-world objects represented in a simulation. The modeling domain of DEEM is flexible, determined by the environment objects available within DEEM and by the collection of models which have been gathered by users to address specific modeling concerns.

DEEM is an object-oriented system that contains a library of reusable objects. The objects in the library have been designed for use in a wide variety of applications with varying levels of resolution. DEEM also employs a sophisticated Context Manager that uses an expert system to assist the user in setting up the application to match the needs of the scenario under consideration. These determinations are made based on an analysis of the "context" of the scenario being considered. During the development of a scenario, DEEM can dynamically change the resolutions being employed in order to efficiently provide the correct level of detail required for the application.

DEEM is also designed to be able to easily interface with existing models. In this way, DEEM can import the various physics and process models that are required to provide the functionality for a given simulation. The majority of these models already exist within the DoD R&D community.

2.1 JWARS ENVIRONMENT OBJECTS AND FUNCTIONALITY

In determining what environmental objects and functionality would be required to support the JWARS test-bed, an analysis of the JWARS Prototype Use Cases was performed to identify what environmental objects would be required and all potential environmental interactions. These "real world" interactions were then mapped against the requirements for the JWARS Prototype Use Cases and a final list of interactions to implement within DEEM was established. In these Use Cases, clouds were the ultimate source of the environmental impacts.

DEEM has been used to support a number of programs (*e.g.* U. S. Department of Energy, the Joint Staff/J-8, Forces Command, U. S. Corps of Engineers/South Florida Water Management District, and the Joint Simulation System Joint Training Federation Prototype) to study environmental impact on military and civilian operations. As a result, Argonne was able to leverage that previous sponsorship to provide many of the objects and functionality required to support the JWARS prototype development. Figure 1 shows the DEEM entity objects that have been included in the version of DEEM developed for use during the JWARS prototype development effort. All of the objects with solid lines have been implemented in software and those objects with environmental functionality tied to the JWARS prototype are shown as heavy lines. The Space object, shown with a dashed line, is planned for future development.

The data used were for the Bosnia area of the former Yugoslavia. Terrain elevation and surface data were obtained from NIMA. Meteorological and oceanic data were obtained from the Master Environmental Library. The NIMA Planning Interim Terrain Data (PITD) "Vegetation" Thematic Files were used to create and load appropriate surface-covering objects: Forest, Plantation, Grassland, etc. The PITD could also be used in the construction of surface drainage features and transportation networks. The PITD for the Bosnia study area was provided at a 1:250,000 resolution. The PITD "Surface Materials" Thematic File was used to create and load soil cover objects.

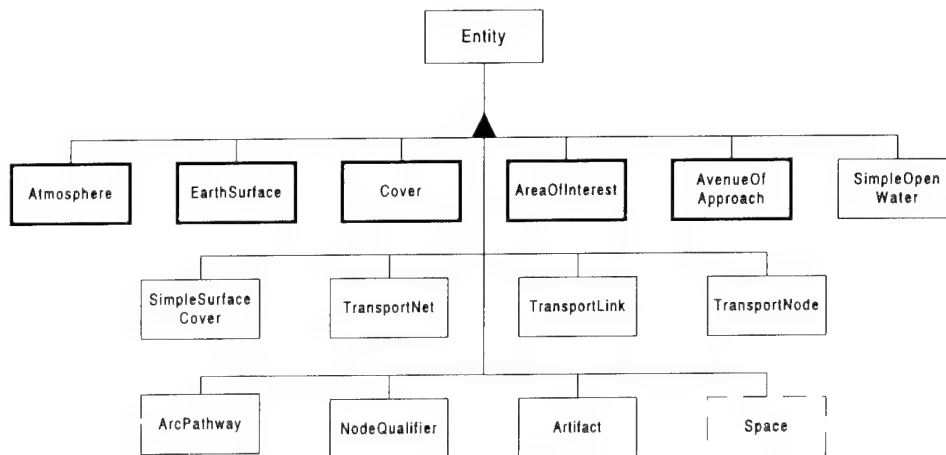


Figure 1. Inheritance relationship of the DEEM Entity objects included in the JWARS Prototype. Those objects with heavy lines have been implemented with functionality used by the JWARS Prototype.

2.2 ENVIRONMENTAL FUNCTIONALITY

In the JWARS prototyping effort, the primary focus on the environment was in terms of the impacts of on mobility and the ability of platforms to engage targets. In both cases, clouds were the dominant environmental factor. In order to provide this environmental functionality, a suite of models was obtained from a number of authoritative DoD sources and integrated into DEEM. Each model was integrated "as is" with no change to the physics or algorithms. If a model was provided to Argonne as source code, it was integrated into DEEM in whatever native programming language it was developed in. The models were also designed to operate from standard, authoritative data sources that could be provided to JWARS by the Joint Data Support program, another partner in the JAMIP effort.

For the mobility determinations, precipitation impacted the soil strength which is one factor in determining the speeds at which vehicles can travel over the ground. Weather conditions were allowed to evolve over a 12 hour period and the cumulative precipitation over the 12 hour period was used, along with information about soil, slope, roughness, and vegetative conditions, in the NATO Reference Mobility Model, the Army standard model used in calculating maximum vehicle speeds over terrain. With the maximum vehicle speeds determined, mobility corridors and avenues of approach could be calculated for different units and different movement strategies. Figure 2 shows an example of a set of maximum vehicle speeds and divisional mobility corridors calculated for the JWARS prototype using DEEM.

For the acquisition of targets by airborne platforms, the impact of clouds was on whether or not pilots could see their targets. Cloud amounts were calculated in each of the atmospheric levels and the total amount of cloud obscuration between the sensing platform and the ground target determined. These results were used in making a determination of whether or not the target would be engaged. In the prototyping effort, the determination of total obscuration was assumed to apply for visible wavelengths only because the airborne platform models did not include any sensor performance details. In the production version of JWARS, more detailed sensor performance estimates based on more realistic cloud simulations will be made.

3. CONCLUSIONS

The Department of Defense has embarked on a program to develop an advanced simulation system to support the Joint analytical community. This new program, the Joint Warfare System (JWARS), is one part of a larger effort, the Joint Analytic Model Improvement Program, to enhance and improve the overall modeling and simulation effort of the Joint community.

JWARS simulations will be impacted by environmental factors. DEEM, the Dynamic Environmental Effects Model, is being used by JWARS to provide a context sensitive, dynamic environmental representation

over varying spatial and temporal regimes. The modeling domain of DEEM is flexible, determined by the environment objects available within DEEM and by the collection of models which have been gathered by users to address specific modeling concerns.

4. ACKNOWLEDGMENTS

Work supported under a military interdepartmental purchase request from the U.S. Department of Defense, Joint Chiefs/J-8, through U.S. Department of Energy contract W-31-109-Eng-38.

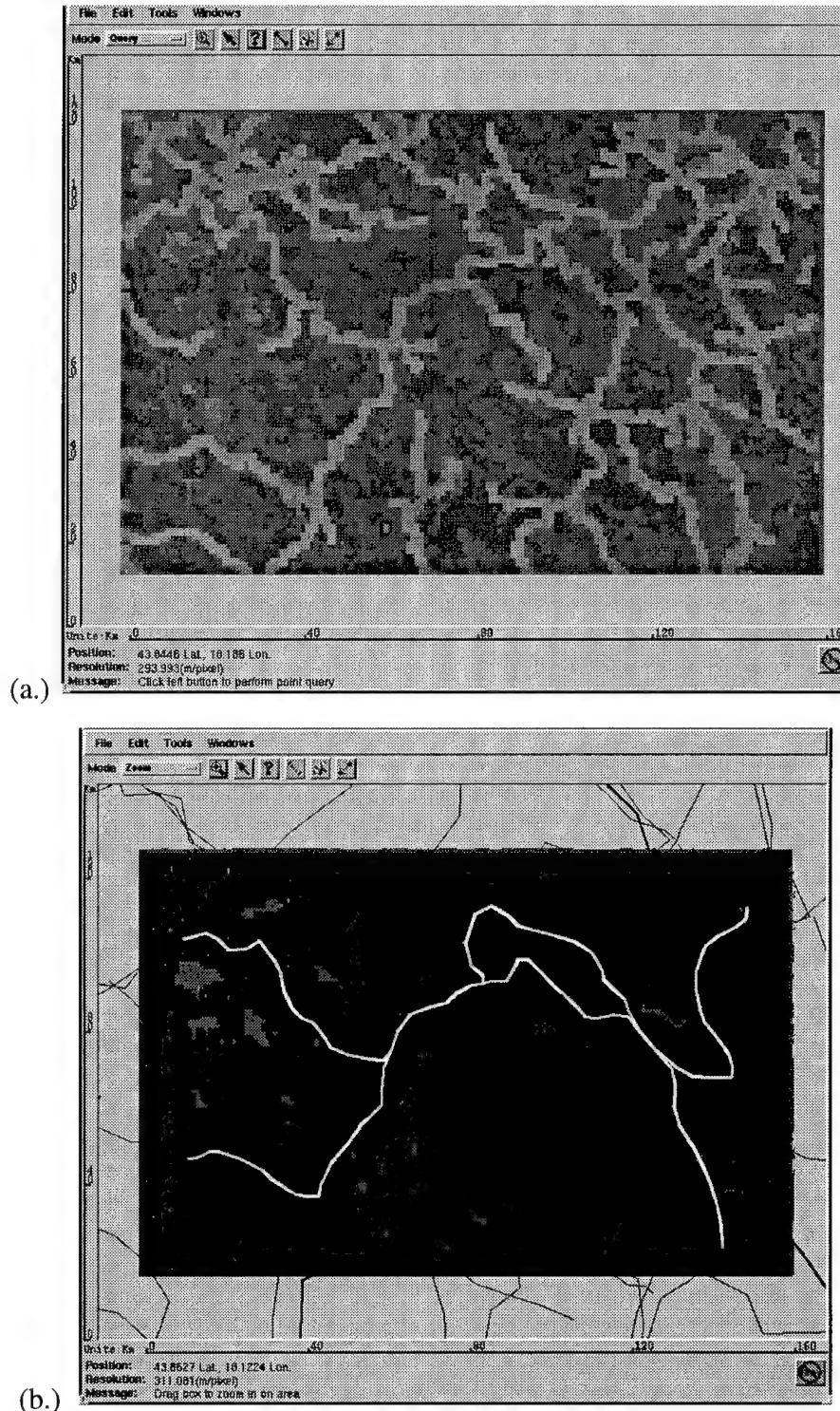


Figure 2. Calculations from DEEM showing the environmentally dependent (a.) maximum vehicle speeds and (b.) resulting divisional mobility corridors generated using the vehicle speeds.

**SESSION III:
CLOUD M&S APPLICATIONS TO WAR GAMING
STUDIES AND ANALYSES**

References in some of the preprints had to be deleted by the editor because they referred the reader to papers with limited distribution that were not available to the public.

THE IMPACT OF CLOUDS ON AN ENGAGEMENT-LEVEL SIMULATION

Capt Mark M. Edwards, USAF
Capt Edward E. Hume, Ph.D., USAF
Lt Col Frank A. Zawada, USAF
Phillips Laboratory
Geophysics Directorate
Analysis and Simulation Division
Hanscom AFB, MA 01731

Abstract

The battlespace environment consists of terrain, battlefield contaminants, the atmosphere, etc. From the point of view of the air-to-ground war, the parts of this environment of greatest concern are clouds and atmospheric absorption. Clouds obscure targets and make even the most intelligent guided weapons useless. Atmospheric absorption degrades a target's signal, effectively obscuring it, forcing the weapon to be brought closer to the target and, perhaps, within the effective range of the target's defenses. Clearly, these are important effects. Until now, technological constraints have kept the full battlespace environment out of distributed simulations. However, the Geophysics Directorate of the Phillips Laboratory has developed a prototype capability to incorporate the effects of clouds and atmospheric absorption into distributed simulations. This paper describes that prototype and demonstrates the effects that these phenomena have on the behaviors of simulated entities.

1. Introduction

The use of modeling and simulation (M&S) by the Air Force and the DoD is rapidly increasing. M&S is being used as a means to solve problems in a time of fiscal shrinkage. It can be used to provide effective and safe training for various sized groups from an individual in a cockpit to a battle staff. M&S also saves time and money during the acquisition of new weapon systems by allowing R&D problems to be solved without the expense of building and testing prototypes.

Modeling and simulation has been used extensively in the past by AF and DoD to perform two basic functions, analysis and training. These functions have been integrated into all echelons of the AF. The analysis community has used M&S to give better answers. Included under the umbrella of analysis are things like operational effectiveness, basic research, force structure decisions, and weapon employment. Training concentrates on better skills for the war fighter. It encompasses things like mission planning and rehearsal, mission simulators, air operation center, and JFACC¹.

The recent decreases in military operating budgets have forced the US armed services to investigate alternative methods of training and conducting proficiency evaluations. Distributed simulation, where many individual simulators are linked together and interact in a common virtual battlespace, has tremendous potential to meet these needs. However, in order to be effective, not only must the operations of the equipment be simulated faithfully, so must the battlespace environment and its effects on the weapons systems being simulated.

1.1 The Environment in Modeling & Simulation

Currently, most M&S and wargames simply don't use weather to fight in. This approach is sometimes called "perfect weather" because it has no effect on the simulation - it's perfect. Not having a realistic environment in M&S has a major impact on the overall quality of the exercise and must be addressed to make the next significant gains in performance and fidelity of M&S. In real life, having "perfect weather" in which to fight a war is not going to happen.

Nor does the warfighter want it to happen. The fact is, the ideal time to fight a battle is when the weather puts the enemy at a disadvantage while friendly forces can capitalize on it.

One concept of putting the environment in M&S is the seamless environment is presented in Figure 1. This figure shows that the weather information to be included in the simulation must come from authoritative sources, preferably the same sources that will supply the weather data during operations.

The incorporation and distribution of the weather in a simulation can be accomplished via a "weather object" or server. In this "object" all the identified parameters are included. This object must be a part of the simulation and know how to supply that data. The key idea is that the weather object knows how to read and handle the weather parameters and format them in such a way that they can be distributed throughout the simulation and be useful.

To use the weather parameters to effect an engagement-level simulation it is necessary to determine whether or not the weapon system sensors can detect a target with sufficient signal strength to lock-on and track it. For example, if the sensor is an infrared device, then the infrared signature of the target and its background must be determined. The contrast between these two signatures becomes the result. Determining the target/background contrast is called "scene generation" in the representation of the seamless environment.

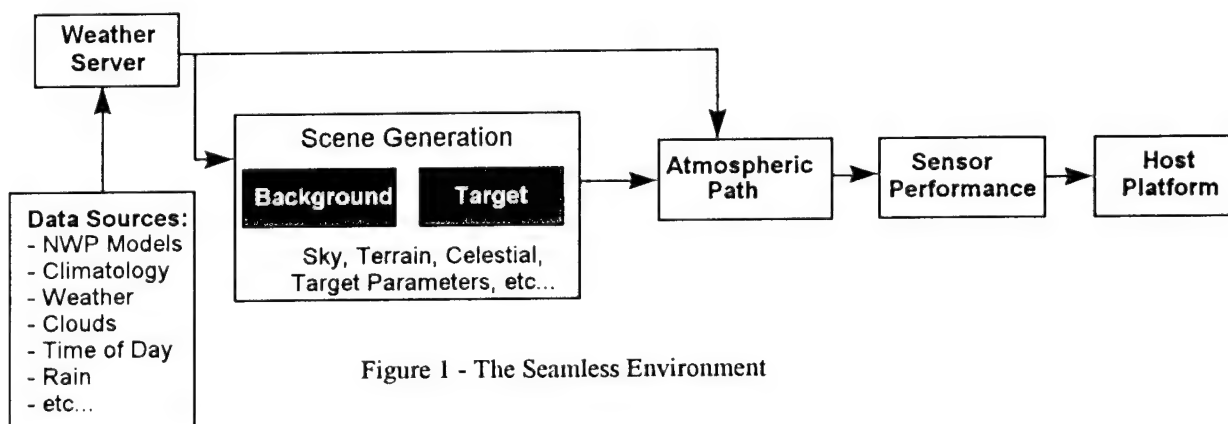


Figure 1 - The Seamless Environment

After computing the contrast of the target and background the atmosphere between the target and the sensor must be addressed. At the very least, the atmosphere will contain particles that will absorb, reflect and refract the incoming signal. Therefore, the amount of usable energy from the target incident upon the sensor's detector will always be less than that predicted by $1/r^2$, where r is the slant range between the two. Other obscurants, such as clouds, smoke, haze, and the like, need to be factored in as well.

When the amount of target/background energy incident upon the sensor aperture is known, then a simple sensor model can determine if this amount of energy meets the minimum required in order to be registered by the detector. Additionally, a higher strength signal is usually required in order for the sensor's electronics to lock-on and track a target. If the target can be tracked, then that information is passed to the host platform.

While the host platform is not specifically part of the seamless environment, if the environmental effects are not used by the host, the environment loses all importance in the simulation. If the sensor is able to lock-on and track a target, then that information is presented to the host, which could be a man-in-the-loop simulation or a computer generated force. Once the target is presented, then the host makes a decision whether or not to pursue that target.

2. Environmental M&S Projects

As simulations became more and more interoperable, users began demanding more realism. Attention has focused onto the lack of a realistic environmental representation and prompted organizations like the Defense Advanced Research Projects Agency (DARPA) and the Defense Modeling and Simulation Office (DMSO) to address these needs. Several projects resulted from this effort, like the Master Environmental Library (MEL)² and the Total Atmospheric Oceanic Server (TAOS)³.

The problem of incorporating a realistic environment into simulations can be decomposed into three distinct parts. The first of these is data sources. If a simulation is to provide a realistic atmospheric environment in which it's entities can interact, then the data used to create that environment must, itself, be realistic. Therefore, the data must come from sources that are reliable and authoritative. That is the province of the Master Environmental Library.

By itself, data from authoritative sources is meaningless. In order for that data to make a difference in a simulation there must be a mechanism for introducing that data into the simulation and distributing it to the entities and components that need it. Additionally, data from different sources needs to be integrated so that it can be distributed as a single environment. This task was designated as the responsibility of the Total Atmospheric Oceanic Server.

Finally, once the data is available in the simulation, a simulated entity must know how to use it in order for the environment to have an effect on that entity's behavior. Clearly, there is no point in introducing environmental data into a simulation if there is no impact on the behavior of the simulated entities.

2.1 The Electro-Optical Tactical Decision Aid (EOTDA) Server

The final part of incorporating the environment into a distributed simulation is to make the entities within that simulation capable of using the data that has been provided. Without this step, the previous two efforts are wasted. The Phillips Laboratory Geophysics Directorate (PL/GP) recognized this problem and developed a prototype program to address this need. Called the EOTDA Server, it provides Computer Generated Forces (CGFs) within a simulation the ability to determine whether or not a certain potential target is actually within a specified weapon system's performance envelope given a specific set of atmospheric conditions. Although the EOTDA server was just a first-step in the area of computing atmospheric effects, it successfully demonstrated that such effects are necessary for realistic simulations and that a client/server architecture could be appropriate for such a task⁴.

3. The Atmospheric Effects Server

The Atmospheric Effect Server (AES) is the next step in making simulations environmentally realistic⁵. Whereas the EOTDA Server only calculated the transmission loss of the atmosphere due to liquid water and other aerosols, the AES adds the capability to factor in the effect of clouds. The basic architecture of the AES shares much in common

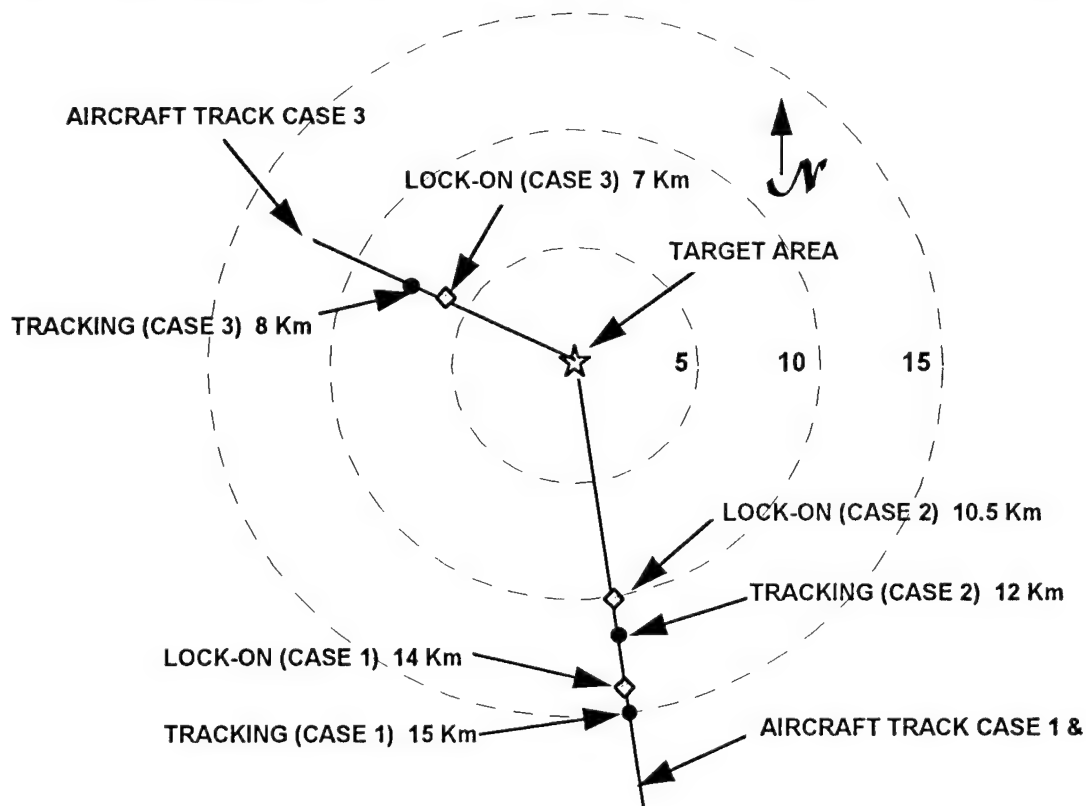


Figure 2 - AES Test Case Results

with its predecessor, the EOTDA Server. Like the EOTDA Server, the AES is based on the client/server architecture. A CGF can request that the AES determine whether or not a given target is "visible" to a specified sensor. The main difference lies in the transmission loss. In the EOTDA Server the transmission loss module was simply a Beer's Law approximation based on the LOWTRAN transmission code. In the AES this is called the IRTDA². The AES adds a module for determining the target's signal extinction due to the intervening clouds. This module is called the CTDA². The results of the IRTDA and the CTDA are merged to generate the detection and lock-on ranges for the target under the supplied weather conditions. Currently the AES is limited to the infrared 8-12 μm band, but it can be extended to the visible band as well.

3.1 Application of AES in DIS

A scenario was applied to the AES in a manner similar to the EOTDA server described in the previous section. A scenario centered around the city of Mostar, Bosnia was selected and several T-72 tanks were placed at an intersection in the city. An F-16 armed with an IR-guided Maverick missile was chosen as the CGF and weapon system. Three representative weather scenarios were generated. The first of these was what exists in simulation facilities today, a scenario with no weather or atmospheric effects (This test case is depicted as Case 1 in Figure 2). The second scenario introduced atmospheric path loss due to the environment but no clouds (This test case is depicted as Case 2 in Figure 2). The final scenario included path losses as well as cloud deck over 90% of the target area (This test case is depicted as Case 3 in Figure 2).

These three test cases clearly demonstrate the effect of the AES and utility of incorporating environmental effects into simulation. Given that simulation will play a greater role in the training and mission rehearsal areas, pilots using these simulations must be able to depend on them to be accurate. The AES, while still a limited prototype, is stepping towards realizing the necessary environmental effects within a distributed simulation.

4. Conclusion

Realizing environmental effects within a distributed simulation is a difficult task. If it were not, then it would have been done already. However, there are several efforts underway to do just that. The DMSO-sponsored Master Environmental Library is being developed to provide access to data from authoritative environmental data sources. The Total Atmospheric Oceanic Server program sponsored by DARPA is being developed to integrate and distribute data from sources connected to MEL into distributed simulations. Finally, the Phillips Laboratory Geophysics Directorate's Atmospheric Effects Server is demonstrating how this data can affect entities with distributed simulations. Much work remains to be done ironing out interfaces, improving performance, and adding services. However, the need for a realistic environment in simulations is clear and environmental effects have been demonstrated in a distributed simulation.

5. References

- 1 Air Force Modeling and Simulation Master Plan, HQ (USAF/XOM), 15 January 96
- 2 Lowe, S., et.al, "Product Generation within the Master Environmental Library (MEL)," Workshop Papers - 1997 Spring Simulation Interoperability Workshop, vol. 2, 3-7 Mar 97, pp 999-1005.
- 3 Whitney, D., et.al, "A Composable Architecture for Synthetic Natural Environment Simulation Services", Workshop Papers - 1997 Spring Simulation Interoperability Workshop, vol. 2, 3-7 Mar 97, pp 815-821.
- 4 Edwards, M., et.al, "Architectures for Computing Atmospheric Effects Within a Distributed Environment," Workshop Papers - 1997 Spring Simulation Interoperability Workshop, vol. 1, 3-7 Mar 97, pp 561-568.
- 5 Edwards, M., et.al, "Realizing Environmental Effects Within a Distributed Environment," Proceedings, Electromagnetic/Electro-Optics Prediction Requirements and Products Symposium, 3-5 June 1997, pp 345-354.

CLOUD TRANSMISSION EFFECTS IN DISTRIBUTED SIMULATION

Joel B. Mozer, Steven M. Ayer, Guy P. Seeley
USAF Phillips Laboratory
Geophysics Directorate
Optical Effects Division
Hanscom AFB, MA 01731

Maureen Cianciolo
TASC, Inc.
55 Walkers Brook Drive
Reading, MA 01867

ABSTRACT

Distributed simulation is an increasingly important part of modeling and simulation activities in the DoD due to diminishing development and training budgets relative to the sophistication of modern weapon systems. A crucial, but often ignored, component of this type of simulation is the effect of the natural environment on an engagement scenario. We have developed a prototype capability to generate and disseminate atmospheric data within a Distributed Interactive Simulation (DIS) environment. This capability utilizes a variety of models and simulations to generate the appropriate 3D atmospheric constituent data using a combination of satellite analysis algorithms, mesoscale numerical weather prediction model diagnostics, and Phillips Laboratory's Cloud Scene Simulation Model (CSSM). The transmission effects of the simulated environment on a weapon system are determined via a modified version of the Electro-Optical Tactical Decision Aid (EO/TDA) program. This paper outlines the construction of this prototype capability.

1. INTRODUCTION

The inclusion of the effects of weather in modeling and simulation of DoD engagement-level campaigns presents a unique set of problems in terms of the atmospheric data that must be provided. Typically these simulations require data at relatively high spatial resolutions—much higher than is provided by conventional weather data sources. In some cases knowledge of how the atmosphere changes over the course of a few minutes is needed. However, these short time scales are not available from traditional weather observations or numerical weather forecasts. Typically, the information required to assess the impact of the weather on a particular weapon or sensor is not generally available at all. For example, eye visibility or visual range is a typically observed meteorological parameter and may be useful to a pilot; however, the relevant parameter to a thermal imager is the visibility in the infrared spectrum, which is not generally reported.

In any one-on-one or few-on-few simulation of an engagement where the impacts of the weather on the weapons and sensors is desired, one must obtain, or assume, information on the detailed components of the atmosphere (e.g. rain, fog, winds, etc.). In some circumstances, the distribution of weather elements over a broad region is required to determine an overall weather impact on a weapon. For example the lock-on-range of an infrared air-to-air seeker will depend on the contrast of the target against its background. The nature of this background will be strongly influenced by the overall atmospheric conditions. In other cases, the specific distribution of clouds between two lines-of-sight must be known. This is the case with a weapon system that uses a laser designator to guide munitions to the target.

This latter type of situation implies that detailed (i.e. high-resolution) knowledge of the three-dimensional distribution of clouds is important. For a simulation of an engagement, it would be useful to simulate the atmospheric conditions that existed over a given region at a given point in time. However, adequate information is not generally available from conventional sources of historical weather and atmospheric data.

For example, no combination of ground-based weather observations, numerical weather prediction model forecasts, and weather satellite imagery can, by itself, give adequate information about where individual clouds exist over a 20-km engagement region and what their detailed structure is. The best one can hope for is to extract all of the useful information from these sources of data and perform intelligent, physically sound, simulations to interpolate down to the fine spatial and temporal scales needed in a simulation.

In this paper we present a prototype application of cloud simulation technology that was performed to support a simulated DIS-based engagement between an F-16 with an infrared-guided missile against a T-62 tank over the city of Mostar Bosnia in conditions mimicking those over the region in September, 1995. The details of the construction of this simulation and how the environmental data was utilized are presented in a companion paper in these proceedings [1].

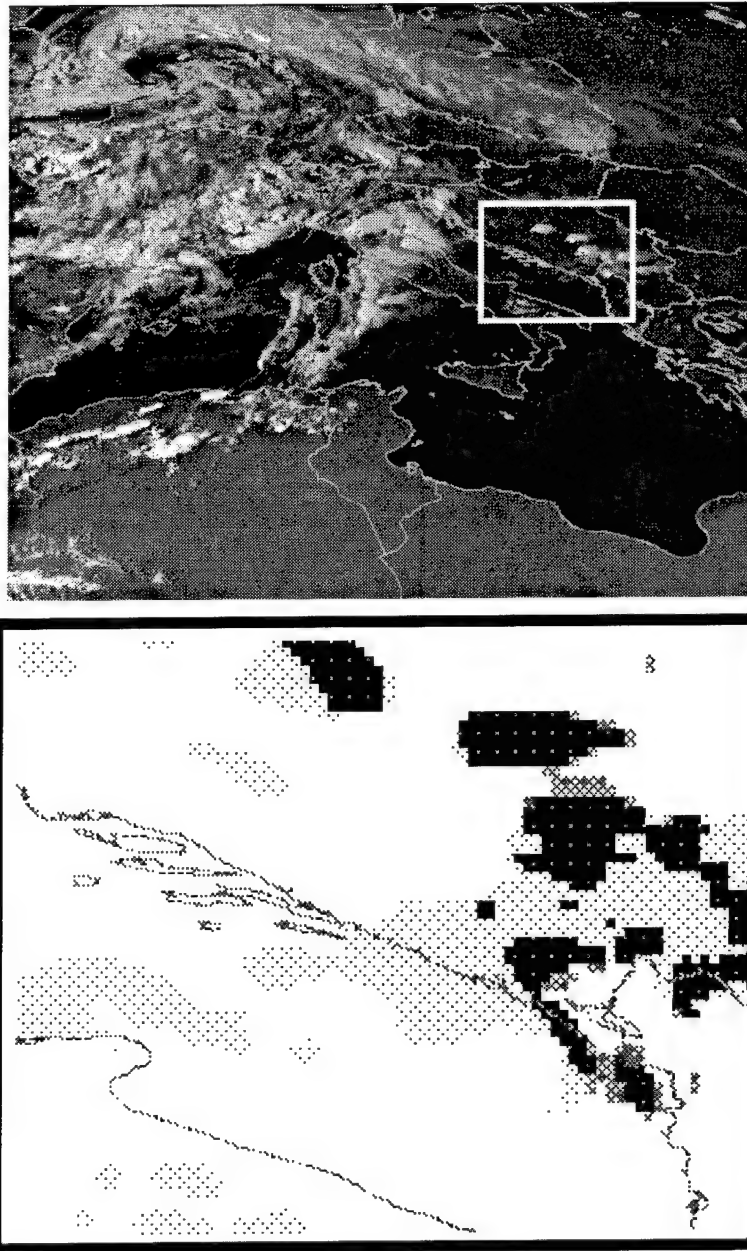


Figure 1(a) Meteosat-6 visible satellite image for September 5, 1995 at 0000 GMT (b) SERCAA analyzed cloud field for the region contained in the region indicated in (a). Grey shaded represent distinct cloud types.

2. APPROACH

2.1 CONSTRUCTING THE WEATHER

The first step in defining the weather conditions for this scenario was to collect the meteorological data. These came from two sources: a geostationary satellite and the gridded fields used to initialize a past global numerical weather prediction model. The satellite data was from the European Meteosat-6 and consisted of one visible and one infrared image, each with an 8-km pixel resolution. Figure 1(a) shows a section of the visible image encompassing Bosnia for September 5, 1995 at 0000 GMT. The gridded fields were obtained from the National Center for Environmental Prediction (NCEP) database and were a part of the global National Meteorological Center (NMC) first-guess fields and consisted of a full set of standard meteorological fields for the same date and location as the satellite imagery.

The primary value of the NMC data set was to provide the initial and boundary conditions to run the Penn State / National Center for Atmospheric Research Mesoscale Model 5 (MM5). The MM5 model was run, using the NMC data as a first-guess, to generate a 24-hour forecast of wind, temperature, pressure, and moisture over a 200x200-km domain at 10-km horizontal grid resolution. The principal value of this MM5-generated data was to transform the relatively low-resolution NMC data into a higher resolution in both space and time in order to be useful in the engagement scenario. Figure 2 shows a vertical cross section of geopotential heights and relative humidity derived from the MM5 output.

We analyzed the satellite imagery using a suite of algorithms from the Survey of Environmental Requirements for Cloud Analysis and Archive (SERCAA) project [2]. This process takes multispectral satellite imagery as input and outputs an objective analysis of the cloud coverage, types and altitudes for up to four vertical layers. Figure 1(b) shows the results of the SERCAA analysis on a subregion of the Meteosat-6 image. The cloud parameters output by the SERCAA algorithms were primarily used as inputs to the Cloud Scene Simulation Model (CSSM) which generated consistent, high-resolution synthetic cloud fields over the exercise domain.

The CSSM is an empirical model that generates high-resolution, four-dimensional, multi-layer cloud fields consistent with large-scale input weather conditions. That is, it simulates realistic structure, with typical resolutions of 10-100 m, within a domain defined by general meteorological characteristics. On 3D field is generated for each specified output time and contains cloud water content values arranged on a regular volumetric grid. The CSSM simulates a variety of cloud types including cirriform, stratiform, and cumuliform types. More information about the CSSM is given in [3].

For the present demonstration, the CSSM generated clouds over a 20x20-km domain at a 100-m grid resolution. The inputs to the CSSM in this case were the MM5 meteorological fields and the SERCAA-derived cloud parameters. By taking this approach, we achieved maximum consistency among all of the constituents of the environment that affected the simulated engagement.

2.2 USING THE DATA

The goal of this work was to demonstrate the capability to construct a consistent meteorological environment and make it available to affect a DIS-based engagement scenario. To achieve this goal in the simplest manner, we chose to place all of the environmental data in one repository. This took the form of a single binary data file in the standard NetCDF format. For the purpose of this demonstration, this data file was used in a pre-distributed sense in that it was made available to any process or entity in the simulation, but no part of the raw data was actually transferred during the simulation. The data file consisted of the 3D, 15-km resolution MM5 output fields (winds, pressure, temperature and moisture fields), the 2D, 8-km resolution SERCAA analysis (cloud type, amount, and altitude) and the 3D, 100-m resolution CSSM cloud grid.

A single consumer of this data existed in this demonstration. This was the Atmospheric Effects Server (AES) and is described in [1]. The AES used the gridded data file to determine infrared lock-on range from an aircraft-based IR seeker to a T-62 tank based on the environmental conditions. A principal factor in determining this lock-on range is the transmission of IR radiation in the presence of clouds. To calculate this, an application was developed which would utilize the data in the gridded file to calculate the integrated extinction coefficient along the line-of-sight between the aircraft and the target. This extinction was combined with the extinction due to the cloud-free atmosphere as calculated by a modified form of the Electro Optical / Tactical Decision Aid (EO/TDA). The end result is a single lock-on range based on the environment described in the gridded data file.

3. CONCLUSIONS

We have demonstrated the capability to construct a consistent weather environment for use in DIS-based simulations using a combination of historical meteorological data and consistent simulation. Although this demonstration is somewhat simplistic, it addresses many of the problems encountered in such activities—particularly the approach to filling the “data void” created by insufficient meteorological observations. The goal of this work was not to provide a comprehensive set of tools for performing these types of simulations. In fact, much work is currently being done to provide these tools, such as with the Master Environmental Library (MEL) and the Weather In Distributed Simulation – Total Atmosphere Ocean Server (WINDS-TAOS) projects. Our intent, rather, was to illuminate the requirements and problems including environmental effects in simulations and to provide a platform to evaluate these other tools as they come available and mature.

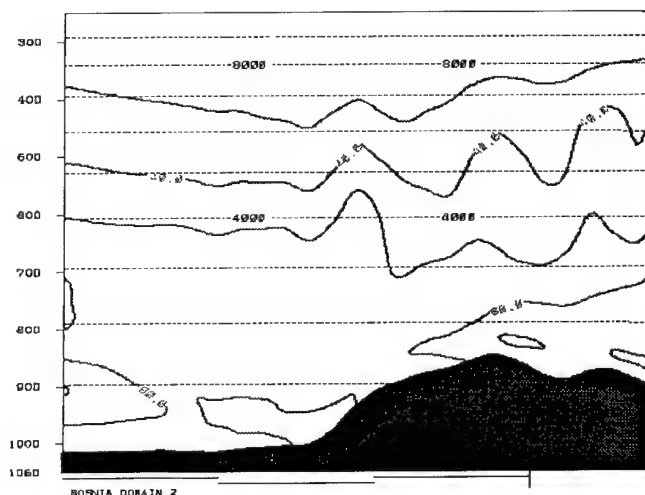


Figure 2. Vertical cross section from MM5. Solid lines are contours of relative humidity, dashed lines are geopotential heights in meters.

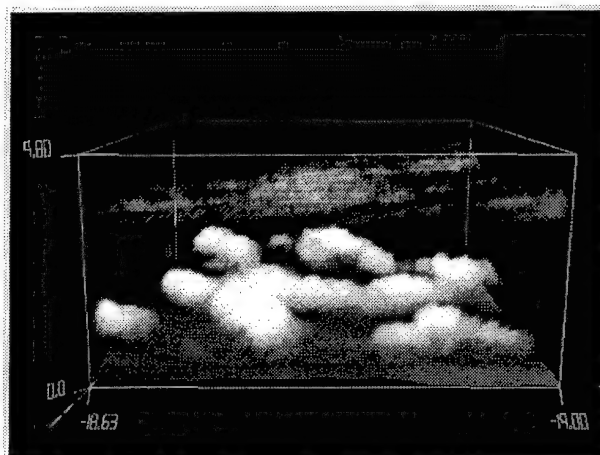


Figure 3. CSSM-generated cloud field over Mostar

REFERENCES

- [1] Edwards, M. M., E. E. Hume, and F. A. Zawada, 1997: Realizing Environmental Effects Within a Distributed Simulation. CIDOS-97.
- [2] Ivaldi, C.F., J.Doherty, C.C. Scott, and G.B. Gustafson, 1994: Support of environmental requirements for cloud analysis and archive (SERCAA): Database management facility. PL-TR-94-2290, USAF Phillips Laboratory, Hanscom AFB, MA, 77 pp. ADA293938
- [3] Cianciolo, M. E., M. E. Raffensberger, E.O. Schmidt, J.R. Stearns, 1996: Atmospheric scene simulation modeling and visualization. PL-TR-96-2079, USAF Phillips Laboratory, Hanscom AFB, MA, 110 pp. ADA312179

CLOUD SIMULATION FOR A FLIGHT MISSION REHEARSAL SYSTEM

Louis Hembree
Naval Research Laboratory
Marine Meteorology Division
Monterey, CA 93943-5502

ABSTRACT

Flight simulations are used by the aviation community for training. Within the Department of Defense they are also used to plan and rehearse missions. Current flight mission rehearsal systems incorporate little environmental information. One environmental parameter that has a large impact on aircraft missions for the U.S. military is cloud. This presentation describes the development of a prototype incorporation of clouds into a mission rehearsal system. A cloud scene simulation model was used to generate cloud information and using visualization tools was incorporated into the PowerScene mission rehearsal system. Future efforts include the integration of clouds into the Navy's operational mission rehearsal system, TopScene, and an effort to develop methods to forecast the required input parameters using mesoscale models.

1. INTRODUCTION

Over the past several years the role of simulation within the Department of Defense (DoD) has been increasing. Within the context of this paper, the broad concept of modeling and simulation (M&S) refers to the use of models and simulations for the purpose of training or for the development of data as a basis for making better managerial or technical decisions. The models within this context are different than the models we think of in the atmospheric community (e.g., mesoscale forecast models, chemical transport models). Many of the models in the M&S community deal with issues such as engineering, logistics, military operations, and training. As an example, simulators are commonly used today to train aircraft pilots. Not only are the costs reduced by not having to fly an actual aircraft, but pilots can also practice maneuvers and recovery techniques that are too dangerous to practice in a real aircraft. As another example, simulators are used to simulate troop movements and engagements with a computer-generated enemy.

Currently most M&S efforts include very little, if any, appropriate environmental information and associated environmental effects. Without realistic environmental information and effects, incorrect conclusions may result, or a negative training environment is produced. Efforts are now under way to increase the overall realism of simulations and opportunities exist to incorporate more realistic environmental information and effects into the simulations.

The role of M&S in tactical aircraft training, mission rehearsal and mission planning is increasing. There are several reasons for this. For example, a pilot cannot fly over the target and study it at his/her leisure to familiarize themselves with the target to select the optimum approach and egress routes. With a mission rehearsal simulation, the pilot can "fly" simulated missions and examine various options.

One aspect of the environment that could play a critical role in the success or failure of a mission is the presence or absence of clouds. Clouds can obscure the target; fog and smoke can decrease visibility. Cloud ceilings impact safety. In addition, weapon and sensor effectiveness can be decreased significantly. The PowerScene mission rehearsal system was used to demonstrate a prototype inclusion of realistic clouds into mission rehearsal system. This effort required us to first identify a cloud simulation model to generate cloud water distributions and second identify methods to render the clouds within the simulated scene. Finally we integrated the cloud model and rendering methods into the PowerScene mission rehearsal system.

2. PROTOTYPE DEVELOPMENT

There are several technical steps that need to be addressed to incorporate clouds into a mission rehearsal system. These are shown in Figure 1. A cloud simulation model must first be run with the resulting output provided to the mission rehearsal system, and the clouds rendered and incorporated into the displayed scene. The rendering rate must be high enough to allow the users to interactively "fly" through the scene in real time.

2.1 CLOUD MODEL

The Cloud Scene Simulation Model^{1,2} was used to model cloud structures. The CSSM was developed by the U.S. Air Force Phillips Laboratory and TASC, Inc.^{1,2}. CSSM was developed specifically to support the DoD simulation community; its typical simulation domains and resolutions match those of PowerScene and similar mission rehearsal systems. It uses readily available meteorological input data, such as wind, temperature, and moisture information (typically available from atmospheric soundings and surface observations or numerical model output). CSSM is also relatively fast. CSSM is a parametric model that takes advantage of several computationally efficient stochastic field generation algorithms to synthesize the overall external structures and internal water density fields of a variety of cloud types. Typical scenes take only seconds to build on a standard workstation.

The CSSM uses stochastic field generation techniques and knowledge of atmospheric structure and physics to model four-dimensional (spatial and time) cloud scenes. The model begins by specifying the horizontal distribution of cloud elements across the scene. It uses a fractal algorithm³ to build that distribution, careful to satisfy the input layer coverage conditions. Parameters within the fractal algorithm are tuned to best replicate the spatial characteristics of each individual cloud type.

For stratiform and cirriform cloud types, vertical cloud structure is derived from the horizontal field values, and a four-dimensional version of the fractal algorithm is employed to simulate water density perturbations everywhere within the cloud structure. The perturbation field is then converted to absolute liquid water content (LWC) using computed field statistics and a mean LWC profile. Various parameters within the density perturbation model are estimated for different cloud types based on an analysis of aircraft-based cloud measurements. Comparisons of the modeled LWC fields with observations have shown that the cloud model captures the structure of observed cloud fields.

2.2 VISUALIZATION METHODOLOGY

An efficient and economic approach for rendering volumetric data was required. The rendering methodology had to satisfy the following requirements: 1) the images had to be derived from three dimensional cloud data such as that available from the CSSM; 2) it must allow for intervisibility effects between any two points; 3) it must accommodate varying levels of data resolution to support varying levels of graphics hardware fidelity and databases, and 4) it must be relatively fast. A basic visualization methodology developed by Loral^{4,5,6} was selected for this prototype development.

A geometric-primitive aggregation approach was chosen as the best approach. This approach groups many small graphic primitives together to provide a total cloud structure. It has the potential to produce a very accurate overall appearance. Each primitive has its own attribute settings. Therefore, density and lighting variations throughout the cloud can be accurately modeled. The intervisibility problem is also solved with this technique. The disadvantage of this approach is the large number of graphic primitives required, *i.e.*, a large number of polygons are required. When looking through many layers of primitives, the pixel processing load can become excessive. Some form of pixel process control is required. An angle-oriented textured polygon approach was selected. This approach uses only one polygon per primitive. The polygons are oriented in real time so that they are always perpendicular to the line of sight. A texture is applied to make them appear spherical resulting in a realistic visual effect.

2.3 POWERSCENE

PowerScene is a general-purpose scene-generating system developed by Cambridge Research Associates. PowerScene is capable of being adapted for various purposes. A unique application for the U.S. Navy and U.S. Air Force has been as a mission planning/rehearsal/preview system. The generated scenes can be viewed

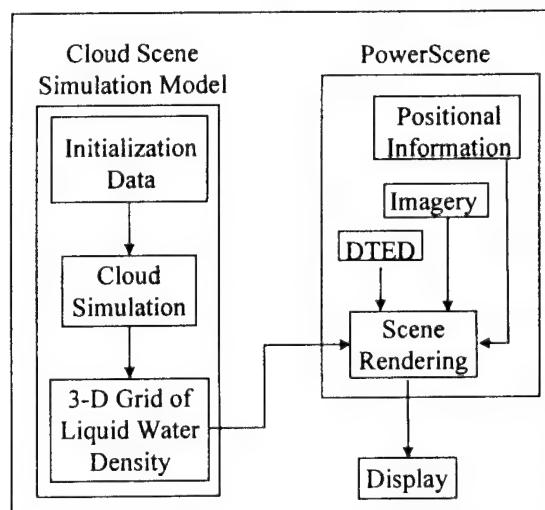


Figure 1: Diagram of how cloud information was incorporated into PowerScene.

using standard CRTs, projection systems in simulator domes, or helmet mounted displays. In its aircraft-simulation mode, the user's viewpoint can move across country-sized data bases. The user can thus pre-fly missions along programmed routes without control inputs. The user can also pre-fly in a simulated autonomous flight mode using either realistic stick and throttle controls, or a joy stick. In the autonomous flight mode, using stick and throttle controls, maneuvering is restricted by the flight dynamics and characteristics of the simulated aircraft; the viewpoint cannot, for example, be stopped for extended study of a scene. The simpler joystick controlled viewing mode relaxes these constraints and permits the user to move arbitrarily around the simulation area, stopping, starting, and moving sideways as needed. Using any of these viewing methods, the user can become familiar with the target mission areas and thus identify a preferred route and approach prior to the mission.

The terrain scene is created from two main data sources: 1) Defense Mapping Agency (DMA) digital terrain elevation data (DTED), and 2) photographic imagery of the terrain. The terrain database for the entire area of interest is assembled converted to triangular meshes for graphical rendering. Unlike many other simulators and visualization systems, the entire terrain data base need not be loaded into the host computer's primary (main) memory all at once. Instead, the applicable area is paged in from peripheral (disk) memory as the viewpoint moves from one region to another. The size of the simulated area is thus limited only by available disk space, rather than by the main-memory size.

Imagery is obtained primarily from two sources: aerial photographs and satellite data. The aerial photographs have resolutions as detailed as 2 meters. The imagery is images from different sources are combined into a mosaic to provide continuous coverage of the area. The imagery is then applied as a texture on the polygonal mesh surface created from the DTED data.

2.4 INTEGRATION

A prototype integration has been completed. The CSSM cloud field was created and then read by PowerScene. The prototyping concentrated on the rendering methodology and was a proof of concept. Figure 2 shows a typical rendering of a cumulus cloud field in PowerScene. A user could fly through the resulting scene using either the free flight method or the joy stick. As the user flew through the rendered cloud the visibility of the objects obscured by the cloud would change according to the amount and density of the cloud along the line of sight.

The rendering rate varied from approximately 1.5 frames per second when the entire rendered cloud field was in the scene to a full 30 frames per second when no clouds were present. The decrease in rendering speed when the entire cloud field is being rendered is due to the large number of cloud elements that are being rendered. All elements, including hidden elements, are being rendered. The rendering rates could be increased by using more current hardware and software.

This example illustrates the realistic nature of the cloud rendering and that the intervisibility is realistically modeled. The amount of attenuation is dependent on the path, path length, and the intervening clouds.

3. CONTINUING EFFORTS

There are two new projects that serve as continuation of the effort to incorporate realistic clouds in mission rehearsal systems. These projects are:

- Cloud Parameters and Littoral Visibility for Modeling and Simulation, and
- Atmospheric Information for Navy Flight Mission Rehearsal.

The Cloud Parameters and Littoral Visibility for Modeling and Simulation is sponsored by the Air and Space Executive Agent for Modeling and Simulation. This project includes a joint task with Phillips Laboratory Geophysics Directorate to develop methods to provide estimates of cloud parameters (base, top, fractional amount, and type) using output from mesoscale forecast models.

The Atmospheric Information for Navy Flight Mission Rehearsal is sponsored by the Space and Naval Warfare Systems Command (SPAWAR). Its objective is to develop methods for providing and incorporating atmospheric information into Navy flight mission rehearsal and planning systems. The initial effort is directed

at incorporating clouds into the Navy's operational flight mission rehearsal system, TopScene, and developing the mechanisms for TopScene to obtain the information required in an operational environment. TopScene was developed and supported by the Naval Air Systems Command (NAVAIR).

The TopScene program office conducted a survey of users to identify requirements. One of the top requirements for strike warfare was the inclusion of atmospheric phenomena such as clouds. Even when all types of missions were included, atmospheric phenomena were in the top 30% of the requirements.

4. SUMMARY

The prototype demonstrated the basic viability of incorporating clouds into flight mission rehearsal systems. Realistic scenes including clouds that allowed real-time interactive fly-through were created. Frame rendering rates were not as high as desired but could be improved significantly with recent improvements in hardware. New projects are developing methods to provide the required inputs from model outputs and incorporating clouds into an operational flight mission rehearsal system.

5. ACKNOWLEDGEMENTS

This integration effort was sponsored by the Office of Naval Research (ONR). The Loral visualization work was supported by Advanced Research Projects Agency (ARPA), U.S. Army Topographic Engineering Center (TEC), and ONR. The development of PowerScene has been sponsored by the Naval Air Systems Command, HQ U.S. Air Force, and the Defense Mapping Agency. The CSSM development has been supported by the U.S. Air Force Phillips Laboratory, Geophysics Division, ARPA, TEC, and the Defense Modeling and Simulation Office.

6. REFERENCES

1. Cianciolo, M. E., and R. G. Rasmussen, 1992: Cloud Scene Simulation Modeling - The Enhanced Model, TASC Technical Report, PL-TR-92-2106, April 1992. [NTIS AD-A 265 958]
2. Cianciolo, M. E., 1995: A cloud model to support real-time scene visualization. *Proceedings of the Eleventh International Conference on Interactive Information Processing Systems for Meteorology, Oceanography, and Hydrology (IIPS)*, Dallas, TX, Am. Meteor. Soc., pp 35-38
3. Saupe, D., 1989: Point evaluation of multi-variable random fractals, *Visualisierung in Mathematik und Naturwissenschaft*, H. Jurgens and D. Saupe, Eds., Springer-Verlag, Heidelberg, 1989, pp 117-129.
4. Cianciolo, M. E., and B. Soderberg, 1994: Modeling the cloud environment in distributed interactive simulations. *Proc. 16th Interservice/Industry Training and Education Conference*, Orlando, FL, Nov. 1994, pp 10-4.
5. Soderberg, B. T., and M. A. DeLoura, 1995: Adding cloud visualization to a real-time simulator, Loral ADS Final Report, Contract N0. DACA76-91-C-0006, May 1995. (Available from U.S. Army Topographic Engineering Center, 7701 Telegraph Rd, Alexandria, VA, 22315)
6. Soderberg, B. T., and J. Gardner, 1994: Dynamic environment modeling in distributed interactive simulation - Final Report, Loral ADS and Grumman Data Systems, DACA76-91-C-0006, May, 1994. (Available from U.S. Army Topographic Engineering Center, 7701 Telegraph Rd, Alexandria, VA, 22315)



Figure 2: Typical scene created when clouds were incorporated into PowerScene.

SIMULATING THIN-CLOUD EFFECTS ON MULTI-SPECTRAL TARGET DETECTION

Joseph G. Shanks, Frederick C. Mertz
Photon Research Associates, Inc.,
San Diego, California 92121 USA

William A.M. Blumberg
U.S.A.F. Phillips Laboratory, Optical Environments Div.
Hanscom AFB, Massachusetts 01731-5000 USA

ABSTRACT

Intervening clouds are a pervasive problem for high altitude optical sensors dedicated to surveillance of ground or low-altitude targets. While thick clouds have a more dramatic effect on performance, thin clouds are much more common, and problematic: they must first be detected, and then compensated for to the extent possible so as minimize their effect on processor performance. Intervening clouds will effect the spatial character of the upwelling radiance (reducing target contrast and blurring fine spatial features) and its spectral signature. The *CLDSIM* (Cloud Scene Simulation Code) has recently been upgraded to incorporate the blurring effect of thin clouds on cloud/terrain scenes, and it will be exercised to illustrate the effect of intervening clouds on a multi-spectral surveillance sensor operating in the Thematic Mapper spectral bands. In particular, the effect of varying cloud thickness on processor performance will be described and illustrated. These results could be combined with cloud climatology statistics to describe the effect of cloud cover on system performance in a given theater.

1. INTRODUCTION

Recent advances in many disciplines has supported the development of a new class of spaceborne, passive Vis-LWIR sensors. Collecting hyper-spectral data with global coverage at ground-sample-distances of ten to one hundred meters this generation of platforms, when coupled with modern communications and computing technologies promises to revolutionize remote-sensing. In particular, the enhanced spatial and spectral resolution promises to resolve many targets (interpreted generically as *features of interest*) essentially undetectable with current systems (NOAA-AVHRR or Landsat-TM data, for example).

However, this potential will be realized only when the contaminating effects of clouds and the atmosphere are minimized--a challenging task requiring both *detection / characterization* of the intervening medium and radiative *correction* for target detection and analysis. Detection of thin clouds is particularly challenging and the objective of this paper is to illustrate the effect of thin clouds on the spatial and spectral signature of an underlying ground target, for a TM-class sensor.

2. PROBABILITY OF THIN CLOUD COVER

The likelihood that thin clouds may be encountered on a global scale is illustrated in Figure-1, which shows the Mean probability of thin cloud cover (all altitudes) for the years 1989 through 1995. This figure was generated from the monthly cloud climatology data bases developed by Don Wylie (U. Wisconsin, Madison) using the *CO₂ slicing* technique. [Wylie, 1997; Robinson, *et al.*, 1994; d'Entremont, *et al.*, 1993] This database has been interrogated with the *CLDVIS* g.u.i. included with the SBIRS Model Toolkit.

*To be presented at the "Cloud Impacts on DoD Operations and Systems '97" Conference,
23-25 September 1997, Naval War College, Newport, RI*

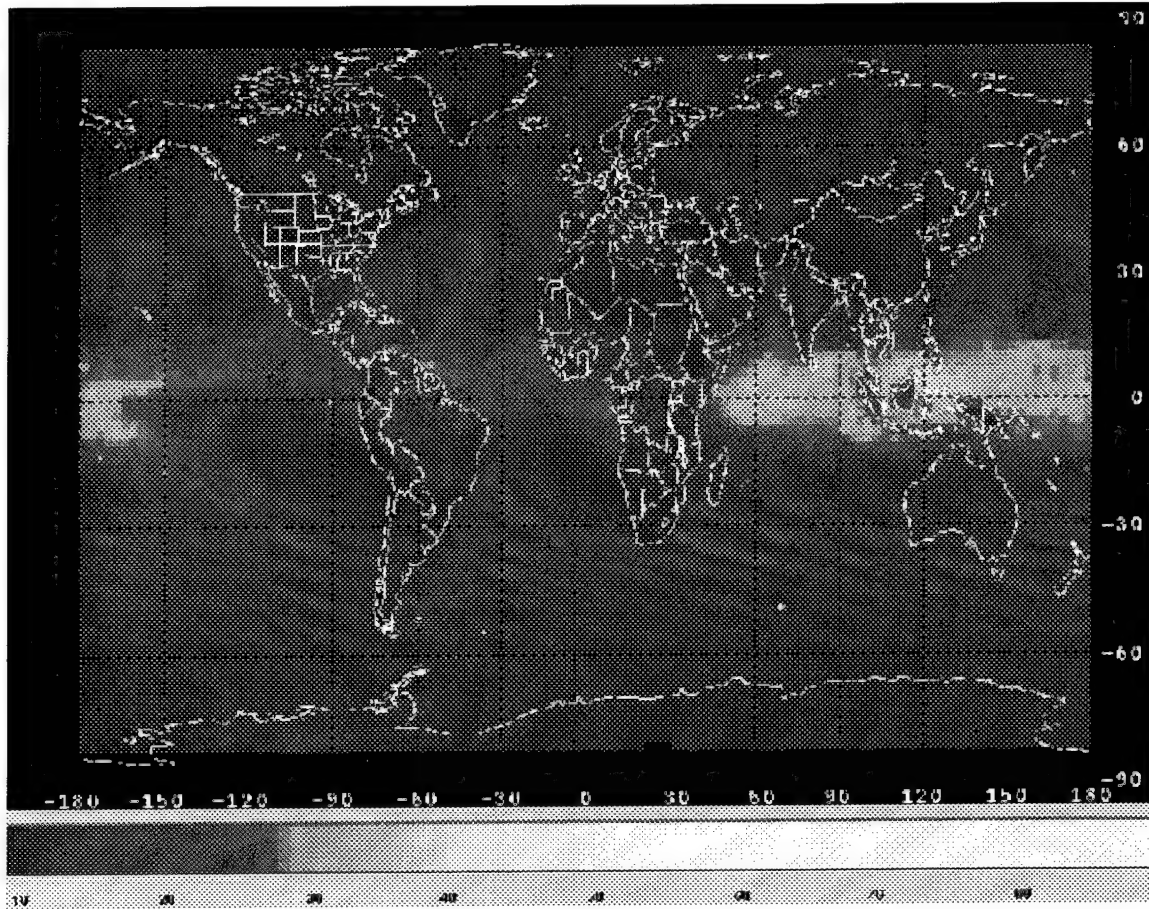


Figure 1. Global Thin Cloud Cover, $\epsilon_{LWIR} \leq 0.3$, (1989 - 1995)

3. SIMULATION OF THIN CLOUD EFFECTS ON TARGET RADIANCE

The SBIRS Model Toolkit's principal capability is the generation of integrated cloud / terrain radiance imagery using the *CLDSIM*, *GENESSIS* and *MOSART* codes. Previous reports have described the operation of the *CLDSIM* code in some detail [Mertz, *et al.*, 1996] and so the topic will only be briefly reviewed. The key operational assumption of the current model is that the cloud-top may be treated as a faceted surface (with flat cloud-bottom) for radiance prediction and projection into the focal-plane. The direct solar-scattered radiance from clouds is modelled as

$$L_{scat} = \int F(\lambda) \Phi(\theta_s; \lambda) \cos(\theta_s) \rho(\theta_s, \Omega_o; \lambda) T_{atm}(\theta_s, \Omega_o; \lambda) d\lambda \quad (1)$$

where " $F(\lambda)$ " is the spectral response of the system, " T_{atm} " is the transmission of the atmosphere (sun - cloud - observer) and " ρ " is the BRDF. The (spectral) solar flux, Φ , and atmospheric transmission are computed by the *MOSART* code (distributed by the Phillips Laboratory at Hanscom AFB, MA) while the BRDF describes the detailed scattering properties of the cloud. Thus, the BRDF depends on both the micro-scale parameters of the cloud (size, shape and volume density of scatterers) and meso-scale parameters (cloud thickness, etc.). The most recent comparison of *CLDSIM* against SWIR data showed agreement within 20 % in predicting the mean and standard deviation of the cloud radiance [Shanks, *et al.*, 1997, Mertz, *et al.*, 1996].

The cloud transmission in version 1.2 of the SMT is modelled by calculating a *diffuse cloud transmission* at every pixel using a 3-stream radiative-transfer model [Coakley & Chylek, 1975, as implemented by Goody & Yung, 1989], and applying a normalized, adaptive OTF (optical transfer function) to the upwelling radiance image at the cloud base. The OTF is approximated by a gaussian kernel of width specified by the in-band optical properties (K_σ , ω_σ , g), local cloud thickness and the LZA

(look zenith angle). A Henyey-Greenstein phase-function is used for all cloud types. Non-nadir viewing implies that the blur kernel will be asymmetric. The radiative-transfer problem is solved empirically using an order-by-order expansion in which the first two terms are calculated exactly with a smooth transition to a "directed diffusion" solution for $N > 2$. For additional discussion, see Ben Dor, *et al.*, 1995; Heggstead, H.M., 1971; Linsens & Bohren, 1994; Liou, *et al.*, 1990; Sadot, *et al.*, 1995.

Sample output from the code is shown in Figure-2, in which two point targets have been inserted into a terrain image using the the *Iraq-Syria* data base in a transmissive SWIR band, underlying a portion of the *Monsoon Cirrus* cloud data base. The intervening cloud layer effects the appearance of the target on the right in various ways: the peak radiance is reduced by a factor of two and the radiance gradient drops by a factor of approximately four due to the blurring effect. As both the mean transmission and degree of blurring are spectrally dependent, thin clouds will effect both the *spatial* and *spectral* character of the signature, contaminating and perhaps defeating conventional retrieval algorithms designed to operate with a cloud-free line-of-sight. In this regard, note that the spectral character of the absorption due to liquid water droplets (as reflected in the albedo) is significantly different than that due to water vapor and that the width of the blur kernel is roughly proportional to the $\text{Sqrt}[1 - g^2]$ for thin clouds, where "g" is monotonic in the size parameter, $X = 2 \pi R / \lambda$ and "R" is a mean dimension of the scatterers.

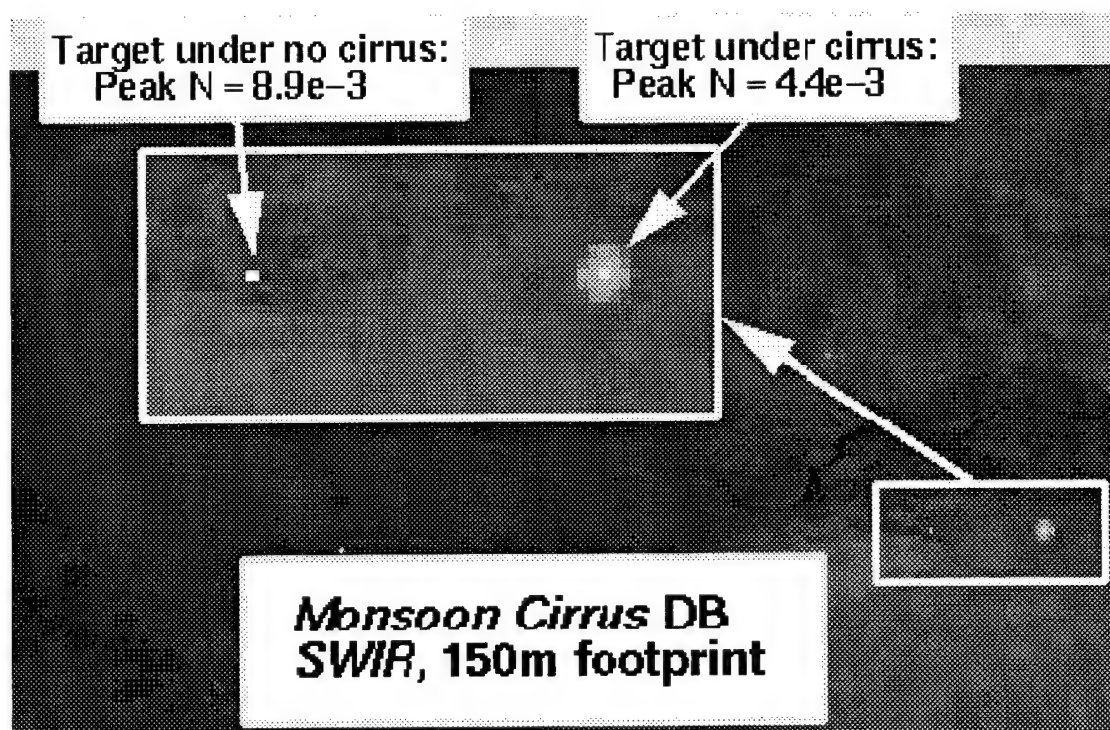


Figure 2. Blurring Effect of Thin Clouds Simulated by *SMT / CLDSIM*

Fortunately, this means that the spectral effect of thin clouds will be less prominent for cirrus than for water clouds. [Smith, *et al.*, 1989;]

4. MULTI-SPECTRAL SAMPLE SET AND PROCESSING PLAN

The objective is to illustrate the effect of intervening cloud on spectral and spatial algorithms for target detection and characterization, using a *LandSat* class multi-spectral sensor. A large building will be embedded in desert terrain and spectral image stacks generated for cloud-free, thin-cloud and thick-cloud ($\tau_{\text{swir}} > 0.9$) layers. Sensor effects will be modelled by addition of representative random noise and the

effect of cloud cover on the radiance, spatial structure (as reflected in the radiance *gradient*) and spectral structure will be illustrated, along with the consequent effect on standard features used for target detection and characterization.

5. REFERENCES

- Ben Dor, B., Bruscalioni, P., Devir, Donelli, P., Ismaelli, A.,
"Cloud, fog and aerosol effect on the MTF of optical Systems"
(*Proc. of the SPIE/EOS Symp. on Passive IR Remote Sensing of Clouds and the Atm.*, Paris, Sept 25-28, 1995)
- Coakley, J.A., Chylek, P.,
"The Two-Stream Approximation in Radiative Transfer: Including the Angle of the Incident Radiation"
J. Atmospheric Sci., 32, 409 (1975)
- d'Entremont, R.P., Wylie, D.P., Peduzzi, D.C., Doherty, J.,
"Retrieval of Cirrus Radiative and Spatial Properties Using Coincident AVHRR and HIRS Satellite Data"
(*Passive IR Remote Sensing of Clouds and the Atmosphere, SPIE Vol. 1934*, D.K. Lynch, ed., 1993) page 180
- Goody, R.M., Yung, Y.L.,
Atmospheric Radiation, Theoretical Basis
(Oxford U. Press, New York, 1989) 519 pages
- Heggstead, H.M.,
"Multiple-Scattering Model for Light Transmission through Optically Thick Clouds"
J.O.S.A., 61, 10, 1293 (1971)
- Linskens, J.R., Bohren, C.F.,
"Appearance of the Sun and the Moon Seen Through Clouds"
Appl. Optics, 33, 21, 4733 (1994)
- Liou, K.N., Takano, Y., Ou, S.C., Heymsfield, A.J., Kreiss, W.,
"Infrared Transmission Through Cirrus Clouds: A Radiative Model for Target Detection"
Appl. Optics, 29, 13, 1886 (1990)
- Mertz, F.C., Shanks, J.G., Craven, S.J.,
"A Cloud Radiance Comparison: *CLDSIM* Predictions & *LandSat* Data (*Stratocumulus, Monsoon Cirrus*)"
(P.R.A. Report *SQ+MC_951213*, January 1996) 134 pages
- Robinson, I.S., Rudy, D.J., Gonzalez, M.M.,
"Frequency of Cloud Cover at Altitude: Implications for Surveillance Systems"
(*Aerospace Report ATR-94(8019)-1*, September 1994, 28 pages)
- Sadot, D., Shamriz, S., Dror, I., Kopeika, N.S.,
"Prediction of overall atmospheric modulation transfer function with standard weather parameters: comparison with measurements of two imaging systems"
Optical Eng., 34, 11, 3239 (1995)
- Shanks, J.G., Mertz, F.C., Westmoreland, S.J., Blumberg, W.A.M., Robinson, I.S., Lisowski, J.L., Thorwart, M.J., Bishop, K., Eloranta, E.W., Piironen, A.,
"A Comparison of Predicted Cloud Radiance with *MSTI-3* and *ARES* Data in the SWIR Spectral Region"
(*IRIS T.B.D. Conf.*, Monterey, Feb. '97)
- Smith, W.L., Ackerman, S.A., Huang, A.H-L,
"Remote Sounding Through Semi-Transparent Cirrus Cloud"
(*Proceeding of the F.I.R.E. Science Meeting*, Monterey, CA, July '89. page 363)
- Wyle, D.P. See <http://wylie.ssec.wisc.edu>, (1997)

CLOUD MODELING AND INFRARED SPATIAL STRUCTURE

Robert A. McClatchey,¹ Robert J. Jordano, and A.T. Stair, Jr.

Visidyne, Inc.

Burlington, MA 01803, U.S.A.

Col. William Smith

BMDO/TOS

Arlington, VA 22202, U.S.A.

ABSTRACT

Space-based surveillance systems operating in infrared spectral regions generally utilize an atmospheric absorption band to screen out surface and low atmosphere radiometric clutter. However, the design that is optimum for screening low atmosphere and surface clutter also assures that intended targets cannot be observed except at high altitudes. Thus, the design of such systems is a compromise between the minimization of clutter and the ability to observe targets. Generally, clouds are a major source of this infrared clutter. Our objective here is to design a realistic modeling capability to specify 3-dimensional cloud scenes over any point on the globe at any time of the year. Our approach is to utilize archived global cloud data combined with our knowledge of the fractal nature of clouds. These cloud scenes can then be used to generate the upwelling radiation as observed by an orbiting satellite with specified sensors located anywhere in the thermal infrared. Such a capability will enable the evaluation of new surveillance concepts to the earliest design stage.

1. INTRODUCTION

Space-based surveillance systems operating in infrared spectral regions generally utilize an atmospheric absorption band to screen out surface and low atmosphere radiometric clutter. This concept has been used in the development of space-based systems for more than 20 years (See Wolfe & Zissis², 1985, and Jamieson³, 1976). Systems operating in the 2.7 μm band depend primarily on water vapor to provide this screening (although there is also some absorption due to carbon dioxide in this spectral region). Systems operating in the 4.3 μm region depend on carbon dioxide for screening. Most of the water vapor is located in the lower half of the troposphere and this fact coupled with the inherent strength of the 2.7 μm water band enables mid- and high level clouds to be observed by a space-based system. The altitude where clouds will be observable will depend on the exact spectral band-pass and the water vapor distribution from space to cloud-top.

The 4.3 μm band of carbon dioxide is fundamentally much stronger and becomes opaque near the band center for paths originating from a much higher altitude than at 2.7 μm . Because the 4.3 μm band absorption depends on the carbon dioxide abundance in the atmosphere, it is far more stable (less variable) than absorption in the 2.7 μm region. This is true because of the nearly uniform mixing of carbon dioxide in the atmosphere. The screening effect of these two spectral regions can be seen by examining the MODTRAN-generated spectra shown as Figures 1a-1c.

Radiation received by a space-based sensor near 2.7 μm is dominated by solar scattering during the day. In the 4.3 μm region, the radiation can have both a thermal emission and a solar scatter component, depending on the altitude of cloud-tops in the field of view. Another complicating factor is the nadir angle of measurement - the larger the nadir angle, the greater the absorption for a given cloud-top altitude in either spectral region. The existence of irregular-shaped clouds of different sizes and at different altitudes in the

field of view of the space-based sensor will represent the major source of radiation variability (or atmospheric clutter).

As a result of many years of atmospheric transmission model development, we are well-prepared to determine the effect of the clear atmosphere on radiation reflected from a solid object at the surface or within the atmosphere and we are also well-prepared to determine the emission of the atmosphere and surface if we know the surface emissivity, the thermal structure of the atmosphere and the profiles of absorbing gases. But, we are not so well prepared to attack this "clutter" problem when we are dealing with clouds. Let us separate the cloud problem into its two major elements: 1) Cloud morphology and 2) Cloud radiative characteristics. They are both more difficult to deal with than the clear atmosphere, but of the two, cloud morphology offers the greater challenge. And, as we've noted above, clouds represent the key problem in defining atmospheric clutter for a space-based surveillance system. The remainder of this paper will deal with the cloud morphology problem as it affects atmospheric clutter.

1.1 CLOUD MORPHOLOGY

Our objective is to design a realistic cloud modeling capability to specify 3-dimensional cloud scenes over any point of the globe at any time of the year. We wish to create ensembles of scenes whose sizes and shapes represent real world conditions for any location in a statistical sense. Recognizing that most space-based measurements useful in studying cloud fields are limited in pixel size, we would also like to use the model developed here to extrapolate to clouds of smaller size than the measurements provide, if possible. Our goal is to provide realistic cloud fields down to a size domain of 100 meters.

Tools available to us in this effort include: 1) Global weather satellite cloud observations in various spectral bands down to a pixel size of 1 km; 2) Global Landsat data in visible and infrared bands with pixel sizes down to 120 m (infrared) and 30 m (visible); 3) Global statistical models derived from satellite, and ground-based observations; 4) Archived global cloud model (USAF Nephanalysis Model) derived from satellite and surface-based observations; 5) Special satellite systems with limited data sets down to 80 meters; 6) Fractal techniques for attempting to unify these data and to render realistic cloud scenes.

1.2 FRACTAL ANALYSIS AND POWER SPECTRAL DENSITY

The power spectral density associated with background clutter is generally used to determine false alarm exceedances when searching for targets. And we have some indication of the power spectral density of cloud systems based on a number of fractal analyses provided in the past several years. Whether or not PSDs are sufficient to define exceedances needs to be further evaluated. But, for our purposes here, we will assume that PSDs derived from satellite-based cloud data can be used and review the state of affairs.

Utilizing satellite- and radar- determined cloud and rain areas between 1 and 1.2×10^6 square kilometers, Lovejoy (1982)⁴ plotted image area against perimeter and obtained a straight-line plot covering the entire 6 orders of magnitude in area as shown in Figure 2. The implication of this figure is that clouds (and precipitation particles) are statistically self-similar over a wide range of sizes. That is, a cloud scene viewed with a relatively low resolution measuring system will look the same statistically as a cloud scene viewed at much higher spatial resolution. If true, this would appear to provide a mechanism for extrapolating to even smaller sizes with some assurance that the statistical properties of sizes and edges are correct. The satellite measurements in the Lovejoy work were from GOES infrared imagery and both satellite observations and radar observations were taken over the Indian Ocean. This assured a smooth sea background and focused on tropical convective clouds and cloud clusters. Would the same kind of plot be obtained in mid-latitudes? Would the same kind of plot be obtained over land areas?

The development of Power Spectral Densities to describe the spatial structure of cloud systems assumes that the energy at wavenumber k will be of the form, $E = k^{-\beta}$ where β is the spectral exponent. And the energy spectrum is both the ensemble-averaged and angle-integrated squared modulus of the Fourier transform of the

image. Our analysis seeks to determine the values of β and to establish the constancy of β with wavenumber. Such analyses have been performed by Lovejoy and Shertzer⁵, 1995, and others, and we have summarized the major points of these analyses.

Figure 3, taken from Lovejoy and Shertzer, 1995⁶, utilizes both visible and infrared measurements from LANDSAT, GOES and Nimbus-9 and deduces similar (but not identical) β values ranging from 1.4 to 1.91. The data lie on a remarkably straight line in the log-log plots. These data cover size ranges from 4000 km to 160 m and do not suggest a scale break (i.e., change in slope) except with the slight hint of a change in slope for scales smaller than ~300 m in the case of the LANDSAT data.

A more detailed breakout of NOAA-9 AVHRR visible data provides the results shown in Table 1 (from Pecknold, et al, 1997⁷) where different cloud types were separately examined.

TABLE 1	
Cloud Type	β Value
Cirrus Clouds	1.57 - 1.92
Stratus Clouds	1.6 - 1.84
Altostratus	1.91
Nimbostratus	1.88
Alto cumulus	1.88
Cumulus	1.04 - 1.21
Mesoscale Conv. Complex	1.56 - 1.83

1.3 THE GENERATION OF CLOUD FIELDS

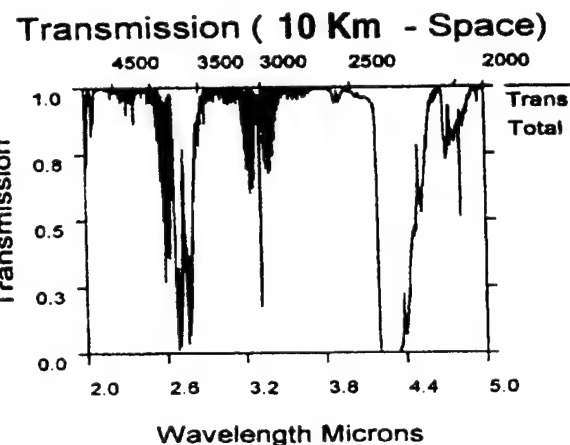
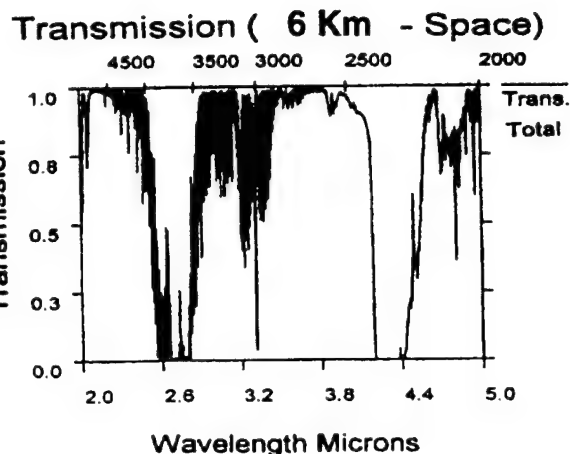
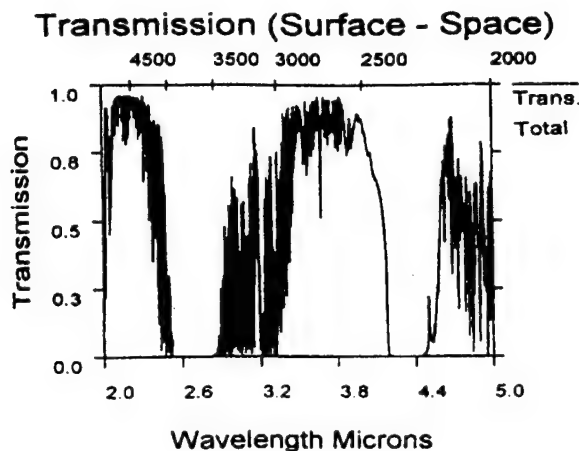
The concept suggested here is to utilize regional or global cloud specifications from a model such as the USAF Nephanalysis model and to extrapolate to smaller sizes using the knowledge provided by fractal power spectral analyses. Techniques are available to create artificial 3-dimensional cloud scenes from this information (such as the Cloud Scene Simulation Model - see Cianciolo and Rasmussen, 1992⁹, and the CloudscapeTM model -). The CloudscapeTM model then subjects the results of this morphological cloud scene to a radiative transfer calculation utilizing externally - supplied cloud microphysical information. The result is a radiation background scene which can be "viewed" from any geometry, taking account of intervening atmospheric absorption effects and from which radiometric "clutter" can be determined at any desired wavelength as seen by a space-based sensor. An ensemble of such scenes created as described above would then provide the statistical atmospheric background clutter model that we desire.

ACKNOWLEDGMENT

This work is conducted under the RAMOS (Russian-American Observational Satellites) Program, sponsored by BMDO (Lt. Col. J. Airis, RAMOS Program Manager) under contract No. C913868 with Space Dynamics Laboratory, Utah State University.

REFERENCES

1. Robert A. McClatchey, McClatchey Associates, Consultant for Visidyne, Inc.
2. Wolfe, W.L. and Zissis, G.J., 1985, The Infrared Handbook, ERIM, ONR, Wash. D.C., 1985.
3. Jamieson, J.A., 1976, "Passive Infrared Sensors Limitations on Performance," Applied Optics, 15, April 1976.
4. Lovejoy, S., Area-Perimeter Relation for Rain and Cloud Areas, Science, Vol. 216, 9 April 1982.
5. Lovejoy, S. and Schertzer, D., How Bright is the Coast of Brittany?, Fractals in Geoscience and Remote Sensing, Image Understanding Research Vol. 1, Eds. G. Wilkinson, K. Kanellopoulos, and J. Megier, Institute for Remote Sensing Applications, Proc. Of Joint JRC/EARSeL Expert Meeting, Ispra, Italy, April 1994, ECSC-EC-EAEC, Brussels, 1995, pp. 102-151.
6. Pecknold, S., Lovejoy, S., Schertzer, D., and Hooge, C., Multifractals and Resolution Dependence of Remotely Sensed Data: GSI to GIS, Scale in Remote Sensing and GIS, Eds. D.A.Quattrochi and M.F.Goodchild, 1997 by CRC Press, Inc.
7. Cianciolo, M.E. and Rasmussen, R.G., Cloud Scene Simulation Modeling: The Enhanced Model, PO-TR-92-2106, April 1992. ADA265958
9. DeVore, J.G., et al, CloudscapeTM model, 1995.
10. Cianciolo, M.E. and Rasmussen, R.G., Cloud Scene Simulation Model, 1992.



Figures 1a-c: Atmospheric transmission for the US Standard Atmosphere calculated using MODTRAN 3.5. Fig. 1a is for a path from the space to the surface viewing the nadir; Fig. 1b is for a path from space to 6 km viewing the nadir; and Fig. 1c is for a path from space to 10 km viewing the nadir.

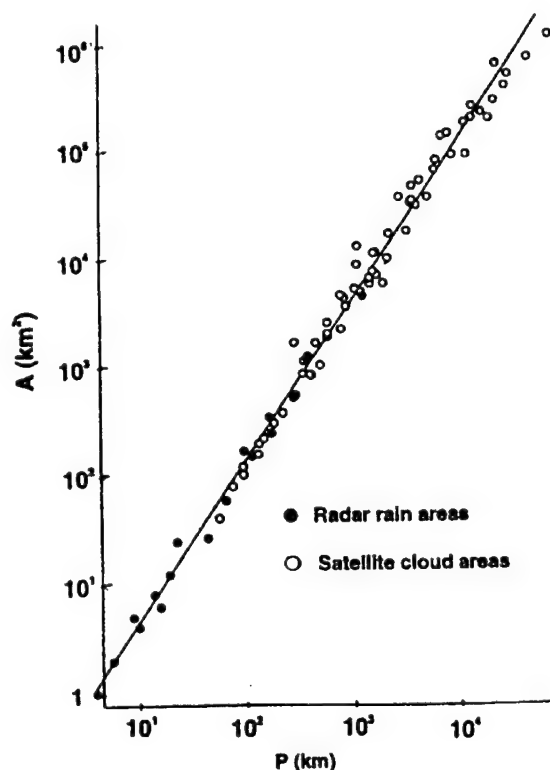


Figure 2: Area plotted against perimeter of rain and cloud areas determined from radar and satellite data (from Lovejoy, 1982).

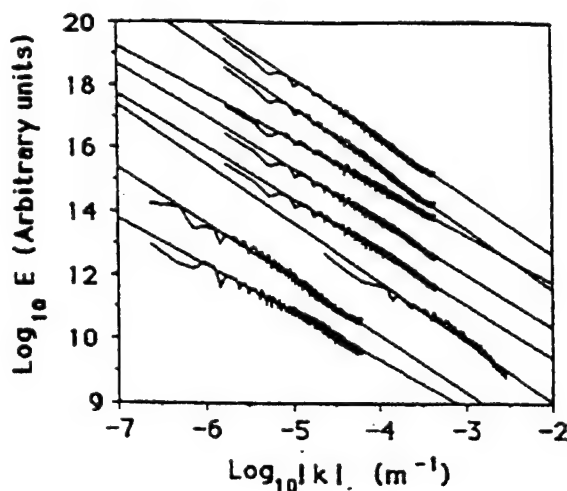


Figure 3: Average power spectrum for satellite images grouped according to the satellite and the frequency range of the images (from bottom to top): LANDSAT (visible) $\beta = 1.7$, GOES (visible) $\beta = 1.4$, GOES (infrared) $\beta = 1.7$, Nimbus-9 (channels 1-5) $\beta = 1.67, 1.67, 1.49, 1.91, 1.85$ (from Lovejoy and Schertzer, 1995).

**SESSION IV:
CLOUD AND CLOUD EFFECTS MODELING**

References in some of the preprints had to be deleted by the editor because they referred the reader to papers with limited distribution that were not available to the public.

MODTRAN4: SIMULATING ATMOSPHERIC RADIATION BUDGETS FOR CLOUDED ATMOSPHERES

G.P. Anderson, J.H. Chetwynd

PL/Geophysics Directorate, 29 Randolph Rd., Hanscom AFB, MA 01731
617-377-2335, Fax 377-8900, 'ganderson@plh.af.mil'

A. Berk, L.S. Bernstein, P.K. Acharya

Spectral Sciences, Inc., 99 S. Bedford St., Burlington, MA 01803

H.E. Snell

Atmospheric and Environmental Research, Inc., 840 Memorial Dr., Cambridge, MA 02139

E.P. Shettle

Naval Research Laboratory, Washington, D.C. 20375

ABSTRACT

The new MODTRAN4 band model, with its correlated-k Beer's Law algorithm, can efficiently and correctly (usually within 3-5%) calculate the scattering and absorption signatures of realistic molecular, aerosol and cloudy environments in the lower and middle atmosphere. The current approach for molecular scattering accommodates line overlap and partial correlations between both molecular species and the solar irradiance, while maintaining automated band model spectral resolution at 2 or 15 cm^{-1} . This new level of evolution and validation will permit improved syntheses and analyses of actinic (direct plus scattered) solar and thermal energy sources and their flux divergence within the stratosphere and troposphere. This capability is a by-product of the direct calculations of transmittance, radiance and irradiance, including thermal, solar, and lunar sources. Validated energy budgets can then serve as validation surrogates for applications related to surveillance and background simulations within clouded environments.

For instance, rapid calculation of IR cooling rates for a variety of thermal and constituent profiles demonstrates the flexibility of the approach and the sensitivity to latitudinal and dynamic variability. Comprehensive validation is provided through two basic avenues. The first involves direct comparisons with line-by-line calculations, as exemplified by FASE (the line-by-line algorithm jointly developed from FASCODE by DoD and DOE) which provides the molecular standard for layer effective optical depths, single scattering albedos, and transmittances. This enables the MODTRAN4 algorithm to be refined for more adaptable spectral resolution plus efficient determination of those layer quantities necessary for multiple scattering applications; e.g. DISORT. The second validation step centers on comparisons against a variety of measurements, mostly airborne visible and IR up-welling radiances, including both clear and clouded skies.

1. INTRODUCTION

With the development of MODTRAN4 (Bernstein, et al., 1996), a flexible tool for radiative energy budget calculations is now available. While this version of MODTRAN is grounded in the prior series of AF radiative transfer band model (BM) algorithms (LOWTRAN, Kneizys, et al., 1980, 1983, 1988, through MODTRAN3, Berk et al., 1989, 1995), it is distinct in its ability to employ Beer's law ($T_v = \exp(-k_{v,i} n_i)$) to describe local layer, species-specific transmittance for input to the radiance calculations. While this capability is not always necessary, it allows appropriate handling of multiple scattering (m.s.) using existing non-BM algorithms (DISORT, Stamnes et al., 1988, and Isaacs et al., 1987). MODTRAN4, while maintaining the basic 2 cm^{-1} spectral resolution, can now complement the m.s. routines by introducing a Correlated-k (CK) capability which is expressly compatible with Beer's law formulations. MODTRAN4 also provides greatly improved predictive capabilities under cloudy and/or heavy aerosol loading conditions in both the visible and IR by allowing the explicit definition of water and ice cloud vertical profiles and spectral data, either by scaling and combining default model clouds or by redefining entirely new model clouds with micro-layering options.

It can be shown that this combination of improvements will permit rapid identification of atmospheric contaminants/signatures in window regions as well as accurate spectral calculations of heating/cooling rates in the presence of clouds for both thermal and solar spectral regimes. Finally, in the regions of molecular opacity, where weighting functions peak in the atmosphere, it is expected that MODTRAN4 can play a role in very quick 'primitive' retrievals, avoiding the large number of line-by-line (LBL) calculations necessary for initiating derivative (perturbation) matrices (Anderson et al., 1993). While the error estimates and residuals associated with a 2 cm^{-1} algorithm will be larger than those associated with LBL retrievals, the speed advantage for image processing might warrant this initial approach.

2. ADDITION OF A CORRELATED- k CAPABILITY TO MODTRAN

Addition of a CK capability to MODTRAN (Bernstein et al., 1995) provides an accurate and fast means for evaluation of the effects of clouds and heavy aerosol loading on retrievals (both surface properties and species concentration profiles) and on atmospheric radiative heating/cooling calculations. These radiative transfer computations require coupling the effects of gaseous molecular absorption due primarily to water vapor, carbon dioxide, and ozone, with particulate multiple scattering due to volcanic aerosols, ice crystals, and water droplets. In order to adapt a band model approach for use in scattering calculations it is necessary to express the band model transmission function in terms of a weighted sum of Beer's law exponential terms. Thus, a method for determining the weighing factors and monochromatic absorption coefficients for the MODTRAN band model is required. An abbreviated discussion of the CK approach as tailored for integration into MODTRAN is given below; for a more complete discussion of the CK method the reader is referred to Lacis and Oinas (1991).

For simplicity, consider the problem of determining the average transmittance, as defined by Beer's law, for a homogeneous path over a finite spectral interval. The generalization to inhomogeneous paths is straightforward. The path transmittance can be exactly determined through evaluation of:

$$T(u) = \frac{1}{\omega_2 - \omega_1} \int_{\omega_1}^{\omega_2} d\omega \exp(-k(\omega)u) ,$$

where ω is frequency, $k(\omega)$ is the monochromatic absorption coefficient, and u is absorber column density. The basis of the CK approach is that evaluation of $T(u)$ by integration over frequency can be replaced by an equivalent integration over the distribution of absorption coefficient values $f(k)$ in the spectral interval

$$T(u) = \int_0^{\infty} dk f(k) \exp(-ku) .$$

The distribution function $f(k)$ is not smooth or monotonic; it generally consists of a series of sharp spikes which reflects the sharp line structure of $k(\omega)$. It then becomes more computationally convenient to work with the smooth and monotonic cumulative probability distribution function

$$g(k) = \int_0^k dk' f(k') .$$

where $k(g)$ is given by the inverse of $g(k)$, $k(g) = g^{-1}(k)$.

The MODTRAN band model for a single species is based on four parameters: (1) the integrated line strength S in a spectral interval $\Delta\omega$ ($\Delta\omega = 1 \text{ cm}^{-1}$ in MODTRAN), (2) the effective number of equivalent lines n (non-integer values of n are acceptable) in the interval, (3) the average pressure broadening Lorentz line width γ_L , and (4) the Doppler line width γ_D . These parameters are determined directly from the 1996 HITRAN parameter line compilation (Rothman et al., 1996).

3. INITIAL VALIDATION OF MODTRAN4 MULTIPLE SCATTER SOLAR

Development of MODTRAN4 was necessary because MODTRAN3 predictions of multiply scattered solar radiances in spectral regions with non-continuum molecular absorption may be inaccurate. This scenario cannot be validated by comparisons to FASCODE (Clough et al., 1988) because it lacks a solar capability. Thus, initial validation of MODTRAN4 multiply scattered solar calculations were made directly to measurements.

In previous studies (Anderson et al., 1997) a comparison of calculated radiance predictions to airborne measurements (Malherbe et al., 1995) was performed by ONERA and CELAR a circular variable filter cryogenic spectrometer (1500 - 5500 nm, 2% spectral resolution). The aircraft altitude was 3.0 km, the cloud top was 2.5 km, the sensor line-of-sight (LOS) zenith angle was 104°, and the solar zenith and relative azimuth angles were 48° and 137°, respectively. The calculations included: (1) results from NAULUM (Malherbe et al., 1995), a new radiative transport model developed at ONERA, (2) MODTRAN3 calculations without the CK approach, and (3) MODTRAN4 calculations performed with the CK approach. The MODTRAN4 cloud model upgrade enabled the cloud profile and spectral data to be explicitly entered for the MODTRAN calculations. Both MODTRAN calculations employed a simpler two-stream multiple scattering model (Isaacs et al., 1987); the discrete ordinate model in MODTRAN, DISORT (Stamnes et al., 1988), was run with 8-streams over a limited spectral sub-region and produced similar results. The fit was excellent. However, when the sun fell into the near line of sight (eg. 11°), the fit could not properly capture the forward scattering lobe. This problem is being addressed.

4. COOLING RATES IN THE PRESENCE OF CLOUDS

An important part of model development is continual comparison with measurements and theoretical predictions. In recent years the ARM community participants, particularly Clough and colleagues, have undertaken the extension of the work originally begun by F. Luther and R. Ellingson, as represented in the dedicated issue of *J. Geophys. Res.*, 96, May 1991. The cooling rate discussions therein have been augmented by more recent studies by Clough et al., 1992, Bernstein et al., 1996, and Kimball, 1992, for instance. In Figure 1a the cooling due to all gases in the tropical atmosphere emitting in the 0-3000 cm⁻¹ spectral range is represented, including a 0.5 km thick cirrus cloud centered at 150 mb.; integrated results can be seen in 1b. This result is preliminary, but MODTRAN4 now allows for the inclusion of such clouds with multiple scattering and micro-layering. The dashed cooling curve was calculated (INCORRECTLY) with a single run of MODTRAN3 fluxes, while the solid and dotted curves resulted from two single runs of MODTRAN4. Initial results show a clear dependence on the mode of implementing the cloud within the code, with as much as 0.5K/day difference between separate MOD4 calculations. Certainly much additional theoretical and validation work needs to be done, but without good measurements, the impact of cloud cooling will remain uncertain. The implications of this surrogate study for cloud modeling of line-of-sight or imaging studies (transmittance and background radiance) suggests that the edges of clouds are going to be particularly sensitive to the assigned optical properties and spatial sampling. Note that the gray scale cannot connote the differences between heating and cooling. Please contact the author for reference to the color version.

5. CONCLUSIONS

MODTRAN4 shows great promise as a research tool for better understanding of the role of clouds in the atmosphere, both within the 'energy budget' and within the visual 'field of operation', actual and simulated. In general the calculations can be done rapidly and with accuracy that approaches LBL numerical solutions. Important current caveats center on improved optical properties of clouds and their physical descriptions (ice and water), issues of current research activity.

6. REFERENCES

- G.P. Anderson, J.H. Chetwynd, A. Berk, L.S. Bernstein, P.K. Acharya, **An Algorithm for Hyperspectral Remote Sensing: Solar and Thermal Regimes** Optical Society of America, Proceedings of Optical Remote Sensing of the Atmosphere, Sante Fe, Feb 10-14, 1997.
- Kneizys, F.X., M.L. Hoke, L.W. Abreu, E.P. Shettle, 'MODTRAN2: Suitability for Remote Sensing', *Proc. of SPIE, 1954, Remote Sensing*, 1993.
- Berk, A., "Upgrades to the MODTRAN Layer Cloud/Rain Models," Report. No. SSI-SR-56, Spectral Sciences, Inc., 99 S. Bedford St., Burlington, MA, 1995..
- Berk, A., L. S. Bernstein, and D. C. Robertson, "MODTRAN: A Moderate Resolution Model for LOWTRAN7," Rep. GL-TR-89-0122, Air Force Geophys. Lab., Bedford, MA, 1989. ADA214337
- Bernstein, L. S., A. Berk, D. C. Robertson, P. K. Acharya, G. P. Anderson, and J. H. Chetwynd, "Addition of a Correlated-*k* Capability to MODTRAN," Proceeding of the 1996 IRIS Targets, Backgrounds, and Discrimination Meeting, 1996.

Bernstein, L.S., A. Berk, P.K. Acharya, D.C. Robertson, G.P. Anderson, J.H. Chetwynd, L.M. Kimball, "Very Narrow Band Model Calculations of Atmospheric Fluxes and Cooling Rates Using the MODTRAN Code," *J. Atm. Sci.*, 53, 2887-2904, 1996.

Clough, S. A., F. X. Kneizys, G. T. Anderson, E. P. Shettle, J. H. Chetwynd, L. W. Abreu, and L. A. Hall, 1988, "FASCOD3 Spectral Simulation" Proceedings of the International Radiation Symposium, Lenoble and Geleyn, Deepak Publishing.

Clough, S.A., M.J. Iacono, J.-L. Moncet, "Line-by-Line Calculations of Atmospheric Fluxes and Cooling Rates: Applications to Water Vapor", *J. Geophys. Res.*, 97, 15761, 1992.

Isaacs, R. G., W. C. Wang, R. D. Worsham, and S. Goldenberg, 1987, "Multiple Scattering LOWTRAN and FASCODE Models," *Applied Optics*, 26, 1272-1281.

Kimball, L.M., "Investigation of Atmospheric Heating and Cooling Balance Using MODTRAN3", *AFOSR Summer Faculty Report*, 1995.

Kneizys, F.X., Shettle, E.P., Gallery, W.O., Chetwynd, J.H., Abreu, L.W., Selby, J.E.A., Fenn, R.W., McClatchey, R.A., **Atmospheric Transmittance/Radiance: Computer Code LOWTRAN 5**, AFGL-TR-80-0067, AD A058643, 1980.

Kneizys, F.X., Shettle, E.P., Gallery, W.O., Chetwynd, J.H., Abreu, L.W., Selby, J.E.A., Clough, S.A., Fenn, **Atmospheric Transmittance/Radiance: Computer Code LOWTRAN 6**, AFGL-TR-83-0187, AD A137796, 1983.

Kneizys, F.X., Shettle, E.P., Chetwynd, J.H., Abreu, L.W., Anderson, G.P., Gallerv, W.O., Selby, J.E.A., Clough, S.A., **Users Guide to LOWTRAN 7**, AFGL-TR-88-0177, 1988. ADA206773

Lacis, A. A., and V. Oinas, "A description of the Correlated K Distribution Method for Modeling Nongray Gaseous Absorption, Thermal Emission, and Multiple Scattering in Vertically in Homogeneous Atmospheres," *J. Geophys. Res.*, 96, 9027 - 9063, 1991.

Malherbe, C., P. Simoneau, A. Boischot, G. Durand, J. Deschamps, and G. Gregoire, 1995, "Radiative Transfer Model in a Cloudy Atmosphere: A Comparison with Airborne Cumulus Measurement," Proceedings of the SPIE Conference on Passive IR Remote Sensing of Clouds and the Atmosphere III.

Rothman, L. S. et al., 1996, "The HITRAN Molecular Database: Edition of 1996," Released as a CD-Rom, June, 1996. ('rothman@plh.af.mil')

Stamnes, K., S. C. Tsay, W. J. Wiscombe, and K. Jayaweera, "Numerically Stable Algorithm for Discrete-Ordinate-Method Radiative Transfer in Multiple Scattering and Emitting Layered Media," *Applied Optics*, 27, 2502-2509, 1988.

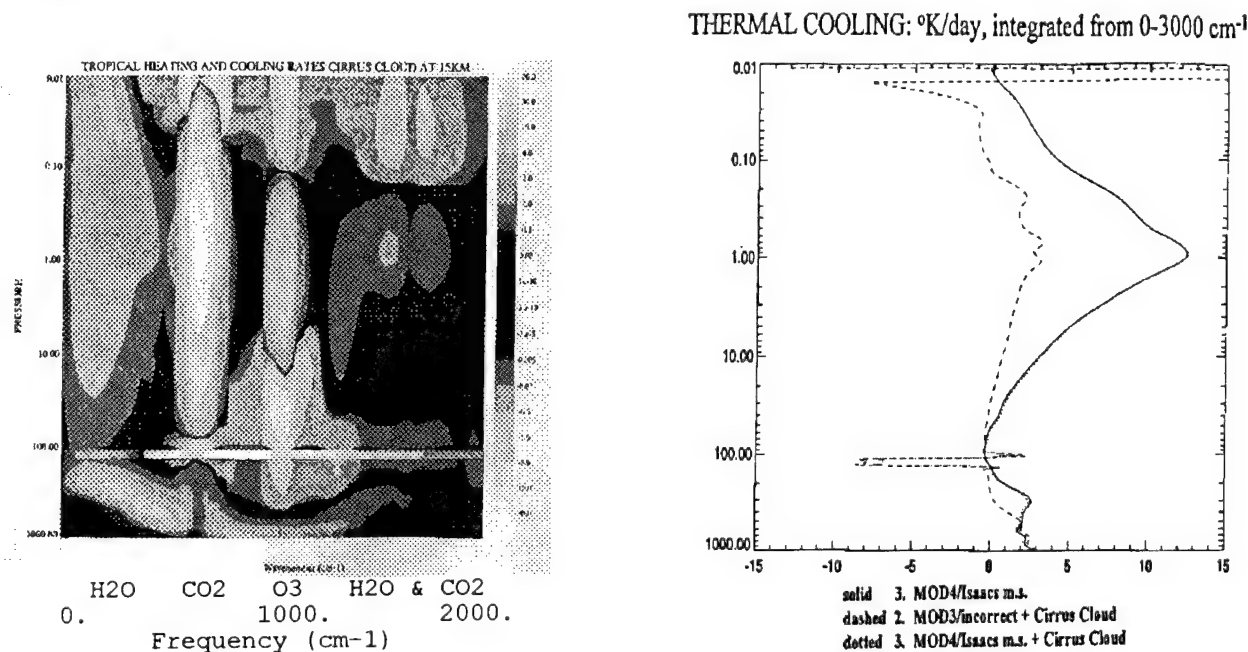


Figure 1: Tropical cooling rate calculations with cirrus cloud inserted at tropopause; discrimination between cooling and heating requires color definition, lost in this representation. The spectrally integrated cooling rate (1b) covers the range from 0-3000 cm⁻¹. This type of calculation can be carried out for the whole MODTRAN domain, including solar scattering.

RADIOMETRIC VALIDATION OF CSSM

Joel B. Mozer, Guy P. Seeley
USAF Phillips Laboratory
Geophysics Directorate
Hanscom AFB, MA 01731

Alan Wetmore, Patti Gillespie, David Ligon, and Samuel Crow
US Army Research Laboratory
Adelphi, MD

ABSTRACT

The Air Force Cloud Scene Simulation Model (CSSM) is capable of generating physically realistic, high resolution, synthetic cloud data in four dimensions using a combination of empirical and physical techniques. These data have uses in many DoD applications that require an accurate radiometric depiction of the clouds, such as for a sensor simulation of target scenes which contain cloudy backgrounds. These applications typically require that a rigorous radiative transfer calculation be performed on the cloud data. We are developing techniques to validate the CSSM in terms of its suitability for such purposes. The Army Boundary Layer Illumination Radiance Balance (BLIRB) model has been systematically coupled to the CSSM in order to produce radiometric scenes of synthetic clouds. The statistical characteristics of these scenes are compared with radiometric images of real clouds to evaluate the physical fidelity of the CSSM/BLIRB combination. In this paper we present the preliminary results of these comparisons and suggest directions for future work to improve the CSSM for radiometric scene generation purposes.

1. INTRODUCTION

Atmospheric clouds critically affect many Department of Defense systems, sensors and operations. In some situations clouds in the battlespace simply act as obstacles which block line-of-sight visibility. This is the case when a thick cloud deck over a battlefield precludes an aircraft-based reconnaissance or battle damage assessment mission. In other situations, clouds have a more insidious effect such as with an IR sensor where the radiation detected by the sensor is modified by clouds in such a way that the maximum lock-on-range to the target is decreased. This may result in a pilot being forced to fly closer to an enemy target than if no clouds were present.

In the first class of problems, clouds can theoretically be avoided (or taken advantage of) by simply knowing exactly where the clouds are, or are forecast to be, over the battlespace. In the second case, however, consideration of the optical and radiative properties of the clouds must be made. For example, an infrared space-based surveillance system that employs automated target detection algorithms to identify missile threats may be subject to false-positive triggers due to bright glint, which is a result of the reflection of sunlight off of clouds. In this example, designers of the sensors and algorithms must be able to account for these spurious triggers by understanding the radiative processes in clouds (solar scattering in this case) and being able to differentiate the cloud-induced noise from real targets.

This latter class of problem is the subject of the present work. Specifically, we are constructing the capability to generate synthetic atmospheric scenarios, including clouds, which can be used to simulate the radiometric conditions in a battlespace. We are creating this capability through a marriage of the US Air Force's Cloud Scene Simulation Model (CSSM) and the Army's Boundary Layer Illumination Radiation Balance Model (BLIRB). It is important that synthetic cloud scenarios closely mimic real-world conditions to have value in the decision making process. This effort to radiometrically validate the CSSM/BLIRB capability quantifies how close the current system comes. This paper describes preliminary results and plans for this effort.

Section 2 includes a brief overview of the CSSM and BLIRB models, Section 3 gives a description of the validation approach and describes the preliminary results along with a discussion of the ongoing work.

2. OVERVIEW

The CSSM was developed by The Analytic Sciences Corporation (TASC) for the US Air Force Phillips Laboratory to generate high resolution synthetic cloud fields for use in DoD modeling and simulation activities [1]. The CSSM takes as input atmospheric wind, temperature and moisture data, such as from a radiosonde or numerical weather prediction, along with cloud parameters (cloud type, amount, coverage, etc.) for a given region. The output of the CSSM is a four-dimensional field of cloud Liquid Water Content (LWC) which is consistent with the input information, but at a much higher spatial and temporal resolution.

The CSSM uses a fractal algorithm to generate the variable structure which is characteristic of clouds. The free parameters of this fractal algorithm were determined via an analysis of aircraft measurements of liquid water content in real clouds. This empirical process is augmented within the CSSM with simple physics-based algorithms to add realism to the structure, development and motion of the cloud fields. The current version (CSSM v. 2.0) is capable of generating complex cloud scenes consisting of multiple layers of up to 12 different cloud types, including structures such as cloud streets and lee wave clouds.

The CSSM does not directly produce information about the radiometric effects of clouds. However, the nature of the CSSM output, a high-resolution volumetric description of the physical properties of the clouds, lends itself to a post-processing calculation to determine the optical and radiometric properties of the cloud scene. The CSSM output has been used in this regard for several applications using a variety of radiative transfer techniques.

BLIRB is a component of the Weather and Atmospheric Visualization for Environmental Simulation (WAVES) suite of tools. One purpose of WAVES is to give the user the ability to modify images to include the effects of weather and the atmosphere. BLIRB is the 3-D spectral radiative transfer code used within WAVES. Other components include VIEW, output database access code for line of sight path radiance/transmittance evaluations, PixelMod, for image spectral estimation and atmospheric effects modifications of images, and ATMOS, a turbulence model.

WAVES performs range-dependent calculations using line of sight radiative transfer methodology for image modification. These line of sight calculations require a description of the radiation fluxes and extinction throughout the local environment. Radiation fluxes, turbulence parameters, and extinctions are calculated by the first phase of the WAVES models. Image modification is done by the PixelMod program using line-of-sight data created by the VIEW program using the three-dimensional databases created by the BLIRB program [2].

The foundation of the WAVES suite of algorithms is an 8-stream, or 24-stream, radiative transfer model, BLIRB. BLIRB accounts for the scattering in the atmosphere, and LOWTRAN (soon to be MODTRAN) is used for the molecular absorption. BLIRB was developed for near-earth scenarios, and deals with a region up to 10 km in length and width and a height of either 5 or 12 kilometers AGL (above ground level). This allows most cloud-related phenomena to be explored. BLIRB uses an iterative discrete-ordinates approach to calculate the direct solar (or lunar) flux, the directional radiances, and the total local extinction and scattering for all points on a grid with typical spacing of 250 meters. It performs these calculations for spectral bands defined as in MODTRAN-7. These calculations allow complex inhomogeneous cloud fields to be used as input. This extension beyond the one-dimensional vertical profiles available in MODTRAN-7 is essential to realistic modeling of the battlefield. The directional effects allow for realistic changes in the appearance of scenes as the observer rotates, the inhomogeneity allows for clouds to engulf the observer or target, or pass between them, all in a self-consistent, radiometrically correct manner.

The result of the BLIRB model is a database of extinction, scattering and directional radiances, that depend on the wavelength and position in 3D space. These values are used by viewing and imaging tools as they project lines-of-sight through space from the observing sensor to the elements that make up the scene [3].

Evaluation BLIRB for simple cloud geometries has been reported in [4]-[6]. These evaluations have shown reasonable agreement of the BLIRB model with standard models, but have also exposed weaknesses. These areas are current research areas for BLIRB.

3. APPROACH

The principal focus of the radiometric validation effort is to assess and improve the physical realism of 2D synthetically-generated cloud scenes. Our approach to this goal is to start with the simple, gross characteristics of synthetic images as compared to images of real clouds and progressively work towards more subtle and complex comparisons. The basic idea is to select a set of representative metrics for cloud-containing images and compare the statistics of these metrics for a large sample of real and synthetic images of similar cloud fields. The results of these comparisons will then be used to evaluate and adjust, if necessary, the simulation methodology.

Figure 1 shows a fundamental comparison of total solar insolation as a time series measured and calculated at a single point. The measurements are from the ongoing experimental test and the model results are from the simple Shapiro three-layer cloud model called Insol . This model calculates bulk solar flux at the surface based on simple surface meteorological observations including cloud layers and types. Insol is in operational use in the DoD and provides a simple baseline to which more elaborate calculations can be compared.

The first step of this approach is to determine the appropriate metrics. The first category of metrics emphasize the bulk statistical properties of the rendered image at the expense of spatial information. "Classical" statistical measures such as mean, variance, skewness and kurtosis fall into this category. These measures are often difficult to use in interpreting complex imagery. A promising approach that we have investigated is the Chi-Squared testing of histogram distributions as detailed in [8].

Another category of metrics emphasizes spatial properties of the synthetic imagery. These types of metrics are largely independent of the details of the radiative transfer scheme and depend strongly on the shape of the generated cloud fields. Examples of these types of measures are spatial image spectra in Fourier or wavelet bases and spatial correlation functions. We report some results on spatial cloud spectra from ground based instrumentation in another paper presented at this conference [9].

Both spatial and bulk metrics need to be examined for a variety of wavebands to verify proper spectral behavior. An overall figure of merit can be constructed by determining the distance between a representative set of real and synthetic scenes in metric space. Determining the weight of each specific metric is a difficult problem. We believe metrics that have a clear physical interpretation and thus a quantifiable effect on the generated imagery should be most heavily weighted in the figure of merit.

4. CONCLUSIONS

We have described the preliminary approach to the radiometric validation of the Cloud Scene Simulation Model / Boundary Layer Illumination Radiance Balance model combination. The principal motivation for this effort is to demonstrate the feasibility for using synthetically-generated cloud scene imagery quantitatively for use in a variety of design, evaluation, training and planning applications. This work is ongoing and only a preliminary review of the approach is given in this paper. A more complete set of results and conclusion will be presented in a future report.

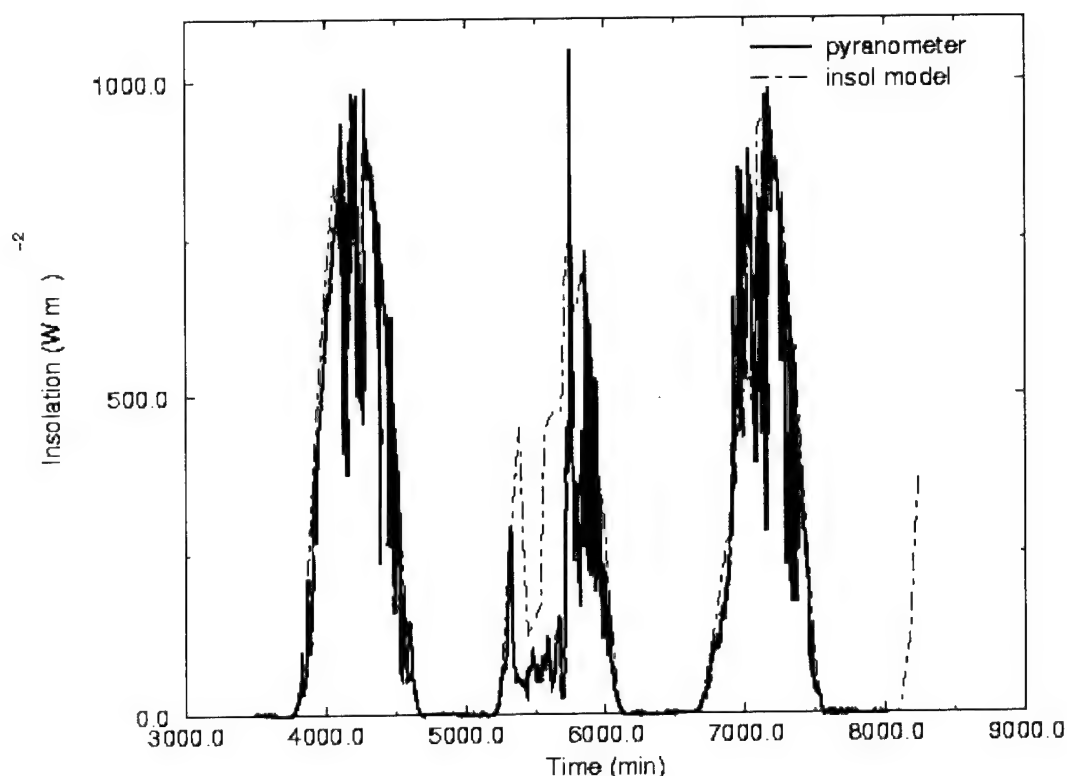


Figure 1. Comparison on pyranometer measurements and Insol model calculations

REFERENCES

- [1] Cianciolo, M.E., M.E. Raffensberger, E.O. Schmidt, J.R. Stearns, 1996, "Atmospheric Scene Simulation Modeling and Visualization", Phillips Laboratory, Hanscom AFB, MA, PL-TR-96-2079 ADA312179
- [2] Wetmore, A. E., and Zardecki, A., "The Boundary Layer Illumination and Radiative Balance Model (BLIRB)," Proceedings of the Cloud Impacts on DOD Operations and Systems 1993 Conference, PL-TR-94-2188, pp. 201-206, Ft. Belvoir, VA, November 1993. ADA286658
- [3] Tofsted, David, Patti Gillespie, and Alan Wetmore, "The WAVES Modeling Suite: Extensions and Evaluation Update", Ground Target Modeling Vehicle Conference, August 1995.
- [4] Gillespie, Patti, Michael Rollins, and David Tofsted, "Evaluating the WAVES Model Using Image Statistics", 1996 Battlefield Atmospherics Conference, White Sands Missile Range, NM, December 1996.
- [5] Wells, Michael B., "Monte Carlo Code for Evaluating the Boundary Layer Illumination and Radiation Balance Model (BLIRB)", ARL-CR-193, January 1995.
- [6] Wells, Michael B., "Monte Carlo Calculations for Evaluating the Boundary Layer Illumination and Radiation Balance Model". ARL-CR-205, November 1995.
- [8] Welsh, J. P., "Smart Weapons Operability Enhancement (SWOE) Joint Test and Evaluation (JT&E) Program," "SWOE Report 94-10, August 1994.
- [9] Seeley, G., J. B. Mozer, and E. Emory, CIDOS-97, September 1997.

VALIDATION OF CLOUDSCAPE® AF WITH AIRCRAFT DATA

R.J. Thornburg, J.G. DeVore, J.H. Thompson, R.J. Jordano, T.L. Stephens
Visidyne, Inc.
Huntsville, AL 35801
Telephone: (205) 880-3411
Telefax: (205) 880-3284
E-mail: thornbrg@visidyne.com

ABSTRACT

This paper describes the validation of CloudScape® AF, a tool developed to compute radiometrically accurate images of clouds to support the design of DoD space-based surveillance sensors. CloudScape® AF computes these images by employing physics-based radiative transfer models and fast, numerical integrations through a three-dimensional grid of liquid water or ice particulates. This paper shows good agreement between CloudScape® AF predictions and multi-spectral (3.33 - 4.75 μm) aircraft measurements of marine stratus clouds taken by Sandford. Plans are discussed for additional comparisons against data taken by such platforms as the ARES aircraft, MSX, and MSTI-III in support of the Space Based Infrared Systems (SBIRS) Program.

1. INTRODUCTION

Careful spectral band selection is important in the design of space-based surveillance sensors in order to reduce the effects of natural background clutter. As system requirements become more stressing, the need increases to measure and model accurately the clutter effects of clouds, both in absorption and window regions, and over a range of altitudes. Data from several recent measurement programs, such as ARES, MSTI-III and MSX, serve as the foundation of our understanding of the clutter problem. However, due to the limited set of spectral bands, viewing geometries and cloud morphologies available from any finite measurement campaign, these measurements must be supplemented by accurate models developed to extrapolate the data for system studies. For optimal utility, such models need to be computationally efficient to allow designers to examine the full parameter space needed to make system trades.

This paper describes the modelling and validation of CloudScape® AF, which was developed under Phase I and II SBIR awards from Phillips Laboratory to provide a fast and accurate rendering of clouds. The paper describes the calculational flow and model assumptions of CloudScape® AF, followed by a comparison of the code's predictions against aircraft measurements of marine stratus clouds in the 3.33 - 4.75 μm spectral range. The paper closes with future validation plans and conclusions.

2. MODEL DESCRIPTION

In order to calculate cloud radiances, CloudScape® AF requires information about the spatial distribution of cloud water and ice particulates, as well as information about the intensity of important radiometric fluxes. CloudScape® AF and its supporting code, CloudGen/Weather™ have internal models of these input quantities, but for greatest fidelity, these inputs are taken from DoD standard codes. Figure 1 shows the typical calculational flow for such a case. On the left, CloudScape® AF receives a gridded array of cloud mass density that has been extracted from data or synthesized by CSSM (the Cloud Scene Simulation Model)², and then reformatted by CloudGen/Weather™. On the right, CloudScape® AF receives a database containing solar or lunar irradiance at the cloud, earthshine, skyshine, path radiance and transmission. This database is constructed by exercising MOSART³ parametrically over a series of solar and observer line-of-sight geometries, using the MD (Mosart Driver) tool. CloudScape® AF interpolates this database to obtain results for the specific geometries of interest to the user.

CloudScape® AF computes solar scattering from a cloud by taking steps along each line-of-sight through the gridded database of cloud water and ice, and computing at each step the single and multiple scattering of solar radiation into the sensor field of view. The computation involves adjusting the extinction coefficient by making the standard approximation that highly-peaked, forward scattered radiation is returned to the direct beam, by computing single scattering exactly, and by estimating

multiple scattering based on build-up factors that depend on the probability that light will escape the cloud after various orders of scattering. Further description and validation of this scattering model against theoretical predictions and Monte Carlo calculations for stratiform and cumuliform geometries is described elsewhere⁴. The resulting computation is quite rapid, so that scattering computations for a 128 x 128 pixel array of lines-of-sight can take less than 40 seconds on an SGI workstation.

3. SPECTRAL VALIDATION AGAINST AIRCRAFT MEASUREMENTS

Several spectral cloud measurements were obtained by the Air Force Geophysics Laboratory during the course of the IR Signature Studies program, although they appear not to have been widely reported. However, Zachor, Holzer and Smith⁵ report on one set of spectra they obtained from Brian Sandford. This set, designated 726/7/FB43, involved a uniform stratus layer off the coast of central California near San Luis Obispo. On September 28, 1977 the AFGL aircraft flew at 6.0 kft (1.83 km) viewing the top of the thick stratus layer at 3.0 kft (0.9 km). The solar elevation angle was 8.88°, while the line-of-sight depression angle was 5.0°. Spectra were reported from 1800 to 3600 cm⁻¹, although spectrometer calibration error and noise limited the useful data to 2100-3000 cm⁻¹ (3.33 - 4.76 μm). The sun was in the west, and spectra were reported near the four compass cardinal points, giving measurements at forward scattering, backward scattering and scattering near right angles.

To generate predictions from CloudScape® AF for this case, MOSART was run using a Mid-Latitude Summer atmosphere with a 5 km meteorological range to set the boundary layer haze values. Since the droplet size distribution was not measured, the standard LOWTRAN value of a 3.33 μm droplet diameter was used⁶. Although CSSM or CloudGen/Weather™ could have been used to generate a structured liquid water field, in order to simplify the comparison, a flat, unstructured field was constructed with CloudGen/Weather™.

Figure 2 shows the comparison between the measurements and the CloudScape® AF predictions with Figure 2a showing the forward and backward scattering cases and Figure 2b showing the side scattering. The measured data were reported spectrally, but have been binned into 25 cm⁻¹ wide bins for the comparison. Above 4.2 μm, scattering is unimportant and for all scattering angles both the data and the code results follow nearly the same line. In the scattering region below 4.2 μm, the side scattering agrees with the measurements to within the variability of the data, represented by the two spectra. The forward scattering spectra show excellent agreement below about 3.8 μm, but CloudScape® AF overpredicts the scattering by up to 30% in the region between 3.8 μm and 4.2 μm. In addition, CloudScape® AF underpredicts the backscatter peak. A likely cause for both of these results is the small meteorological range chosen for the MOSART run. The extremely hazy conditions resulting from this choice results in too much of the solar irradiance being scattered out of the beam in the cloud-free atmosphere, where it contributes to the forward scattering path radiance. The scattered solar irradiance is then not available to contribute to the backscatter peak coming from the Mie scattering in the cloud.

CONCLUSIONS

The demanding requirements placed on satellite surveillance systems require that careful engineering studies be performed to maximize target signal in a cluttered environment, and fast-running, versatile radiometric codes be developed to support such studies. This paper has described CloudScape® AF and showed it gave good agreement with spectral measurements of a marine stratus deck using standard settings for the unknown atmospheric profile and droplet size inputs. The authors plan more stringent validation tests using coordinated measurements by ARES, MSX, MSTI and lidars such as those reported by Shanks⁷, and those made for the First ISSCP Regional Experiment (FIRE)⁸.

ACKNOWLEDGMENTS

This work is conducted under the RAMOS (Russian-American Observational Satellites) Program, sponsored by BMDO (Lt.Col. J. Airis, RAMOS Program Manager) under contract No. C913868 with Space Dynamics Laboratory, Utah State University. We particularly acknowledge Col. Bill Smith of BMDO for his active participation and support.

REFERENCES AND FOOTNOTES

2. Cianciolo, M.E., and M.E. Raffensberger, Atmopsheric Scene Simulation Modeling and Visualization (AMV): Cloud Scene Simulation Model User's Guide, TIM-07169-2, TASC, Reading, MA, April 1996.
3. Cornette, W.M., P.K. Acharya, D. Robertson, and G.P. Anderson, Moderate Spectral Atmospheric Radiance and Transmittance Code (MOSART). PL-TR-94-2244 (4 Vols), Phillips Laboratory, Hanscom AFB, MA, 7 Nov 1995. V 1: ADA304038; V 2: ADA304180;
 V 3: ADA304072; V 4: ADA304073
4. DeVore, John G., James H. Thompson and Ross J. Thornburg, January 1996, "Physics-Based Background Visualization from Volumetric Cloud Descriptions Using CloudScape™", The 1996 Meeting of the IRIS Specialty Group on Targets, Backgrounds and Discrimination, volume I, pp 277-286, Sandia National Laboratory, Albuquerque, NM, January 30-February 1, 1996.
5. Zachor, A. S., J. A. Holzer, and F. G. Smith, 1979, IR Signature Study, AFAL-TR-79-1012, Air Force Avionics Laboratory, Wright-Patterson AFB, OH.
6. Quoted in Thomas, Michael E. and Donald D. Duncan, 1993, "Atmospheric Transmission", in Atmospheric Propagation of Radiation, F. G. Smith, ed., volume 2 of The IR/EO Systems Handbook, ERIM, Ann Arbor, MI, pp.105-109.
7. Shanks, J.G. et al., 1997, "A Comparison of Predicted Cloud Radiance with MSTI-3 and ARES Data in the SWIR Spectral Region", The 1997 Meeting of the IRIS Specialty Group on Targets, Backgrounds and Discrimination, Naval Postgraduate School, Monterey, CA, February 4-6, 1997 and references therein.
8. Cahalan, Robert F. and Jack B. Snider, 1989, "Marine Stratocumulus Structure", *Remote Sensing Environ.*, vol 28, pp. 95-105.

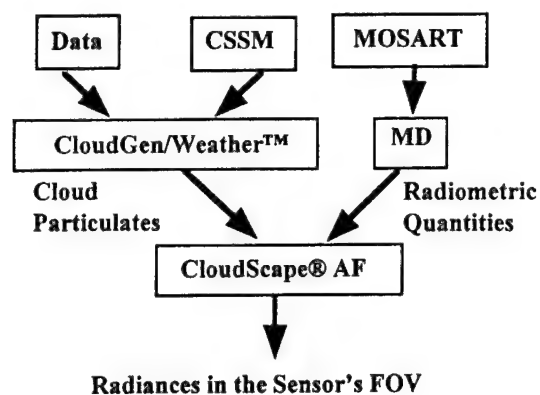


Figure 1. Calculational flow in CloudScape® AF.

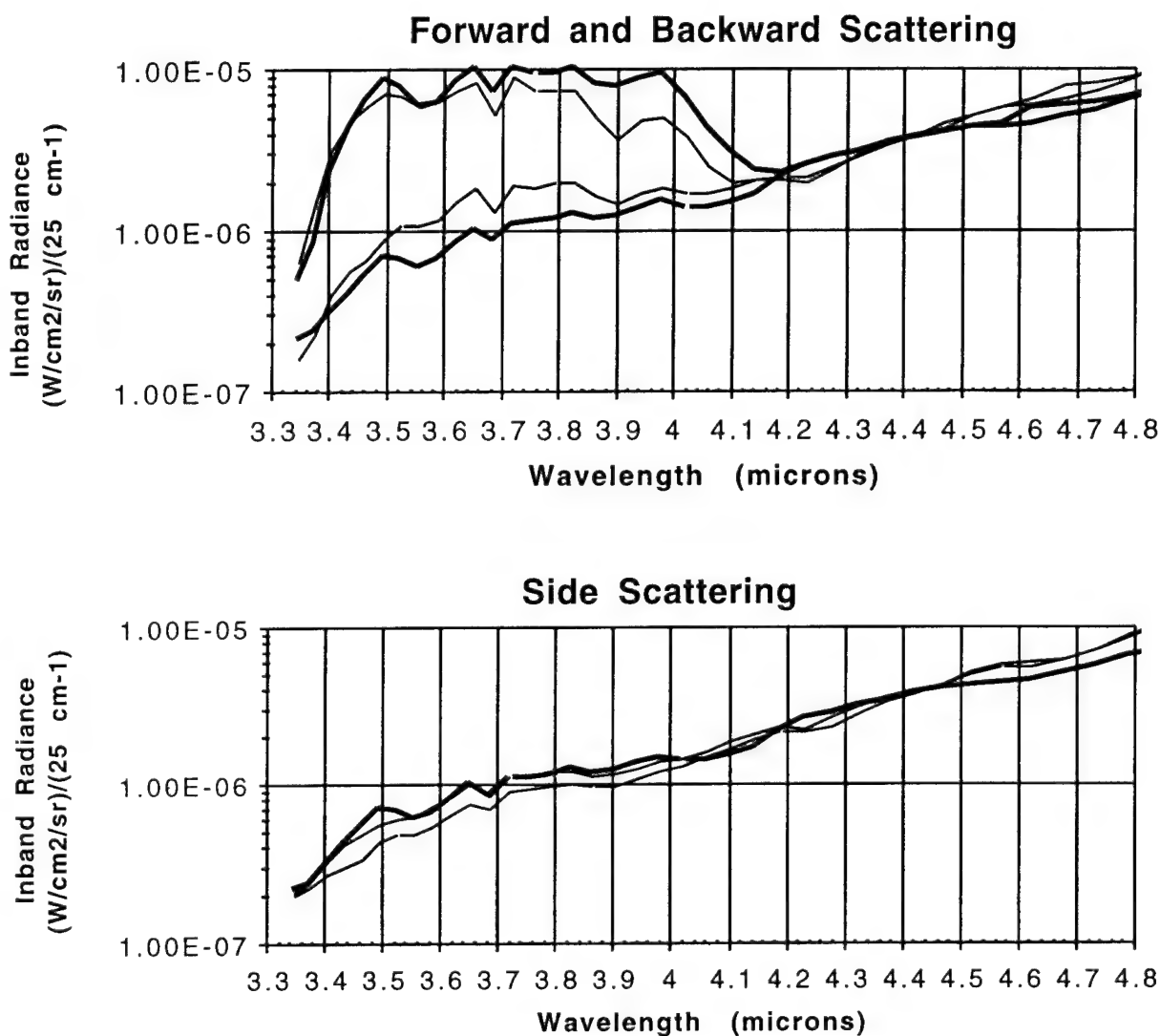


Figure 2. Comparison of CloudScape® AF predictions against aircraft measurements. Thick lines denote predictions while thin lines represent data. The scattering angle for the forward scattered case is 14.9°, and for the backscattered case it is 174.1°. For side scattering, the scattering angle is 95.2° and 96.2°.

CLOUD PHENOMENOLOGY RELEVANT TO SPACE BASED INFRARED SYSTEMS

Hsiao-hua K. Burke and J. William Snow
MIT Lincoln Laboratory
244 Wood Street
Lexington, MA 02173

CAPT David O'Donnell
United States Air Force
SMC/MTAS
Los Angeles, CA

ABSTRACT

Background phenomenology databases and models are essential for the design and operational assessment of electro-optical sensing systems. Space based infrared (IR) systems need cloud information for clutter characterization. This paper reviews cloud phenomenology relevant to space based IR systems. It also discusses how spatial, microphysical and radiative parameters of clouds are inter-related and how measurements need to be conducted to derive the necessary cloud information.

1. INTRODUCTION

Cloud phenomenology is of particular interest in the design and assessment of IR surveillance satellite systems because clouds are a major source to background clutter that the system must mitigate. Cloud databases and models provide the means for accessing the accumulated knowledge acquired from laboratory and field measurements and the associated theories necessary to extend from this limited information and characterization of clouds to the full range and detail of conditions in which sensor systems must operate.

In Section 2, an overview of the cloud parameters that are of relevance to infrared surveillance systems is presented. In Section 3, a review of cloud parameters is made. Some of their inter-relationships are illustrated. In Section 4, it is demonstrated how field measurements should be conducted to establish the understanding for system requirements. These findings are summarized in Section 5.

2. REQUIRED CLOUD INFORMATION FOR SPACE BASED IR SYSTEMS

Direct cloud information required by space based IR systems is discussed here along with the corresponding relevance. There are six key cloud parameters:

* This work is sponsored by the Air Force under Contract F19628-95-C-0002.

Cloud Top Height: This information allows for the estimate of when “cloud break” occurs during a missile trajectory as well as for quantifying the detectability of other targets. [The Conference Preprint cover illustrates cloud top detection results.]

Fraction and Spacing: For various military applications, the knowledge of cloud amount by layer and horizontal scale to characterize the background is needed.

Cloud Optical Depth: Typically, for thin clouds, optical depth information is necessary in order to retrieve information beneath such cloud.

Directional Reflectivity: For sensors operating in the SWIR, cloud bidirectional reflectivity information is required to interpret the solar component of the measured signature.

In-Band Emissivity: For IR sensors operating in the MWIR and LWIR, interpretation of the thermal component of the cloud signature is provided for.

Cloud Movement: For fast moving high altitude clouds, cloud movements need to be differentiated from “target” movements.

3. REVIEW OF CLOUD PARAMETERS

There are many cloud parameters commonly referred to. Generically they can be categorized as spatial, microphysical and radiative. Spatial parameters include number of layers, fractional coverage and spacing (length scale), top height, base height (thickness), morphology (type), and movement (horizontal). Microphysical parameters include condensed water content, particle size distribution, phase (habit) and ice particle morphology. Radiative parameters include optical depth, emissivity, bidirectional reflectance distribution function (BRDF), single scattering albedo and scattering phase function. Three spatial and three radiative parameters, identified in Section 2., are considered key for IR space sensor phenomenology.

Many of these parameters are inter-related. For example, the bidirectional reflectance distribution function (BRDF) is directly related to cloud spatial structure, atmospheric profiles through cloud, particle size distribution and particle morphology. Similarly, optical depth and emissivity are related to cloud top and base heights, particle size distribution and phase.

Figure 1 illustrates how BRDF can be obtained from measurements. Figure 2 illustrates a microphysical approach to determining cloud optical depth. Conversely as shown in Figure 3, cloud optical depth can be obtained through satellite remote sensing approaches. The understanding of this level of information need ensures that appropriate and sufficient field measurements are conducted.

4. FIELD MEASUREMENT REQUIREMENTS

Some dedicated field measurements are required to obtain the direct data product values used, for example, in the construction of realistic cloud scenes. Additionally, measured cloud physical and optical property databases can be employed to validate or modify models. In order to achieve these objectives, further field measurements may be needed to obtain "truth" data. On the mesoscale to synoptic scale, meteorological satellite data, surface and other air-borne observations are required. On the local to micro-scale, finer resolution sensors (e.g., LANDSAT) and ground based RADARs and LIDARs can establish cloud microphysical characteristics such as particle properties. Figure 4 demonstrates the data collection, analysis and product flow for a field data collection experiment.

As discussed in Section 2, there are six key cloud parameters required for space based IR systems. Here they are listed again with identified primary sources of data and models needed to adequately specify each:

Cloud Top Height: Ground based LIDAR or RADAR, meteorological satellite (window IR band).

Fraction and Spacing: High resolution and meteorological satellite imagery.

Cloud Optical Depth: Meteorological satellite, LIDAR, aircraft measurement, and models (see Figures 2 and 3).

Directional Reflectivity: Meteorological satellite and other data, plus models (see Figure 1).

In-Band Emissivity: Meteorological satellite imager or sounder (e.g. the Conference Preprint cover graphic).

Cloud Movement: Sequential satellite images.

5. SUMMARY

Space based infrared system design and operational applications needs for cloud information are identified. Cloud parameters and some of their inter-relationships are illustrated. Subsequently, measurements and analysis efforts can be defined to meet the requirements. The approach focuses on the applications of space based infrared systems so that necessary and sufficient cloud measurement and modeling steps are taken.

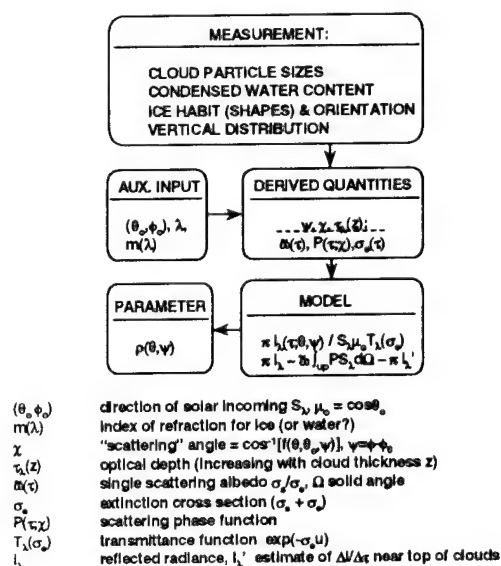


Figure 1 CLOUD DIRECTIONAL REFLECTIVITY (BRDF, $\rho(\theta, \psi)$)

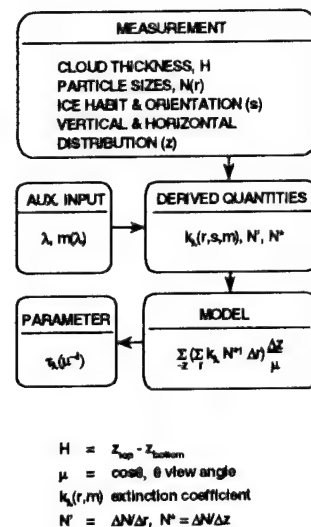


Figure 2 CLOUD OPTICAL DEPTH, $\tau_\lambda(\mu^{-1})$
- MICROPHYSICAL APPROACH -

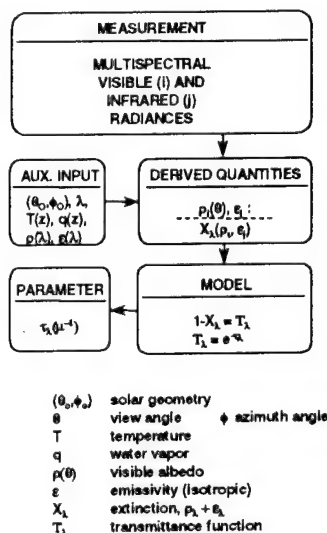


Figure 3 CLOUD OPTICAL DEPTH, $\tau_\lambda(\mu^{-1})$
- SATELLITE REMOTE SENSING APPROACH -

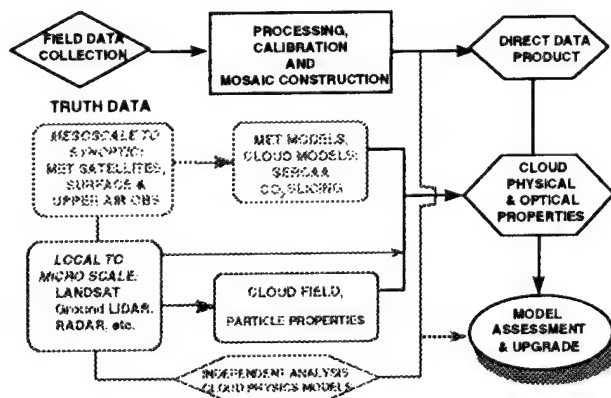


Figure 4 EXAMPLE: DATA COLLECTION, ANALYSIS, AND PRODUCT FLOW

ATMOSPHERIC CORRECTION THROUGH TRANSMISSIVE CLOUDS

J. William Snow, Hsiao-hua K. Burke, Michael P. Jordan,
Daniel C. Peduzzi, and Kristine E. Rhoades
MIT Lincoln Laboratory
Lexington, MA, 02173, USA

ABSTRACT

Surface parameter retrieval from satellite using infrared sensors is impeded by clouds. Routinely, when clouds are present retrievals are not performed. The frequent occurrence of clouds warrants investigation of possible methods to quantify and eliminate the cloud attenuation of surface radiance. Transmissive clouds, defined here as having optical depth less than 0.5, allow correctable amounts of surface radiance to emanate from the top of the atmosphere.

A methodology for diagnosing the atmospheric conditions indicative of such clouds is developed which utilizes numerical model profiles of water vapor and temperature. Mid-wave infrared (MWIR) satellite data are then reconstructed to provide accurate surface radiance using readily available atmospheric information and MODTRAN. The retrieved surface temperatures in transmissive cloud cases are encouraging - bias and rms being 0.1 K and 1.0 K.

1. INTRODUCTION

The objective of a recent Lincoln Laboratory Innovative Research Program (IRP)* is the reconstruction of surface emitted MWIR radiance in conditions of no-cloud and of transmissive cloud. The atmospheric attenuation of radiance in the MWIR by water vapor and aerosols in no-cloud conditions, and also by cloud particles in transmissive cloud cases is quantified at the resolution of the typical satellite imager (1-4 km). For the cases tested, it is demonstrated that with transmissive clouds less than 1.5 km in physical thickness, the surface radiance can be reconstructed without significant degradation in accuracy over the no-cloud cases. GOES-8 individual image pixel radiances from Ch 2 - MWIR (3.7 - 4.1 μm) are the data; in conditions of uniform thin cirrus clouds, as determined by inspection of coincident GOES visible and longwave infrared (LWIR) imagery. The IRP final report, Burke et al (1997), explains more completely the methodology.

The MWIR, broadly defined as 3-5 μm , includes absorption and window bands. Surface parameter detection commonly employs the 3.7-4.0 μm window. This MWIR window is advantageous for surface temperature retrieval in thin cloud conditions because: 1) condensed water, i.e., cloud particle absorption is less (by nearly a factor of 40) than in the 10 - 12 μm LWIR window, and 2) water vapor absorption is also less (by a factor of 50 to 100). Other advantages, which are evident from log-differentiation of the expression $L = a T^b$ (L - radiance, T - temperature), are: 3) at terrestrial temperatures the sensitivity (change in radiance \div change in temperature) is nearly 2.5 times greater in the MWIR than in the LWIR (exponent $b_4 \cong 10$, $b_{11} \cong 4$), and 4) uncertainty in the surface emissivity (contained in a) is less consequential. Disadvantages are: 1) radiation intensity at terrestrial temperatures is significantly less than in the LWIR, and 2) during daytime, the MWIR signal is a combination of thermal emission and solar reflection. But, in the aggregate, the advantages outweigh the disadvantages, especially during nighttime where transmissive clouds are present.

* Innovative Research Program principal support is from USAF Contract F19628-95-C-0002.

2. METHODOLOGY

The architecture of the MWIR correction technology is shown in Figure 1 where - proceeding upward, the attenuation by atmospheric gases and aerosols is treated - proceeding downward, the effects of transmissive clouds are evaluated - and proceeding from left to right, the actual MWIR correction is made. The sequential data processing and analysis steps are illustrated in Figure 2. Atmospheric attenuation is assessed by radiative transfer computations using the Air Force MODTRAN transmission-radiance model; this is the fundamental correction tool. Atmospheric specification (bottom Figure 1), the basic input to the computations, is obtained from routine geophysical data products, which are developed in large part from satellite sounder sources. Specifically, the NCEP 'Eta' numerical prediction model vertical profiles of relative humidity (RH) and temperature (available for 00 and 12 Z) are used.

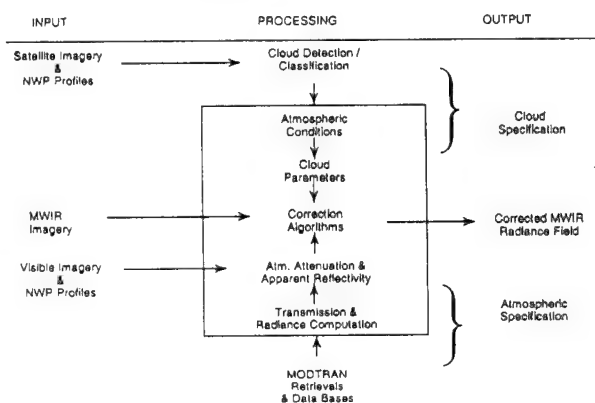


Figure 1. Architecture of the MWIR data correction technique.

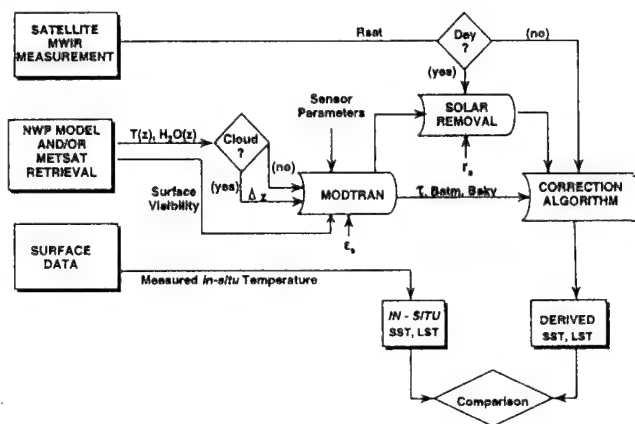


Figure 2. Data processing and analysis procedure.

Cloud specification begins with inspection of multi-channel GOES imagery and proceeds with the analysis of Eta profiles. The specification consists of two separate procedures, one diagnostic, the other analytical. Cloud presence is diagnosed using critical relative humidity RH_c expressions. First, it is found that whenever the actual RH profile remains below RH_c (%) = $(80 - 10z)$, z (km) ≤ 8 , no clouds are present in the low and middle troposphere. Second, cirrus cloud presence and physical thickness is diagnosed where actual RH exceeds RH_c (%) = $100 [C \exp (a(T-273))]$, $a = 0.00924$, $C = 0.88$, T (K), an expression taken from Liou et al (1990). Only conditions of: 1) no low or middle clouds and 2) cirrus physical thickness less than 1.5 km are considered for surface radiance correction. The cirrus diagnostic procedure is shown in Figure 3.

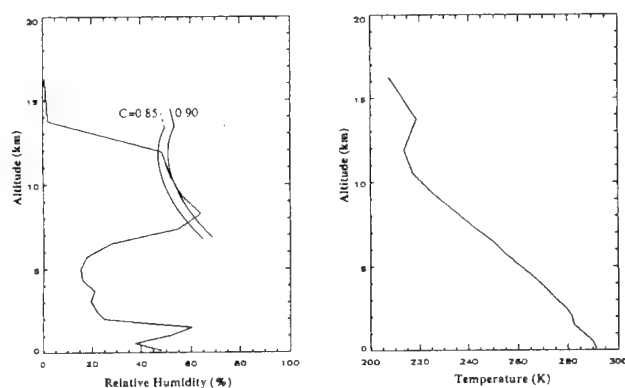


Figure 3A. Diagnostic test for vertical extent of cirrus cloud. C's for generation and sublimation.

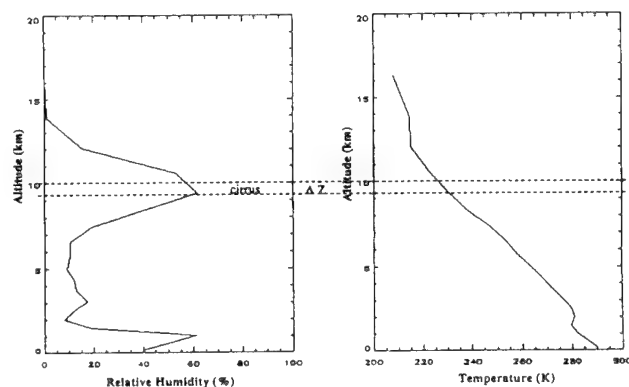


Figure 3B. Example of thin cirrus cloud. 'Eta' profiles of humidity and temperature.

Basically, three cirrus parameters are needed to quantify attenuation of radiation: the extinction coefficient β_e , the single scattering albedo ω , and the asymmetry factor g . The analysis of profile data is used in assigning these parameters. The principle parameter is β_e ; once its value is computed, the cirrus type is determined and the other needed parameter values are obtained from tabular data presented in Table 5.2, Liou (1992) and Table 1, Stone et al (1990). The ice-water-content IWC and effective spherical ice particle radius r_e are needed to compute β_e . From the extensive cirrus data presented in Table 2, Heymsfield and Platt (1984), $IWC (g m^{-3}) = \{[30.0 - 4.5 (253 - T_c)^{1/2}] \times 10^{-3}\} H$. Both of the needed atmospheric values are obtainable from Eta profiles: T_c (K), the mean cloud temperature, and $H = [(RH_m/RH_c)^3 - 0.5]$, a humidity adjustment factor with RH_m being the maximum within-cirrus RH-value. Furthermore, using $r_e (\mu m) = 10.0 + 0.5 (T_c - 213)$, then $\beta_e = IWC (a + b/r_e)$ can be computed, with the constant values taken from Table 3, Fu and Liou (1993), specifically, $a = -6.656$ and $b = 1843.0$ within the MWIR window band.

The basic correction algorithm is contained in Figure 4. There are 3 types of radiation emanating from the top-of-atmosphere and constituting the infrared satellite measured radiance R_{sat} . These are surface emitted radiance - the signal which is to be corrected, radiance emitted by atmospheric constituents, and radiance downward-directed from the sky, reflected by the surface and attenuated en-route back out through the atmosphere in the satellite line-of-sight direction. Within the LWIR these 3 types are the measured quantity day or night. But in the MWIR, in daytime, two additional components of solar origin are included - surface reflected and atmospherically back-scattered solar MWIR radiance. During the daytime R_{sat} is reduced by the magnitudes of these components, using MODTRAN, before the retrieval of surface temperature is made.

Typically, in the MWIR and with atmospheric conditions of no-cloud and nominal aerosol load, the relative magnitudes of the components incident on a satellite sensor, $B_s:Batm:Bsky$, shown in Figure 4, may be in the proportions $\sim 90:10:2$. For thick (totally opaque) cloud conditions, the proportions become $\sim 5:95:1$, an uncorrectably small surface signal. A thin cirrus case may have proportions $\sim 60:40:2$, versus the LWIR proportions $\sim 40:60:2$ under similar cloud conditions - evidently, correction is more feasible in the MWIR. MODTRAN computes the path transmittance τ , as well as the downward sky irradiance and upward atmospheric path radiance. Surface emissivities are obtained from various databases. It is worth noting that the correction algorithm is equally applicable to surface emissivity retrieval if surface temperature is otherwise known.

$$B_s = \frac{R_{sat} - (1 - \epsilon_s) \tau B_{sky} - B_{atm}}{\epsilon_s \tau}$$

$$T_s = \text{Planck}^{-1}(B_s)$$

WHERE $R_{sat} (\text{Night}) = \text{SATELLITE MEASURED SPECTRAL RADIANCE}$
 $R_{sat} (\text{Day}) = \text{MEASURED RADIANCE} - \text{SOLAR COMPONENTS}$
 (atmospheric scattering & ground reflection)
 $T_s = \text{SURFACE TEMPERATURE}$
 $\epsilon_s = \text{SURFACE EMISSIVITY}$
 $B_s = \text{CORRECTED SURFACE SPECTRAL RADIANCE}$
 $\tau = \text{GROUND - TO - SPACE TRANSMITTANCE}$
 $B_{sky} = \text{DOWNWARD SKY SPECTRAL RADIANCE}$
 $B_{atm} = \text{UPWARD ATMOSPHERIC PATH RADIANCE}$

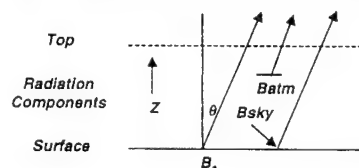


Figure 4. MWIR correction algorithm utilized.

3. RESULTS

During this program more no-cloud cases (47) were processed than transmissive cloud cases (16). The results for both conditions are given in Figure 5. The no-cloud bias (-0.14 K) and rms (0.54 K) statistics for nighttime ocean surface temperatures, 32 cases, are excellent. Because of the limited number of transmissive cloud cases, the results for nighttime ocean (7), nighttime land (5), and daytime ocean (4) are combined. The range of measured surface temperatures is greater than 20 C. The bias (-0.14 K) and rms (1.04 K) are encouraging, in spite of the small sample size. As a sensitivity analyses, the same processing was carried out for the nighttime ocean transmissive cloud cases using the coterminous GOES 10.5 and 11.5 μm LWIR pixel

data instead of MWIR data. The resulting bias and rms are: 1.70 K and 2.04 K for 10.5 μm , and 2.26 K and 2.62 K for 11.5 μm data. Clearly, even modest numbers of ice crystals strongly affect radiative transfer in the LWIR. Although effective in the MWIR, the relatively elementary method applied here does not adequately reconstruct surface radiance in the LWIR when thin cirrus clouds are present.

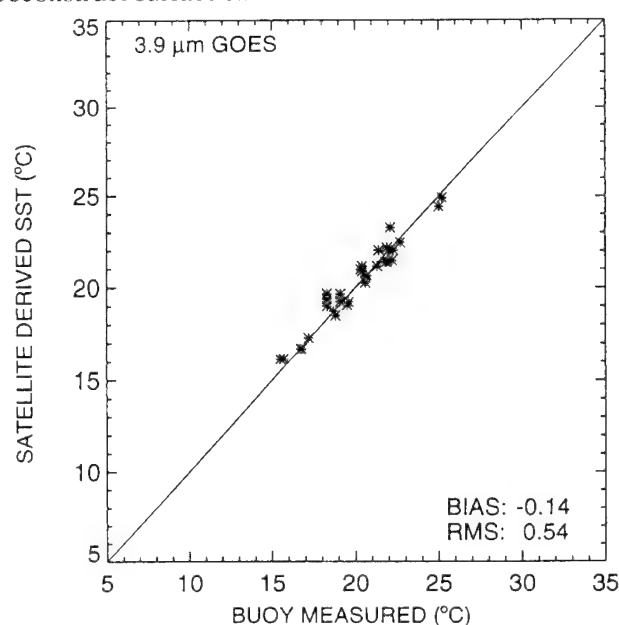


Figure 5A. Surface temperature retrieval results for 32 night, ocean, no-cloud cases.

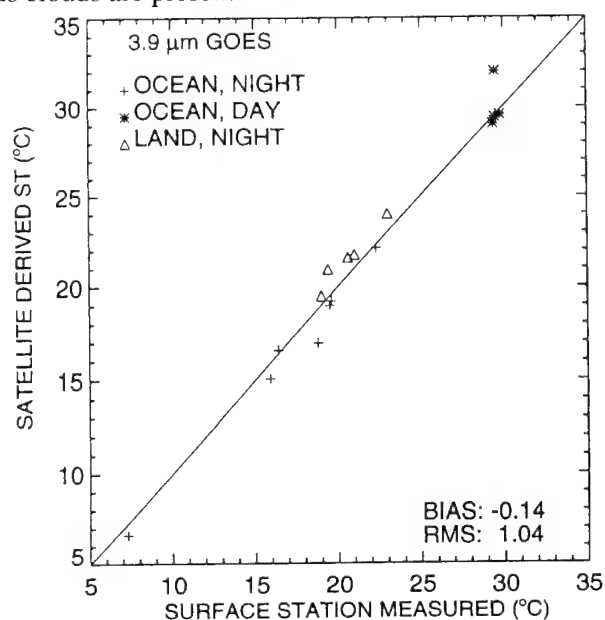


Figure 5B. Surface temperature retrieval results for all transmissive cloud test cases.

4. CONCLUSIONS

A surface radiance retrieval algorithm for the MWIR is developed (Figure 4), the accuracy of which is enhanced by using existing NOAA operational products (Eta output) combined with state-of-technology radiative transfer modeling (MODTRAN Report 1996). A methodology for determining the presence, physical thickness, and optical properties of thin cirrus is also proposed based upon documented cloud properties and local profiles of water vapor and temperature. The results, i.e., the surface temperatures computed from reconstructed MWIR radiances in these transmissive cloud cases, are encouraging - bias and rms of 0.1 K & 1.0 K.

5. REFERENCES

- Burke, H.K., J.W. Snow, J.P. Kerekes, M.P. Jordan, K.E. Rhoades, C.A. Upham, D.C. Peduzzi, 1997. MWIR Atmospheric Correction Experiments. Project Report IRP-20, MIT Lincoln Laboratory, Lexington, MA, 66 pp.
- Fu, Q., and K.N. Liou, 1993. Parameterization of Radiative Properties of Cirrus. *J. Atmos. Sci.*, 2008-2025.
- Heymsfield, A., and C.M.R. Platt, 1984. A Parameterization of the Particle Size Spectrum of Ice Clouds in Terms of the Ambient Temperature and Ice Water Content. *J. Atmos. Sci.*, 846-855.
- Liou, K.N., 1992. *Radiation and Cloud Processes in the Atmosphere*. Oxford Univ. Press, NY, NY, 487 pp.
- Liou, K.N., Y. Takano, S.C. Ou, A. Heymsfield, and W. Kreiss, 1990. Infrared Transmission Through Cirrus Clouds: A Radiative Model for Target Detection. *Appl. Optics*, 1886-1896.
- MODTRAN Report 1996: The MODTRAN 2/3 Report and LOWTRAN 7 Model. Contributing authors: Kneizys, F.X., et al. Phillips Laboratory, Geophysics Directorate (GPOS), Hanscom AFB, MA, 261 pp.
- Stone, R.S., G.L. Stephens, C.M.R. Platt, and S. Banks, 1990. The Remote Sensing of Thin Cirrus Cloud Using Satellite, Lidar, and Radiative Transfer Theory. *J. Appl. Meteor.*, 353-366.

The Fractal Behavior of Cloud Systems¹

**Kenneth E. Eis, John M. Forsythe, Donald L. Reinke
Cooperative Institute for Research in the Atmosphere
Foothills Campus, Colorado State University
Fort Collins, CO 80523**

ABSTRACT

The DOD and other agencies interested in cloud simulations have used fractal-based synthetic cloud generators since Lovejoy (1982) showed the fractal behavior of clouds. Fractal generators are attractive because they allow control of the synthetic cloud's statistical moments. Simulated scenes can be produced at a variety of scales with two seed numbers: the fractal dimension, and the mean cloud cover. This paper analyzes the temporal and spatial behavior of the fractal dimension of cloud systems of scale sizes from 1280 km to 10 km. The variations in the fractal dimension over time and space will be shown to be significant and must be considered by the simulations community.

BACKGROUND

Clouds, like many other natural features, can be artificially rendered using fractal methods. Simulators are currently being developed that create individual clouds with realistic radiative properties that make them invaluable to engineering and sensor development. Caution should be taken however when the use of fractal methods is scaled up to the generation of cloud systems. Just as cloud cover probability can't be reasonably assumed to be the same over large areas of the earth, the fractal dimension of cloud systems can not be assumed constant for large areas or for long periods of time. Our analysis used the CHANCES database Reinke (1995) to perform a fractal analysis for a large portion (Equator to 30N) of the Northern Hemisphere for June and July, 1994. The analysis used the Box Counting technique to determine the fractal dimension for areas within the region composed of 256 by 256 cloud/no cloud pixels. Each pixel was a 5 by 5-km area taken from the CHANCES constant area nephanalysis database. Since the radiance data was also available from the CHANCES data, a cloud/no cloud analysis for three different cloud top temperatures were computed (253, 263, and 273 degrees K). Approximately 1600 hourly domains were interrogated for fractal dimension for this two month period.

ANALYSIS

The resulting fractal analysis was analyzed by fitting the points generated from the Box Counting technique. The resulting 6 data points are plotted on a log-log plot and a least squares fit applied. The resulting slope is the fractal dimension for the 256 by 256 domain. In addition to the total fit the data was also broken into two data groups, the top including the top three data points and a bottom group containing the smallest three scale sizes. A least square fit for each of these groups is again applied. The subsequent slopes were then filtered by their R^2 regression fit.

¹ This work is sponsored by the Center for Geosciences Phase II under grant DAAH04-94-G-0420

RESULTS

Figure 1 shows the variation in fractal dimension of the total region. Each pixel in this figure is the 256 by 256 analysis domain.

Figure 2 shows a scatter diagram of cloud cover percentage vs fractal dimension for each of these domains. All three temperatures showed the same signature. This scatter plot shape is a significant finding for the fractal simulation researcher in that it bounds the fractal dimension with cloud cover percentages.

Figure 3 shows the temporal variation for an area off the Florida coast for a period of 500 consecutive hours. The fractal dimension dependence with cloud cover percentage is clearly evident.

Figure 4 is the scale break. These values were determined by using the high and low least squares fit values and computing the intersection of the two lines (fractal dimension slopes). Only values where the R^2 regression = 1.0 were used in these computations so natural scatter in the plots were avoided. A scale break (if one was found) is significant in that the fractal dimension changes value and the scale break length.

CONCLUSIONS

- Cloud system fractal dimensions vary considerably with space and time. Average fractal dimensions can't be used for large temporal or spatial regions. (New results are encouraging that show fractal dimensions having a strong functional relationship to mean cloud cover for limited times and areas)
- Fractal dimensions for cloud systems vary with cloud top temperature. This verifies that clouds are multi-fractal.
- Fractal dimension values are bounded by an envelope that is functionally dependent upon the cloud cover percentage. This finding will allow fractal cloud scene generators to be run more efficiently.
- A majority of the 1280 by 1280 km areas analyzed exhibited scale breaks in their fractal dimension. The breaks predominated at scales less than 97 km. This size is significant (twice the RTNEPH pixel size) because any determination of fractal dimension based on a database of 47 km resolution or larger would only see the larger scale size fractal dimension. If that fractal dimension were to be used to extrapolate to smaller cloud features, and fractal scene generators were used to produce clouds at sizes smaller than 97 km, the scenes may give inaccurate results

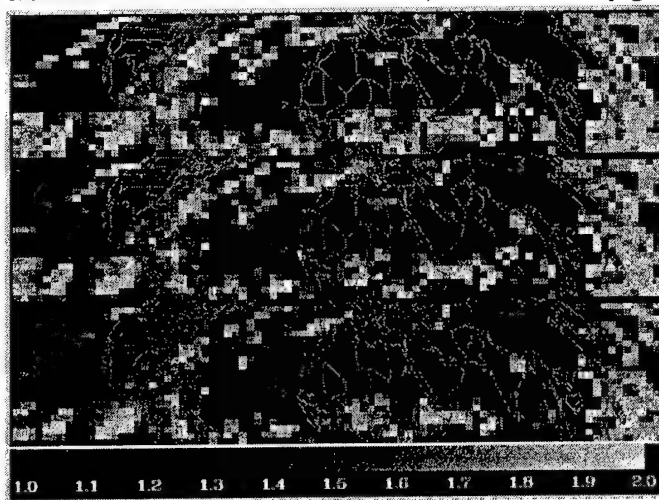


Figure 1 – Fractal Dimension analysis of 1280 by 1280 km pixels for cloud top temperatures of 273, 263, and 253 degrees Kelvin. Grey scale represents the dimension. Note that the fractal dimension varies significantly in space.

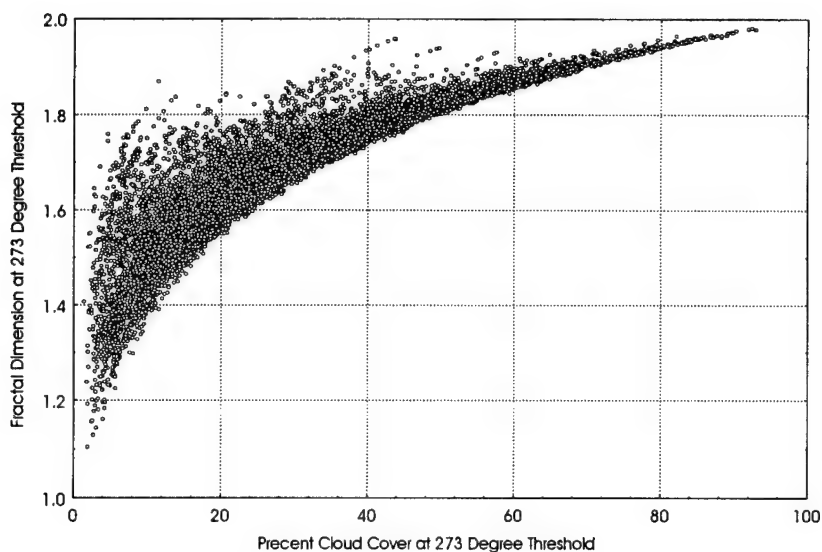


Figure 2- Plot of mean cloud cover vs Fractal Dimension at images at 273 degree cloud top temperature

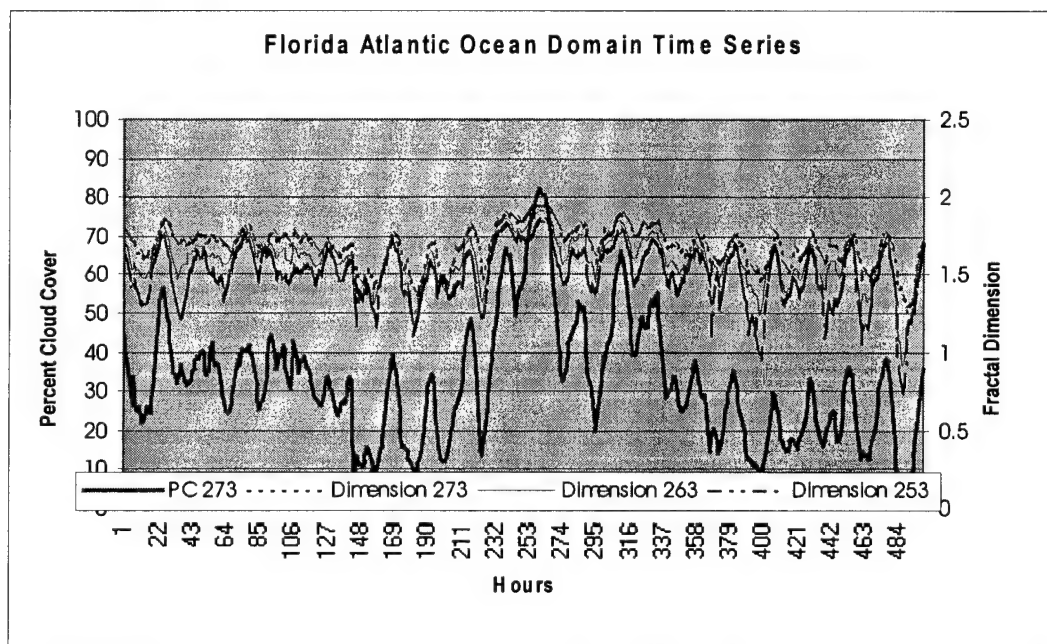


Figure 3 – Temporal variation of fractal dimension for one 1080 by 1280 domain off the coast of Florida for a 500 hour period.

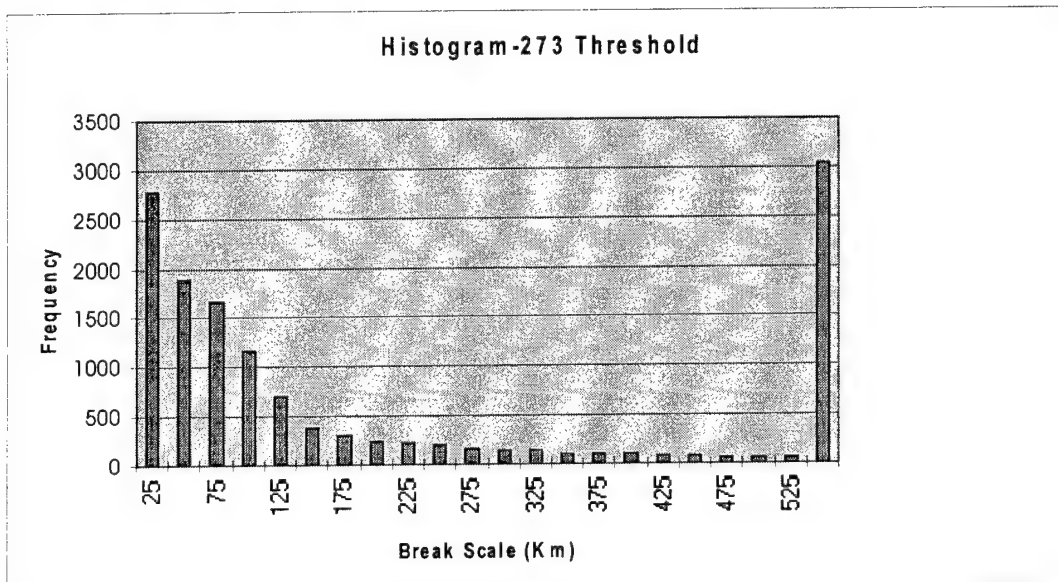
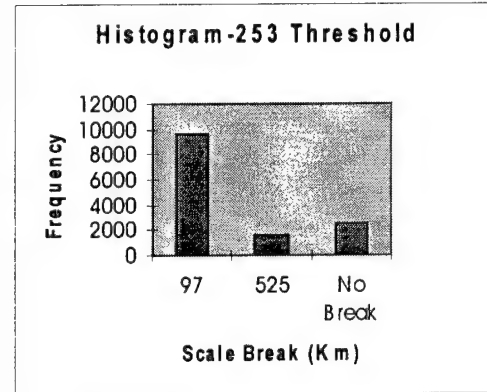
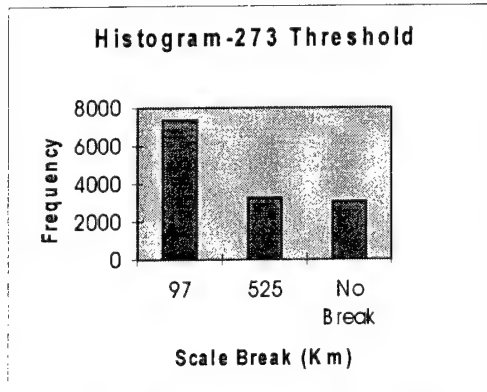


Figure 4 – Scale break distribution for the 273 and 253 degree cloud top temperature fractal slope analysis

A METHOD FOR CALCULATION OF NEAR-HORIZONTAL CLOUD FREE LINE OF SIGHT PROBABILITIES

Eric L. Strobel and Dwayne Pribik
Schafer Corporation
Arlington, Virginia, 22209

ABSTRACT

Cloud databases derived from satellite and ground observations contain statistics such as percent cloud coverage per altitude band. The data are provided in cells having standard width, depth and height. Such information is difficult to utilize when determining probability of cloud free line of sight (PCFLOS) statistics along near-horizontal paths. An algorithm has been developed for performing these calculations. A Monte Carlo calculation is performed, producing a tabular function, $P(x,d)$, for PCFLOS through a single data cell. $P(x,d)$ is related to the percent cloud coverage in that cell (x) and the normalized horizontal path length through the cell (d). The PCFLOS between two locations (for example, between two aircraft) may then be built up by progressing along the line of sight through the cells in the dataset, accumulating the contributions from each cell. The details of the algorithm are presented. A computer code implementing the algorithm is discussed. Results from several example calculations are also given.

INTRODUCTION

This work was prompted by examining an airborne IR sensor system for observation of objects aloft, and possibly on the ground. The operation of such a system requires lines of sight which are not blocked by clouds. The design of these sensor systems requires an estimation of the probability of cloud-free line of sight (PCFLOS). Furthermore, such an estimation must be grounded in actual data.

First, existing approaches to computing PCFLOS were examined. These approaches are typically oriented toward near-ground to satellite paths. Calculation of near-horizontal PCFLOS is possible in some cases by differencing two appropriately chosen paths, but this is inconvenient and it would be difficult to embed such calculations into another code. The decision was therefore made to develop a new algorithm.

Attention turned to selecting an appropriate dataset. Initially, the SAGE II dataset¹ was considered because the data were taken horizontally, making them more sensitive to clouds with small optical depths. However, the SAGE II data are relatively sparse spatially and temporally. In addition, the SAGE II transmittance profiles often cut off (are completely blocked) at altitudes higher than potential airborne viewing platforms. These issues led to consideration of RTNEPH² and HIRS.³ These datasets are more voluminous in geographic and temporal coverage. These data are provided as percent cloud cover in each 3-D bin. This reduces the problem to interpreting such data to obtain PCFLOS for a near-horizontal path.

The details of an algorithm providing such an interpretation of the data are discussed in the following section. A simulation applying the algorithm is then described and some sample results are presented. The last section summarizes the work and discusses future directions.

ALGORITHM

The data in RTNEPH or HIRS are delimited by geographic location and altitude where the horizontal dimensions of a data cell are much greater than the vertical dimension. This leads to data cells in a 'pizza box' shape. We can take advantage of this and reduce the problem to a two dimensional traversal of a square, utilizing the cell's data value (% cloud) and the path length through the cell to provide a function for the probability of successfully traversing the cell. These single cell values may then be used to build the PCFLOS for the path from the sensor to the object.

The single cell PCFLOS function is denoted as $P(x,d)$, where $x = \% \text{ cloud cover}$ and $d = \text{traversal distance}$. The distance d is normalized to the cell horizontal dimension. The range of x values are $0 \leq x \leq 100\%$, with the boundaries representing no blockage and total blockage. The range of d values are $0 < d \leq \sqrt{2}$, where the bounds are 'nicking' the corner and following the diagonal.

$P(x,d)$ is constructed by a Monte Carlo process in which a large number of paths are taken across a box which is randomly filled with $x\%$ cloud. A conservative assumption made is that the cloud is totally opaque. This eliminates the need to obtain extra cloud information, such as cloud type or optical depth.

The base grid size is comparable to the thickness of the original 'pizza box.' This is consistent with the cloud opacity assumption since vertical detection of cloud in an altitude bin is equivalent to stating the vertical line of sight stopped in that bin. The cloud is formed on this grid by randomly selecting a seed point. The cloud grows from this seed with its nearest neighbors becoming part of the cloud with some high probability. A point from the edge of this cluster is randomly chosen and its nearest neighbors which aren't yet part of the cloud join the cloud with the above probability. A 'snapshot' of the process is illustrated in Figure 1 for the upper right hand corner of the grid. Iterations continue until the box is covered to $x\%$, wrapping at the box edge as necessary. The resulting set of points is visually cloudlike.

The paths across the box are taken as follows. A large number of points are equally spaced on each side of the box. The points and sides are sequentially numbered. Paths are then traced from all points on one side to all points on the other three sides. The geometry of any path is algebraically expressible in terms of the point number along the side and the side number. This allows easy computation during the Monte Carlo function generation process. The number of path endpoints on each side was chosen to be ~ 2.5 times the number of grid points to avoid any lattice periodicity sampling effects. This is depicted in Figure 2 on a simplified 3×3 grid, with a few example paths shown.

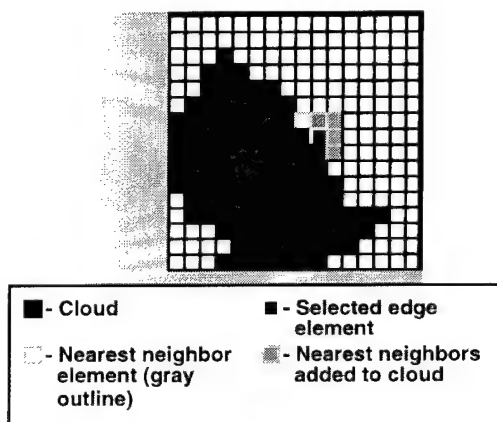


Figure 1. Cloud generation example.

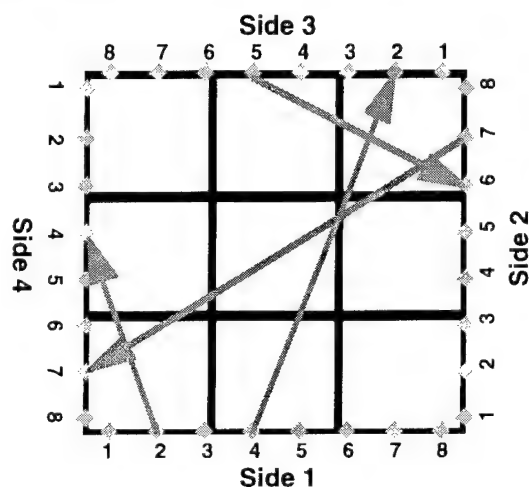


Figure 2. Path generation example.

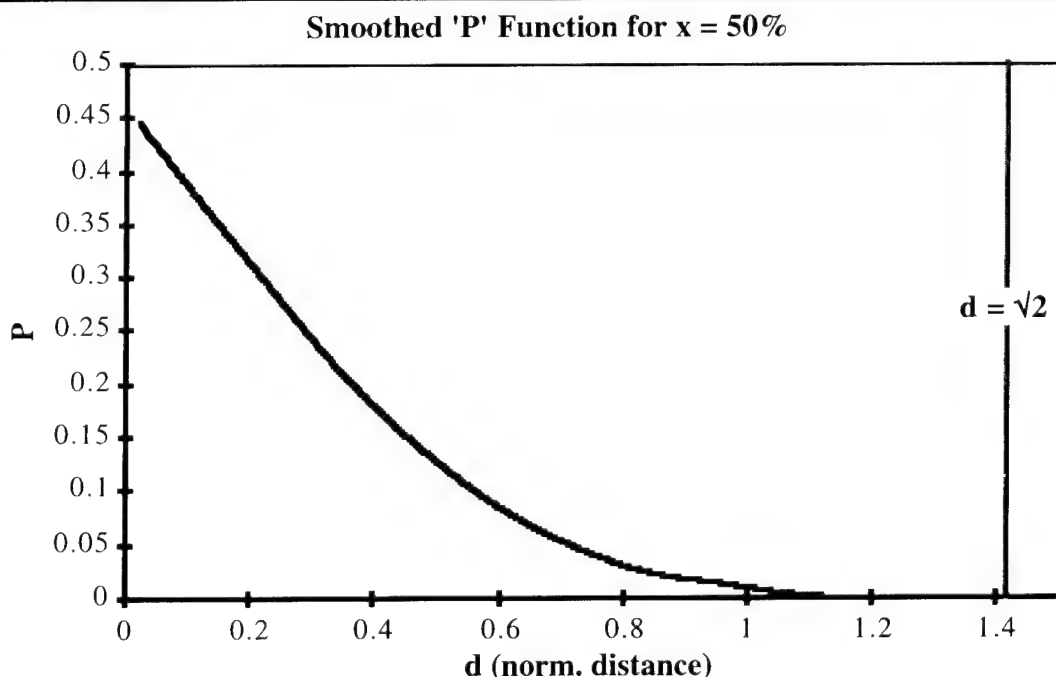


Figure 3. An example of $P(x,d)$ for $x = 50\%$.

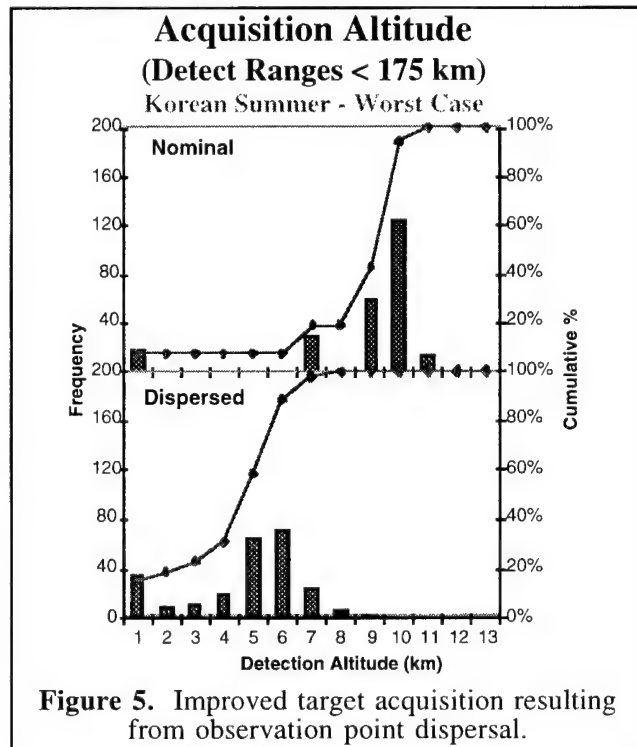
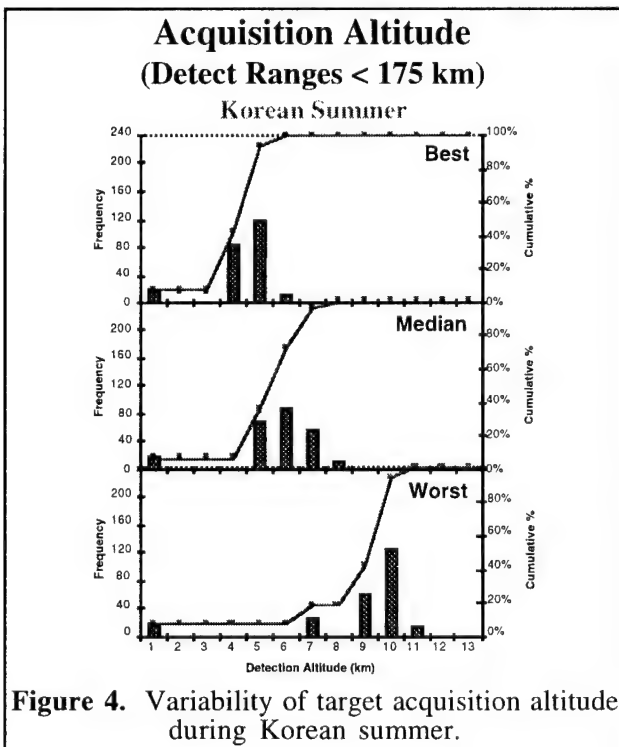
$P(x,d)$ may now be produced. At increments in x of 2%, a cloud is generated to cover the appropriate percent of the box. Every path, i.e., all paths originating on side 1 to all other sides, then all paths from side 2 to all other sides, etc., is tested for blockage. The results are recorded. A new cloud is now randomly generated and the process repeats until the chosen number of Monte Carlo iterations are performed. The results are constructed into a histogram showing the fraction of paths successfully traversing the cell for each path length. This histogram is a slice of the $P(x,d)$ function at constant x .

For a reasonable number of Monte Carlo iterations, the histogram goes to $P \sim x$ for $d \rightarrow 0$, falling off at larger d . The histogram, though, is fairly 'noisy.' Since this is simply a geometry and probability problem, it should be possible to derive P analytically, resulting in a smooth P . Failing such a derivation, the approach taken is to numerically smooth the histogram (Figure 3). The family of smoothed histograms for all x values forms the look-up table which is $P(x,d)$.

Given P , the PCFLOS for the full path from sensor to object is calculated as follows. If the object is above the sensor's horizon, the path is traced until a boundary between data cells is crossed. The distance traveled through the cell just departed is normalized and used as d in the look-up to determine that cell's P value. This operation is done in three dimensions and the full distance is used, as opposed to the horizontal component of the distance. In the rare instance that $d > \sqrt{2}$, the look-up value for $d = \sqrt{2}$ is used. The cell's x (% covered) value and d are then used to look-up P for that segment. The PCFLOS along the path may then be accumulated by multiplying the P values from each segment.

APPLICATION

The PCFLOS algorithm was integrated into a preliminary simulation code for testing purposes. The targets follow Earth-centered inertial trajectories which are polynomial in time. These are pre-computed and assembled into input files for the simulation. The user must specify the latitude, longitude and altitude of the (fixed) sensor platforms, as well as the year, date, time, and values of some control variables (such as the minimum acceptable PCFLOS for a path, typically 90%). Lastly, provision is made to 'batch' a number of runs, permitting the examination of PCFLOS over a range of dates and the averaging of results over a number of years. The simulation has not yet been cross-checked against other simulations or actual data, therefore results of this code should be considered estimates. The results should be useful in examining trends. Two examples of the use of this code follow.



The geographic region chosen for these examples is the Korean peninsula. This locale is of interest not only politically, but climatologically, due to the summer rainy season. For these examples, several hundred objects following vertically ascending trajectories were observed by a number of airborne

platforms at 20 kilometers altitude (chosen to be well above any clouds). The RTNEPH database was used. Each season was sampled at 5 day intervals, making a total of 13 trials per season. Each trial represents an average over six years of data.

The first example demonstrates the wide variety of conditions during the summer. For this case, the sensor platforms were clustered into groups of two or three in an area smaller than a data cell. Three such groups were placed in the area of interest, with separations of several cell sizes. This permitted probing the effects of spatial diversity at small (\sim cell size) and large ($>$ cell size) scales. The results, shown in Figure 4, are for the entire set of observation points. Detection is declared if any observation point has a PCFLOS to the object $> 90\%$. In the figure, the best, worst and median days are the six year averaged trials having the lowest, highest and median values of mean target acquisition altitude, respectively. Possible detection ranges were limited to 175 kilometers. Figure 4 shows that systems operating in Korea must deal with target acquisition altitudes which may vary by about a factor of two.

The second example is an outgrowth of the first. Upon examining the details of the previous example, it appeared that increasing sensor dispersal would improve results. This makes sense, as typically high cloudiness is somewhat localized. Increasing the spatial diversity of the observation points increases the probability that one of these points can view past the edge of the high, blocking clouds. Figure 5 depicts the drastic detection altitude improvement yielded by increasing spatial diversity. The 'nominal' case corresponds to the 'worst' case from the Figure 4. These examples show that the simulation is capable of supporting useful system-level comparisons.

CONCLUSIONS

An algorithm for utilizing percent cloud cover data to determine near-horizontal probabilities of cloud free line of sight has been presented. The algorithm should be easily implemented on any computer capable of handling the underlying cloud dataset. Furthermore, the algorithm is modular and may readily be embedded in a larger system simulation. This method is shown to be capable of supporting some qualitative analyses. Use of this method in a preliminary analysis tool has exposed areas in which the implementation may be improved. These are being pursued. This algorithm is presently being integrated into an architecture assessment code. Lastly, approaches for verification are being looked at.

ACKNOWLEDGEMENTS

The research in this paper was carried out with funding from the BMDO Surveillance and Interceptor Technology Directorate. The authors are indebted to Larrene Harada for her invaluable discussions and explanations.

REFERENCES

1. L. E. Mauldin, N. H. Zaun, M. P. McCormick, J. H. Guy, and W. R. Vaughn, "Stratospheric aerosol and gas experiment II instrument: a functional description," *Opt. Eng.* **24**, 307-312 (1985).
2. T. M. Hamill, R. P. D'Entremont, and J. T. Bunting, "A Description of the Air Force Real-Time Nephanalysis Model," *Weather and Forecasting*, Vol. 7 #2, 288-306 (1992).
3. Wylie, D. P., W. P. Menzel, H. M. Woolf, and K. I. Strabala, "1994: Four Years of Global Cirrus Cloud Statistics using HIRS," *J. of Clim.*, 7, 1972-1986.

A RELOCATABLE CLIMATE WINDOW FOR GENERATING CLOUD SCENARIOS INCLUDING STRUCTURE AND PHYSICAL ATTRIBUTES

Albert R. Boehm
Hughes STX Corporation
2501 Ermine Drive
Huntsville, AL 35810

ABSTRACT

The object is to produce a computer representation of the climate variables needed for propagation for any region. Standard climatological data sets, e.g. upper air temperatures, dew points, and pressure heights, are input as well as specialized data sets such as CFLOSA which specifies the probability of clouds at altitude. The Crane or alternately the Tattleman model is used to specify rain rates.

1. INTRODUCTION

Calculation of electro-optical propagation requires a set of physical variable to be specified along a ray. Cloud and rain droplet distributions are an important part of this set but also are the most variable. However, it is desirable for all of the required variables to be readily available in a compact climatological data set. By climatological the meaning is that, not only are individual means available, but the complete distribution of each variable is specified along with its correlation with other variables. Furthermore, such a data set is needed if Monte Carlo simulation of the variables is to be realistic.

2. DATA

A program called WXFit inputs several standard and special data sets to produce a site specific data set. The site is located in a latitude/longitude region known as the site window. Typically this window is 100 by 100 km and has homogeneous climatology although two or more separate climate regimes may be specified. The output of WXFit is the climatology for the window in a standard format called V2 which includes upper air, surface, cloud, and rain climatology.

2.1 Data Inputs

Means and standard deviations by month of upper air winds, temperature, dew points, and pressure heights are obtained from the GUACA (Global Upper Air Climatic Atlas) which is available on CD-ROM. Surface values are obtained from International Station Meteorological Climate Summary which contains over 6000 stations and is also available on CD-ROM. This data is by month and time of day.

2.2 Rain Rates

Rainfall rates are from Crane's Revised Two Component Model which provides rain rate and droplet distributions in 12 regions that cover the earth. Crane also provides droplet distributions and spatial correlation between rain cells. Optionally, if local tuning is desired, Tattleman's² rain rate model can be selected.

2.3 Cloud Data

Cloud information is inputted from a special version of CFLOSA³ which provide correlation parameters as well as cloud climatology at a point. Parameters include sky dome mean correlation, large scale (~300km) correlation, and probability of cloud in the vertical. These parameters along with the vertical and horizontal statistics found in deBarry and Moller³, Matveev⁴, and Willand and Boehm⁵ specify the vertical and horizontal structure of clouds in the region including cloud layers, cloud spacing, and droplet distributions.

2.4 Sufficiency

Are the above input data sets sufficient to specify the electro-optical climatology for a region? The answer is yes and no. With two exceptions, all of the major physical values needed to calculate transmission are specified by their climatological distributions as well as their spatial structure. The two exceptions are aerosols and optical turbulence which are planned for later versions but are not included in the present V2 version. Furthermore, none of the distributions or spatial structure specifications are known with great precision. Part of the problem will be solved by more and better data sets. But it is the nature of the atmosphere to be variable and variable on all scales. For example, the liquid water content in cumulus has been measured to vary three orders of magnitude!

3. USAGE

The output of the virtual climate generator is a site specific file including all the required parameters needed to calculate propagation. Depending on the application, these files can be used with PLEXUS, MODTRAN, FASTRAN, or other propagation codes to calculate transmission. However, their main use is to provide the basis for simulating virtual weather scenarios with the proper frequency of occurrence for a particular area, month, and time of day.

4. ACKNOWLEDGMENTS

This work was supported in part by the Geophysics Directorate of the Phillips Laboratory with Mr. Donald D. Grantham and Dr. Joel Moser as contract monitors under contract number F19628-93-C-0051 and by the US Army Space and Strategic Defense Command with Chuck LaMar as project leader.

5. REFERENCES

1. Crane, Robert K., 1996: *Electromagnetic Wave Propagation Through Rain*, John Wiley & Sons, New York.
2. Tattleman, P., Larson, K.P., Mazzella Jr., A. J., 1995: A climatology Model fro 1-minute Precipitation rates, *J. Applied Met.*, **34**, No. 5, 1020-1027.
3. deBarry, E., and Moller, F., 1963: The vertical distribution of clouds, *J. Appl. Meteorol.*, **2**, 806-808.
4. Matveev, L.T., 1984: *Cloud Dynamics*, D.Reidel Publishing Co. Boston, MA, p235-239.
5. Willand, J. and Boehm, A., 1995: Vertical Cloud Layer Statistics derived from echo intensities received by a 35-GHz Radar, **PL-TR-95-2034**, Phillips Lab., Hanscom AFB, AD A294 826.
6. Boehm, A., 1997: The CFLOSA (Cloud-Free Line-Of-Sight Aloft) PC program, CIDOS-97 Preprint, STC Corp.

DENSE CLOUD RADIATIVE TRANSFER SCENARIOS AND MODEL VALIDATION

David H. Tofsted
U.S. Army Research Laboratory
White Sands Missile Range, NM 88002-5501, USA

Sean G. O'Brien
Physical Science Laboratory
Las Cruces, NM 88003, USA

ABSTRACT

The BLITS (boundary layer illumination and transmission simulation) three-dimensional (3-D) radiative transfer model has been compared to a sequence of cloud scattering scenarios developed to test the reliability and accuracy of the model under varying 3-D cloud conditions. The model performs extremely well (0.7 percent RMS error) at the highest resolution, where the modeled cloud cell geometry is sufficient to resolve the density differences between separate clouds. Single axis optical depths per cell were allowed to vary from less than one up to 64.

INTRODUCTION

The Battlefield Environment Division of the Army Research Laboratory's Information Science and Technology Directorate has been developing three-dimensional radiative transfer (RT) models in conjunction with efforts to characterize near surface propagation conditions. Among the models developed is the boundary layer illumination and transmission simulation (BLITS). This model is a possible candidate for upgrading the BLIRB (boundary layer illumination and radiation balance) model currently used in the WAVES (weather and atmospheric visualization effects for simulation) modeling suite. BLITS has been tailored to better treat 3-D dense natural cloud conditions,¹ since partly cloudy skies can have marked impacts on visual systems performance via illumination variations, affecting limiting path radiance, sky-to-ground ratio, and other measures used in determining systems performance.² Illumination can also be integrated across the ultraviolet (UV) to near infrared (IR) to determine the net solar loading on the surface as a function of position. Solar loading affects the surface energy budget, thereby impacting infrared systems performance. A typical sample scene based on the output of the BLITS model is seen at figure 1.

Though it is believed the BLITS model performs well for virtually all radiative transfer scenarios, it was necessary to determine the degree of accuracy of the model under stressing conditions. To gauge this performance BLITS was initially compared to computed scattering scenario results derived from open literature materials. However the available scenarios were limited to cases where the scattering volume was uniformly filled with scattering material. These scenarios were processed using standard Monte Carlo techniques in which the scattering properties of the material were prescribed prior to the numerical experiment. The experiment itself then consisted of randomly passing 'photons' into the material and determining the statistics of which cell walls the photons exiting the material were passing through. In the most well known of these experiments, McKee and Cox³ determined the mean statistics of photons exiting through the top, base, and collectively through the sides of uniformly filled cubical model volumes. Incident photons were set to enter the volume from either the top or the east wall from a plane parallel incident light source. Data were collected for a sequence of three zenith angles for the incident energy (0°, 30°, and 60°), where the 0° incident energy entered only the volume's top face, and the remaining scenarios saw energy entering only the top and eastern wall of the volume. The density of the media was varied for each of these three scenarios.

The BLITS model was first tested against the McKee and Cox uniform cloud scenario results.³ However, the best test of a 3-D model is truly 3-D density variations. Also some means of testing the reasonability of the Monte Carlo model itself was necessary. It was thus decided that the McKee and Cox scenarios would form a limiting case for the 3-D scenarios developed.

SCENARIOS USED

To extend the original uniform cubical cloud comparison data set of McKee and Cox scenario computations, the original scattering volume was reapportioned such that the same amount of scattering aerosol material as in the original scenarios was concentrated in 8 cubes placed in the corners of the modified scattering volume. The modified concentration was parameterized by the factor P ($0 < P < 1$). $P=0$ means all the aerosols are infinitely compacted at the 8 corners of the cubic volume. Of course, this also implies that the aerosols have a zero cross sectional area to the incident radiation, and thus $P=0$ equates to a vacuum scattering condition. On the other hand, $P=1$ implies the aerosols are uniformly distributed and equates to the scenario used by McKee and Cox. By varying P , then, we can bound the results obtained in these numerical experiments on both the high and the low sides. These constraints allowed us to validate the Monte Carlo model.

The P parameter is computed based on its relation to the fractional size of 8 cubic elements at each of the 8 corners of the larger cubic scattering volume. Let the parameter q be the fractional single-axis length of each subcube to the length of the overall volume. Each sub-cube is therefore q^3 in size. Since there are 8 such subvolumes within the overall scattering volume, if the original scattering extinction within the volume, as measured for the McKee and Cox experiments, were σ , then if all the scattering material were uniformly redistributed within these subvolume elements, a modified material extinction coefficient equal to $\sigma' = \sigma/(8q^3)$ must be used. The remainder of the volume is assumed to be a vacuum.

The parameter q ranges from 0 to $1/2$, corresponding to a range between vacuum results and the McKee and Cox scenario. The relationship between P and q is that P measures the ratio of q to the single-axis center-to-center distance between two subvolume elements. Since each of the subvolume elements has a corner located at one of the 8 corners of the volume (see figure 2), the center to center distance will be $1 - q$. We thus have, $P = q/(1 - q)$.

Besides checking the original McKee and Cox scenario results ($P = 1$), additional test results were obtained for P values of $1/3$, $3/5$, and $7/9$.

To test the BLITS model under stressing conditions these scenarios were run under various resolutions of the modeled volume. That is, the BLITS model computations are based on dividing a scattering volume into a series of cubical cells of arbitrary size. To stress the model the above scenarios were evaluated under $1 \times 1 \times 1$, $2 \times 2 \times 2$, $4 \times 4 \times 4$, $8 \times 8 \times 8$, $16 \times 16 \times 16$, and $32 \times 32 \times 32$ cell resolution cases. For the $P = 1/3$ case $q = 1/4$, so only cell resolutions of at least 4 per axis were able to resolve the variations. For the $P = 3/5$ case, $q = 3/8$ and only 8 or more cells per axis were able to resolve the density variations. For the $P = 7/9$ ($q = 7/16$) case only 16 or more cells per axis would be able to resolve the variations.

RESULTS

The results of the Monte Carlo model can be presented in a series of 9 3-D plots: one each for each of 3 output regions (top, base, sides) and each input streaming photon direction (0° , 30° , and 60°). Due to space limitations it is only possible to present two of these plots (figures 3 and 4). The plot vertical dimensions measure the fractional flux exiting the given face (McKee and Cox cases all involved conservative scattering assuming non-absorptive media), the 'X' axes measure the scattering medium's nominal optical depth σ prior to modification due to concentration (σ'), and the 'Y' dimensions measure the amount of scatterer concentration into the 8 corner regions via the parameter P .

We reran the original McKee and Cox scenario data using our in-house Monte Carlo model. Noting some minor errors found in the McKee and Cox results by Davies,⁴ our results match the vacuum results for zero optical depth of the media, as well as matching the McKee and Cox results for large optical depths. To control the accuracy of the Monte Carlo model results, it was necessary to monitor the accuracy of the model outputs by computing the mean μ as well as the variance ν^2 of each output statistic. Due to the weak law of large numbers it was possible to test the accuracy of a given solution by invoking the Chebyshev inequality.⁵ In our case, we wanted a solution accurate to within 2 percent to a 75 percent confidence level by selecting parameters $\epsilon = 0.02$ and $A = 0.5$ such that $2 = 100\epsilon$ and $75 = 100(1 - A^2)$.

The statistics were computed by computing sample means (μ_N) and variances (ν_N^2) of a set of independent and identically distributed random variable (X_i) with mean μ and variance ν^2 . Due to the law of large numbers $\nu_\mu^2 = \nu_N^2/N$, and invoking the Chebyshev inequality leads to a test condition $\nu_N \leq \sqrt{N}\mu\epsilon A$. Using this condition it is possible to determine any Monte Carlo statistic to an arbitrary desired accuracy and confidence level. Note, however, that the results are determined to an accuracy determined by the product of ϵA . Thus the results apply equally well to a solution within 5 percent accuracy at a 96 percent confidence level.

The calculations made by the BLITS model can then be compared for resolved and unresolved cloud volume cases. The worst case was the single cell volume resolution. Figure 5 shows the data comparison for this case. The RMS error was 7.2 percent compared to the Monte Carlo results. These errors are largely due to the volume handling method within BLITS. There, each cell characterizes volumetric scattering effects using mean volume illumination factors. Also transmission and surface scattering calculations are made. However, it appears that the single cell case shows significant error even for the uniform cube case.

The $2 \times 2 \times 2$ case also has difficulties accurately characterizing anything but the uniform cube scenario, and its RMS error is similar to that of the single cell case (5.55 percent). To illustrate the differences, figure 6 shows the $2 \times 2 \times 2$ resolution results where the central core shows a better performance for the uniform volume case. Figure 7 then shows the remaining under-resolved cases and figure 8 shows a sampling of resolved cases. The $16 \times 16 \times 16$ and $32 \times 32 \times 32$ cases show RMS errors of 0.749 and 0.735 percent, respectively, indicating that the match between the Monte Carlo results and the BLITS results for these cases exceeds the Chebyshev accuracy criterion. Since the Chebyshev inequality only places a lower bound on the accuracy of a given result, the close correspondence between the BLITS results and the Monte Carlo data indicates that the Monte Carlo results are actually more accurate than is reflected by the test used above. In part, this is because the Chebyshev test is applied to only the worst of the 3 output wall mean fractional fluxes measured.

CONCLUSIONS

The comparisons developed for this paper indicate that the BLITS model accurately simulates cloud scattering features, with RMS errors as low as 1 percent compared to Monte Carlo results. Since the Monte Carlo results themselves have accuracies of approximately 2 percent, this indicates that the BLITS model results are highly accurate and reflective of the actual scattering properties of nonuniform cloud fields. Results for lower spatial resolution volume models indicate that BLITS still performs well in an RMS sense, yielding energy conservation, though not necessarily the correct directional distribution of energy.

REFERENCES

1. O'Brien, S. G., and D. H. Tofsted, 1997, "Visualization of dense cloud radiation data in modeling and simulations," in *Visualization of Temporal and Spatial Data for Defense Applications*, SPIE, 3085:82-93, N. L. Faust and J. D. Illgen, eds., Orlando, FL.
2. Tofsted, D. H., and S. G. O'Brien, 1997, "Characterizing the effects of natural clouds on scene simulations," in *Targets and Backgrounds: Characterization and Representation III*, SPIE, 3062:188-198, W. R. Watkins and D. Clement, eds., Orlando, FL.
3. McKee, T. B., and S. K. Cox, 1974, "Scattering of visible radiation by finite clouds," *J. Atmos. Sci.*, 31:1885-1892.
4. Davies, R., 1978, "The effects of finite geometry on the three-dimensional transfer of solar irradiance in clouds," *J. Atmos. Sci.*, 35:1712-1725.
5. Stark, H., and J. W. Woods, 1986, *Probability, Random Processes, and Estimation Theory for Engineers*, Prentice-Hall, Englewood Cliffs, NJ.

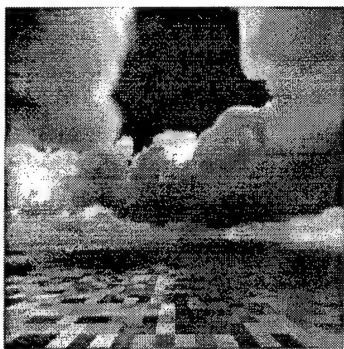


Fig. 1: Rendered image of a cloud filled scene.

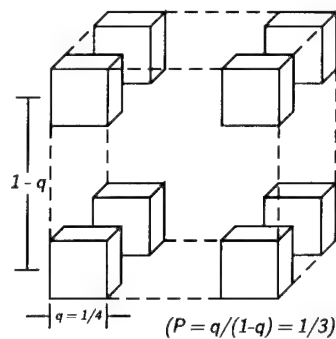


Fig. 2: Multi-cell scattering geometry ($P=1/3$).

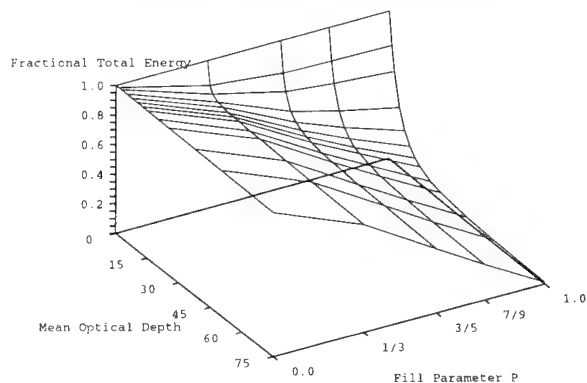


Fig. 3: Monte Carlo results for 0° incident energy exiting the modeled volume base.

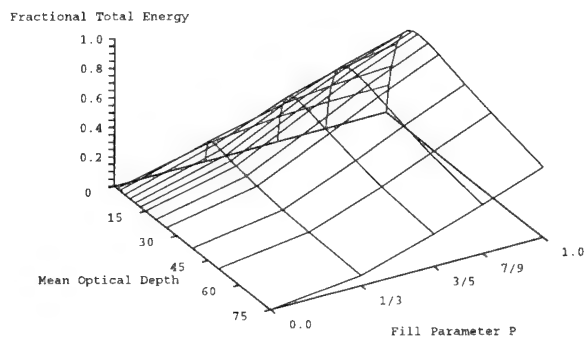


Fig. 4: Monte Carlo results for 0° incident energy exiting the modeled volume sides.

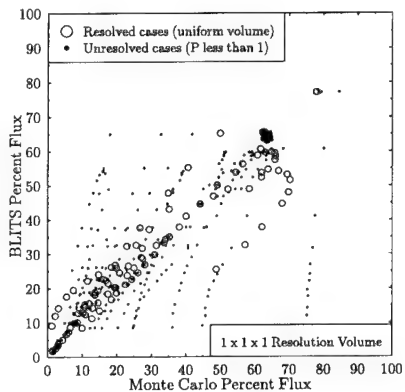


Fig. 5: Single cell model scatter diagram.

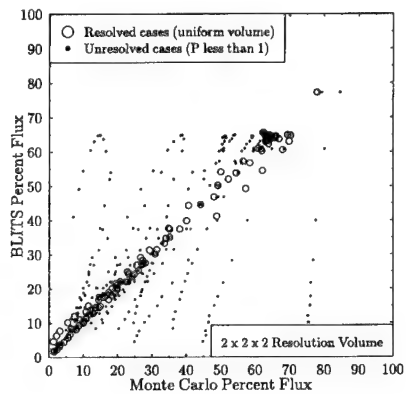


Fig. 6: $2 \times 2 \times 2$ cell model results.

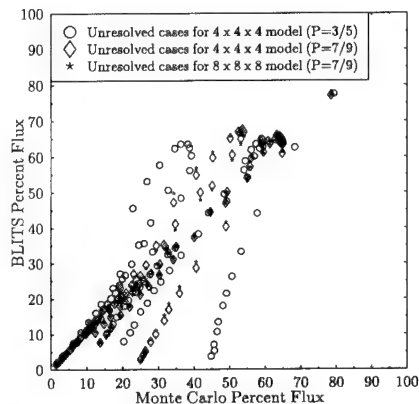


Fig. 7: 4^3 and 8^3 cell unresolved cases.

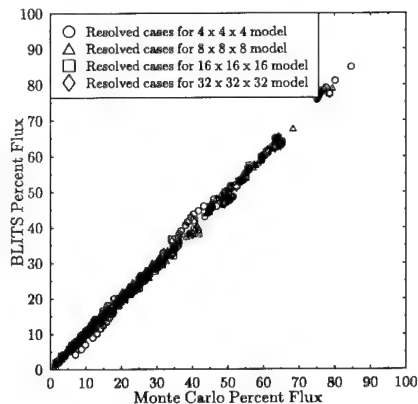


Fig. 8: 4^3 , 8^3 , 16^3 , and 32^3 cell resolved cases.

Lattice Boltzmann equation models: A new approach for microscopic simulation of cloud physics

Xiaowen Shan and Joel Mozer
Phillips Laboratory, Geophysics Directorate
29 Randolph Road
Hanscom Air Force Base, Massachusetts, 01731-3010

Abstract

Several DoD target modeling applications require knowledge of the radiant energy delivered to a target area over many hours. To address this, the lattice Boltzmann Equation (LBE) method will be presented as a new approach for the simulation of the microscopic physics in clouds. This method simulates the fluids at the level of distribution function, and therefore, allows the interparticle interaction being incorporated into macroscopic hydrodynamic simulation. With the interparticle interaction properly defined, the fluid can be assigned a rather arbitrary equation of state. As a consequence, it will exhibit the liquid-vapor phase transition naturally. Different processes, such as nucleation, diffusion, and coalescence can be simulated using a simple uniform algorithm which can be easily parallelized. The application of the LBE method to the study of droplet formation and development will also be presented.

1 Introduction

Accurate knowledge of the microscopic details of cloud and precipitation drops, such as the shape, terminal velocity and size distribution is needed for purposes such as carrying out cloud computation, interpreting Radar data, and predicting radiative transport properties of the cloud. The formation and evolution of small water droplets in air is a rather complex physical process involving hydrodynamics, thermodynamics and the theory of multiphase flows. Due to the extreme complexity, microscopic simulation of cloud particles by traditional methods is very difficult if possible. The recently developed lattice Boltzmann method for fluid simulation simulates fluid motion at the level of distribution function. This gives us the access to the information about the molecular interaction, which is the fundamental mechanism responsible for the complexities involved in fluid systems with multiple phase and phase change. It provides an efficient method for the simulation of microscopic cloud physics.

2 Lattice Boltzmann equation method

The lattice Boltzmann method is originated from the lattice Gas cellular automaton (LGA) [1], in which particles move on a regular lattice and collide with each other on the nodes. The algorithm consists of two steps: the streaming step and the collision step. In the streaming step, the particles move from each node to its neighboring nodes. Only one particle is allowed to move between one lattice link. Therefore, the state at each node can be characterized by no more than b bits of information, where b is the number of neighbors that each node has depending on the lattice structure. In the collision step, the result of a particular configuration of incoming particles has to satisfy the requirement that the particle number and the momentum are both conserved. More complex LGA models also impose the conservation of kinetic energy. The macroscopic fluid density, velocity and energy in models with energy conservation are evaluated by averaging over an area that is small compared with the fluid scale yet contains enough number of particles. When the total number of allowed particles at each node is small, the collision step can be implemented efficiently using a table-lookup algorithm. With the conservation requirements and that the lattice must have enough symmetry to ensure isotropic, the macroscopic

density and velocity can be shown to obey a set of equations very similar to the Navier-Stokes equations. It was hoped that this simple algorithm can be implemented very efficiently with possible hardware acceleration to provide an efficient computational fluid dynamics (CFD) tool. However, the averaging step time-consuming. It increases the actual computation cost considerably. In addition, a few artifacts also make the LGA impractical for engineering purposes.

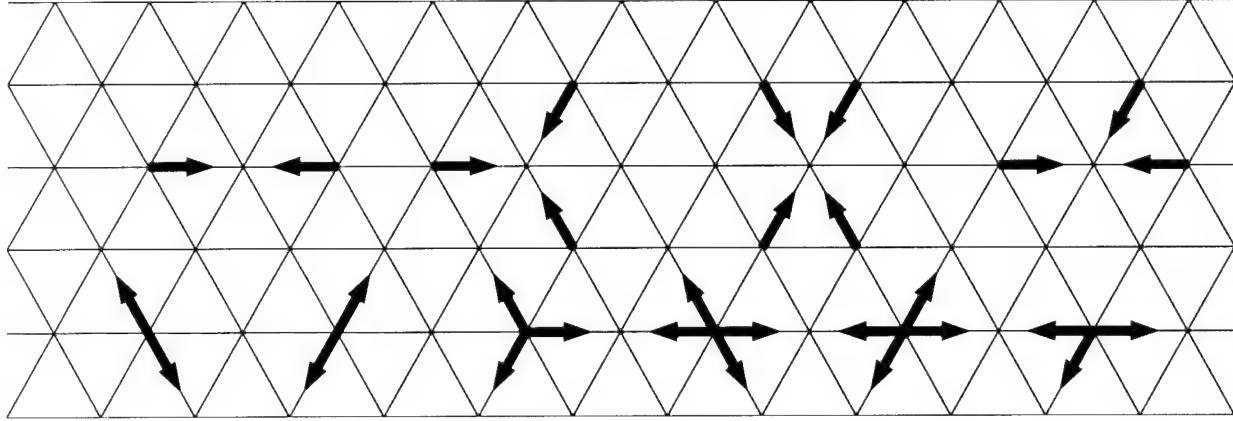


Figure 1: The collision rules of the FHP Lattice Gas cellular automaton. In the top row are the incoming states and the possible result of the collision are in the bottom row.

While deriving the macroscopic equations for the LGA, a Boltzmann equation, known as the lattice Boltzmann equation can be written down which governs the evolution of the “averaged” distribution function of the particles on the lattice. It was soon realized that instead of following the motion of each individual particle, the Boltzmann equation could be solved as efficiently as the LGA algorithm [2]. By working with the distribution function, the high statistical noise is removed from the system. Moreover, the lattice Boltzmann equation can be further simplified by replacing the complex collision term with a simple collision term known as the BGK collision model following the names of Bhatnagar, Gross and Krook [3]. This collision model relaxes the distribution function to the equilibrium distribution function in a single relaxation time, τ . On a D dimensional lattice, noting the population of the particles having the velocity \mathbf{e}_a at lattice site \mathbf{x} and time t by $n_a(\mathbf{x}, t)$, where $\{\mathbf{e}_a; a = 1, \dots, b\}$ is the set of vectors of length c pointing from \mathbf{x} to its b neighboring sites, the lattice Boltzmann equation with BGK collision term is:

$$n_a(\mathbf{x} + \mathbf{e}_a, t + 1) - n_a(\mathbf{x}, t) = -\frac{1}{\tau} \left[n_a(\mathbf{x}, t) - n_a^{(\text{eq})}(\mathbf{x}, t) \right]. \quad (1)$$

Here, the equilibrium distribution function $n_a^{(\text{eq})}(\mathbf{x}, t)$ is the Maxwell-Boltzmann distribution function in the original BGK model. For the lattice version, it has been shown [4, 5] that the following form will ensure that the correct Navier-Stokes equations can be obtained at the macroscopic level:

$$n_a^{(\text{eq})}(\mathbf{x}, t) = \begin{cases} n \left(\frac{1-d_0}{b} + \frac{D}{c^2 b} \mathbf{e}_a \cdot \mathbf{u} + \frac{D(D+2)}{2c^4 b} \mathbf{e}_a \mathbf{e}_a : \mathbf{u} \mathbf{u} - \frac{D \mathbf{u}^2}{2c^2 b} \right); & a = 1, \dots, b \\ n \left(d_0 - \frac{\mathbf{u}^2}{c^2} \right); & a = 0 \end{cases}, \quad (2)$$

where n and \mathbf{u} are the density and velocity of the fluid respectively, and d_0 is a constant. Similar to LGA, a LBE code consists of a streaming step and a collision step. In stead of boolean bits, a distribution function of $b + 1$ floating numbers is defined at each site. In the streaming step, the components of the distribution function are “streamed” to the neighboring sites; the density and velocity are then evaluated; with which the equilibrium distribution function for the next step can be constructed according to Eq. (1). Using the LBE method, numerical benchmark simulations for several flow configurations such as two and three dimensional decaying turbulence [6, 7] and Cavity flow [8] have been performed. The conclusion is that in terms of both accuracy and efficiency, the LBE method is at least as good as conventional CFD methods *e.g.* finite difference and spectral method.

3 Interparticle interaction in LBE models

One of the most important advantages of the LBE method is that by simulation fluid motion at the distribution function level, we have more detailed information about the motion of the fluid particles. It is this microscopic physics that is responsible for the complexities in flows with multiple phases and phase changes. Traditionally taking into account the details at this level into a flow simulation is very expensive. Soon after the introduction of the LGA, attempts have been made to simulate complex fluid with phase changes using LGA [9, 10] and LBE equivalents was soon developed [11]. In these models particle velocities and distribution functions are altered to effectively introduce interaction between particles over a long distance. Phases of different densities separate and an interface with surface tension forms in between. However, these models introduce the particle interaction in a rather naive way so that they have problems as lack of Galilean invariance and isotropy.

In previous works [12, 13], a lattice Boltzmann model for simulating multiple component multiphase flows was developed. Interparticle forces was systematically incorporated into the LBE models by defining interaction potentials between particles of different components. A distribution function $n_a^\sigma(\mathbf{x}, t)$ is defined for the σ -th of the total of S components, and it satisfies Eq. (1) with it's own relaxation time τ_σ and equilibrium distribution function $n_a^{\sigma(\text{eq})}(\mathbf{x}, t)$ which is given by $n_a^{\sigma(\text{eq})}(\mathbf{x}, t) = N(n_\sigma, \mathbf{u}_\sigma^{(\text{eq})})$, where $\mathbf{u}_\sigma^{(\text{eq})} = \mathbf{u}' + \tau_\sigma \mathbf{F}_\sigma / \rho_\sigma$, $\rho_\sigma = m_\sigma n_\sigma$, and m_σ are the mass density and molecular mass respectively. We let the force between particles of components σ at site \mathbf{x} and that of component $\bar{\sigma}$ at site \mathbf{x}' be proportional to the product $\psi_\sigma(n_\sigma(\mathbf{x}))\psi_{\bar{\sigma}}(n_{\bar{\sigma}}(\mathbf{x}'))$. The arbitrary function $\psi_\sigma(n_\sigma)$ is the "effective mass." The total molecular force exerted on the particles of component σ at site \mathbf{x} , $\mathbf{F}_\sigma(\mathbf{x})$, is given by

$$\mathbf{F}_\sigma(\mathbf{x}) = -\psi_\sigma(\mathbf{x}) \sum_{\mathbf{x}'} \sum_{\bar{\sigma}} G_{\sigma\bar{\sigma}}(\mathbf{x}, \mathbf{x}') \psi_{\bar{\sigma}}(\mathbf{x}') (\mathbf{x}' - \mathbf{x}), \quad (3)$$

where the Green's function defines the relative strength of interaction between different components. It satisfies the relation $G_{\sigma\bar{\sigma}}(\mathbf{x}, \mathbf{x}') = G_{\bar{\sigma}\sigma}(\mathbf{x}', \mathbf{x})$. It can be shown that the multiple-component LBE system defined above satisfies the Navier-Stokes equation with an equation of state of a non-ideal gas mixture. For the simplest case when there is only one component in the system, the equation of state is given by

$$p = \frac{c^2}{D} \left[(1 - d_0)n + \frac{b}{2} G \psi^2(n) \right]. \quad (4)$$

The second term is due to the interaction, which when properly chosen, will make the pressure a non-monotonic function of the density. A liquid-vapor type of phase transition can be simulated. In addition to the Navier-Stokes equation that the fluid mixture satisfies, each component in the multiple component system satisfies a diffusion equation [14, 15]. By adjusting the relative strength of interaction, more complicated phase transitions can occur.

4 Microscopic simulation of clouds

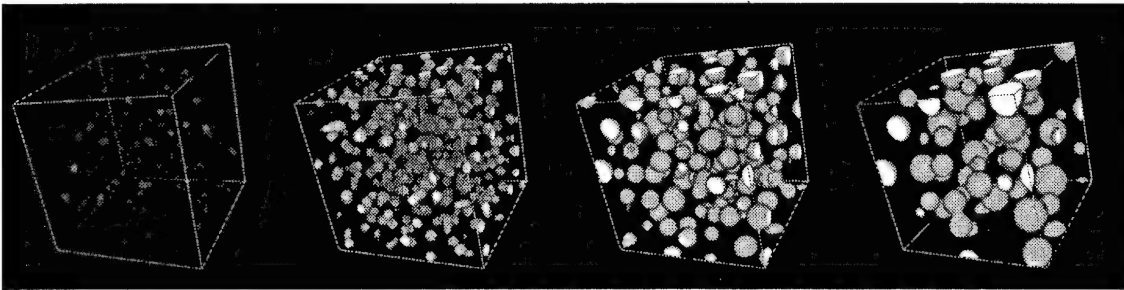


Figure 2: Microscopic simulation of drop formation using lattice Boltzmann method.

We have performed preliminary study of water condensation in air using the multiple component LBE model described above. Two components are used to simulate water and air molecules respectively. The first component

(water) has a non-ideal equation of state, and the second component is an ideal gas. The simulation was started from the state with both components homogeneously distributed with small random perturbation. The water vapor is over-saturated and spontaneously condenses into liquid drops. The subsequent development is a combination of nucleation and drop coalescence. The evolution of the density field of water, color-coded from black to white, is presented in Fig. 2. The numerical simulation of the drop formation process involves many physical processes in clouds such as nucleation, diffusional growth, and drop collections. More detailed and quantitative studies of the cloud properties are currently being carried out and will be presented in future presentations.

References

- [1] U. Frisch, B. Hasslacher, and Y. Pomeau. Lattice-gas automata for the Navier-Stokes equation. *Phys. Rev. Lett.*, 56:1505, 1986.
- [2] G. R. McNamara and G. Zanetti. Use of the Boltzmann equation to simulate lattice-gas automata. *Phys. Rev. Lett.*, 61:2332, 1988.
- [3] P. L. Bhatnagar, E. P. Gross, and M. Krook. A model for collision processes in gases. I. Small amplitude processes in charged and neutral one-component system. *Phys. Rev.*, 94(3):511–25, May 1954.
- [4] Hudong Chen, Shiyi Chen, and W. H. Matthaeus. Recovery of Navier-stokes equations using a lattice- gas Boltzmann method. *Phys. Rev. A*, 45(8):R5339–42, April 1992.
- [5] Y. H. Qian, D. d’Humières, and P. Lallemand. Diffusion simulation with a deterministic one-dimensional lattice-gas model. *J. Stat. Phys.*, 68(3-4):563–73, Aug 1992.
- [6] Shiyi Chen, Zheng Wang, Xiaowen Shan, and G. D. Doolen. Lattice Boltzmann computational fluid dynamics in three dimensions. *J. Stat. Phys.*, 68(3-4):379–400, Aug. 1992.
- [7] Daniel O. Martínez, William H. Matthaeus, Shiyi Chen, and David Montgomery. Comparison of spectral method and lattice Boltzmann simulations of two dimensional hydrodynamics. *Phys. Fluids*, 6:1285, 1994.
- [8] Shuling Hou, Qisu Zou, Shiyi Chen, G. Doolen, and A.C. Cogley. Simulation of cavity flow by the lattice boltzmann method. *J. Comp. Phys.*, 118(2):329–47, May 1995.
- [9] Daniel H. Rothman and Jeffrey M. Keller. Immiscible cellular-automaton fluids. *J. Stat. Phys.*, 52(3-4):1119–27, August 1988.
- [10] C. Appert and S. Zaleski. Lattice gas with a liquid-gas transition. *Phys. Rev. Lett.*, 64(1):1, Jan. 1990.
- [11] A. K. Gunstensen, D. H. Rothman, S. Zaleski, and G. Zanetti. Lattice Boltzmann model of immiscible fluids. *Phys. Rev. A*, 43(8):4320–7, April 1991.
- [12] X. Shan and H. Chen. Lattice Boltzmann model for simulating flows with multiple phases and components. *Phys. Rev. E*, 47(3):1815–19, March 1993.
- [13] X. Shan and H. Chen. Simulation of non-ideal gases and liquid-gas phase transitions by lattice Boltzmann equation. *Phys. Rev. E*, 49(4):2941–8, April 1994.
- [14] Xiaowen Shan and Gary Doolen. Multi-component lattice boltzmann model with interparticle interaction. *J. Stat. Phys.*, 81:379, 1995.
- [15] Xiaowen Shan and Gary Doolen. Diffusion in a multi-component lattice boltzmann equation model. *Phys. Rev. E*, 54(4):3614, 1996.

A LATTICE BOLTZMANN CLOUD MODEL WITH MOISTURE PARAMETERIZATION

Susan Triantafillou, Xiaowen Shan, Joel B. Mozer
Phillips Laboratory, GPOF
29 Randolph Road
Hanscom Air Force Base, Massachusetts 01731-3010

ABSTRACT

This paper describes a model that is being developed to provide simulations of atmospheric macroscopic cloud evolution. Work on this problem is ongoing and preliminary results will be discussed. The solution method is a three-dimensional, multicomponent lattice Boltzmann model combined with a moisture parameterization. The components represent air, water vapor, cloud water, and temperature and the parameterization specifies phase changes of water. An advantage of this kind of model is that it lends itself to parallel computation, and thus available computational power can be exploited. An important application of the model is as a tool in weather prediction.

1. INTRODUCTION

A challenge in modeling atmospheric clouds is capturing the extremely complex physical processes that occur on a vast range of spatial and temporal scales. Since explicit treatment of all of these processes is computationally expensive, typically parameterization is used to treat processes that occur at unresolved scales, while selected processes are predicted explicitly. This leads to specialized cloud models. For example, a microphysical modeling approach might be appropriate for tracking the evolution of individual droplets and ice crystals, while a macroscopic cloud model would be useful for describing the evolution of an entire thunderstorm.

The Department of Defense requires information on both the microphysical and macroscopic scales in order to determine critical impacts on systems and operations. For example, the sizes and shapes of individual droplets and ice crystals make up an important factor for electro-optical propagation through clouds, while storm development is important to consider in mission planning. These competing requirements have led to the need for research aimed at bridging the gap between microscopic and macroscopic cloud models. In this regard we have sought numerical algorithms and techniques which are amenable to the cloud problem and take advantage of modern scalable computer hardware. Algorithms based on the lattice Boltzmann equation (LBE) that are implemented on parallel processors are a promising find in this search.

In a LBE model the fluid material is viewed in terms of fictitious particles that occupy lattice sites. In each discrete time step particles are advanced, or streamed, to adjacent lattice sites according to statistical velocity distributions. This leads to a collision of particles arriving at the same given site from various directions. The collision results in a reassignment of velocity distributions in such a way that the advancement and collision steps satisfy mass and momentum balances. The details of the lattice Boltzmann model are given in several publications, including [1] and [5].

The LBE scheme is well suited to parallel computation because of a low communication to computation ratio. While the streaming step requires communication of information about neighboring sites, the ratio is dominated by the single-site computation required for the collision step. A speed-up of 5.5 has been achieved by parallelization of this scheme [5].

Lattice Boltzmann models have been developed to describe small-scale flows, including flows involving phase changes [4]. Since small-scale computations are not practical for the purposes of the

present study, the particles used here represent collections of particles used in previous lattice Boltzmann models. That is, discrete elements may represent smaller-scale structures, such as turbulent eddies.

The aim of this research is to create a lattice Boltzmann model of mesoscale atmospheric motions including cloud-forming processes. To achieve this, the model must be developed to simulate features of large-scale flows that were not relevant in previous LBE model implementations. These include stratified fluids, large-scale eddies, and Coriolis effects. The model is being developed in two stages. In the first stage a dry air flow is modeled; in the second stage moisture is incorporated using a cloud parameterization.

2. MULTICOMPONENT LATTICE BOLTZMANN METHOD

The LBE method has been used to simulate flows governed by the Navier-Stokes equations. A multicomponent lattice Boltzmann method can be used to describe flows involving two or more substances or multiple phases of a substance [4]. Shan [3] showed that a multicomponent method could also capture thermal effects by treating the temperature as an additional component. This treatment, in which the temperature acts as a passive scalar, is an alternative to incorporating the energy equation into the LBE method. The passive scalar approach eliminates the numerical stability problems that are introduced when the energy equation is incorporated into a LBE model.

3. DRY AIR FLOW

The first problem is that of uniform flow of dry, stratified air past a mountain. The LBE model requires two components: one for air and one for temperature. This approach is adapted from the method introduced by Shan [3] who solved a problem of dry air flow with heat transfer in a rectangular domain. The present problem is distinguished from Shan's problem by the more complicated boundary and the large-scale forces that are addressed here.

This problem can be solved analytically for extreme Rossby numbers and therefore these cases are approximated to validate the LBE model. The case of a large ($\gg 1$) Rossby number, indicating a small Coriolis effect, corresponds to a narrow mountain or a strong wind. The solution features gravity waves and contains no cyclonic bending. On the other hand, when the Rossby number is small ($\ll 1$), the Coriolis force is important, as in the case of a weak wind or a broad mountain. The resulting flow exhibits cyclonic bending ahead of and behind the mountain peak and anticyclonic bending in the vicinity of the peak.

4. RESULTS AND CONCLUSIONS

The lattice Boltzmann method can potentially speed the computations required for cloud modeling. This potential depends on successful use of the method in solving large-scale problems. It has been shown that a large-scale problem involving only air flow and thermal effects can be simulated using the LBE approach. Research on the inclusion of moisture is ongoing.

5. FUTURE WORK

Vapor and liquid water will be incorporated as two additional model components. As flow conditions change, mass may be transferred from one component to another to reflect phase changes. Phase transitions are specified by a cloud parameterization used in the Penn State/NCAR Mesoscale Model (MM5) [2]. The MM5 equations are chosen for the present study so that comparisons can be made

between results of the MM5 model and those of the lattice Boltzmann model (with MM5-type phase changes).

The moisture equations specify a system of advection, diffusion, and forcing. The advection and diffusion of the moisture components will be computed according to the LBE approach. An additional step will transfer mass from one component to the other based on forcing.

Future work also includes the incorporation of additional moisture processes, such as rain water and ice processes.

REFERENCES

- [1] Alexander, F. J., H. Chen, S. Chen, and G. D. Doolen, Lattice Boltzmann model for compressible fluids, *Phys. Rev. A*, **46** 4, 1992, pp. 1967 – 1970.
- [2] Grell, G. A., J. Dudhia, and D. R. Stauffer, A description of the fifth-generation Penn State/NCAR Mesoscale Model (MM5), NCAR/TN-398 + STR, June 1994.
- [3] Shan, X., Simulation of Rayleigh-Benard convection using a lattice Boltzmann method, *Phys. Rev. E*, **55** 3, 1997, pp. 2780 – 2788.
- [4] Shan, X. and H. Chen, Simulation of nonideal gases and liquid-gas phase transitions by the lattice Boltzmann equation, *Phys. Rev. E*, **49** 4, 1994, pp. 2941 – 2948.
- [5] Succi, S., Lattice Boltzmann method: A review with a glance at astrophysics, *Cellular Automata: Prospects in Astrophysical Applications* edited by J. M. Perdang and A. Lejeune, World Scientific, New Jersey, 1993.

**SESSION V:
CLOUD PREDICTION**

References in some of the preprints had to be deleted by the editor because they referred the reader to papers with limited distribution that were not available to the public.

DIAGNOSIS OF CLOUD VARIABLES FROM MESOSCALE NUMERICAL WEATHER PREDICTION MODEL FORECASTS

Donald C. Norquist
Phillips Laboratory, Geophysics Directorate
Hanscom AFB, MA 01731-3010 USA

ABSTRACT

Cloud mission impact variables, such as cloud amount, type, base and top altitude, and ceiling altitude are not explicitly predicted by current mesoscale numerical weather prediction models. Two statistical methods of relating numerical weather prediction forecast variables and geographic variables to cloud mission impact variables have been developed and demonstrated. In this demonstration, MM5 weather model forecasts were combined with RTNEPH cloud analyses over running 10-day periods. Application of these relationships to subsequent forecasts yielded cloud diagnoses. These were verified against valid-time cloud analyses. Results indicate that the basic distribution of clouds can be predicted.

1. Introduction Department of Defense (DoD) military services require a knowledge of present and a prediction of future meteorological conditions to support a variety of operations. In addition to standard observed and predicted meteorological quantities, a number of variables not explicitly predicted by numerical weather prediction (NWP) models are needed. Prominent in their importance to DoD operations are the so-called cloud mission impact variables (CMIVs). CMIVs include fractional cloud cover (herein called cloud amount), cloud type, cloud base altitude, and cloud top altitude, and cloud ceiling altitude.

Several past studies examined the feasibility of applying a diagnostic approach of cloud prediction to global NWP model forecasts and gridded cloud analyses. Trapnell¹ applied the "cloud curve algorithm" procedure of Mitchell and Hahn² to Air Force Global Weather Center (AFGWC) global spectral NWP model forecasts and AFGWC RTNEPH cloud analyses. Cianciolo³ applied a model output statistics approach to a one-year sample of AFGWC global NWP model forecasts and RTNEPH cloud analyses. Norquist et al.⁴ used a similar approach to forecasts from the Phillips Laboratory (PL) global spectral NWP model forecasts and RTNEPH analyses. Finally, Nehrkorn and Zivkovic⁵ compared several methods of diagnosing cloud cover using the PL global model and RTNEPH cloud analyses. All of these studies involved the diagnosis of cloud amount only, and only on the global scale. A consistent finding was that the schemes with the lowest root-mean-square (RMS) errors had unrealistic frequency distributions, while those that sought to retain the frequency distribution of the cloud amounts had higher RMS errors.

This paper describes a method developed at PL to diagnose all of the required CMIVs from theater-scale (covering areas 500-2000 km on a side) NWP model forecasts. The results of employing this method using data sets of gridded cloud analyses and mesoscale NWP model forecasts are evaluated and discussed.

2. Method I chose to use a model output statistics approach to the CMIVs forecast problem. This type of statistical prediction technique involves developing statistical relationships for the observed "predictand" as a function of a number of relevant predicted and fixed geographic "predictors." These relationships are usually developed over a suitably lengthy time series of both the predictor and predictand for a given location, then applied to future specifications of the predictors to diagnose the future predictand values, thus the "forecast."

In my method, the predictand-predictors relationships are developed from a randomly-selected sample of theater gridpoints at which predictand and predictor values are available. However, because gridpoints from many locations within the theater are used at each forecast time, a much smaller period of forecast times can be

used. For example, I used a ten-day development period in this demonstration. This approach has the advantage of quickly adapting to any changes in the forecast model or predictand specification, but has the potential disadvantage of limiting the development sample to fewer weather types.

Two statistical methods have been used to develop the predictand-predictor relationships for the CMIVs: multiple linear regression (MLR) and multiple discriminant analysis (MDA). MLR minimizes the mean-squared difference between a linear combination of selected predictors and the predictand in deriving the coefficients of the relationship between them. MDA, a categorical regression procedure, identifies a group of predictor values associated with each of the categories of the predictand. MDA generates coefficients of a discriminant function for each category, which when applied to the predictor values yield the probability of each category being the correct one. The actual category value assigned to the diagnosis must then be chosen on the basis of the diagnosed probabilities. The predictors used in each development period (at most 20) are selected from a large pool of potential predictors using a forward stepwise regression technique.

The MLR technique, when developed and applied to forecast values of the selected predictors, tended to produce acceptable RMS error levels but poor representations of the predictand frequency distribution. In particular, MLR diagnosed too few occurrences of zero and 100% cloud amount, and too many cases of partly cloud conditions. To address this, I developed a category selection method to be used in conjunction with MDA that would force a preservation of the frequency distribution as specified in the development sample of the predictand. The application of MDA to all of the CMIVs requires that the non-categorical ones be segmented into categories across their expected range of values. Table 1 lists the categories used for each of the CMIVs.

TABLE 1. CMIV Categories Used in MDA

CMIV	<u>1</u>	<u>2</u>	<u>3</u>	<u>4</u>	<u>5</u>	<u>6</u>
Amount %	0	05-20	25-40	45-60	65-80	85-100
Type - Low	Cb	St	Sc	Cu		
Middle	As	Ns	Ac			
High	Cs	Cc	Ci			
Base Alt. *,	0.0-0.2	0.2-0.4	0.4-0.6	0.6-0.8	0.8-1.0	
Thickness+,						
Ceiling Alt. ^						

*B.A.=[BA(AGL)-Deck Base]/[Deck Top-Deck Base], +Thickness=(Layer Top-Layer Base)/Factor, Factor=4000m (H,M), 8000m (L), ^C.A.=Ceiling Alt./10800m

3. Data RTNEPH cloud analyses were used in this demonstration because of their ready availability to both the operational and research communities, and the fact that they include gridded specifications of all of the required CMIVs. There are known deficiencies in the RTNEPH cloud specification that are well documented.⁶ Software developed in this project was designed to be general enough to handle any specification of the CMIVs with little modification. Future improvements in cloud specification should yield improvements in cloud forecasting using any method.

We acquired RTNEPH data sets for the Northern Hemisphere for January and July 1992. We used the data only where the observations on which the analyses were based were no more than two hours old. A statistical evaluation of the data influenced the design of our technique as applied to RTNEPH. First, it was clear that the frequency distribution of cloud amounts showed a predominance of clear and overcast. This fact reinforced the need for the MDA with the frequency distribution preserving category selection method. Secondly, I found that the association of groups of cloud types by the reported base altitude as mentioned in the RTNEPH user's guide is strictly adhered to in the data. Clouds with bases no higher than 1029 m above ground level (AGL) are considered low clouds, those with bases above 1029 m but lower than 5028 m AGL are middle clouds, and those with bases above 5028 m AGL are considered high clouds. Thirdly, it was clear from the statistics that only middle and low deck clouds are likely to have more than one layer reported at any RTNEPH gridpoint. Therefore, the technique was set to diagnose no more than one high cloud layer and no more than two middle and low cloud layers. Reported cloud layers were assigned to one of the three cloud decks (H,M,L) by their base altitude. Within the middle and low decks, the layer with the greater cloud amount was assigned to the

"primary" cloud layer, while any other cloud layer with a lesser cloud amount (including zero) was assigned to a "secondary" layer.

I used gridded forecasts from the Penn State/NCAR MM5 mesoscale meteorology model to supply the forecasts. For the development/demonstration project, we set up the MM5 to coincide with a theater-sized subset of the RTNEPH gridpoints. The forecast domain for a selected theater centered over northern Italy had a 40x40 gridpoint array with a 47.625 km grid spacing on a polar stereographic projection. The forecast domain was nested within a domain three times larger in both dimensions. We used global weather model forecasts for January and July of 1992 from the Medium-Range Forecast (MRF) model of the National Centers for Atmospheric Prediction, which were acquired from NCAR, as initial and boundary conditions for the MM5. The MM5 analysis package RAWINS was used to perform an analysis of the MRF fields at 0-hour forecast time. Resulting analyses and the boundary conditions were interpolated vertically to 22 model sigma layers [$\text{sigma} = (\text{pressure} - \text{ptop}) / (\text{psfc} - \text{ptop})$], where psfc is surface pressure and ptop is a fixed model top pressure.

Twice-daily 0-36 hour MM5 forecasts were generated for the periods 1-22 January and July 1992. To develop separate statistical relationships for the 6-hour forecast intervals, each 6-hour forecast duration and the 3-hour duration immediately preceding it were used to derive a number of prognostic and diagnostic quantities at each gridpoint and vertical model level. Then at each gridpoint, the model layers which lie within each cloud deck (H,M,L) were mass-weighted averaged to form a single forecast predictor value for each cloud deck.

The predictors for each 6-hour interval forecast duration are combined with the RTNEPH cloud predictands valid at the forecast time at one out of every four gridpoints (selected randomly) of each twice/day time, separately for each deck. Once ten days of these predictor-predictand sets are generated, the MLR and MDA methods are invoked to derive the linear cloud predictand-predictor relationship for each CMIV. The 10 leading cloud amount predictors for the 10-day period 12-21 January 1992 are listed in Table 2. The predictand-predictor relationships developed over the most recently completed 10-day period are applied to both twice-daily forecasts initialized on the day following the completion of the 10-day period. This results in diagnoses of the gridded CMIVs at forecast times.

TABLE 2. Leading Predictors for Cloud Amount in Each Deck, 12-21 January 1992

<u>High</u>	<u>Middle</u>	<u>Low</u>	<u>Total</u>
Hours sunlight	RH, high deck	Diag. Total Cld Amt	Max. RH^4
u wind, t-3	Precip. water, t-3	u wind, t-3	cos (latitude)
MSL pressure	v wind	v wind	RH, low deck
RH w.r.t. ice	cos (latitude)	Hours sunlight	Hours sunlight
RH	wind speed, low deck	RH max., high deck	RH^2
dθ/dz, low deck	Diag. # of cloud layers	RH^4 , t-3	Hours darkness
RH, low deck	sin (latitude)	Total cloud water, t-3	v wind
RH^4	Max. RH^2	RH max., middle deck	v wind, t-3
Percent surface water	dθ/dz, low deck	cos (latitude)	wind shear, low deck
RH max.	cos (longitude)	surface wind x Z (sfc)	dθ/dz, low deck

4. Results From the two-dimensional maps of diagnosed cloud amount distribution (to be shown at the conference), it was obvious that the realism of the MLR diagnoses suffers from the over-prediction of small but non-zero cloud amounts, and an over abundance of mid-range cloud amounts. The MDA diagnosis avoids this problem, and in this case shows a similar frequency distribution of cloud amount categories as in the RTNEPH depiction. Statistics computed over the 10-day verification period confirm that these characteristics remain consistent with time.

A number of statistical skill scores were generated in the quantitative comparison of the cloud diagnoses with the verifying RTNEPH. In Table 3, results of two such skill measures for cloud amount are shown. RMS error scores for the two methods favor MLR as expected. On the other hand, MDA tended to perform better in percent diagnosed in the correct cloud amount category. This is probably due in part to our attempts to replicate

the RTNEPH's categorical frequency distribution. However, MDA must be capable of accurately indicating the most probable predictand category in order to show skill.

We also generated skill scores for the other CMIVs. Results show that biases are small, and other measures of skill are comparable to those of cloud amount. Some of these, and visual depictions of the other CMIVs, will be shown in the meeting.

TABLE 3. Verification Skill Scores for Cloud Amount Categories 1-6, 12- and 36-hour Forecasts

	Root-Mean-Square Error (Category)								Percent Diagnosed in Correct Category							
	High		Middle		Low		Total		High		Middle		Low		Total	
	12h	36h	12h	36h	12h	36h	12h	36h	12h	36h	12h	36h	12h	36h	12h	36h
1/12-21																
MLR	1.2	1.2	1.5	1.6	2.1	2.1	1.9	2.0	40	42	39	39	29	27	38	36
MDA	1.5	1.5	1.9	2.0	2.3	2.4	2.2	2.3	76	74	69	68	49	48	50	46
Persist.	1.4	1.5	1.8	1.9	2.4	2.7	2.2	2.5	79	77	72	69	50	42	47	40
7/12-21																
MLR	1.1	1.1	1.2	1.2	1.3	1.3	1.4	1.5	45	42	54	54	53	52	50	49
MDA	1.2	1.3	1.5	1.5	1.8	1.9	2.0	2.1	79	74	70	70	45	44	39	36
Persist.	1.4	1.4	1.6	1.6	2.0	2.2	2.0	2.2	71	72	69	68	39	35	35	30

CONCLUSIONS

Cloud mission impact variables can be diagnosed with some skill from mesoscale numerical weather prediction forecasts using statistical forecast methods, when skill is measured in improvement over persistence. Multiple linear regression can show considerable skill in root-mean-square error, but at the cost of not reproducing the frequency distribution of the reference cloud analysis. Multiple discriminant analysis, when combined with a category selection method that preserves the frequency distribution of the cloud data, loses skill somewhat with respect to multiple linear regression in root-mean-square error, but generally represents an improvement in percentage diagnosed in the correct category. The latter ability results in a more realistic visual depiction of the diagnosed cloud scene from multiple discriminant analysis.

REFERENCES

1. Trapnell, R.N., Jr., 1992: Cloud curve algorithm test program. PL-TR-92-2052, Phillips Laboratory, Hanscom AFB, MA 170pp. [NTIS ADA 253918]
2. Mitchell, K.E., and D.C. Hahn, 1989: Development of a cloud forecast scheme for the GL baseline global spectral model. GL-TR-89-0343, Geophysics Laboratory, Hanscom AFB, MA 147pp. [NTIS ADA 231595]
3. Cianciolo, M.E., 1993: Short-range cloud amount forecasting with model output statistics. PL-TR-93-2205, Phillips Laboratory, Hanscom AFB, MA 154pp. [NTIS ADA 274769]
4. Norquist, D.C., H.S. Muench, D.L. Aiken, D.C. Hahn, 1994: Diagnosing cloudiness from global numerical weather prediction model forecasts. PL-TR-94-2211, Phillips Laboratory, Hanscom AFB, MA 152pp. [NTIS ADA 289456]
5. Nehrkorn, T., and M. Zivkovic, 1996: A comparison of diagnostic cloud cover schemes. *Mon. Wea. Rev.*, **124**, 1732-1745.
6. Hamill, T.M., R.P. d'Entremont, and J.T. Bunting, 1992: A description of the Air Force real-time nephalanalysis model. *Wea. Forecasting*, **7**, 288-306.

STATISTICAL CONTRAIL FORECASTING

Artie Jackson
Brian Newton
Doug Hahn
Allan Bussey
Phillips Laboratory, Bedford MA

ABSTRACT

Current operational Air Force contrail forecast procedures still rely on the Appleman technique developed in the 1950's with minor modifications. The Appleman technique depends on accurate measurements or forecasts of ambient flight level temperature, relative humidity and pressure as well as the amount of heat and water vapor in the exhaust plume of an aircraft to determine if the aircraft will produce a contrail. Current atmospheric measurement and numerical weather prediction technologies do not provide a sufficiently accurate description of ambient flight level conditions, thus operational contrail forecasts based on the Appleman technique are relatively poor. The Statistical Contrail Forecast algorithm developed at Phillips Laboratory makes use of logistic regression techniques to relate contrail-YES/contrail-NO observations with coincident-in-time/space atmospheric measurements. The ability of the Statistical Contrail Forecast technique to account for biases in atmospheric measurements results in a significant improvement in contrail forecasts when compared to current operational Air Force contrail forecasts.

1. INTRODUCTION

The Atmospheric Sciences Division of Phillips Laboratory has recently initiated a program to study the formation of contrails by jet aircraft. The objective of the program is to measure the spatial distribution of atmospheric variables, particularly water vapor, with ground, air and space-based sensors with the ultimate goal to improve the capability to forecast the occurrence of contrails generated by jet aircraft. The centerpiece of the project thus far has been a Field Program conducted in eastern Massachusetts during a two week period in September 1995, in which coincident in time/space radiosonde measurements and aircraft contrail-Yes/contrail-No observations were made.

The objective of the project is to develop techniques which produce improved contrail forecasts. Current Air Force operational contrail forecast procedures still rely on the Appleman technique (Appleman, 1953) developed in the 1950's, with minor modifications (Schrader, 1996). The contrail forecast technique reported on in this paper is a statistical algorithm making use of logistic regression techniques to relate contrail-YES/contrail-NO observations with coincident-in-time/space atmospheric measurements.

The long-range objective of the project is to apply the statistical regression contrail prediction techniques to Numerical Weather Prediction (NWP) model output and real-time satellite sounding data.

2. CONTRAIL FIELD PROGRAM/DATA SET

The Contrail Field Program was conducted in eastern Massachusetts during the 10 day period September 18-22, 25-29, 1995. Radiosondes were launched from 5 sites every 3 hours from 12 GMT to 00 GMT (daylight hours) to measure the distribution of temperature, humidity and winds within the project's domain. The 5 sites included Phillips Laboratory in Bedford, University of Massachusetts in Lowell, Beverly Municipal Airport in Beverly, The Phillips Laboratory Weather Test Facility at Otis Air Force Base in Falmouth, and the National Weather Service radiosonde launch site in Chatham. Coincident space-based sounding and imagery data, and a TPQ-11 vertically pointing cloud radar (35 Ghz) data were also archived.

In addition to collecting meteorological data, observers at each radiosonde launch site documented aircraft observations. Through communication with an observer at the FAA Air Route Traffic Control Center in Nashua, New Hampshire and an observer at each radiosonde site, an aircraft observation consisted of visually observing an aircraft within the celestial dome of a radiosonde site, whether or not the aircraft was producing a contrail, the aircraft's altitude, aircraft type and aircraft speed. Thus a comprehensive data set has been collected consisting of upper-air observations and aircraft contrail-YES/contrail-NO observations. Throughout the Field Project, approximately 220 radiosondes were launched and 557 aircraft (355 contrail-YES, 202 contrail-NO) were observed and documented.

3. AIR FORCE GLOBAL WEATHER CENTRAL (AFGWC) CONTRAIL FORECAST TECHNIQUES

AFGWC operational contrail forecast techniques during the past 40 years have been based on the Appleman (1953) technique. The Appleman technique depends on accurate measurements of ambient flight-level temperature, relative humidity and pressure as well as the amount of heat and water vapor in the exhaust plume of an aircraft to determine if the aircraft will produce a contrail. Several modifications have been suggested over the years to account for the variations of water and heat production in the plumes of major types of modern jet aircraft (Peters, 1993 and Schrader, 1996). A contrail forecast scheme developed for AFGWC by Bjornson (1992) used discriminant analysis techniques to relate temperature, altitude and vertical motion to contrail formation showed some improvement over the Appleman technique, but overall results were inconclusive.

In this paper we will compare the results of our new statistical logistic regression algorithm to the operational AFGWC contrail forecast algorithm using the updated contrail factors suggested by Schrader (1996). To test the AFGWC algorithm, we input pressure at the flight level of each aircraft observation from our Field Program data set, the bypass ratio of the observed aircraft and the relative humidity appropriate for the flight altitude from the Stratospheric Aerosol and Gas Experiment II (SAGE 2) (McCormick and Chiou, 1994) data base (a climatological relative humidity data base) currently used to supply relative humidity values for the AFGWC operational contrail forecast algorithm. A critical temperature is then calculated from the input parameters for each aircraft observation. For the AFGWC algorithm, statistics are calculated allowing for 0, 2 and 5 degree differences between the observed temperature at flight level and the calculated critical temperature for that aircraft observation. Typically, if the atmospheric temperature (measured or forecast) is less than or equal to the calculated critical temperature, contrails are forecast. If the atmospheric temperature is greater than the calculated critical temperature, contrails are not forecast.

4. LOGISTIC REGRESSION STATISTICAL CONTRAIL FORECAST TECHNIQUE

The long-term goal of this project is to use Numerical Weather Prediction (NWP) model forecast data as input to new contrail forecast techniques to improve operational contrail forecast capabilities. Current operational contrail forecast techniques produce poor forecasts because they require accurate input data. NWP model forecast data and climatological relative humidity data used as input to these techniques often do not represent the true state of the atmosphere, thus resulting in poor contrail forecasts. Our intent is to take advantage of regression techniques to account for the biases of inaccurate atmospheric measurements, NWP model forecast data and aircraft engine-related factors.

Due to the dichotomous nature of the dependent variable (contrail formation = 1, no contrail formation = 0), logistical regression was chosen to develop the contrail forecast algorithm. Logistical regression determines the relationship between the predictand and a finite number of predictors. In this case, the predictor pool consisted of measured and derived atmospheric parameters from the radiosonde measurements and aircraft observations coincident in space and time obtained during the Contrail Field Program.

Due to the limited size of our data set, 557 contrail-YES/contrail-NO observations, the data set was divided into four "quadrants". The first quadrant consisted of every fourth observation, starting with the first observation, the second quadrant consisted of every fourth observation, starting with the second observation, etc, for the remaining two quadrants. A logistical regression model was developed using all the observations in quadrants 1,2 and 3. The model was tested using the data from quadrant 4. Another logistical regression model was developed using all the observations in quadrants 2,3 and 4. That model was tested using the data from quadrant 1. In all, four logistic regression models were developed on three fourths of the data and tested on the remaining fourth of the data. With a limited data base, testing the logistic regression algorithms in this way provides some confidence in the stability of the technique if results of the four tests are of comparable quality.

Another logistical regression model, Incestuous Logistic Regression (ILR) was developed using the entire data set (all 557 contrail-YES/contrail-NO observations). The model was then tested using the same entire data set. This test is obviously incestuous, but often provides valuable insight when using a small data set.

5. RESULTS

Table 1 compares results of the logistic regression Statistical Model (SM) and the AFGWC Model. Note that results for each component of the quadrant approach (SM Quad1-4) are shown, including a Quadrant Average/Total (SM Quad Avg) which is the average/total of the four quadrant models' statistics. The statistics calculated for each test include the probability of detection (POD), false alarm rate (FAR), critical success index yes/no (CSIY, CSIN), percent correct (PC) and Hanssen and Kuipers' (1968) discriminant "V" score (VDS). The VDS ranges from -1 (no skill) to 1 (total

accuracy). The VDS accounts for biases in a test where events (contrail occurrences) and non events (contrail non-occurrences) are not equally represented.

The SM Quadrant Average algorithm (SM Quad Avg) significantly outperforms the AFGWC model for all statistics except FAR. In Table 1, the AFGWC Model statistics are calculated allowing a 0, 2 and 5 degree Celsius error (AFGWC 0,2,5) in the critical temperature output by the model. The SM Quad Avg outperforms the AFGWC model even allowing for an unreasonable 5 degree Celsius error in the critical temperature. Allowing a more reasonable 2 degree Celsius error in the AFGWC Model, the VDS is .57 for the AFGWC 2 model, while the VDS for the SM Quad Avg is .66. POD for the AFGWC 2 model is .64, while the POD for the SM Quad Avg is .91. Percent Correct (PC) for the AFGWC 2 model is .74, while the PC for the SM Quad Avg is .85. In all aspects except FAR, the SM Quad Avg performance is superior to the AFGWC 2 model. The smaller FAR for the AFGWC 2 model is somewhat deceiving because the AFGWC/Appleman model characteristically underpredicts contrail occurrences (Speltz 1995, Peters 1993). Note in Table1, that the AFGWC 2 model only predicted 226 of 355 contrail occurrences while the SM Quad Avg predicted 322 of 355 occurrences. The strong tendency of the AFGWC/Appleman model to underpredict the occurrence of contrails results in a small FAR. The AFGWC model statistics (POD, FAR, VDS) allowing for no error (AFGWC 0) in the critical temperature are significantly worse than the SM Quad Avg model, and they are consistent with those reported by Speltz (1995) and Peters (1993).

TABLE 1: COMPARISON OF LOGISTIC REGRESSION STATISTICAL CONTRAIL PREDICTION MODEL AND AFGWC CONTRAIL PREDICTION MODEL

Correct: Total of correct forecasts
 Yes/FYes: Observed Yes, Forecast Yes
 Yes/FNo: Observed Yes, Forecast No
 No/FYes: Observed No, Forecast Yes
 No/FNo: Observed No, Forecast No

POD: Probability of Detection
 FAR: False Alarm Rate
 CSIY: Critical Success Index/Yes
 CSIN: Critical Success Index/No
 PC : Percent Correct
 VDS: Discriminant V Score

	# Correct	Yes/FYes	Yes/FNo	No/FYes	No/FNo	POD	FAR	CSIY	CSIN	PC	VDS
SM ILR	484	328	27	46	156	.9239	.1230	.8180	.6812	.8689	.6962
SM Quad1	119	84	6	14	35	.9333	.1429	.8077	.6364	.8561	.6476
SM Quad2	121	80	8	11	41	.9091	.1209	.8081	.6833	.8643	.6976
SM Quad3	122	80	4	13	42	.9524	.1398	.8247	.7119	.8777	.7160
SM Quad4	112	78	15	12	34	.8387	.1333	.7429	.5574	.8058	.5778
SM Quad Avg	474	322	33	50	152	.9084	.1342	.7958	.6472	.8510	.6598
AFGWC 0	317	116	239	1	201	.3268	.0085	.3258	.4558	.5691	.3218
AFGWC 2	414	226	129	14	188	.6366	.0583	.6125	.5680	.7433	.5673
AFGWC 5	422	306	49	86	116	.8620	.2194	.6939	.4622	.7576	.4362
Contrail Yes Obs	355										
Contrail No Obs	202										

The top five predictors chosen by the SM in order of importance are: 1.Temperature, 2.Flight Level Wind Speed, 3.Maximum Wind Speed Direction, 4.Maximum Wind Speed Height and 5. Saturation Mixing Ratio. Predictor 1, temperature, is obviously a very important parameter in predicting contrail formation, and it is well measured by radiosondes, thus the SM has determined it to be the most important parameter in diagnosing contrail formation. Predictors 2, 3 and 4 indicate a strong relationship between contrails and the flight level synoptic situation. In diagnosing the presence of clouds using multiple linear regression techniques, Norquist, et al (1994) also found wind parameters to be strong predictors. Other predictors in the top ten chosen by the SM include several other wind-related parameters, flight altitude and flight level pressure.

The most notable parameters excluded from the SM algorithm top ten predictors are relative humidity-related parameters. Several relative humidity (RH) parameters were included as predictors, including flight level RH, 200 mb RH and 300 mb RH. Flight level RH ranked 14th. The poor quality of RH measurements at very cold temperatures (T less than -40 degrees C) available from radiosondes result in weak relationships between radiosonde measured humidity and contrail formation. This resulted in decreased importance of relative humidity-related predictors in the SM. Improved radiosonde RH measurements at cold temperatures would undoubtedly benefit the AFGWC Appleman algorithm which requires accurate measurements, however, this deficiency provides an opportunity for the SM to be superior.

In Table I, results for the Incestuous Linear Regression model are labeled as SM ILR. The ILR model only slightly outperforms the SM, thus increasing confidence in the results obtained for the SM.

6. SUMMARY

The logistic regression SM developed to predict contrail formation provides results which are superior to operational AFGWC contrail prediction techniques. Comparing the SM Quad Avg algorithm to the AFGWC 2 algorithm, the SM outperforms the AFGWC algorithm in Percent Correct by 10.8 percent (.851, .743 respectively). The SM significantly outperforms the AFGWC algorithm in Probability of Detection by 27.1 percent (.908, .637 respectively). The SM outperforms the AFGWC algorithms by a far greater margin if no error in critical temperature (AFGWC 0) is considered. The long-term objective of this project is to use NWP model forecast data as input to new contrail forecast techniques. The ability of the regression techniques to account for biases in atmospheric measurements, NWP model forecast data and aircraft engine-related factors provides a distinct advantage over the operational Appleman technique which requires accurate measurements or predictions to produce accurate contrail forecasts, and suggests that using NWP model forecasts as input to regression-based contrail forecast techniques will lead to improved contrail forecasts.

7. ACKNOWLEDGMENTS

We thank Mr Scott Lambert from the FAA Air Route Traffic Control Center in Nashua, New Hampshire for providing their facilities, allowing us to document aircraft type, altitude and speed in real time. The aircraft data obtained was invaluable to this study. We also thank Captain Mark Schrader, Headquarters Air Weather Service, USAF for keeping us up to date on AFGWC contrail prediction algorithms.

8. REFERENCES:

- Appleman, H.S., 1953:** "The Formation of Exhaust Condensation Trails by Jet Aircraft", Bulletin of the American Meteorological Society, Vol 34, pp 14-20.
- Bjornson, B.M., 1992:** "SAC Contrail Formation Study", USAFETAC/PR-92/003, USAF Environmental Technical Applications Center, Scott AFB, IL.
- Hanssen, A.W. and Kuipers, W.J.A., 1968:** "On the Relationship Between the Frequency of Rain and Various Meteorology Parameters", Koninklijk Nederlands Meteorologisch Institute, Med Ed. Verhand., Vol 81, pp 2-15.
- McCormick, M.P. and E.W. Chou, 1994:** "Climatology of Water Vapor in the Upper Troposphere and Lower Stratosphere Determined from SAGE II Observations", Preprints, Fifth Conference on Global Change Studies.
- Norquist, D.C., Muench, H.S., Aiken, D., and Hahn, D.C., 1994:** "Diagnosing Cloudiness From Global Weather Prediction Model Forecasts", PL-TR-94-2211, Phillips Laboratory, Hanscom AFB, MA, 139 pp., ERP No. 1156. ADA289456
- Peters, J.L., 1993:** "New Techniques for Contrail Forecasting", AWS/TR-93/001, HQ Air Weather Service, Scott AFB, IL.
- Schrader, M.L., 1996:** "Calculations of Aircraft Contrail Formation Critical Temperatures", Submitted to Journal of Applied Meteorology.
- Speltz, D.J., 1995:** "Validation of the Appleman Contrail Forecasting Scheme Using Engine-Specific Aircraft Data", Preprints, Cloud Impacts on DOD Operations and Systems Conference 95.

ADVCLD: Air Force Global Weather Center's Updated Cloud Forecast Model

Thomas J. Kopp, Margaret M. Wonsick, Louis E. Cantrell, and Francis D. Bieker
Headquarters Air Force Global Weather Center
Offutt AFB, NE, 68113-4039

ABSTRACT

Recently, the Air Force Global Weather Center (AFGWC) updated its cloud forecast capability, replacing the older 5Layer and TRONEW cloud forecast models with Advect Cloud (ADVCLD). ADVCLD produces 3-hourly cloud forecasts out to 12 hours at 25 nm resolution and out to 48 hours at 50 nm resolution. The cloud forecast comprises a total cloud amount plus cloud amounts at five specific levels. ADVCLD employs a semi-Lagrangian advection technique in three-dimensions to forecast cloud motion. Cloud amounts are parameterized by Condensation Pressure Spreads (CPS). Initial CPS values come from the AFGWC Real-Time Nephanalysis (RTNEPH, Hamill 1992). Since actual clouds initialize ADVCLD, the model has a powerful advantage over numerical techniques which must infer cloud cover from other parameters. ADVCLD hemispheric Root Mean Square Errors (RMS) begin at 30% for a 3-hour forecast, increase to 40% at 12 hours, and gradually increase to 40-45% at 48 hours. Certain regions, especially most mid-latitude locations, exhibit better error statistics.

INTRODUCTION

AFGWC has provided customers with global cloud forecasts for over 20 years. National Programs are currently supported by the High Resolution Cloud Prognosis (HRCP) model (Crum, 1987), but until ADVCLD became operational all other customers depended upon a pair of 20-year old cloud forecast models referred to as 5Layer and TRONEW. The 5Layer model was a 100 nm resolution cloud forecast which was valid only for mid-latitude and polar regions, while TRONEW was a simple persistence forecast for all tropical locations. Improved capabilities in wind forecasts and model processing rendered these two models obsolete.

In order to correct this deficiency, AFGWC designed a new cloud forecast model named ADVCLD. ADVCLD improves upon the previous models with better resolution, improved trajectories, longer forecast range, and the extension of trajectory techniques into the tropics. This short paper will briefly describe how ADVCLD makes a cloud forecast, and will present quantitative results.

METHOD

ADVCLD begins by preparing the initial wind and moisture fields required to forecast cloud. The model converts all input moisture variables to CPS units. CPS represents the upward displacement, in pressure coordinates, necessary to saturate a parcel. Low values of CPS indicate a nearly saturated parcel, while larger values are indicative of drier conditions. The first CPS values are obtained by converting cloud amounts within RTNEPH into CPS units using empirically derived look-up tables (Edson, 1965). After clouds have been incorporated, cloud free areas are initialized by dew point depression data from the Navy Operational Global Atmospheric Prediction System (NOGAPS). These dew point depressions are also converted to CPS units.

Winds are also obtained from the NOGAPS model. The winds are stored at AFGWC on a 2.5 by 2.5 degree grid. These winds are then interpolated to a 50 nm grid used by ADVCLD. Once the winds are interpolated, the trajectories may be calculated. The trajectory components for each forecast hour are based on the average NOGAPS winds for the preceding 3-hour time period:

$$dx = \bar{u}dt \quad (1)$$

$$dy = \bar{v}dt \quad (2)$$

$$dp = \bar{w}dt \quad (3)$$

Note that dx , dy , and dp represent upstream displacement from the trajectory endpoint to the trajectory origin. They are subtracted from the gridpoint to determine the trajectory origin. This "backward" trajectory saves regridding the field at each time step, and adds stability to the model. Since dt is specified by the forecast length, the model only requires the mean winds to determine the upstream displacement in the x , y , and p directions. ADVCLD calculates the mean winds through a series of Taylor series and matrix operations, and the upstream displacements follow directly from (1) - (3).

Once the trajectories and CPS values are determined, the cloud forecast is produced. Cloud amounts are forecast for each of 5 specific levels (gradient, 850, 700, 500, and 300 hPa). For all but the gradient level, horizontal motion is determined by subtracting the trajectory from the gridpoint of interest to locate the trajectory origin, and rounding this value to the nearest gridpoint. The vertical component modifies the CPS values -- upward motion decreases CPS while downward motion increases CPS. The CPS may also be modified by entrainment, which is simulated by weighting the CPS values at the end point and the origin. These weights can be "tuned" by forecast hour. The gradient level is similarly advected, but with decreased horizontal displacements so friction is taken into account. Vertical displacements at the gradient level may be modified by the surrounding terrain.

After the CPS values have been established for all 5 levels, a horizontal smoother is applied at all gridpoints and at each layer to prevent holes in the clouds due to shearing. Once the final CPS values are produced, they are converted back to level cloud amounts. Total cloud amounts are determined by stacking the layer cloud amounts at each grid point. The stacking algorithm considers overlapping cloud layers, preventing excessive and unrealistically high cloud amounts.

RESULTS

ADVCLD is verified both qualitatively and quantitatively on a daily basis. An example of ADVCLD's cloud forecast is given in Figure 1. The top left figure is an analysis at 15Z 29 July 97, while each successive figure represents the 12 hour forecast (upper right), 24 (lower left), and 36 hour (lower right) forecast verifying at the same time (i.e. the 12 hour forecast is from the 03Z run on 29 July).

Cloud features are remarkably well forecast, even out to 36 hours. Note the frontal bands over Europe and the synoptic cloud field in western Canada. Tropical clouds are also captured, as indicated in tropical Africa and the equatorial Pacific. Despite a lack of convective physics in ADVCLD, the model is able to capture most cloud features even in locations dominated by convection. Cloud free areas are also maintained throughout the forecast. Generally clear skies over the western Pacific and the United States are present in all the forecasts.

A quantitative analysis of ADVCLD is given in Table 1. The Root-Mean Square Error (RMS) is given for total cloud on each hemisphere and certain user-defined regions. On a hemispheric scale, the RMS remains below 40% throughout most of the forecast. RMS values out to 48 hours (not shown), remain near 40. On a regional scale the RMS is even better for most mid-latitude locations, and the RMS is outstanding over the deserts. The numbers increase somewhat for Europe, polar regions (not shown), and the tropics. Much of the error, as indicated by Figure 1, is due to cloud features correctly forecast in occurrence but slightly off in location.

The increase in RMS over regions such as the tropics are also due to ADVCLD's lack of boundary layer processes. ADVCLD is strictly based on trajectories, limiting its ability to forecast clouds in the tropics. ADVCLD will capture cloud development and dissipation related to synoptic scale processes, but has more difficulty at detecting smaller scale features. If the RTNEPH misses a stratus cloud deck, the CPS values at low levels will be too high, and the low clouds will not be forecast. This is a common problem over Europe. Finally, ADVCLD is only as good as the winds input into the model. A poor wind field will increase the RMS. Vertical motions in the tropics are difficult for any numerical model, yet these winds will strongly affect tropical cloud forecast amounts. Despite these limitations, ADVCLD consistently and reliably forecasts cloud cover for most mid-latitude and even tropical cloud systems.

CONCLUSION

ADVCLD was implemented in December 1996 to improve the cloud forecasting capability at AFGWC. ADVCLD is the world's only hemispheric cloud forecast model initialized by an actual cloud field, and has proven itself as a reliable and accurate source for cloud forecasts. ADVCLD has been chosen as the cloud forecast model for the Cloud Depiction and Forecast System II scheduled for implementation at AFGWC around the year 2000. ADVCLD forecasts will be available soon to military ID/password holders through the AFGWC web site.

REFERENCES

- Crum, T.D., 1987: AFGWC Cloud Forecast Models. AFGWC Tech. Note AFGWC/TN-87/001, Air Force Global Weather Central, Offutt AFB, Nebraska, 66 pp.
- Edson, H., 1965: Numerical Cloud and Icing Forecasts. 3WW Tech. Note 3WW/TN-13, 3rd Weather Wing (Air Weather Service), Offutt AFB, Nebraska, 97 pp.
- Hamill, T.M., R.P. d'Entremont, and J.T. Bunting, 1992: A Description of the Air Force Real-Time Nephanalysis Model. *Wea. Forecasting*, **7**, 288-306.

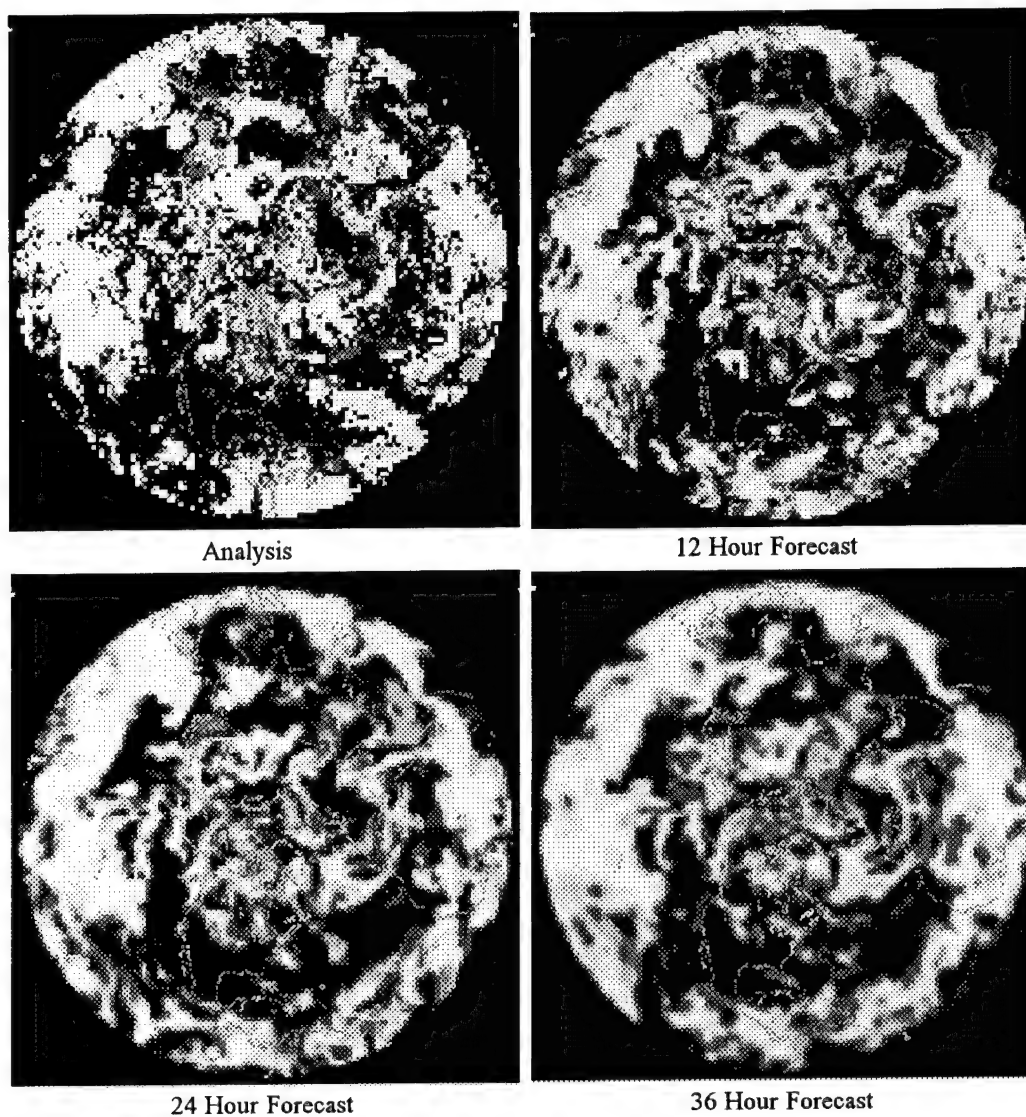


Figure 1. Polar-stereographic hemispheric cloud projection centered on the North Pole. Source: RTNEPH valid 29 Jul 97 / 1500UMT.

	3 hour	6 hour	9 hour	12 hour	18 hour	24 hour	36 hour
N. Hemi	30.8	37.9	39.3	42.1	39.8	41.1	42.5
S. Hemi	30.6	35.4	37.2	39.4	38.4	37.1	39.5
Europe	30.7	37.2	37.9	42.3	39.0	36.4	36.0
NH Desert	12.2	16.7	19.0	23.9	24.0	27.5	26.0
So Amer	23.2	36.3	39.1	41.9	38.9	37.7	42.3

Table 1. Root mean square deviations computed from comparing ADVCLD forecasts to the RTNEPH valid at the same time.

CLOUDY REGIONS BELOW THE MARINE STRATUS DECK

James W. Telford

Atmospheric Concepts
1975 Fallen Leaf Crt., Reno NV, 89509

ABSTRACT

Marine stratus clouds respond to changes in sea surface temperature. Aircraft observations near sunrise show some of these changes and associated effects on the cloud. Even though the subcloud air is stable to dry convection there is no decoupling from the surface as the lack of wind shear and the upward passage of moisture attest. Rising saturated parcels carry moisture continually up from the sea surface. Over cooler water the rising parcels are not buoyant enough to reach and penetrate cloud base, and so they accumulate below cloud as cloudy regions until warmer water is encountered. These effects are determined in detail by entrainment of subsaturated air into the cloudy regions and such effects have previously been shown to determine cloud drop spectra and liquid water content. The basic understanding of this phenomenon is approaching the stage where developing modeling techniques will provide predictive schemes.

1. INTRODUCTION

Many observations over the sea have established that fog is very frequently found over cooler water. Some recent observations have shown fog which formed in an offshore flow over the cool inshore water persisted for tens of miles until it flowed over warmer water, where it rose from the surface, changed to small cumulus clouds and then totally evaporated (Telford, J.W., and S.K. Chai, 1993).

Similarly, when stratus cloud moves with the wind over cooler water the cloud base tends to descend (Rogers, D.P. and J.W. Telford, 1986) and sometimes, when the decrease in surface temperature is larger than usual, new cloud layers form below the earlier layer above. Sometimes several layers form. This paper reports observations showing the response of the sub-cloud layer when a passage over cooler water is followed closely downwind by warmer water. This situation leads to patches of cloud and greatly reduced visibility in the relatively clear sub-cloud layer next to the sea. Such sea surface conditions occur when there is upwelling in the sea near the coastlines.

The highest incidence of marine stratus occurs over the eastern Oceans, both near the west coasts of North and South America over the Eastern Pacific and near Western Europe and South Africa. These cases involve a warm overlying subsiding air mass and long fetches, with the air close to the sea surface in temperature. These cloud layers tend to persist if the air above is warmer, as often occurs with continental air in the late summer when deep convection produces potentially warmer dry air aloft, which slowly subsides in high pressure regions. Other cases occur when cold air flows out over a warmer sea on the Eastern shores of both China and the United States of America. Then cloudy layers form in cooler surface air on leaving the coastline and encountering warmer water (Driedonks, A. G. M., and P. G. Duynkerke, 1989).

1.1. AIRBORNE OBSERVATIONS

The observations discussed here were obtained just beyond the coast, west and north of San Francisco, CA. The upwelling in the ocean provides the abrupt sea surface temperature changes which stimulate the responses in the air mass that we wish to study. The data discussed here was obtained on September 11, 1996, with the flight commencing at 4 AM from Livermore CA.

Figure 1 provides an isometric view of the flight profile. The outgoing track to the north

was completed at an altitude of 500 ft. At the north point (to the right) we took vertical soundings from 500' to 10,000'. Cruising back above cloud tops and above the outgoing track, a further four soundings were obtained above the sea where the water temperature was measured on the way out. The wind in and below cloud was measured and found to be flowing from the north roughly parallel to the aircraft track, with an on-shore component relative to the track of 10 to 20 degrees.

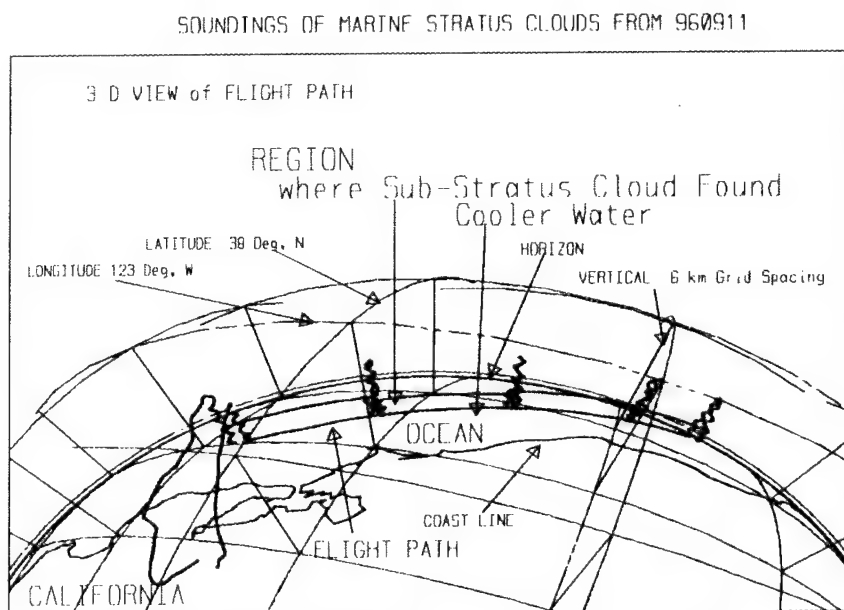


Figure 1. Flight path of aircraft on 11 September 1996. The aircraft departed Livermore California at 4 am and proceeded out from the coast and spiraled down below the marine stratus cloud to 170 m (500 ft) altitude. We then flew entirely below cloud to the northwest parallel to the coast and at about 5:30 am began a sounding up to 10,000 ft (3000 m). Descending through cloud to 500 ft (170 m) and up again to 3500 ft (1000m) at cloud top the return track began with further soundings at the positions shown. Sunrise was observed during the next sounding at about 6:30 am. There were no overlying clouds visible to the south and the traces of cloud to the north were some distance away.

Above the cloud layer the wind was from the south or south south west. The wind speed was 5 to 7 m/sec.

The region where the sub-stratus cloud was observed is shown by an arrow just upwind of sounding "D" if the soundings are designated A, B, C, D, and E, from the upwind end on the right in Fig. 1. The coolest sea

surface temperature is similarly marked just downwind of sounding "C".

From Fig. 2 the cloud structure changes after traversing sea water at different temperatures can be described. The water surface temperature between soundings B and C is at 15°C, as is the water below sounding A. Between A and B, upstream of B, the water is cooler at a little over 13°C, and sounding B shows a cloud liquid water profile with a slope close to the undiluted adiabatic profile given by the adjacent straight line. This indicates that the cloud layer was being supplied with water from below and that the cloud top entrainment was much less active. The new parcels of moist air from the cooler surface were still buoyant enough to reach cloud and stir it enough to keep it well mixed, but were not buoyant

MARINE STRATUS CLOUDS

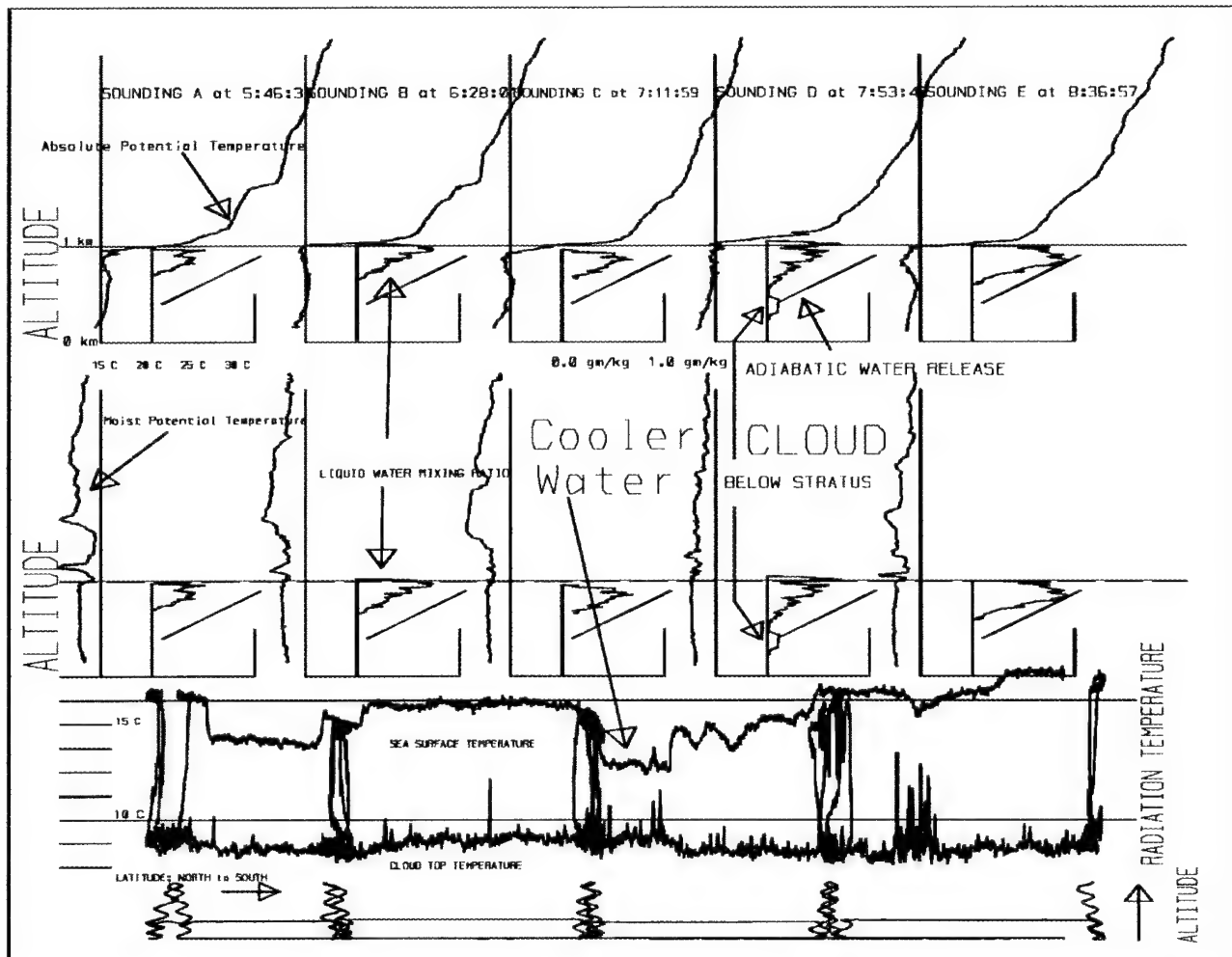


Figure 2. The climbing section of the five soundings. From the bottom the graphs show the altitude of the aircraft plotted against latitude, with north to the left. Above that the surface temperature from the radiation thermometer is displayed with the higher temperatures measured on the outgoing track below cloud showing the sea surface temperature changes at different positions. The lower trace is the cloud top temperature. The five graphs above the temperature in the figure show the moist potential temperature and cloud liquid water, and, on top, the absolute potential temperature and liquid water mixing ratio. The water shows where the cloud is, and the adjacent straight line gives the slope of well mixed adiabatic liquid water. The parcel of liquid water below the stratus cloud in sounding "D" is of particular importance

enough to stir in more subsaturated dry air from the subsaturated air above cloud.

Sounding C, after a substantial passage over the water with the temperature of 15°C, shows the effects of increased cloud top entrainment of subsaturated air. The liquid water content just below cloud top is much reduced below the value which would result from uniform in-cloud mixing, as is the cloud near cloud base. The subsaturated air entrained from above evaporates the cloud drops and reduces the cloud liquid water content. The evaporation also

produces cooled denser negatively buoyant blobs which descend through the cloud to near its base, so the liquid water content near the base is also reduced.

Sounding D shows the **substrates cloud**. It follows passage over water with a surface temperature somewhat cooler than the sea upstream of sounding B. This effect is profoundly different. The buoyancy of many saturated parcels leaving the colder sea surface are now not sufficient to carry them into the stratus cloud, so they accumulate underneath where we observed them as cloudy regions. The cloud above also shows the effects of receiving more water from below in parcels which are not buoyant enough to penetrate to cloud top and hence add water at lower levels within the cloud.

Sounding E shows the result of heating the **substrates cloud** when warmer water is again reached. The new found buoyancy from the warmer water has carried these cloudy parcels throughout the top half of the stratus cloud with the peak liquid water content at mid-cloud corresponding directly with undiluted uplift of the substrates cloud. The cloud drop sizes near cloud top show that the cloud is there the same as at the peak liquid water content. but subsequent dilution from the entrainment of subsaturated air from above the cloud has reduced the drop number concentration to give the liquid water content shown.

1.2. CONCLUSION

The data reported here show that sub stratus cloud forms as a direct result of the passage of a stratus deck of cloud over water 2 or 3 °C cooler than the water further upstream. If warmer water is then encountered these cloudy patches below the stratus deck are carried up into the stratus and temporally increase its cloudy density. All these vertical transport processes are the result of density differences created by the latent heat of evaporating or condensing cloud drops. The local release of buoyant parcels creates roughly spherical vortex circulations which can carry moisture and heat appreciable distances up or down (Telford, 1996). These spherical vortices have been modeled mathematically and will, hopefully be further developed into predictive schemes to show when substrates clouds can be expected.

2. ACKNOWLEDGMENTS

This research has been funded by the National Science Foundation under Grant ATM-9596249. The author is particularly pleased to acknowledge the support of the University of Wyoming flight crew without whom the high quality and reliable data used in this paper could not have been gathered.

3. REFERENCES

- Driedonks, A. G. M., and P. G. Duynkerke, 1989, Current Problems in the Stratocumulus-Topped Boundary Layer, *Boundary-Layer Meteorol.* 46, 275-304
- Rogers, D.P. and J.W. Telford, 1986: Metastable stratus tops. *Quart. J. Roy. Meteor. Soc.*, 112, 481-500.
- Telford, J.W., and S.K. Chai, 1993: Marine Fog and its Dissipation over Warm Water. *J. Atmos. Sci.*, Vol. 50, No. 19, pp. 3336-3349.
- Telford, J.W., 1996: Clouds with turbulence; the role of entrainment. *Atmos. Research.*, 40, 261-282.

ENSEMBLE CLOUD MODELING FOR MESOSCALE FORECAST

Ted Yamada
Yamada Science & Art Corporation
Santa Fe, NM 87501, USA

ABSTRACT

An ensemble cloud model (Mellor¹) was incorporated into the three-dimensional atmospheric model HOTMAC, Higher Order Turbulence Model for Atmospheric Circulation (Yamada and Bunker²). HOTMAC, which is based on a set of second-moment turbulence-closure equations (Mellor and Yamada³) computes not only the mean but also variances of mixing ratios of water vapor, cloud water, and rain water. Those variables are used to determine the probability density function, which is used in the ensemble cloud model. Other HOTMAC outputs include fractional cloud volume, which is the ratio of cloud volume to the grid volume.

1. INTRODUCTION

The purpose of the study was to examine how well a three-dimensional mesoscale model can simulate the airflows and cloud distributions over complex terrain. Theoretically, condensation occurs when water vapor reaches the saturation value. The modeled values for water vapor are grid volume averages which are always less than the saturation values because horizontal grid spacing used in a mesoscale model is normally larger than the cloud size. Thus, numerical models generally underestimate the amount of clouds. Some models lower the saturation values to match predicted cloud amounts with observations.

Another problem encountered in the conventional method is the abrupt change between the cloud and non-cloud status associated with the condensation criteria: Clouds form if water vapor mixing ratios become greater than the modified saturation values and clouds dissipate as soon as the mixing ratios become less than the saturation values.

An ensemble cloud model (Mellor¹; Sommeria and Deardorff⁴) alleviates the two problems discussed above: ambiguity associated with the saturation and abrupt change between cloud and no-cloud status. The ensemble cloud model defines condensation at the saturation value and produces a gradual variation of the amount of clouds with mixing ratio of water vapor.

2. ENSEMBLE CLOUD MODEL

Following Mellor¹ we assume the probability density function G for Θ_l and Q_w to be Gaussian so that

$$G = \frac{1}{2\pi\sigma_{\theta_l}\sigma_{q_w}(1-r^2)^{1/2}} \exp \left[\frac{-1}{1-r^2} \left\{ \frac{\theta_l^2}{2\sigma_{\theta_l}^2} - r \frac{\theta_l q_w}{\sigma_{\theta_l}\sigma_{q_w}} + \frac{q_w^2}{2\sigma_{q_w}^2} \right\} \right] \quad (1)$$

where $\sigma_{\theta l}^2 \equiv \overline{\theta_l^2}$, $\sigma_{q_w}^2 \equiv \overline{q_w^2}$, and $r \equiv \overline{\theta_l q_w} / \sigma_{\theta l} \sigma_{q_w}$. The results will be presented here without details of derivation.

First we define

$$a \equiv \left(1 + Q_{sl,T} \frac{L_v}{c_p} \right)^{-1}, \quad (2)$$

$$b \equiv a \frac{\langle T \rangle^p}{\langle \Theta \rangle} Q_{sl,T}, \quad (3)$$

$$\Delta Q \equiv Q_w - Q_{sl}, \quad (4)$$

$$Q_{sl,T} \equiv \left(\partial \tilde{Q}_s / \partial \tilde{T} \right)_{\tilde{T}=T_l} = 0.622 \frac{L_v}{R_d} \frac{Q_{sl}}{T_l^2}, \quad (5)$$

$$Q_{sl} \equiv 0.622 e_s(T_l) / (P - e_s(T_l)), \quad (6)$$

$$e_s(T_l) = 6.11 \exp \left[\frac{L_v}{R_w} \left(\frac{1}{273} - \frac{1}{T_l} \right) \right], \quad (7)$$

and

$$T_l \equiv (P/P_o)^k \Theta, \quad (8)$$

where Q_{sl} is the mean saturation mixing ratio of water vapor at T_l , the liquid water temperature; $e_s(T_l)$ is the saturation water vapor pressure at T_l and R_w is the gas constant for water vapor. Mellor¹ obtained the following expressions. A function R , which indicates a fractional cloud volume for a given volume of air, is found,

$$R = \int_{-\infty}^{\infty} \int_{-\infty}^{\infty} H(\tilde{Q}_w - \tilde{Q}_s) G d\tilde{Q}_w d\tilde{\Theta}_l = \frac{1}{2} \left[1 + \operatorname{erf}(\tilde{Q}_l / \sqrt{2}) \right], \quad (9)$$

where $\operatorname{erf}(x) = 2 / \sqrt{\pi} \int_0^x \exp(-y^2) dy$ and $H(x)$ is the Heaviside function. For Q_l

$$\frac{Q_l}{2\sigma_s} = RQ_1 + \frac{1}{\sqrt{2\pi}} \exp\left(-\frac{Q_1^2}{2}\right), \quad (10)$$

where

$$Q_l \equiv a\Delta Q / (2\sigma_s), \quad (11)$$

and

$$\sigma_s^2 = \frac{1}{4} \left(a^2 \overline{q_w^2} - 2ab \overline{q_w \theta_l} + b^2 \overline{\theta_l^2} \right). \quad (12)$$

Figure 1 shows the relationship among Q_i , R , and Q_e schematically.

3. RESULTS

The computational domain was 27 km x 19 km x 7 km (vertical) located over the southern area of Taiwan. Horizontal grid spacing was 1 km and vertical grid spacing was 4 m near the surface and increased gradually with height to 600 m near the top of computational domain. There were 26 vertical levels.

Simulation began at 0000 lst (local standard time), July 15 (Julian day 176) and continued for 60 hours. A light southerly wind (2 m/s) was assumed initially. Figure 2 shows the modeled wind distributions at 0400 lst, Julian day 178 at 10 m above the surface. Weak drainage flows and land breezes were developed over the land. Figure 3 shows the modeled wind distributions at 1200 lst, Julian day 178 at 10 m above the surface. Well-developed upslope flows and sea breezes are clearly seen. The convergence of winds over the ridges resulted in upward motion. The air lifted over the ridges condensed and produced clouds. A computer animation of cloud distributions was generated and will be presented at the meeting.

CONCLUSIONS

An ensemble cloud model was incorporated into the three-dimensional mesoscale model HOTMAC. A numerical simulation was conducted to simulate airflows and cloud development over the southern area of Taiwan. Diurnal variations of sea- and land-breezes as well as up- and down-slope flows were simulated well. A computer animation of cloud evolution was generated.

ACKNOWLEDGEMENTS

This work was supported by the U.S. Air Force (Contract No. F08637-95-C-6039).

REFERENCES

1. Mellor, G. L., 1977: The Gaussian cloud model relation. *J. Atmos. Sci.*, **34**, 356-358.
2. Yamada, T. and Bunker, S., 1988: Development of a nested grid, second moment turbulence closure model and application to the 1982 ASCOT Brush Creek data simulation. *J. Appl. Meteor.*, **27**, 562-578.
3. Mellor, G.L. and Yamada, T., 1982: Development of a turbulence closure model for geophysical fluid problems. *Rev. Geophys. Space Phys.*, **20**, 851-875.
4. Sommeria, G. and Deardor, J.W., 1977: Subgrid scale condensation in cloud models. *J. Atmos. Sci.*, **34**, 344-355.

Figure. 1. Fractional cloud volume R , mixing ratio of liquid water $Q_l/2\sigma_s$, and variance of liquid water $\overline{q_l^2}/4\sigma_s^2$, as a function of Q_l .

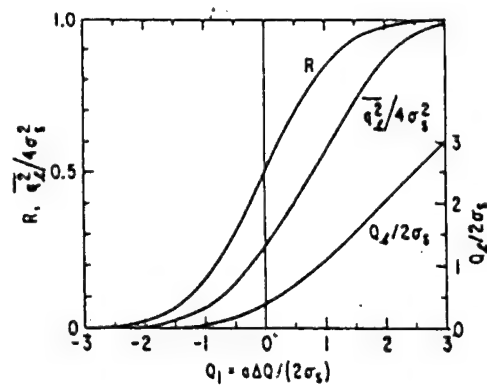


Figure. 2. The modeled wind distributions at 10 m above the surface at 0400 lst, Day 178. Solid lines indicate ground elevations with an interval of 20 m.

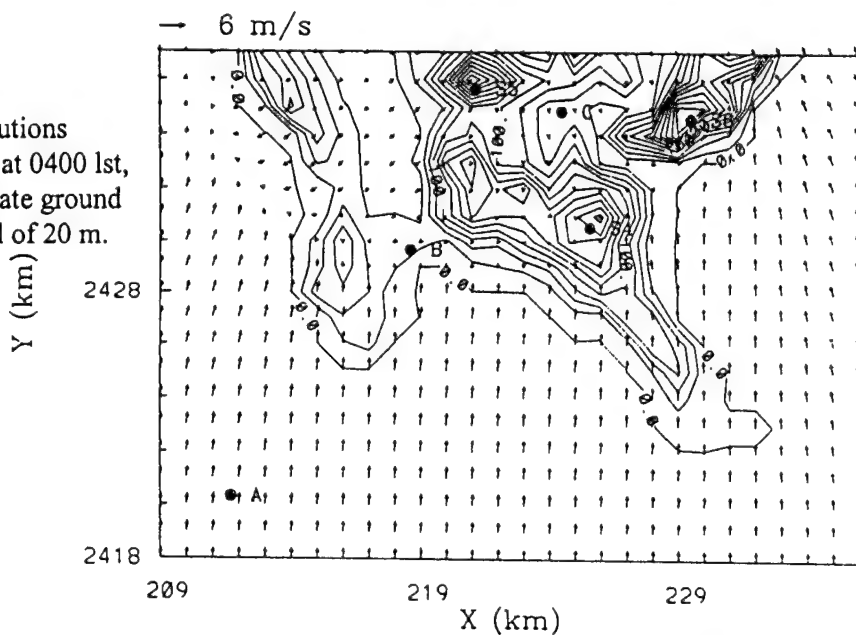
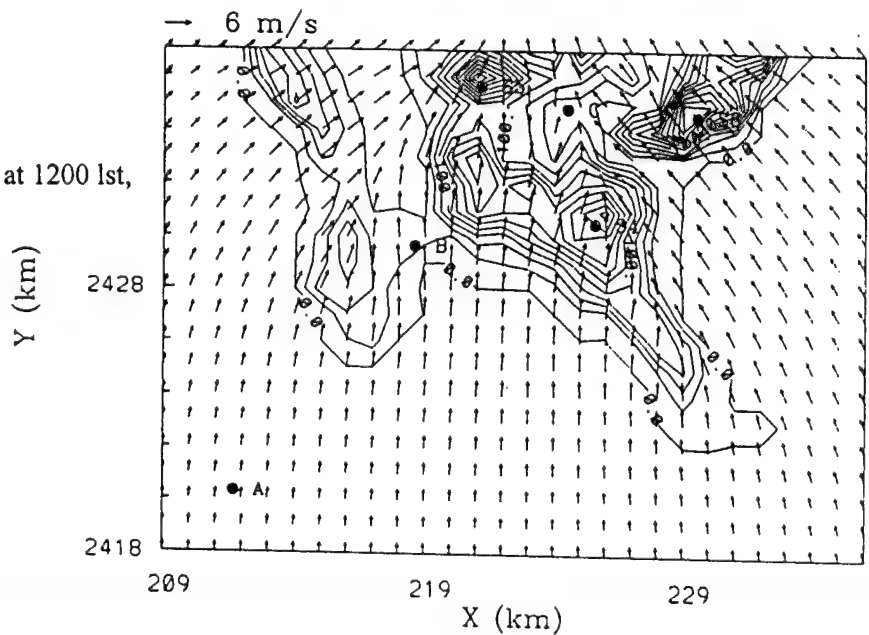


Figure. 3. Same as in Fig. 2 except at 1200 lst, Day 178.



THE CLOUD DEPICTION AND FORECAST SYSTEM II NEPHANALYSIS MODEL

Gary B. Gustafson and Ronald G. Isaacs
Atmospheric and Environmental Research, Inc.

Bonnie McDonald
Sterling Software, Inc.

Manuscript not available at time of printing. Please contact author for further information.

**SESSION VI:
MEASUREMENT SYSTEMS AND SENSORS**

References in some of the preprints had to be deleted by the editor because they referred the reader to papers with limited distribution that were not available to the public.

Optimal Visualization of Multispectral and Multisensor Environmental Satellite Data

Robert P. d'Entremont, Joanne Zhou, and Karen Cady-Pereira

Satellite Meteorology Group

Atmospheric and Environmental Research, Inc.

840 Memorial Drive, Cambridge, MA 02139-3794

James T. Bunting

Remote Sensing Applications Branch / GPOR

Phillips Laboratory, Geophysics Directorate

Hanscom AFB, MA 01731-3010

1. Introduction

A prototype set of display-device-independent software tools has been developed that automatically predicts and applies the best possible enhancements to many channels of satellite multispectral image data. Under this effort, known spectral signatures of clouds and the Earth's surface (e.g., nighttime fog, thin cirrus, snow) were automatically detected and enhanced through selection of optimal sensor channel combinations, and displayed using innovative color composite display techniques. These software applications algorithms significantly expand state-of-the-art meteorological image processing capabilities by automatically adapting to different satellite-dependent spectral, spatial, and radiometric resolutions and to varying combinations of sensor-channel availabilities. The applications programs facilitate intuitive, exploratory display and enhancement of multispectral and hyperspectral environmental satellite imagery in an automated fashion.

2. Identification and Significance of the Problem

Throughout the past decade many color display techniques have been developed specifically for meteorological satellite data (d'Entremont et al., 1987; Negri et al., 1989). A number of them focus on enhancement of differences in observed multispectral albedos and/or brightness temperatures (e.g., Bellec and LeGleau, 1992). Others concentrate on reduction of the dimensionality of the original satellite data via principal component analysis or clustering (Canas and Barnett, 1985). Still others are directed specifically toward the problem of displaying 24-bit full-color image products on devices with only 8 bits of display memory (Klaes et al., 1992).

No single technique accounts for all these issues simultaneously. A review of the current literature illustrates several key points [e.g., see d'Entremont and Thomason, (1987); d'Entremont et al., (1987); Negri et al., (1989); Bellec and LeGleau, (1992); Thomas and Nicholas, (1984); Canas and Barnett, (1985); Kleespies, (1987); Klaes et al., (1992); Thomason and d'Entremont, (1991)]. First,

there are many ways to generate and display color composites, each in some way combining the information content of two or more grayscale images into a single color composite image product.

Second, the importance of multispectral color composites is recognized in terms of (1) simultaneous display of information contained among multiple satellite sensor channels, and (2) the ease of interpretation of a single color composite image in comparison to several single-channel grayscale images for detection and identification of primary cloud classes and discrimination between clouds and the Earth's surface.

Third, among all these studies the use of color is archetypal and fundamental; the use of grayscale images constrains the amount of information that can be conveyed to the user in a single image product. In addition multispectral signatures routinely occur over narrow grayscale ranges, further underscoring the crucial need of color for feature detection.

Fourth, each of the techniques discussed in this section is in theory generically applicable to any type of multispectral image data; in practice, each has particular image channel combinations for which optimal displays can be generated, but other channels for which color displays are adequate but clearly not optimal. No single technique or software package accounts for all these issues simultaneously and in *automated* fashion.

3. Color-Composite Displays

The back cover of this proceedings contains an example of a conventional color-composite image product compared with its corresponding optimally enhanced color composite. In the top is a raw AVHRR MWIR-LWIR full-color image of the northeastern United States and western Atlantic. This is an example of how color composites appear when they are assembled using grayscale imagery that has not been enhanced, but rather simply displayed as the original temperature-to-grayshade data ingested from the satellite. Note that the colors are muted, and the image has an overall pastel appearance to it. Since the colors are not strongly saturated, spectral differences among the cloud classes (e.g., thin cirrus, fog, low clouds, cumulonimbus) and in the sea surface structure (e.g., marine stratus; warm and cold eddies) are difficult to discern. Low and mid-level clouds are barely detectable in the top of the scene. The remainder of the image is essentially cloud-free, including a large sector of the Gulf Stream region of the western Atlantic and most of the northeast U.S. Very little spatial variation in land-surface and sea-surface temperatures (LSTs and SSTs, respectively) is discernible in this image.

The bottom image shows the corresponding color composite with automated land- and sea-surface detection and enhancement enabled. Note the detail that now can be seen in both the land- and sea-surface temperature structures. The Delmarva peninsula, the south coast of New Jersey, and the Hudson River are all clearly detectable. So too are the cooler mountaintops of the Adirondacks, Catskills, and the Green and White mountains of New England. Some of the land surface appears brownish red in color (e.g., Delaware and eastern Virginia),

indicating the presence of very thin ground fog through which land surface features are still discernible. Note too the enhanced detail in SST spatial structure, including the Gulf Stream's north wall and associated eddies. Also noticeable in the bottom center of this image (over the sea surface) are tints of very pale blue. This represents the presence of very thin cirrus through which LST and SST features are still discernible.

The wide range of hues, saturations, and intensities in this composite dramatically illustrate the ability of the automated display toolkit to use color in an optimal way to effectively and successfully convey a large amount of meteorological and oceanographic information to the novice and experienced user alike. Conventional color composites rarely convey this information with so much detail and clarity.

4. Summary

A prototype integrated software class applications library is under continued development that supports the automated analysis, optimal enhancement, and display of multispectral and multisensor imagery. These applications algorithms significantly expand state-of-the-art environmental satellite image processing capabilities by automatically adapting to different satellite-dependent sensor spectral and radiometric resolutions and to varying combinations of sensor channels. Thus far, technical feasibility has been demonstrated using AVHRR, GOES-Next, and DMSP Operational Linescan (OLS) imager and Special-Sensor/Microwave (SSM/I) data.

Such a display capability has commercial value for many reasons. First, satellite data are collected at many different spectral, spatial, temporal, and radiometric resolutions. The "Multispectral Image (MSI)" display library technology will automatically account for and exploit such differences in an automated fashion, freeing the user of the burden of keeping track of the many sensor attributes. This allows experienced and novice image interpreters alike to focus more completely on multispectral image information content, and less on interpretation of available spectral signatures, how they relate to features of user interest, and how they manifest themselves in color composites.

Second, off-the-shelf versions of image display packages such as Photostyler, PCI, and "xv" work reasonably well for generic image processing functionalities such as non-linear stretching and interactive color editing, but are not well suited for processing of meteorological satellite data because of their complex and specialized information content.

Third, new display capabilities that are both satellite- and display-device independent have clearly beneficial value to the meteorological imaging needs of the DoD and civilian operational and research communities. It can be implemented as a component of the AFGWC Satellite Data Handling System, and the Navy TESS and Air Force STT tactical terminals. It is also of value to users who require quick-look estimates of cloud and surface parameters derived by exploiting the full available information content of multispectral satellite data.

With respect to civilian scientific applications, the MSI image-processing software developed during Phase I can be directly applied to the monitoring of atmospheric and oceanographic properties from spaceborne platforms using all available satellite sensor data, including those collected by the DMSP and NOAA/TIROS polar- and GOES-Next, Meteosat, and GMS geostationary satellite radiometers.

5. References

- Bellec, B., and H. LeGleau, 1992: **The Multispectral Colour-Composite Technique; an Improved Method to Display Meteorological Satellite Imagery.** *Int. Journ. Remote Sensing*, **13**, 1981-1998.
- Canas, A. A. D., and M. E. Barnett, 1985: **The Generation and Interpretation of False-Colour Composite Principal Component Images.** *Int. Journ. Remote Sensing*, **6**, 867-881.
- d'Entremont, R. P., and L. W. Thomason, 1987: **Interpreting Meteorological Satellite Images Using a Color-Composite Technique.** *Bull. Amer. Meteor. Soc.*, **68**, 762-768.
- d'Entremont, R. P., L. W. Thomason, and J. T. Bunting, 1987: **Color-Composite Image Processing for Multispectral Meteorological Satellite Data.** Digital Image Processing and Visual Communications Technologies in Meteorology, *SPIE 846*, 27-28 Oct. Cambridge MA, 96-106.
- d'Entremont, R. P., D. P. Wylie, D. C. Peduzzi, and J. Doherty, 1992: **Retrieval of Cirrus Radiative and Spatial Properties Using Coincident AVHRR and HIRS Satellite Data.** Proceedings, Passive Infrared Remote Sensing of Cloud and the Atmosphere, *SPIE 1934*, 13-15 April, 1993, Orlando, FL, 180-195.
- Klaes, K. Dieter, R. P. d'Entremont, and L. W. Thomason, 1992: **Applying an 8-Bit Multispectral Color Composite Image Simulation Technique to Operational Real-Time AVHRR Data.** *Bull. Amer. Meteor. Soc.*, **73**, 766-772.
- Kleespies, T. J., 1987: **Temporal Display of Meteorological Satellite Imagery on a Static Full-Color Display System.** Digital Image Processing and Visual Communications Technologies in Meteorology, *SPIE 846*, 27-28 Oct., Cambridge MA, 91-95.
- Negri, A. J., R. F. Alder, and C. D. Kummerow, 1989: **False-Color Display of Special Sensor Microwave/Imager (SSM/I) Data.** *Bull. Amer. Meteor. Soc.*, **70**, 146-151.
- Thomas, I. L., and J. V. Nicholas, 1984: **Special Colour Enhancement for Three Channels Having Similar Radiances.** *Int. Journ. Remote Sensing*, **5**, 753-760.
- Thomason, L. W., and R. P. d'Entremont, 1991: **The Simulation of Composite Color Imagery on 8-Bit Display Devices.** Proc. 7th Intl. Conf. Interactive Info. and Processing Systems (IIPS) for Meteorology, Oceanography, and Hydrology, New Orleans, *Amer. Meteor. Soc.*, 360-362.

CLOUDSAT: A SPACECRAFT TO MEASURE THE VERTICAL STRUCTURE OF CLOUDS

Steven J. Walter, Deborah G. Vane, Fuk K. Li
Jet Propulsion Laboratory, California Institute of Technology
Pasadena, CA 91109

Graeme L. Stephens
Colorado State University, Department of Atmospheric Sciences
Fort Collins, CO 80523

ABSTRACT

CloudSat is being developed to measure the vertical structure of clouds from space. It integrates a 94-GHz cloud profiling radar (CPR) with an A-band spectrometer/visible imager (ABSI) and a submillimeter-wave cloud ice radiometer (CLIR). CPR maps vertical cloud profiles with 500 meter resolution. ABSI detects very thin clouds and images the regional cloud field. CLIR retrieves cirrus ice content and crystal size. CloudSat is designed to provide data to improve how clouds and cloud-feedbacks are parameterized in general circulation models (GCMs). It will also demonstrate the utility of space-based cloud profiling for future forecast systems.

INTRODUCTION

CloudSat is a space-based approach to measure the vertical structure of clouds. This mission is being designed to investigate how clouds affect climate. Existing models relating cloudiness, atmospheric circulation, and temperature lack the accuracy needed to meet climate modeling needs. Current and planned observation systems are unable to probe the structure of multilayer clouds which are key to deciphering a range of climate feedback mechanisms. CloudSat is uniquely suited to resolve the mechanisms interrelating climate and clouds.

The original CloudSat mission concept was developed for the cost-constrained NASA Earth System Science Pathfinder (ESSP) mission series. The proposed payload consists of a 94-GHz cloud profiling radar (CPR), an oxygen A-band infrared spectrometer integrated with a visible imager (ABSI), and a submillimeter-wave cloud ice radiometer (CLIR) as shown in Figure 1. This payload will be able to determine the vertical distribution of clouds, measure cloud optical depth, retrieve cirrus ice content, and assist in validating measurements made by the NASA Earth Observing System (EOS). CloudSat will also furnish an important technology demonstration for future scientific, civilian, and tactical forecast systems.

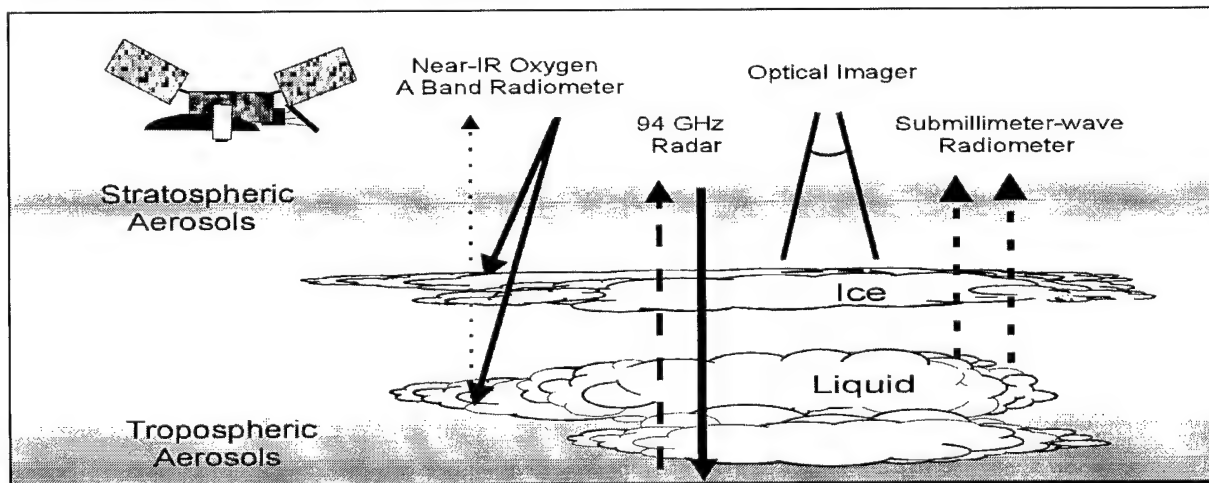


Figure 1. The CloudSat payload will measure the vertical structure of clouds to study the impact that clouds have on climate using a 94-GHz radar, IR spectrometer, submillimeter-wave radiometer, and optical imager.

2. MISSION OBJECTIVES

CloudSat was conceived to investigate the effect of clouds on radiative heating of the atmosphere. It is designed to compile a database of cloud measurements to be used to identify and quantify fundamental climatic processes relating the Earth's energy balance to its hydrological cycle. The ultimate goal is improve the accuracy of climate models by developing more realistic representations of clouds and their influence on climate.

The greenhouse effect determines the global energy balance. When the Earth is in equilibrium, the amount of solar energy illuminating the Earth equals the amount of energy being radiated back to space. Solar energy incident at the top of the atmosphere is scattered, absorbed, and transmitted by clouds, aerosols, and atmospheric gases. Roughly 30% of the radiation is scattered directly back to space, while the rest of the radiation warms the soil, oceans, and atmosphere. As the Earth surface warms, it radiates infrared or thermal energy to space. The amount of energy radiated to space increases with temperature. When the incident solar energy is balanced by the reflected solar energy and the thermal emissions, the planet is in equilibrium. Central to calculating the equilibrium state are greenhouse gases which are transparent to visible light and absorb infrared light. Gases such as water vapor and carbon dioxide let visible light warm the surface while trapping thermal emissions. Hence, an increase in greenhouse gas concentration increases the Earth's temperature. The uncertainty in predictions of greenhouse warming lies in the ability to accurately model feedbacks in the land-ocean-atmosphere system.

There are significant uncertainties in the feedbacks that occur between the hydrological cycle and the Earth energy balance due to the coupling between temperature, circulation, and hydrology (*i.e.*, clouds, precipitation, and distribution of water vapor). For example, the formation of clouds will modify the temperature structure of the atmosphere. A change in temperature then affects atmospheric circulation. In turn, variations in atmospheric circulation will modify the hydrological cycle. Accurate modeling of the interrelationships between these elements is necessary to derive the response of the Earth to a perturbation such as an increase in carbon dioxide.

Understanding and resolving climate feedback mechanisms is an important objective for the NASA EOS mission set. However, planned EOS, GOES, and NPOESS payloads will not be able to detect the presence of multilayer clouds reliably. They are therefore limited in their ability to characterize cloud-induced heating of the atmosphere which is essential to elucidate cloud-climate feedbacks. It is this observational gap that CloudSat intends to fill. The design for CloudSat will provide new insight into climatic processes by:

- Documenting the vertical distribution of cloud systems with 250 to 500 meter resolution.
- Measuring the total cirrus ice content and vertical distribution of ice water to 30%.
- Providing new measurements of optical depth and cloud phase by retrieving the asymmetry parameter.
- Validating EOS cloud and radiative flux products.
- Integrating CloudSat and EOS observations to assess the performance of climate models at simulating atmospheric heating.

3. SCIENCE PAYLOAD

3.1 CLOUD PROFILING RADAR (CPR)

The CloudSat radar, CPR, determines the cloud profile. It operates at 94-GHz using 1.5 kW peak transmit power, a repetition rate of 4700 Hz, and an uncoded pulse width of 3.3 μ s. The radar footprint is roughly 900 meters requiring an antenna diameter of 1.85 meters. The antenna, a center-fed Cassegrain, requires that spacecraft be pointed with an accuracy of 0.5° to minimize direct surface reflections and contamination from sidelobes. The power, mass, dimensions, and data rate for the CloudSat payload are summarized in Table 1.

The choice of radar frequencies is a trade-off between sensitivity, technological limits, and atmospheric attenuation. Radar backscatter from hydrometeors (ice crystals, cloud droplets, and precipitation) increases dramatically with increasing frequency. This needs to be balanced against atmospheric transmittance and the

performance of radar technology which both degrade at higher frequencies. The choice of 94 GHz means that a small percentage of the time when very thick clouds or heavy precipitation is present, the radar will not be able to penetrate the cloud base. The mission objective dictates this choice. To derive radiative heating, it is more important to be able to detect thin high clouds than it is to determine the base of a heavy cloud deck.

The radar has been designed with pulse coding capability to enhance sensitivity to mid- to high-level thin clouds. When pulse coding is selected, the radar transmits 33.3 μ s pulses at a 900 Hz repetition rate. Pulse coding increases sensitivity at the expense of generating range sidelobes from the surface and highly reflective clouds. The range sidelobes associated with the earth surface will obscure clouds near the ground. Thus, it is envisioned that coded pulses will be interspersed with uncoded pulses in order to resolve both thin clouds and surface-level clouds. The sensitivity of the radar is projected to be -32 dBZ for uncoded pulses and -38 dBZ for coded pulses.

TABLE 1. PAYLOAD RESOURCE SUMMARY

Instrument	Mass	Avg. Power	Length	Width	Height	Data Rate
CPR Antenna	21.6	-	1.85 (diam.)	1.85 (diam.)	0.27	
CPR Electronics	69.1	209-266 [†]	0.3	0.7	0.3	< 15
ABSI	15.0	12	0.45	0.25	0.45	110
CLIR Antenna	5.9	-	1.0 (diam.)	1.0 (diam.)	0.75	
CLIR Electronics	24.2	26	0.45	0.3	0.2	< 3
Contingency	20%	20%				
Total	163	318 [†]				

[†]Range in power requirements is due to difference in power required for coded pulses vs. uncoded pulse operation. The total assumes use of uncoded pulses 70% of the time.

3.2 OXYGEN A-BAND SPECTROMETER AND VISIBLE IMAGER (ABSI)

ABSI is a high resolution spectrometer centered on the oxygen A-band (~770 nm) integrated with a visible imager. The spectrometer/imager will provide the capability of detecting thin clouds and aerosol layers, provide a coarse estimate of their altitude, determine optical depth, and document the morphology of the cloud field. With a signal-to-noise of 1000:1 it will be able to measure an optical depth of 0.02 with 3% accuracy. ABSI will only operate during the daytime because the spectrometer and imager require sunlight.

The visible imager (748 nm \pm 5 nm), provides the context for CloudSat measurements. It will allow researchers to associate cloud profiles with mesoscale weather patterns. For example, it will be able to identify when a cloud profile is associated with a tropical storm, a cumulus column, or a uniform cloud deck. The data from the imager will be highly compressed to reduce its data requirements.

The high resolution spectrometer determines the optical depth and altitude of thin clouds by making high spectral resolution (0.5 cm^{-1}) measurements at the oxygen A-band (761 nm -772 nm). The oxygen A-band is characterized by a "thicket" of closely spaced spectral lines. Therefore, a small change in wavelength will vary the rate at which light is attenuated as it traverses the atmosphere. With measurements made at a wide range of attenuation lengths, it is possible to determine optical depth, photon path length, characteristics of the scattering particle, and altitude.

3.3 CLOUD ICE RADIOMETER (CLIR)

Submillimeter-wave radiometric measurement of cloud ice is a new technique for retrieving cirrus ice mass and ice crystal size. It can be understood intuitively. In the absence of clouds, the Earth appears to emit a

relatively uniform background of submillimeter-wave (> 300 GHz) radiation emitted by mid-tropospheric water vapor. When viewed from space, cirrus clouds will scatter the background emissions back toward the Earth reducing the upward flux of submillimeter-wave energy. Hence, cirrus clouds appear "cool" against the "warm" emission background. The reduction in radiative brightness is dependent on both the number of ice crystals and their sizes. Measurements made at two widely separated frequencies permit variations in thermal flux caused by changes in mean crystal size to be distinguished from changes in ice content.

The CloudSat radiometer is a sensitive heterodyne receiver tuned to 640 GHz and 183 GHz. When coupled with 94 GHz radar measurements, the 640 GHz measurements of atmospheric brightness allows retrieval of ice mass and mean crystal size. Since 183 GHz is situated on a water vapor line, it can yield a similar atmospheric opacity as is observed at 640 GHz. However, it has virtually no sensitivity to cloud ice. Therefore, the measurement at 183 GHz provides an independent measure of variations in the water vapor emission background ensuring that structure in the background does not contaminate the retrievals of ice mass and crystal size.

The Cloud Ice Radiometer (CLIR) receivers will utilize planar-Schottky mixers feeding an IF bandwidth of 1.5 GHz. The receiver will have 0.5 K sensitivity and will be calibrated to better than 1 K accuracy using a cold sky view and an "ambient" target. The radiometer footprint is matched to the radar requiring a 1 meter diameter antenna utilizing a 10 cm secondary that is illuminated by an offset feed.

4. SPACECRAFT REQUIREMENTS

The mission was designed for a lifetime goal of two years to enable more than one seasonal cycle to be observed. The desired orbit is a nearly sun-synchronous orbit (altitude = ~ 475 km, inclination = 97.1°) providing coverage to 83° latitude. Communications is accomplished via an S-band transceiver using an omni-directional antenna and X-band transmitter for data downlink utilizing a helical antenna. Independent calibration of the instrument payload will take advantage of ground-based observational sites such as the DOE Cloud and Radiation Testbeds, NASA airborne science campaigns, and university research facilities worldwide. The total weight of the commercial spacecraft was estimated to be approximately 600 kg requiring an average of 550 W of power. However, since no teaming arrangements have been formalized for future proposals opportunities, it would be inappropriate to identify the original spacecraft manufacturer or reveal proprietary information about their spacecraft bus.

CONCLUSIONS

CloudSat is being developed to measure the vertical structure of clouds from space. It integrates a cloud profiling radar with an A-band spectrometer/visible imager and a submillimeter-wave cloud ice radiometer. This payload is designed to profile clouds with 500 meter resolution, detect very thin clouds, image the regional cloud field, and retrieve cirrus ice content and crystal size. The CloudSat payload will be able to determine the vertical distribution clouds, measure cloud optical depth, retrieve cirrus ice content, and assist in validating measurements made by the NASA Earth Observing System (EOS). CloudSat will also furnish an important technology demonstration for future scientific, civilian, and tactical forecast systems.

The CloudSat concept was originally proposed for the first NASA ESSP mission opportunity. It was ranked very highly, but was not selected due to the ESSP program cost cap. We plan to propose this mission concept to the 1998 ESSP Announcement of Opportunity which may adopt a higher cost cap. The science team is currently exploring the possibility of teaming with international partners and other government agencies that have related interests to facilitate cost-sharing improving the overall competitiveness of the proposal.

ACKNOWLEDGMENTS

This research was partially carried out by the Jet Propulsion Laboratory, California Institute of Technology, under a contract with National Aeronautics and Space Administration.

CLOUD ANALYSIS DURING THE NPOESS ERA

Gary B. Gustafson, Robert P. d'Entremont, David P. Hogan, and Ronald G. Isaacs
Atmospheric and Environmental Research, Inc.

Manuscript not available at time of printing. Please contact author for further information.

USE OF RECONNAISSANCE ASSETS IN SUPPORT OF THEATER WEATHER

Maj Michael S. Kapel, Capt John F. Polander, Mr. Steven P. Weaver
88th Weather Squadron
Wright-Patterson AFB, OH 45433

Mr. Jeffrey Pesler
Aeronautical Systems Center, Reconnaissance Program Office
Wright-Patterson AFB, OH 45433

ABSTRACT

The impact of the environment on modern weapons systems is well known. Data from DESERT STORM indicate that the majority of missed opportunities were the result of weather. Theater commanders need accurate, near-real-time, environmental data over the battlefield. Air Force Weather needs accurate information over data denied and data sparse regions to feed numerical forecast models. The 88th Weather Squadron and the Aeronautical Systems Center's Reconnaissance Program Office (ASC/RA) are investigating ways in which reconnaissance assets can be used to provide data in support of the Air Force Weather mission.

1. INTRODUCTION

The importance of accurate, real time, weather data became apparent during Desert Storm, where weather caused ordnance to go unused over targets and greatly compromised battle damage assessments. Figure 1 shows the percentage of bombs not dropped on target due to weather during the first 45 days of the operation. A USAF Scientific Advisory Board study¹ cited poor confidence in forecast accuracy as a contributing factor to our inability to fully own the weather for battle. Lack of accurate, fine-mesh observations was further identified as a significant shortfall in our ability to forecast weather over the battlefield.

This paper explores the potential use of reconnaissance assets to collect weather data over the battlefield.

2. MODERN WARFIGHTER REQUIREMENTS

Weapons, intelligence, and surveillance systems are effected by atmospheric conditions. Effects range from slight degradation to total system failure. In order for theater commanders to properly employ modern weapons, systems they need accurate and timely battlefield weather forecasts. Weather observations provide the information needed to make accurate forecasts. Information concerning temperature, pressure, humidity, wind, and other atmospheric parameters over the battlefield is used to initialize numerical weather prediction models. Output from these models is interpreted by meteorologists and provided to theater commanders and planners as weather forecasts. The accuracy of information given to the war fighter is completely dependent on the ability of the observation field to accurately depict current (0 hour) weather conditions. Inaccurate or incomplete observation fields affect a war fighter's ability to properly employ ships, aircraft, ground vehicles, and most weapons and surveillance systems. To fully "own the weather for battle" a thorough specification of meteorological parameters throughout the battle space is needed.

Cloud imagery/data are required to predict the location/extent of clouds, the height and thickness of cloud decks, the type of clouds, and the composition of clouds over areas of interest. Properly exploited, such data would increase the accuracy of cloud observation/prediction and would greatly increase the effectiveness of all aspects of air operations by heightening confidence in mission and weapons/sensor selection. High-resolution cloud analyses/forecasts would additionally increase the efficiency of battle damage assessment.

Flight level data are required over areas of interest to increase accuracy of numerical weather models. Temperature, wind (speed and direction), humidity, and aerosol/constituent concentrations are needed. Current numerical forecast models are limited by their input data. Increases in accuracy/resolution of input data would provide

increases in output accuracy. Flight level data can also be used to produce high-accuracy flight plans over areas of interest and can feed models designed to predict sensor performance.

In addition to flight level data, vertical profiles of temperature, humidity, wind (speed and direction), and aerosol/constituent concentrations are required to increase the accuracy of weather forecast models. As with flight level data, atmospheric profiles would provide input to sensor and weapons system performance models. Data from aircraft launched vertical sounders can also be used to calibrate satellite sensors thereby increasing their accuracy.

Finally, surface measurements of pressure, temperature, wind, constituent concentration, and humidity are needed. Again, this data would be used to increase the accuracy of weather forecast models and sensor/weapons system performance models.

3. SCENARIOS FOR THE USE OF RECONNAISSANCE ASSETS IN SUPPORT OF REQUIREMENTS

Reconnaissance assets could provide real time weather observation over previously inaccessible or data denied areas. Both traditional reconnaissance aircraft and Uninhabited Aerial Vehicles (UAVs) could take meteorological observations while over-flying the battlefield. They could additionally be used as platforms for the deployment of dropsondes (for taking vertical profiles) or the deployment of unattended ground sensors (for the collection of surface data). Potential support scenarios range from minimal impact to dedicated weather missions.

In a minimal impact scenario reconnaissance assets are flown, unmodified, on traditional missions. Course deviations in support of weather requirements are minimal. Theater Weather is simply viewed as a customer for data that is gathered. Although some flight level weather data could be gathered from on-board sensors, the primary benefit would be the gathering of timely, high resolution cloud data.

A medium impact scenario involves the modification of the air vehicle by the addition of on-board sensors, the addition of an on-board or towed payload, or a significant deviation in mission profile. In such a scenario, the gathering of weather data near areas of interest would be a significant part of the mission. Flight level measurements of atmospheric parameters could be made using specialized on-board sensors. Vertical soundings could be made utilizing dropsondes released from the vehicle or a towed payload. The benefit of this scenario would be the ability to completely specify the weather in and around areas of interest. This would result in improved short term mission specific forecasts.

High impact scenarios involve the flying of dedicated weather missions. Vehicles would be modified to allow for a "full specification" of the battlefield. They would fly weather missions gathering the information needed to produce high-resolution observation fields for numerical weather prediction models. They would have the capability to do both "in-situ" measurements and vertical profiles. One possible scenario would have them "seeding" the battlefield with unattended ground sensors. The full development of this scenario would result in significant increases in accurate short and long-range weather prediction over the entire battlefield.

The extent to which reconnaissance assets are used in support of Theater Weather would depend on the value-added relative to other potential missions.

4. RECONNAISSANCE PLATFORM APPLICABILITY

Both traditional and uninhabited reconnaissance vehicles have the potential to support Theater Weather. 88th Weather Squadron and the Reconnaissance Program Office at Aeronautical Systems Center are investigating the applicability of several vehicle/sensor systems to weather support. The project is ongoing and information should be regarded as preliminary data from a "work in progress." Systems operated by the Air Force (U-2, Predator), Navy (Altus), and NASA (ER-2) are being considered along with systems currently in development such as "Dark Star" and "Global Hawk."

As a manned operational platform the U-2 has considerable potential to support Theater Weather. The U-2 flies several sensor systems that could be used in cloud analysis/forecasting. Wet Film cameras (IRIS II, IRIS III, and F-489) have sufficient resolution and footprint to aide in a fine scale cloud analysis. They represent a proven reliable technology. Unfortunately, real time images are not available. Due to delays in processing, wet film images would be

best used to study local effects in and around areas of interest. Electronic systems (ASARS and SYERS) are also proven technology currently being used on operational missions. SYERS is of sufficient resolution for cloud analysis and provides its data in near real time. Its footprint, however, is not optimal for the theater weather mission. Like all operational reconnaissance platforms the U-2 offers the advantage of flying over areas of interest. High-resolution cloud analysis and forecasting utilizing U-2 sourced data should be pursued.

The ER-2, flown by NASA, is a research version of the U-2. It flies a variety of research grade sensors that would be useful to Theater Weather. The Airborne Visible and Infrared Imaging Spectrometer (AVIRIS) could be adapted to view clouds at high resolution. It scans 224 spectral bands with a swath of approximately 10.6 km. and a resolution of 66 ft. It is a large and cumbersome instrument that could be made smaller by reducing the number of spectral bands². The Meteorological Measuring System (MMS) is a small lightweight system used to measure winds, pressure, and temperature at flight level. It is extremely accurate and utilizes both GPS and internal INS systems for geolocation. Additional information on ER-2 systems is available over the web at <http://airsi-www.ar.nasa.gov/ER-2/index.html>.

Uninhabited Aerial Vehicles (UAV) are capable of longer missions than their traditional counterparts and don't place aircrews at risk. Unfortunately, they have more limited payloads and are not as technologically mature. Current systems (Predator and Altus) flying an IR/EO sensor package could be used in support of cloud observation and forecasting. A ceiling of 25,000 ft (Predator) and a slow airspeed (Predator and Altus) are limiting factors. Of the two UAVs in development (Global Hawk and Dark Star), Global Hawk holds the most promise for theater weather support. It operates at high altitude, carries a large payload, and is capable of 24 hours loiter time at a range of 3000 nm. It can be outfitted with both a synthetic aperture radar (SAR) and an E-O package. Its long loiter time and high altitude make it ideal for use in specifying weather over the battlefield. In addition to observing clouds, it could be outfitted to take flight level meteorological measurements and serve as a launch vehicle for atmospheric sounders or ground based meteorological sensors.

CONCLUSIONS

Modern weapons systems require accurate weather forecasts for effective employment. One of the most significant barriers to improving forecast accuracy has been a lack of weather observations over hard to access areas. Reconnaissance platforms can help eliminate this shortfall by taking weather observations while over-flying the battlefield. Current capability exists to observe clouds and limited flight level weather from reconnaissance platforms. Further development would allow for a thorough meteorological specification of the battle area. The extent to which reconnaissance assets are modified and/or deployed in support of Theater Weather depends on the value added relative to other missions. Providing "current capability" data from reconnaissance platforms to Air Force Weather is low risk/high value and therefore recommended. Technologies allowing for increased weather observation capability of reconnaissance assets should be investigated and implemented when practical.

ACKNOWLEDGEMENTS

We would like to thank Mr. Andrew Roberts of NASA Ames Research Lab for information regarding their ER-2 program. We would additionally like to thank Mr. Mike Duncan at the Naval Postgraduate School for information regarding instrumented UAVs. Finally, thanks to Major Tracy Knights from the 9th Intelligence Squadron and Captain Anthony Howard from the 13th Intelligence Squadron at Beale AFB for information regarding U-2 capabilities.

REFERENCES

1. US Air Force Scientific Advisory Board, Dr. Gene McCall, Chairperson, SAB Quick Look Study on Weather Monitoring and Forecasting in Theater, 1997.
2. Eastwood, Michael, Member Technical Staff, Imaging and Analytical Spectrometry Group, Jet Propulsion Laboratory, Conversation with Capt John Polander 23 Jul 97.

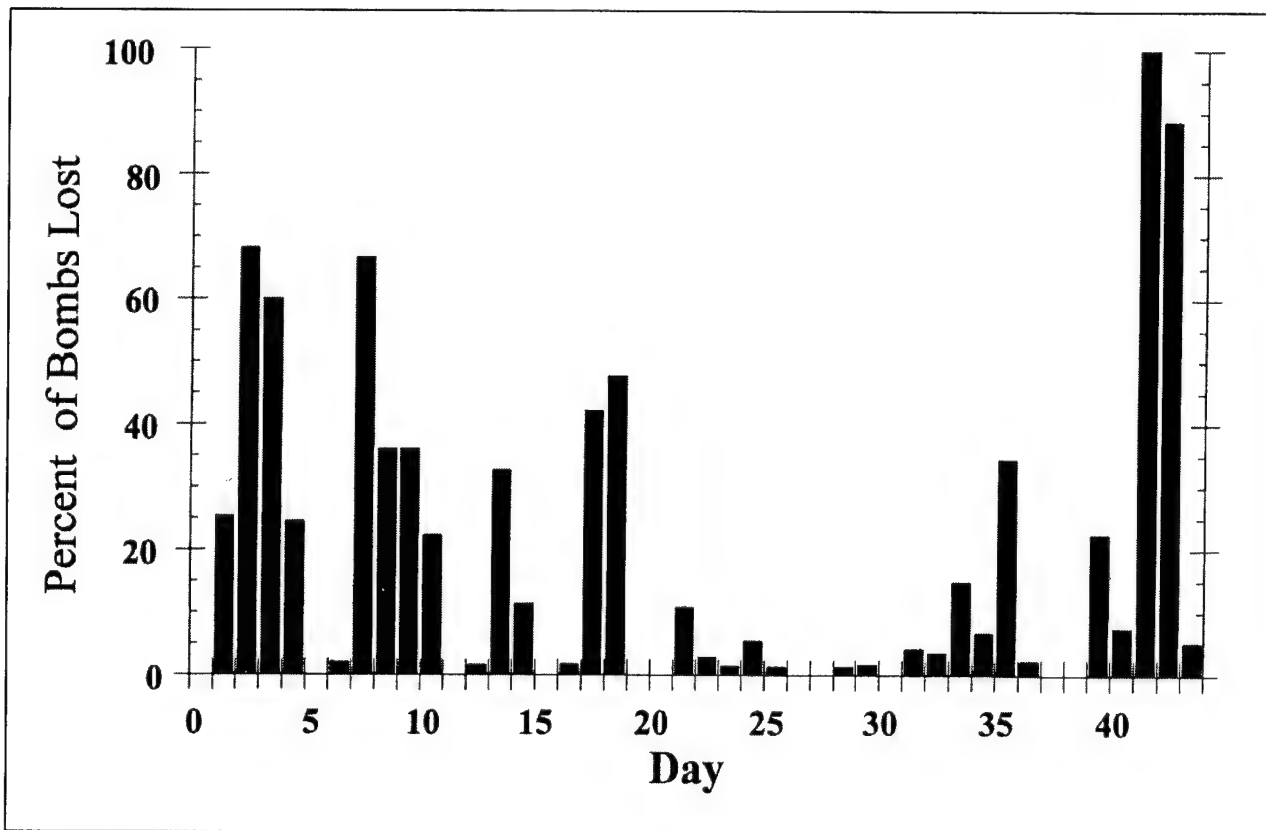


Figure 1. Percentage of bombs not dropped on primary target due to weather during Desert Storm (from Scientific Advisory Board Quick look study "Weather Monitoring and Forecasting in Theater.")

Platform	Status	Mission Profile	Available Sensors	Payload
U-2	Currently Flown by USAF	High Altitude, Medium Duration Flight	Wet Film Cameras Various E-O/Radar Packages	
ER-2	Currently Flown by NASA	High Altitude, Medium Duration Flight	Multi-spectral Scanners Film and Electronic Cameras Various Research Sensors	1,300 lbs. Internal 650 lbs. Nose 650 lbs. Each Wing 350 lbs. Center Pod
Dark Star	In Development	Short Duration (8 hour) Flight Over Heavily Defended Areas	Synthetic Aperture Radar or E-O Package	
Global Hawk	In Development	Long Duration (42 hour) Flight at High Altitude	Synthetic Aperture Radar and E-O Package	2,000 lbs.
Predator	Currently Flown by USAF	Long Duration Flight Slow Speed, below 25,000 ft.	IR/EO Sensor Synthetic Aperture Radar	450 lbs. Internal 150 lbs. Each Wing
Altus	Currently Flown by US Navy	Long Duration Flight Slow Speed below 45,000 ft.	Various Operational and Research Sensors	330 lbs.

Figure 2. Summary of reconnaissance assets of possible use in gathering weather data.

NASA DC-8 AIRBORNE SCANNING LIDAR CLOUD AND CONTRAIL OBSERVATIONS

Edward E. Uthe, Terje E. Oseberg, and Norman B. Nielsen
SRI International
Menlo Park, CA 94025, USA

ABSTRACT

An angular scanning backscatter lidar has been developed and operated from the NASA DC-8 aircraft; the lidar viewing direction could be scanned from vertically upward to forward in the direction of aircraft travel to vertically downward. The scanning lidar was used to generate real-time video displays of clouds and contrails above, below, and ahead of the aircraft to aid in positioning the aircraft for achieving optimum cloud/contrail sampling by onboard in situ samplers. Data examples show that the lidar provides unique information for the interpretation of the other data records and that combined data analyses provides enhanced evaluations of contrail/cloud structure, dynamics, composition, and optical/radiative properties.

1. INTRODUCTION

The environmental consequences of subsonic and supersonic aircraft fleets need better definition for input to the development of future aircraft and their operational scenarios. NASA is developing a capability to predict the effects of current and future aircraft on the environment through a 3-D model consisting of modular parameterizations of effluent emissions and their microphysical and chemical transformations, dynamic behavior, and radiation budget perturbations. Experimental data are needed to better understand relevant atmospheric processes and to develop quantitative relationships that improve the 3-D model performance. Model analyses will be used to assess and report the effects of aviation on the environment.

As part of the atmospheric effects of aviation project (AEAP), NASA formulated an extensive multi-aircraft field program, termed the subsonic aircraft: contrail and cloud effects special study (SUCCESS), that was conducted during April and May 1996. In addition to many advanced and recently developed atmospheric sensors, an angular scanning lidar was installed on the NASA DC-8 research aircraft and operated in support of SUCCESS.

2. LIDAR SYSTEM

The DC-8 scanning lidar employed a conventional two-wavelength (1.064 and 0.532 μm) 35-cm telescope system that previously had been used for both ground-based and airborne operations. The major effort in the DC-8 installation was the development of a scanning capability that provided for observations in the manner shown by Figure 1. Basically, a pressurized motor driven and computer controlled rotating cylinder that contained a 45 degree optical mirror and a 43-cm diameter window was attached to the DC-8 fuselage. Figure 2 pictures the scanning mirror pod along with an aerodynamic fairing located to the rear of the pod. The lidar was installed near the rear of the aircraft as the forward sections were needed for installation of in situ chemical, aerosol, radiation and meteorological sensors. Details of the lidar installation have been presented by Nielsen et al.¹

3. LIDAR OPERATIONS

The primary purpose of the DC-8 scanning lidar was to locate and help direct the aircraft into low density aircraft contrails and cirrus clouds so that they could be sampled by onboard in situ sensors. Lidar backscatter signatures were processed for real-time pictorial display on the DC-8 NTSC video network for viewing by the flight crew and experimenters to help guide flight direction and data collection operations. The digital signatures were also stored on 8-mm Exabyte tape for use in subsequent data analyses programs.

The lidar was normally operated at vertical up or down viewing angles to establish the presence and location of backscattering layers above and below the aircraft. At sampling altitudes the lidar was operated in forward viewing angular scan patterns to map the vertical structure of cirrus and contrails ahead of the aircraft. Figure 3 presents examples of the real-time angular scan display as presented on the DC-8 video network. The intensity modulated display presents a picture of cloud structure with a vertical axis of 1000 ft per division and a horizontal axis of 15 km. The backscatter signature for the last laser firing was plotted below the picture display and text information was given below the signature plot. The laser was fired at a rate of 10 Hz and the scanning mirror was rotated at 1° per second. The starting, ending, and incremental angles as well as the scan rate were computer controlled and easily adjusted by thumb switches.

4. LIDAR DATA EXAMPLES

Figure 4 presents DC-8 lidar data collected on 12 May 1996 with the lidar viewing in a fixed downward direction while the DC-8 was sampling its own contrail generated during an earlier flight over the area. The lidar display clearly depicts times when the contrail is below the aircraft and indicates times when the aircraft penetrated the contrail. These times agree well with times of observed increased water content and NO_x concentrations measured by onboard in situ sensors. The data are well correlated although the water content and NO_x sampling inlets were located on different sides of the DC-8. The combined lidar and in situ observations established times the contrail was above the aircraft as indicated in Figure 4. Onboard radiometric observations agree with this analysis showing cooler IR "surface" temperature and increased upwelling solar flux at times when the contrail was below the aircraft. Although the solar radiometric data have not yet been calibrated or corrected for aircraft motions, it appears that the albedo above the contrail is increased about 30% by the presence of the contrail.

Figure 5 presents angular scan data of DC-8 effluent plume cross sections (plotted with elevation angle and distance from aircraft axes) as the DC-8 closed the distance on its own contrail generated during the first flight of the system on 10 April 1996. The first six contrail cross sections are presented for a wavelength of 0.532 μm and the last cross section is presented for a wavelength of 1.064 μm . The onboard in situ chemical sensors detected the effluent plume at 00:53:03 GMT, the same time as the aircraft penetrated the contrail as inferred by the lidar data.

On 10 May 1996, during DC-8 transport from Salina, Kansas, to Ames Research Center, California, the lidar observed a widespread thin scattering layer at an altitude of about 43,000 ft MSL—above the flight ceiling of the DC-8 during this flight. Figure 6 presents upward-viewing lidar data showing backscatter returns from the layer before and after an aircraft turn that was made at an aircraft altitude of about 17,000 ft MSL. The backscatter from the particulate layer sharply decreases as the aircraft turn is initiated and the laser pulses intersected the layer at non-vertical angles. This behavior has been observed for high-altitude tropical cirrus clouds consisting of horizontally aligned plate-shaped ice crystals² and has been observed by several other lidar researchers.^{3,4} The rate the backscatter decreases with angle is dependent on size, shape, and orientation of the crystals.⁵ The scanning lidar provides a means to measure the zenith-enhanced backscatter without aircraft turns that affect other measurements such as solar and infrared flux. The horizontal alignment has been explained by falling crystals orienting themselves to offer maximum resistance to motion.⁵ Other DC-8 scanning lidar data show intense single-pixel lidar returns probably from individual precipitating ice crystals from aircraft contrails.⁶

5. DoD APPLICATIONS

The DC-8 scanning lidar concept can be readily deployed on DoD transport size aircraft (e.g., ABL, AST, ARGUS, Cobra Ball, etc.). Applications include the following:

- Detection and optical characterization of particulate layers above aircraft ceilings.
- Evaluation of high-altitude cirrus cloud and aircraft emissions on performance of airborne multispectral radiometers and infrared search and track (IRST) sensors, atmospheric propagation of high energy laser beams, and ablation of objects reentering from space.

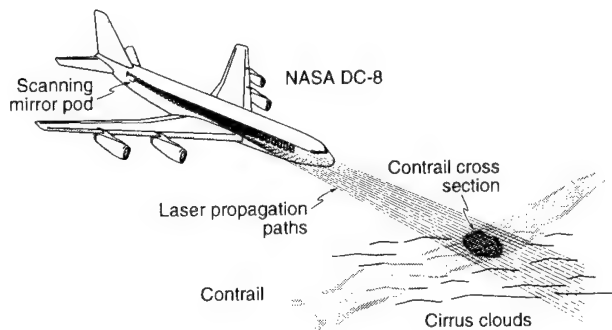


Figure 1. DC-8 scanning lidar illustration.

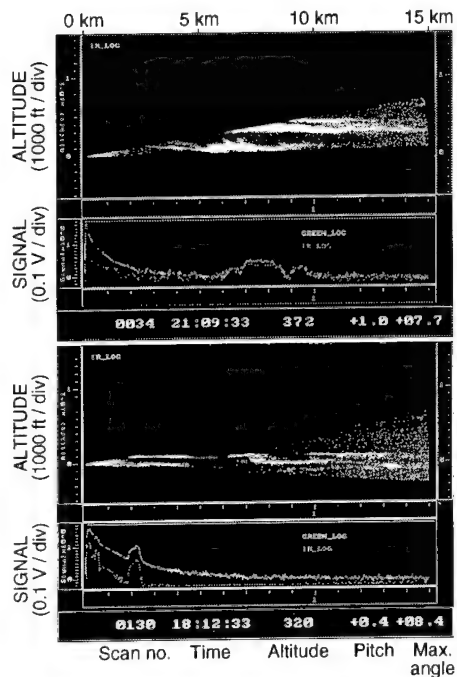


Figure 3. Real-time angular scan video displays generated by the DC-8 scanning lidar system.

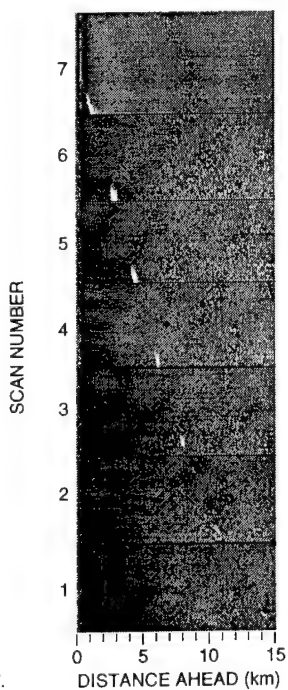


Figure 5. DC-8 lidar forward-viewing scan observations as the aircraft approaches a contrail generated earlier by the DC-8. Data are plotted with a vertical axis of time (scan angle) and a horizontal axis of distance ahead of the DC-8. 11 April 1996, 00:49:21 to 00:50:50 GMT.



Figure 2. DC-8 scanning lidar pod and aerodynamic fairing installation with pod positioned for forward lidar viewing.

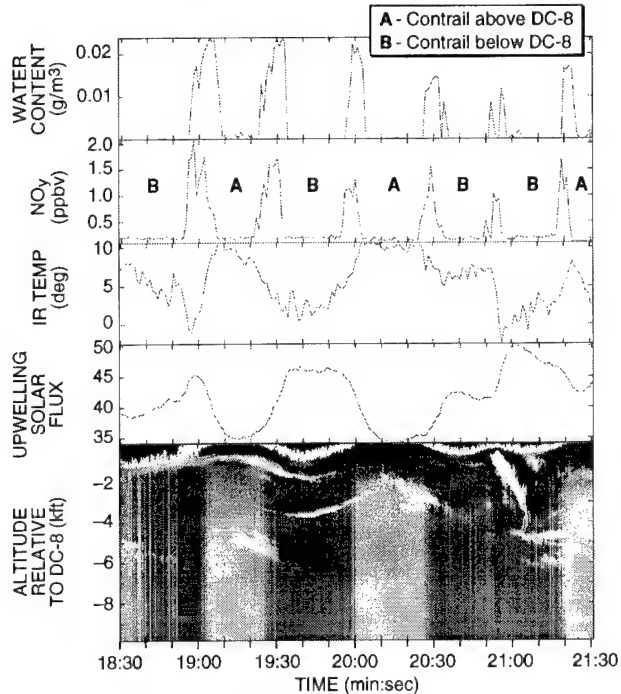


Figure 4. Lidar and selected in situ and radiometric data at times of the DC-8 penetrating its earlier generated contrail, 12 May 1996, 23:18:30 to 23:21:30 GMT. DC-8 altitude approximately 36 kft.

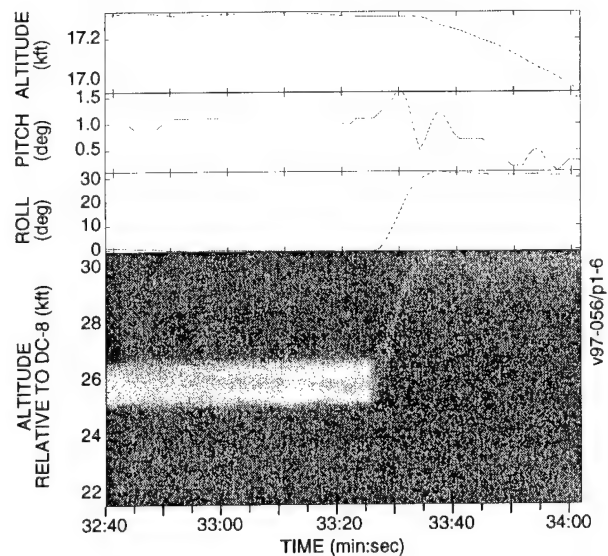


Figure 6. DC-8 lidar observations and selected DC-8 flight parameters showing a sharp decrease in lidar backscatter from a high altitude (43 kft) layer at small angles from the vertical, 10 May 1996, 16:32:40 to 16:34:05 GMT.

- Mapping visible and subvisible cirrus cloud distributions to help position aircraft to minimize atmospheric effects on DoD sensors and operations.
- Tracking aircraft effluents (engine exhaust, laser gases, etc.) to help position aircraft and sensor viewing angles to minimize effluent effects on onboard optical standoff and in situ sensors.
- Inferring atmospheric chemical composition and turbulent properties that can affect standoff sensor performance employing elastic backscatter lidar techniques.

6. ACKNOWLEDGMENTS

The SUCCESS DC-8 scanning lidar program was funded under Cooperative Agreement NCC2-885 with the NASA Ames Research Center. The water content data were provided by H. Gerber,⁷ the NO_y data by A. Weinheimer,⁸ and the solar flux records by F. Valero and A. Bucholz.⁹

7. REFERENCES

1. Nielsen, N. B. et al., "NASA DC-8 Airborne Scanning Lidar Sensor Development," Proceedings of the Second International Airborne Remote Sensing Conference and Exhibition, San Francisco, CA, 24-27 June 1996.
2. Uthe, E. E., and P. B. Russell, "Lidar Observations at Tropical High-Altitude Cirrus Clouds," in *Radiation in the Atmosphere*, H. J. Bolle, ed., Science Press, Princeton, New Jersey, 1976.
3. Intrieri, J. M. et al., "Multiwavelength Observations of a Developing Cloud System: The FIRE II 26 November 1991 Core Study," *J. Atmos. Sci.*, 4079-4093, 1995.
4. Thomas, L. et al., "Lidar Observations of the Horizontal Orientation of Ice Crystals in Cirrus Clouds," *Tellus*, 211-216, 1990.
5. Platt, C. M. R., "Lidar Backscatter From Horizontal Ice Crystal Plates," *J. Appl. Meteor.*, 482-488, 1978.
6. Uthe, E. E., N. B. Nielsen, and T. E. Oseberg, "DC-8 Scanning Lidar Applications During SUCCESS," submitted to *Geophysical Research Letters*, June 1997.
7. Gerber, H. et al., "Measurement of Wave Cloud Microphysics With Two New Aircraft Probes," submitted to *Geophysical Research Letters*, June 1997.
8. Ridley, B. A. et al., "Distributions of NO, NO_x, NO_y, and O₃ to 12 km Altitude During the Summer Monsoon Season Over New Mexico," *J. Geophys. Res.*, 99, 25519-25534, 1994.
9. Valero, F. P. J. et al., "The Atmospheric Radiation Measurements Enhanced Shortwave Experiment (ARESE): Experimental and Data Details," submitted to *J. Geophys. Res.*, 1997.

CLOUD DATABASE COLLECTED IN SUPPORT OF THE
SPACE-BASED INFRARED SYSTEM (SBIRS) PHENOMENOLOGY EXPLOITATION PROGRAM

Thomas R. Caudill, William A. M. Blumberg, Alan Griffin, John Wise
Phillips Laboratory, Geophysics Directorate
Hanscom AFB, MA 01731-3010

Capt. David J. O'Donnell
Space and Missile Systems Center
Los Angeles AFB, CA 90245

ABSTRACT

The SBIRS Phenomenology Exploitation Program (PEP) was formed to provide infrared data and background models to the SBIRS contractors which could be used to assess system performance. To accomplish this task the PEP carried out a number of data collections using satellites, aircraft, lidars, radars, and other instruments. Some instruments collected IR data, while others collected "ground truth" information about the cloud environment to provide more complete descriptions of the scene. The satellites used included the DoD funded MSTI-3 and MSX, as well as the geostationary GOES, METEOSAT and GMS and polar-orbiting NOAA-12 and -14 weather satellites. The ARES aircraft was used to collect spectral data with its 75-channel spectrometer, while the Aeromet HARP aircraft collected radar, lidar and particle probe data in and around the clouds. The University of Wisconsin HSRL and VIL lidars and the University of Massachusetts' CPRS and PL/GP's TPQ-11 radars provided high resolution information about the cloud structure. This dataset is now available to authorized users through the SBIRS Phenomenology Data Analysis Center (PDAC) located at PL/GP.

INTRODUCTION

The SBIRS Systems Program Office (SPO) conducted a program of background data collections, analyses, and modeling as a part of its Phenomenology Exploitation Program. IR data was collected by the Miniature Sensor Technology Integration-3 (MSTI-3) satellite, the Mid-Course Space Experiment (MSX) satellite, and the Airborne Remote Earth Sensing (ARES) aircraft. Additional "truth" data was collected by the High Spectral Resolution Lidar (HSRL), the Volume Imaging Lidar (VIL), the Cloud Profiling Radar System (CPRS), the TPQ-11 (a 35 GHz radar), the High Altitude Reconnaissance Platform (HARP), and meteorological satellite imaging and sounding sensors. In this context, "truth" data is information on terrestrial and atmospheric phenomena relevant to the generation of IR signals. TABLE 1 gives a list of the principal instruments used for data collection as well as providers of other analysis products.

INSTRUMENTS AND ANALYSIS PRODUCTS

The MSTI-3 satellite, launched in May 1996, is in a sun-synchronous orbit at 425 km altitude. MSTI-3 includes a pair of carefully calibrated, very sensitive radiometers. Using a common telescope and two-dimensional pointing system, each radiometer has a 256 x 256 pixel focal plane and its own filter wheel. The filter wheels contain an array of interference filters with state-of-the art transmission edges and very high out-of-band rejection. The filters are primarily located near the 2.8 μm and 4.3 μm absorption bands.

The Airborne Remote Earth Sensing (ARES) Program is administered by the Remote Earth Sensing Program Office under SAF/AQ. The ARES aircraft (a WB-57 flying at 50,000 ft.) was used to collect spectral data with its 2.0 - 6.4 μm , 75-channel spectrometer. The largest scenes collected by ARES are ~100 kilometers in length and one to a few kilometers in width.

The MSX satellite, launched in April 1996, is in a near-sun-synchronous orbit at 902 km altitude. MSX is owned by and operated under contract to BMDO. Its primary instrument for SBIRS was the SPIRIT III radiometer and interferometer which has one array of IR detectors with 2 MWIR spectral filters. Information about the SPIRIT III and other MSX instruments is available in Reference [2].

The University of Wisconsin operated two different lidars (together, in general) for the PEP. The systems are referred to as the High Spectral Resolution Lidar (HSRL) [3] and the Volume Imaging Lidar (VIL) [4], respectively. Using the two instruments in combination allows a (partial) calibration of cloud extinction for the 3-D VIL cloud fields. The lidars have excellent sensitivity and can collect data on optically thin and sub-visual cirrus clouds.

The HSRL is a non-scanning lidar operating at $0.532\ \mu\text{m}$. It provides information on cloud extinction as a function of altitude, cloud base, cloud top (up to optical depth 4) and information on the spatial variations of cloud density (as winds cause clouds to drift through the HSRL beam). Precision retrievals of cloud optical depth are accomplished because extinction along the propagation path is calibrated using the known level of molecular scatter. The molecular return is roughly linear with atmospheric density (whose altitude profile is well known). Knowledge of the extinction allows the lidar return to provide absolute backscatter levels.

The VIL is a high-speed scanning lidar operating at $1.06\ \mu\text{m}$. It only reports relative backscatter as a function of altitude. The backscatter is termed "relative" because there are ambiguities in the proportions of a given return resulting from the cloud scatter of interest (at a particular altitude) versus extinction along the propagation path. The VIL provides less robust information on cloud physics but operates on a high-speed, two-axis gimbal. This gimbal allows the VIL to produce an instantaneous slice through the sky. As clouds drift over the lidar, a full 3-dimensional depiction of a cloud field is created.

The CPRS is a compact, mobile instrument built and operated by the University of Massachusetts-Amherst (UMass) [5]. This system is similar to the VIL in that it can scan perpendicular to the wind vector to build up a three-dimensional representation of a cloud field. The CPRS has the advantage that the millimeter wavelengths are able to penetrate most non-precipitating water clouds allowing collection of information on multi-layer cloud systems. It can also operate in the presence of water clouds that obscure the VIL. The CPRS is a calibrated, dual wavelength (8- and 3-mm) and dual polarization system. The latter characteristic allows separation of spherical and non-spherical particles. It has the disadvantage of reduced scan rates (compared to the VIL), limiting it to a reduced swath. Another problem of using radars for sensing cloud properties is that the millimeter wavelengths are not very sensitive to the smaller particles ($<10\ \mu\text{m}$). These small particles may be important in certain cases (particularly cold high cirrus) since they could make a significant contribution to the optical depth of the cloud in the IR.

The TPQ-11 35-GHz radar at Hanscom AFB provides a dedicated asset to collect coincident truth data on clouds as well as a long term climatology. The latter data set is important because the TPQ-11 can detect multiple layers of cloud even when low altitude water clouds are present [6].

The High Altitude Reconnaissance Platform (HARP) operated by Aeromet, Inc. (Tulsa, OK) utilizes an instrumented Lear-36A jet to measure cloud metrics and microphysics from below, within, or above a cloud deck. HARP has a 35 GHz down-looking radar, an uplooking lidar firing at 0.53 and $1.06\ \mu\text{m}$ wavelengths, and several particle probes (2D-C, 1D-C, FSSP) attached to hard points on the wings. The primary use of HARP was to collect data on particle size, concentration, and shape from the top of clouds down. HARP also reported on atmospheric state at its flight altitude.

Meteorological satellite sensors are divided into two categories: imagers and sounders. Data were collected from the polar orbiting NOAA-12 and -14, and geostationary GOES-8 and -9, METEOSAT and GMS. World-wide imagery was obtained by MIT/LL through the University of Wisconsin's McIDAS connection. Imagers provide multi-spectral data at high spatial resolution (1-5 km, high only compared to the sounders), primarily in spectral bands that have high transmission to the ground. Algorithms exist to detect most clouds with imager

data. The GOES imagers and the AVHRR (aboard NOAA platforms) imagers have the best inherent capability of imagers to detect cirrus clouds. The GOES sounders have 10 km nadir spatial resolution and the HIRS-2 aboard the NOAA platforms have 18 km nadir resolution (though its pixels are not contiguous). The other geostationary platforms do not fly sounders. The sounders have a large number of spectral bands with variable transmission to the ground. Comparison of signals in bands with low and high transmission to the ground allows retrieval of information in the vertical. The sounders are optimal for detection of cirrus, especially optically thin cirrus, and for obtaining cloud heights.

Other meteorological data were also collected in connection with IR measurements. Radiosondes provided standard reports of temperature, pressure, water vapor, and wind speed as a function of altitude. Also collected were regional reports of air and water temperature, observations from ground meteorological stations at 0000Z and 1200Z and mesoscale grids of atmospheric profiles created by numerical weather prediction models.

Although not a data collection instrument, the SERCAA algorithm [7] is the latest development in the processing of meteorological satellite imagery. SERCAA, which stands for Support of Environmental Requirements for Cloud Analysis and Archive, has been developed by Phillips Laboratory and Atmospheric and Environmental Research, Inc. (AER) to provide a global cloud analysis capability using data from multiple military and civilian satellites. The high resolution data from both geostationary and polar platforms is then integrated into a real-time cloud analysis product.

Another issue addressed was the need for a global cloud climatology to assess obscuration of low altitude targets. The climatology created by Dr. Don Wylie of the University of Wisconsin was selected as the baseline data set in this area. Reference [8] describes the many positive assets of the Wylie data and compares it to SAGE and ISCCP data. It also notes that there are substantial disagreements in the literature regarding the amount of cloud present at any one time, particularly clouds above 6 km.

Particle shape is an important parameter in the determination of the angular distribution of the scattered radiation. Non-spherical particles scatter light much differently than spherical particles. To address this issue, the University of Utah has provided information on the scattering properties of non-spherical particles [9]. They have calculated the scattering phase function, single scatter albedo and asymmetry factor for a number of mixtures of randomly oriented ice crystal shapes (based on HARP measurements) over the ARES 2.0-6.4 μm wavelength range. The University of Utah is also developing a method for retrieving cirrus cloud properties using a number of ARES channels.

CONCLUSIONS

Since the high cost rules out any test flights of the new satellites, simulations are a critical tool in the design and assessment of the sensor and constellation performance. However, the fidelity of the simulation output is limited by the quality of the input data. Significant uncertainty in the design/testing process still exists because very little empirical data has been available to support performance simulations. Truth assets provide data on cloud occurrence, cloud physical and microphysical properties, MWIR atmospheric radiance, surface temperature, glint, and other relevant phenomena. Whereas coincident data is intended to aid in model validation, the statistical truth data are geared to understanding the scope and frequency of occurrence of important phenomena. This dataset is now available to authorized users through the SBIRS Phenomenology Data Analysis Center (PDAC) located at PL/GP.

REFERENCES

2. Mill, J. D., O'Neil, R. R., et al., (1994) Midcourse Space Experiment: Introduction to the Spacecraft, Instruments, and Scientific Objectives, *J. of Spacecraft and Rockets*, **31**, No. 5.
3. Eloranta, E. W. and Piironen, P. (1994) An I₂-absorption filter based High Spectral Resolution lidar for measurements of the optical properties of aerosols and clouds, *Atmospheric Propagation and Remote Sensing III*, SPIE, Orlando, Florida, April 5-8, 1994. and Piironen, P. (1994) *A High Spectral Resolution Lidar Based on an Iodine Absorption Filter*, Ph.D. Thesis, University of Joensuu, Dept. of Physics, Finland.
4. Piironen, A. K. (1994) *Analysis of Volume Imaging Lidar Signals*, Ph.D. Thesis, University of Joensuu, Department of Physics, Vaisala Laboratory, Finland.
5. Sekelsky, S. and McIntosh, R. (1996) Cloud Observations with a Polarimetric 33 GHz and 95 GHz Radar, *Meteorology and Atmospheric Physics*, **59**, 123-140.
6. Paulsen, W. H., Petrocchi, P. J., and McLean, G., (1970) *Operational Utilization of the AN/TPQ-11 Cloud Detection Radar*, Instrumentation Paper No. 166, AFCRL-70-0335, U. S. Air Force, Cambridge Research Laboratories, Bedford, MA, June 1970, AD709364.
7. Gustafson, G., et al., (1994) *Support of Environmental Requirements for Cloud Analysis and Archive (SERCAA): Algorithm Descriptions*, PL-TR-94-2114, Phillips Laboratory, Hanscom AFB, MA, AD283240.
8. Wylie, D. P., Menzel, W. P., Woolf, H. M., and Strabala, K. I. (1994) Four Years of Global Cirrus Cloud Statistics Using HIRS, *J. Climate*, **7**, 1972-1986.
9. Takano, Y., and Liou, K. N., (1995) Radiation Transfer in Cirrus Clouds. Part III: Light scattering by irregular ice crystals, *J. Atmos. Sci.*, **52**, 818-837.

TABLE 1. Instrument and analysis summary

Component	Source	Agency	Data Type	Product	Application
ARES	WB57 Aircraft	AF, LMSC (Tilton)	Spectrometer/Radiometer	IR cloud background signatures	Radiometric cloud scene construction
MSTI-3	Satellite	SMC/MTA (O'Donnell)	Filter Radiometers	IR background signatures	Radiometric cloud scene construction
MSX	Satellite	BMDO	Filter Radiometer	IR background signatures	Radiometric cloud scene construction
HARP	Learjet	Aeromet (Rose)	Radar, Lidar, Particle probes	Cloud top, ice shape and size distribution	Cloud parameters along flight track
HSRL	Lidar	U. Wisc. (Eloranta)	Calibrated line-of-sight backscatter	Cloud optical depth, top, thickness	Cloud optical depth as function of alt.
VIL	Scanning Lidar	U. Wisc. (Eloranta)	3-D high resolution images	Navigated 3-D cloud fields	Precise cloud volume structure
TPQ-11	35 GHz Radar	PL/GPA (Caudill)	Radar backscatter	Cloud top, thickness, multilayer	cloud structure
CPRS	Scanning Radar	U. Mass. (Sekelsky)	3-D Radar images	Navigated 3-D cloud fields	Cloud volume structure
SERCAA	NOAA & GOES Imagers	PL & AER (Gustafson)	Multispectral cloud imagery	Large scene cloud top map	Large scene cloud top altitude
CO ₂ Slicing	NOAA & GOES Sounders	U. Wisc. (Wylie)	Multispectral radiance	Vertical cloud properties	Large scene cloud vertical structure
ARES Data Analysis	ARES	U. Utah (Liou)	model radiative properties	Cirrus cloud phase functions/BRDF's	Microphysical cloud properties
Meteorology Data	Satellites, in-situ, and others	MIT/LL (Burke)	Polar & Geo satellite, surface obs, models	Satellite images, surface obs. and model output	Archived met dat and other products

LIDAR OBSERVATIONS PROVIDE INFORMATION ON THE 3-DIMENSIONAL STRUCTURE AND OPTICAL PROPERTIES OF CLOUDS REQUIRED FOR SCENE GENERATION

E. W. Eloranta

University of Wisconsin

1225 W. Dayton St., Madison, WI 53706, US

1. Abstract

Computer simulations can greatly reduce the cost and danger of military training. These simulations require realistic representations of the environment. Clouds impact the operation of military systems and they often play an important role in tactical decisions. Thus, it is important to develop computer algorithms which produce realistic cloud scenes.

Cloud models for military simulations must not only predict the visual appearance of the cloud under various illumination conditions, but they must also predict the appearance of the cloud field at all of the wavelengths used by military sensors. These requirements suggest the use of simplified radiative transfer models in the rendition codes. These radiative transfer codes require information on spatial structure of the clouds and on the optical properties of the cloud. The optical properties depend on cloud micro-physics.

This paper will describe the use lidar to observe the three-dimensional structure of clouds and to provide the cloud optical properties required for developing and testing simulations.

The University of Wisconsin Volume Imaging Lidar (VIL) combines an energetic, high-repetition rate laser with a sensitive receiver and high-speed scanning system. This system is particularly useful for mapping the 3-dimensional structure of cirrus clouds. A typical scan volume maps the cloud structure through the entire vertical extent of the cloud and covers horizontal dimensions of approximately 100 km. Spatial resolutions of 60 m are normally provided. However, resolutions as fine as 15 m can be provided in smaller volumes.

In addition to the VIL, the University of Wisconsin has developed a unique High Spectral Resolution Lidar (HSRL) which provides calibrated measurements of backscatter cross section, optical depth, and depolarization. Ongoing research shows promise of simultaneously providing range-resolved measurements of particle size. Although the HSRL is not currently a scanning system, it provides unambiguous measurements of cloud optical properties along a single pointing direction.

We have operated the VIL and the HSRL simultaneously to observe cirrus clouds. In these experiments the VIL provides the spatial structure of the clouds while the HSRL provides calibrated optical properties. The HSRL observations are then used to provide an approximate calibration for the VIL observed data. The resulting VIL data sets provide measurements of the scattering cross section mapped over large 3-dimensional volumes at time intervals of a few minutes. A typical data volume contains 10's of megabytes of data, and each data set includes many successive time intervals. In addition, we have compiled a large database on the optical properties of cirrus clouds derived from HSRL observations.

This presentation will include visualizations prepared from VIL data using a single scatter radiative transfer model. These will include both cirrus and fair weather cumulus cloud scenes. Statistics on the optical properties and the spatial structure of cirrus clouds will also be presented.

2. Acknowledgements

Funding for this research was provided by Air Force contract F19628-96-C-0097, National Science Foundation Grant ATM-9321330, and by Lockheed Missiles and Space Company contract SK30G4160F.

Comparison of Satellite-Based Cirrus Retrievals With Coincident Ground-Based Radar and Lidar Observations

*Robert P. d'Entremont and Gary B. Gustafson
Satellite Meteorology Group
Atmospheric and Environmental Research, Inc.
840 Memorial Drive, Cambridge, MA 02139-3794*

*Thomas R. Caudill
Remote Sensing Applications Branch / GPOR
Phillips Laboratory, Geophysics Directorate
Hanscom AFB, MA 01731-3010*

1. Introduction

In addition to the wide variability in properties common for other types of clouds, cirrus clouds have transmissivity values t that span the entire possible domain $0 < t \leq 1$. This variability adds complexity to the analysis of cirrus clouds. In comparison to opaque clouds, uncertainties exist in thin cirrus cloud amount, altitude, thickness, and optical properties as retrieved from satellite because the measured cirrus signal is affected additionally by an unknown radiation component from below.

Cirrus radiative and spatial properties are derived using multispectral AVHRR imager techniques. This model is based on radiative transfer principles that intrinsically account for both the semi-transparent nature of thin cirrus clouds and the attenuation effect of atmospheric water vapor in the 3.7- μm MWIR and 10.7- μm LWIR thermal window regions.

Cirrus altitudes and optical depths, both observed and retrieved, are compared using satellite-based AVHRR analyses and either the ground-based TPQ-11 35-GHz radar (over Hanscom AFB) or the HSRL lidar (at Madison, WI) observations for a period in mid-September 1995. Optically thin cirrus clouds are studied that are clearly discernible in lidar observations but extremely tenuous in the MWIR and LWIR window regions. The use of water vapor imagery to enhance cirrus retrievals will also be described.

2. Observation of Cirrus from Satellite

There are many sources of passive satellite data that can be used to detect and analyze cirrus attributes. Among the earliest are visible and infrared data of the 1960s from the TIROS series of polar orbiting satellites, augmented in the early 1970s by geostationary GOES data. Current GOES-Next Imager and Sounder channels useful for detection of cirrus include 3.9, 6.7, 11.2, 12.7, and

the CO₂ 13.3 – 14.5 μm spectral bands. The 3.9, 6.7, and 11.2 – 12.7 μm channels will be discussed in detail shortly; the 6.7 μm water vapor band has proven useful for detection of very thin cirrus over warm backgrounds such as deserts and tropical oceans.

More recent TIROS sensors include the Advanced Very High Resolution Radiometer (AVHRR), a five-channel passive radiometer with detectors that measure upwelling visible (0.63 μm), near-infrared (NIR, 0.86 μm), middle wavelength IR (MWIR, 3.7 μm), and split longwave IR (LWIR, 10.7 and 11.8 μm) energy both day and night. The sounder instruments collectively known as TOVS (TIROS Operational Vertical Sounder) also collect data in the wings of the 15-μm CO₂ absorption band that are useful for detection of thin cirrus and specification of their height. There are also very high spatial resolution (650-m) Defense Meteorological Satellite Program data available in visible/NIR (0.4 – 1.1 μm) and LWIR (10 – 12 μm) bands that are helpful in ascertaining the small-scale spatial attributes of cirrus over global scales.

2.1 Passive Infrared Physics of Cirrus Cloud Signatures

The upwelling spectral thermal radiance I_{obs} measured by a downward pointing radiometer for a field of view completely filled by a non-reflective, thin cirrus cloud is

$$I_{\text{obs}} = (1 - \epsilon) I_{\text{sfc}} + \epsilon I_{\text{cld}} \quad (1)$$

where ϵ is the bulk cirrus emissivity, I_{sfc} is the upwelling radiance emitted by the underlying surface and clear atmosphere, and I_{cld} includes the cirrus blackbody radiance plus the radiance emitted by the atmosphere above the cloud. For purposes of discussion, assume that the radiance data are being measured by the AVHRR MWIR Channel 3 and LWIR Channel 4 sensors. The two cirrus radiance equations are then

$$I_{\text{obs},3} = (1 - \epsilon_3) I_{\text{sfc},3} + \epsilon_3 I_{\text{cld},3} \quad (2a)$$

and

$$I_{\text{obs},4} = (1 - \epsilon_4) I_{\text{sfc},4} + \epsilon_4 I_{\text{cld},4} \quad (2b)$$

where the "3" and "4" subscripts denote the 3.7 and 10.7 μm AVHRR Channels 3 and 4 radiances, respectively. Additionally,

$$\epsilon_3 = 1 - (1 - \epsilon_4)^m \quad (2c)$$

This is the third of a three-set equation (2a), (2b), and (2c) in three unknowns ϵ_3 , ϵ_4 , and T_{cld} . The three measurements (knowns) consist of the exponent "m," and the satellite-measured radiances $I_{\text{obs},3}$ and $I_{\text{obs},4}$ (see d'Entremont et

al., 1990). This three-equation system forms the physical basis for the cirrus retrieval techniques of this study that analyze multispectral infrared satellite radiances.

2.2 Cirrus Retrievals Using 6.7- μ m Water Vapor Imager Data

In light of the 3.7- μ m daytime solar contamination issue, ongoing SERCAA studies are revealing that 6.7- μ m water-vapor radiance data can be used in place of those taken at 3.7 μ m. This finding is significant in that (a) the complexity of retrieving cirrus properties during daytime (due to mixed solar/thermal energy at 3.7- μ m) is eliminated, and (b) there are 6.7- μ m water vapor channels on all currently operational meteorological satellites, both geostationary and polar, save DMSP. Thus with the development of a 6.7- μ m cirrus optical depth and effective altitude algorithm comes a capability for cirrus spatial and optical property analyses that are truly global in nature and that span the full diurnal cycle. The water-vapor cirrus retrieval physics is identical to the MWIR retrieval physics in that Eq. (2a) is written for 6.7- μ m (vice 3.7- μ m) satellite radiance observations. Initial retrieval results over a 10-case data set compare quite well with ground- and aircraft-based observations of cirrus clouds.

3. Cirrus Retrieval Validation Results

The front-cover figure of this CIDOS preprint volume shows direct comparisons between SERCAA satellite-based cirrus retrievals and coincident ground-based 35-GHz radar observations of cirrus base and top. The ground-based radar data were collected as a part of a field experiment conducted over Hanscom AFB, MA and Madison, WI during mid-September 1995. The satellite retrievals were performed using GOES-8 water-vapor and LWIR radiances. On the front cover is shown cirrus altitude retrievals plotted with coincident cirrus radar observations for 2330 UTC at Hanscom AFB on 16 September 1995.

The colors on the plot are representative of the reflected power received as a function of altitude by the active 35-GHz radar, with warm colors (reds, oranges, yellows) corresponding to strong returns and cool colors (green, cyan) corresponding to weaker returns. Dark blue denotes cloud-free observations. Red diamonds denote the SERCAA 6.7-10.7- μ m satellite-retrieved cirrus altitudes that correspond with their respective coincident radar observations. As can be seen, the retrievals match well with observation. Corresponding cirrus LWIR effective emissivities are plotted in yellow squares against the right-hand vertical (emissivity) axis. It is seen that the retrieved emissivities are higher where the radar returns are stronger and vice versa.

The white circles correspond to "blackbody" altitude retrievals obtained

using 10.7- μm brightness temperatures that have been uncorrected for cirrus transmissive effects (i.e., assuming the cirrus is a blackbody cloud). This is the technique typically used by most cloud analysis models to compute cloud altitude for both opaque and transmissive clouds. Altitudes retrieved in this manner agree reasonably well with true cirrus altitudes wherever cirrus transmissivities are low (optically thick cirrus), as is seen on the left side of the plot. However, where cirrus is optically thin, the comparison differences are dramatic: on the right half of the plot are cirrus blackbody retrievals that differ by as much as 6 km from the true, SERCAA-retrieved cirrus altitudes. It is important to note that the green squares denote state of the art in the current Air Force operational global cloud analysis model, the RTNEPH, as well as in the Phase-I SERCAA algorithms being implemented as a part of CDFS-II.

4. Summary

As a part of SERCAA cloud analysis development efforts, new and innovative multispectral infrared cirrus analysis techniques have been developed and successfully applied and validated to real-time cirrus detection and analysis scenarios. Integration of these and other retrieval techniques into the overall SERCAA cloud analysis allows the strongest and most reliable attributes of each technique to be combined into one comprehensive cloud analysis product that is more realistically representative of cirrus spatial and optical properties than the current RTNEPH. With increasing amounts of multispectral infrared satellite data becoming available, the goal is to continue to retrieve from these data high quality augmented radiative, spatial, and microphysical properties of cirrus clouds in real-time and for climatological purposes at finer spatial and temporal resolution.

5. Bibliography

- d'Entremont, Robert P., Donald P. Wylie, J. William Snow, Michael K. Griffin, and James T. Bunting, 1992: **Retrieval of Cirrus Radiative and Spatial Properties Using Independent Satellite Data Analysis Techniques**. Proceedings, Sixth Conference on Satellite Meteorology and Oceanography, Amer. Meteor. Soc., 5-10 January 1992, Atlanta, GA, 17-20.
- d'Entremont, Robert P., Michael K. Griffin, and James T. Bunting, 1990: **Retrieval of Cirrus Radiative Properties and Altitudes Using Multichannel Infrared Data**. Proceedings, Fifth Conference on Satellite Meteorology and Oceanography, Amer. Meteor. Soc., 3-7 September 1990, London, England, 4-9.
- Ou, S. C., K. N. Liou, W. M. Gooch, and Y. Takano, 1993: **Remote Sensing of Cirrus Cloud Parameters Using AVHRR 3.7 and 10.9 μm Channels**. *Appl. Optics*, 32, 2171-2180.

AIRBORNE RETRIEVAL OF CIRRUS CLOUD TEMPERATURE AND COMPOSITION
USING ARES 5.1-5.3 μm AND 3.7 μm RADIANCE DATA

S. C. Ou, K. N. Liou, P. Yang, and P. Polland
Department of Meteorology / CARSS
University of Utah
Salt Lake City, Utah 84112-0110

T. R. Caudill
Geophysic Directorate, Phillips Laboratory
Hanscom AFB, MA 01731-3010

J. Lisowski SCITEC, Princeton, NJ. 08540	B. Morrison Aeromet, Inc. Tulsa, OK. 74170-1767
--	---

ABSTRACT

We present an airborne retrieval method for determining cirrus cloud temperature and composition based on the Airborne Remote Earth Sensing (ARES) 2-6.4 μm 75-channel data. The retrieval method has been applied to the ARES data collected during the Hanscom AFB mission flight, which was carried out on board the WB-57F on September 16, 1995 over western Boston. For validation, the retrieved cloud parameters are compared with in-situ 2D-probe measurements on board the Aeromet's Learjet, and the cloud heights derived from the ground-based 8.6-mm TPQ-11 radar returns.

1. INTRODUCTION

The airborne retrieval method developed utilizes the ARES 5.1-5.3 μm water vapor band-wing channel radiances to compute cirrus cloud temperatures and IR emissivities, from which the associated optical depth is derived based on radiative transfer parameterizations¹⁻³. The ice crystal mean effective size is obtained by matching the computed sum of the 3.7 μm solar reflected and IR emitted radiances with that from ARES Ch. 42 (3.755 μm) radiance. The selection of these channels is based on the examination of the computed weighting functions of a midlatitude summer atmosphere and quick-look images of ARES channels radiances over the WB-57F flight tracks.

Cloudy radiances have been measured by the ARES channels on board the WB-57F high-altitude research aircraft operated by the NASA Johnson Space Flight Center. The ARES sensor for the present study has been operated as a 75-channel imaging spectrometer. It is in a pushbroom mode with 45-pixel array pointing in the nadir direction taking data at the standard rates of 10, 20, 40, or 80 scan/s. We apply the retrieval algorithm to the ARES data collected during a mission flight, which was carried out on board the WB-57F on September 16, 1995 over the western Boston area. For validation purposes, we also acquired meteorological and ice microphysical data collected from the High Altitude Reconnaissance Platform (HARP), which is a Learjet 36A, flying in conjunction with the ground-based sensors and ARES measurements. In addition, the cloud-height data from the ground-based TPQ-11 8.6 mm (35GHz) radar at the Hanscom AFB were also obtained.

2. APPLICATION OF THE RETRIEVAL SCHEME TO ARES DATA

The WB-57F flight on September 16, 1995 was divided into eight flight tracks, among which the data collected for the four straight tracks (#1,3,5, and 8) were analyzed. Figure 1 shows radiance images for the ARES Chs. 41(3.681 μm), 42(3.755 μm), 55(4.747 μm), 60(5.116 μm), and 63 (5.332 μm) over a selected segment of Track 1. The first three channels are within the 3.75 and 4.7 μm window regions, while the last two channels are in the 6.3 μm water vapor band-wing region. For each image, the horizontal and vertical scales are ~500m and 2.5 km respectively. The dark and gray colors are associated with higher and lower radiance values, corresponding to clear and cloudy regions,

respectively. From these images, it is noted that the upper one third of the domain is clear, and the rest of the domain is cloudy. Over the clear area, the images for the three window channels show significant variations of the emitted/reflected radiances due to the inhomogeneity of the surface temperature and emissivity. However, for the two band-wing channels, radiances over the clear area appear to be relatively uniform, as compared to the clear radiances for the window channels, because the significant water vapor absorption/emission effect in the lower troposphere blocks the horizontally inhomogeneous surface emission. The narrow distribution of the clear radiances is a desirable feature for the application of remote sensing algorithms. Smaller spreads in clear radiances lead to less errors in prescribing the mean clear radiances, thus enhancing the retrieval accuracy. Over the cloudy area, it is evident that the images for the $4.7\text{ }\mu\text{m}$ channel as well as for the two band-wing channels contain distinct cloud signatures. For the two $3.7\text{ }\mu\text{m}$ window channels, there is no distinguishable cloud signature due to the compensating effects of strong reflection and weak emission by cloud particles. Radiance images for channels at the absorption band center (not shown here) exhibit no cloud signature. Based on the images shown in Fig. 1, together with the weighting function profiles, we select Ch. 60, 61 ($5.189\text{ }\mu\text{m}$), 62 ($5.261\text{ }\mu\text{m}$) and 63 for the application of cirrus cloud retrieval algorithms. Images for these channels contain definitive cloud signatures and display narrow data spread of clear radiances.

To validate the retrieved cirrus cloud temperature/height, we use the time series of cloud boundary (cloud top and base) altitudes derived from the 8.6-mm radar measurement together with the upper atmospheric temperature measurement by HARP. Figure 2(a) shows the atmospheric temperature profile between 5 and 11 km. These temperature values were obtained between 2029 and 2341 UTC. Within the altitude range, the temperature varies between -5° and -55° C. Figure 2(b) shows the cloud boundary altitudes derived from the 8.6-mm radar measurements between 2000 and 2400 UTC. Within this time period, the 8.6-mm radar observed the continuous presence of a single layer of cirrus cloud. Between 2000 and 2100 UTC, the observed cloud top and base altitudes were at 8 and 6 km, respectively. After 2100 UTC, the cloud-top altitude fluctuates between 8 and 10 km, while the cloud base altitudes largely remains at 6 km, except for the period between 2130 and 2230 UTC. We convert the retrieved cloud temperatures into cloud altitudes using the HARP-derived sounding. (There was no surface sounding launch around the flight time of the WB-57F.) For Tracks 1 and 3, when the WB-57F flew over the radar site, the area happened to be clear, although the radar recorded very thin cirrus. Thus, comparison of the retrieved cloud altitudes with the radar data was not available. For Tracks 5 and 8, the retrieved cloud temperatures over the radar site are -33° and -40° C, which correspond to 8.2 and 9.2 km, respectively. Both altitudes are within the radar-derived cloud boundaries but near the cloud top at the particular WB-57F overpass time.

To verify the retrieved cirrus cloud optical depths and ice crystal mean effective sizes, we use the in-situ ice crystal size distributions obtained by FSSP, 1D-C and 2D-C probes on board the HARP. Between 2030 and 2040 UTC (case 1), and between 2147 and 2157 UTC (case 2), HARP flew a race track pattern which were within a distance of 30 km from the Hanscom AFB, and were approximately collocated and coincident with Tracks 1 and 3 of the ARES flights, respectively. For both cases, the flight altitude was at about 8 km, corresponding to the radar-detected cirrus cloud altitude. We use the 2D-C derived ice crystal size distribution for comparison purposes and employ the Gamma function to extrapolate the 2D-C data ($\sim 100\text{ }\mu\text{m}$) to $20\text{ }\mu\text{m}$.

We have computed the single-scattering properties of the preceding ice crystal size distributions, including the phase function (asymmetry factor), single-scattering albedo, and extinction coefficient, using the unified theory for light scattering by ice crystals developed by our research group. Visible extinction coefficients of 0.54 km^{-1} and 0.57 km^{-1} were obtained for cases 1 and 2, respectively. Moreover, based on the cloud boundary altitudes derived from the 8.6-mm radar measurements, the average cirrus cloud thicknesses during the two periods are estimated to be about 1.75 and 2 km for cases 1 and 2, respectively. It appears reasonable to use the computed extinction coefficients based on single-level aircraft measurements to represent the vertically averaged cirrus cloud extinction coefficients. This is because the vertical profile of the 2D-C median volume ice crystal diameter obtained during the ascending run of the HARP indicated that ice crystal sizes varied by no more than $20\text{ }\mu\text{m}$ between 6.5 and 8 km. The computed optical depths based on the preceding assumption are 0.994 and 1.14 for cases 1 and 2, respectively. The mean retrieved optical depths are 0.89 and 1.42 for Tracks 1 and 3 of the ARES flight. It is evident that the retrieved mean optical depth agrees relatively well with that from the 2D-C probe for Track 1. However, for Track 3, the difference between the two optical depths is on the order of 0.3. There are two reasons for this discrepancy. First, the optical depth

estimate from the 2D-C probe is computed from the composite ice crystal size distribution at a single flight level within the cirrus cloud so that uncertainty is inherent. Second, variability of the retrieved optical depth for Track 3 is much larger than that for Track 1.

Moreover, we also use the mean effective ice crystal size derived from single-level aircraft measurements to represent the vertically averaged cirrus cloud mean effective size. A typical ice crystal shape model is used for this analysis: 50% bullet rosettes, 30% hollow columns, and 20% plates. For each shape, different relationships between the maximum dimension, L , and width, W , are employed in the calculation. For plates, $W = 2.02^{0.449} L$; for hollow columns; $W = 11.3 L^{0.414}$, for $L > 200 \mu\text{m}$; $W = 8.479 + 1.002 L - 0.00234 L^2$, for $L < 200 \mu\text{m}$; and for bullet rosettes, $W = 2.3103 L^{0.63}$. The mean effective sizes for the two size distributions are based on the average of the mean effective size for each shape weighted by the percentage distribution. They are $57.2 \mu\text{m}$ for case 1, and $55.2 \mu\text{m}$ for case 2. The retrieved mean effective sizes are $64.2 \mu\text{m}$ for Track 1, and $53.3 \mu\text{m}$ for Track 3, and both compared favorably with the 2D-C probe derived values.

3. SUMMARY

We have presented a remote sensing algorithm for the retrieval of cirrus cloud temperature (height), optical depth, and ice crystal size based on radiative properties of cirrus clouds. The ARES 5.1-5.3 and $3.7 \mu\text{m}$ channels were used for this purpose. This scheme has been applied to the ARES data collected on September 16, 1995, over the Hanscom AFB area. For validation, the retrieved cloud temperatures compare reasonably well with collocated and coincident values determined from the ground-based 8.6-mm radar. The retrieved optical depth and mean effective size also match the in-situ microphysical measurements.

4. ACKNOWLEDGMENTS

This research work was supported by the Air Force Geophysical Directorate of the Phillips Laboratory under contract F19628-96-C-0052 and by the Air Force Office of Scientific Research under grant F49620-94-1-0142.

5. REFERENCES

1. Ou, S. C., K. N. Liou, and Coauthors, 1995: Remote sounding of cirrus cloud optical depths and ice crystal sizes from AVHRR data: verification using FIRE-II-IFO measurements. *J. Atmos. Sci.*, **52**, 4143-4158.
2. Ou, S. C., K. N. Liou, and B. A. Baum, 1996: Detection of multilayer cirrus cloud systems using AVHRR data: Verification based on FIRE-II-IFO composite measurements. *J. Appl. Meteor.*, **35**, 178-191.
3. Ou, S. C., K. N. Liou, and T. R. Caudill, 1997: Remote sounding of multilayer cirrus cloud systems using AVHRR data collected during FIRE-II-IFO. *J. Appl. Meteor.*, **36**, (accepted).

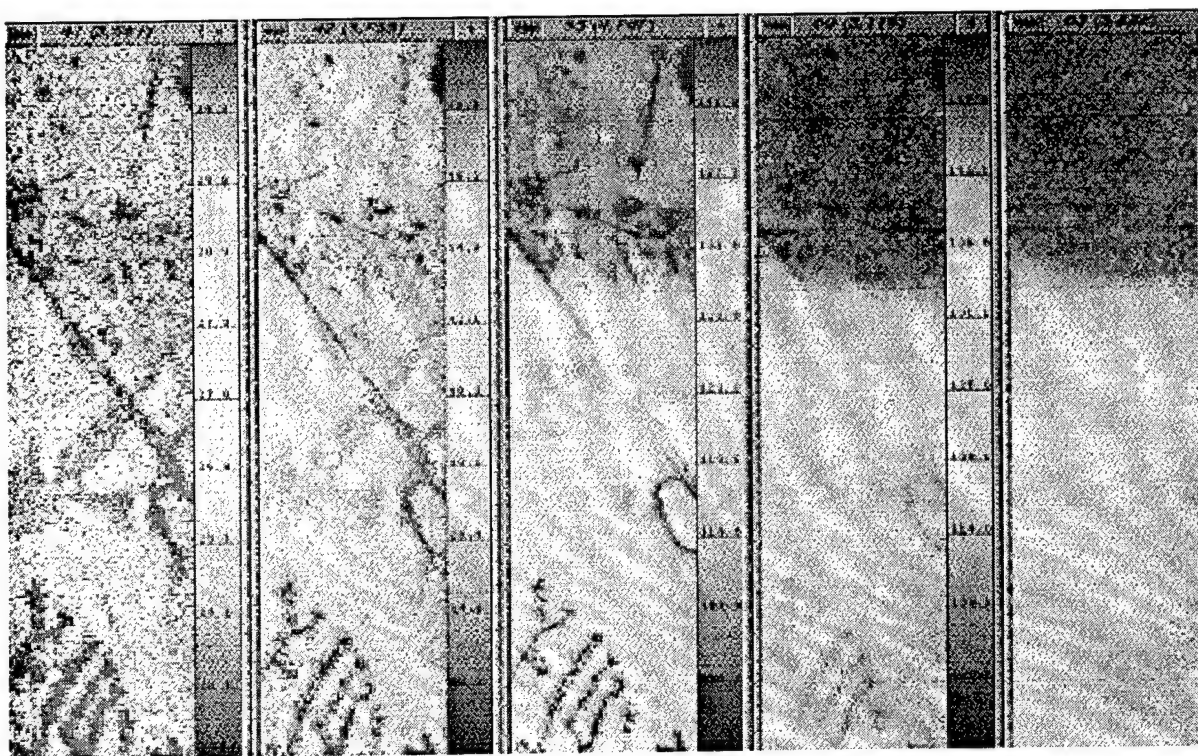


Fig. 1. Radiance images for ARES Chs. 41, 42, 55, 60, and 63 over a selected scene with strong cloud/clear contrast within the Track 1 of September 16 flight.

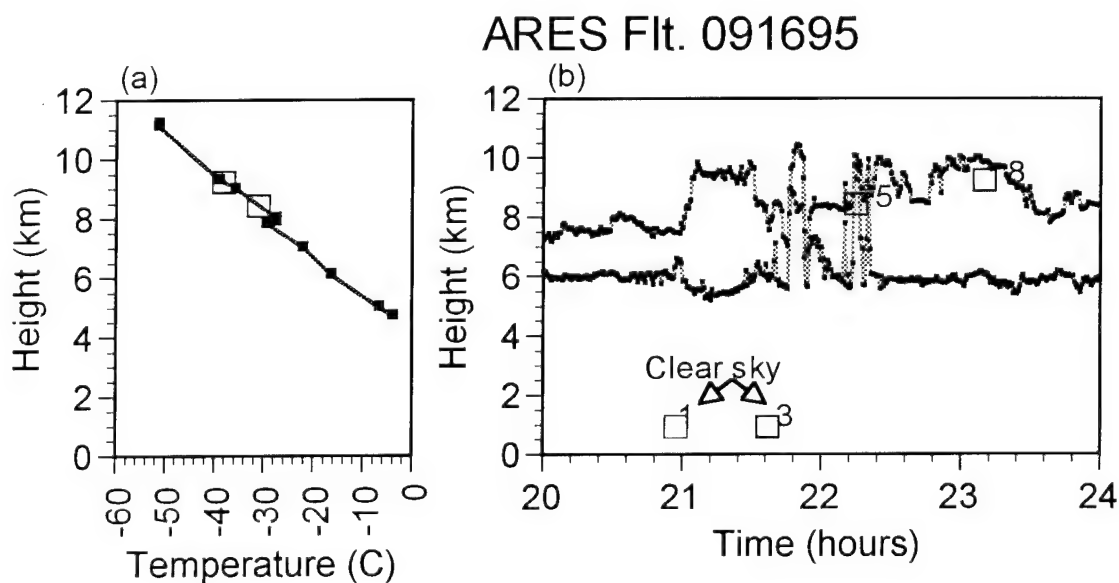


Fig. 2. (a) Partial sounding of the middle and upper troposphere obtained using HARP flight above Hanscom AFB (squares correspond to retrieved cloud temperature). (b) Comparison of cloud top heights (obtained from radar/lidar measurements) and retrieved cloud temperatures. Retrieved temperatures are displayed for Tracks 1, 3, 5, and 8 (in chronological order).

**SESSION VII:
CLOUD DATASETS**

References in some of the preprints had to be deleted by the editor because they referred the reader to papers with limited distribution that were not available to the public.

Global Cloud Data for System Design and Simulation

Donald Wylie
Space Science and Engineering Center
University of Wisconsin-Madison
1225 W. Dayton Street
Madison, WI 53706

W. Paul Menzel
NOAA/NESDIS
Madison, Wisconsin 53706

ABSTRACT

Eight years of global cloud frequency data have been collected from the HIRS on the NOAA weather satellites. These data have been summarized showing the frequencies and heights of clouds globally and the average optical depths of the clouds. The statistics show the probability of clouds obscuring radiative transmission systems. Comparisons to two other cloud data sets, the ISCCP and SAGE also have been made. The HIRS is more sensitive to partially transmissive cirrus clouds than the ISCCP but less sensitive than the SAGE. The methods of sampling and the radiative channels used by each system greatly affected the number of clouds reported and the altitudes assigned to them.

1. The Cloud Detection Method

The High resolution Infrared Radiation Sounder (HIRS) has been flown on the polar orbiting NOAA satellites since 1979. Its original purpose was to make temperature soundings of the troposphere, however, it also has been used for detecting radiatively thin clouds which are difficult to detect by other means. Statistics of global cloud cover have been compiled over the last eight years from the HIRS data. These statistics are being assembled into a data set for estimating the probability of cloud obscurations to electromagnetic transmission through the atmosphere.

HIRS measures terrestrial radiation in partially absorbing CO₂ bands from 13-15 μm . The amount of CO₂ absorption in the band determines the level from which the radiation originated. Bands with strong CO₂ absorption receive radiation from near the top of the atmosphere while bands with weak CO₂ absorption receive radiation from lower levels. These differences allow detection and altitude assignment of radiatively thin clouds without the problems of land surface reflections or low level boundary layer clouds that plague other methods. A full description of the method of cloud detection used on the HIRS data is given in Wylie et al. (1994).

2. Comparison To Other Cloud Statistics

Two other global cloud data sets have recently been compared to the HIRS cloud data. They are the International Satellite Cloud Climatology (<http://isccp.giss.nasa.gov>, Rossow and Schiffer, 1991) and the Stratospheric Aerosol and GAS Experiment (SAGE, see

Wang et al., 1996). The ISCCP uses the 11 μm window channel on five geostationary satellites and the AVHRR instrument on the polar orbiting NOAA satellites. It has encountered problems in detecting radiatively thin clouds because it requires solar reflection measurements from the visible (0.6 μm) channels on these satellites. Radiatively thin clouds have to be distinguished from ground and low underlying cloud reflections and the visible channels on these satellites have to be accurately calibrated. A comparison of ISCCP the HIRS cloud data by Jin et al. (1996) found that the ISCCP reported 15% less cloud cover than the HIRS mostly from under detection of clouds with infrared emissivities < 0.5 , or optical depths, $\tau_{\text{vis}} < 1.3$.

A comparison between HIRS and SAGE data also has recently been made by Wylie and Wang (1997). The SAGE instrument was designed for measuring aerosol and gas constituents in the stratosphere. It is very sensitive to very thin clouds because it scans the atmosphere horizontally by tracking the sun as it appears and disappears over the horizon on each orbit, the solar occultation method. It detects clouds with optical depths as low as $\tau_{\text{vis}} = 0.0002$, which are seldom visible to weather satellite sensors. However the down side is that it collects only two data points on each orbit, giving it a very low sampling frequency. SAGE reports 12-22% more clouds than the HIRS. These clouds were in the optical depth range, $0.02 < \tau_{\text{vis}} < 0.1$. HIRS can not detect clouds with $\tau_{\text{vis}} < 0.1$.

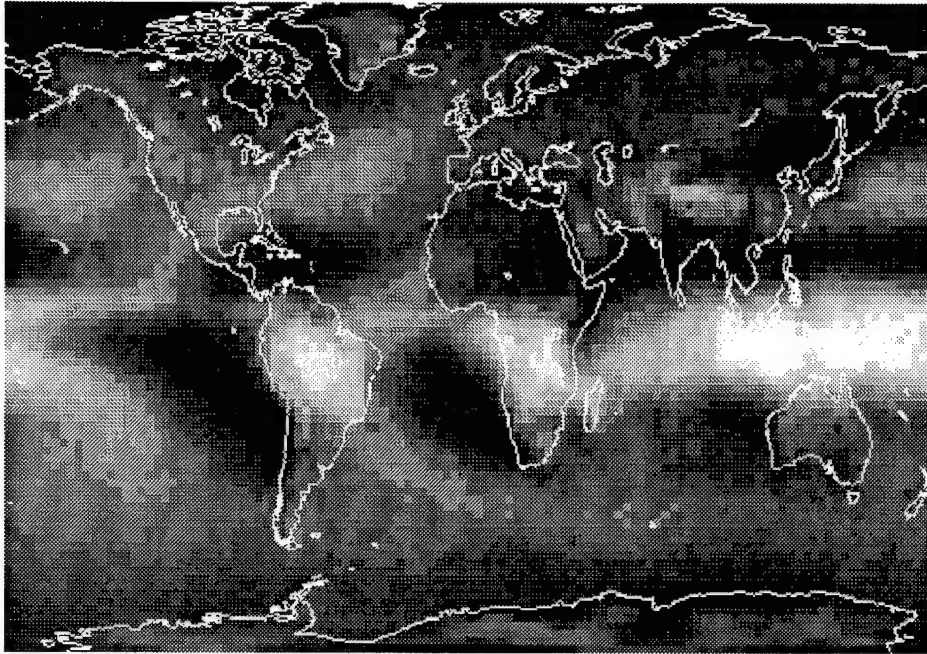
3. Cloud Frequencies and Densities

The frequencies of clouds above 6 km globally are shown in Figure 1. Each panel gives the average frequencies of clouds over a three month season in the eight years of study. The Boreal Winter is the months of December, January, and February, and the Boreal Summer is the months of June, July, and August. Over 50 million HIRS observations have been compiled.

Clouds are extremely frequent in the tropics where some locations have 95-100% cloud cover for the entire season. Other areas of frequent cloud cover were found in the mid-latitude storm belts.

Effective emissivities of the clouds (above 6 km) have been calculated using the radiative measurements of the HIRS at 11 μm considering both the opaque and partially transmissive clouds. The details of this calculation along with global distributions of this radiative parameter are discussed in detail in Wylie and Menzel (1997). The basic behavior of the effective emissivities is shown in Figure 2. Where cloud frequencies were high, above 50%, the effective emissivity was mostly between 40 and 65%. This corresponds to average optical depths of, $1.0 < \tau_{\text{vis}} < 2.1$. In less frequent areas the effective emissivities tended to be lower because the clouds tended to be more fractured and only partially covered the HIRS sensor fields of view. However, Figure 2 indicates that some dense clouds with effective emissivities $> 60\%$ did occur where high clouds were less frequent ($< 50\%$). Most of these occurrences were in high latitudes from infrequent storms.

FREQUENCY OF CLOUDS ABOVE 6 KM
BOREAL WINTER



BOREAL SUMMER

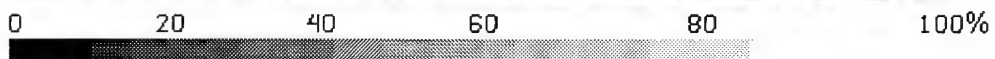
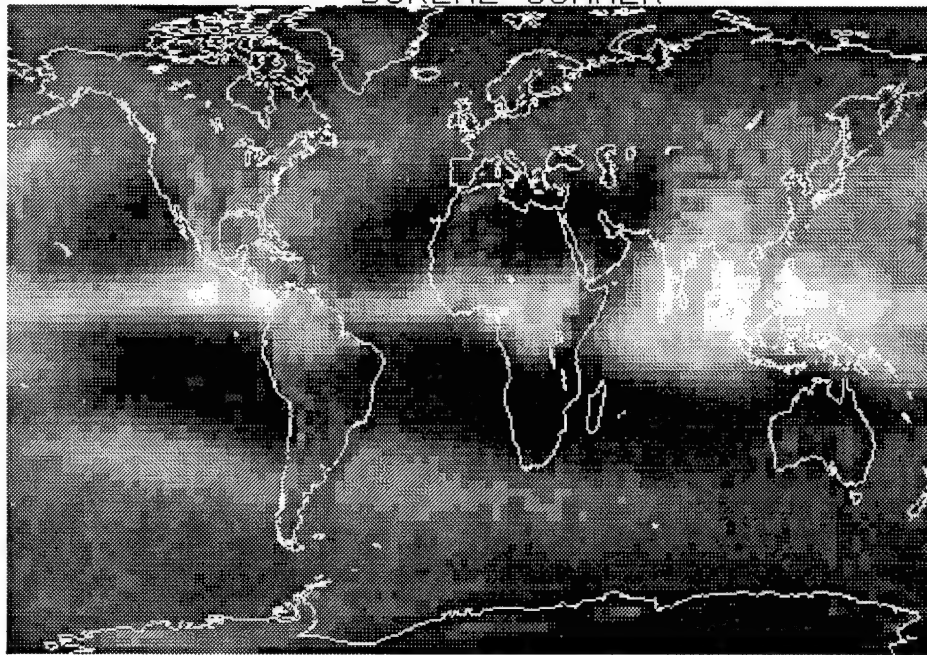


Figure 1: The frequency of clouds above 6 km detected from the HIRS data. boreal winter is the months of December, January, and February, and boreal Summer is the months of June, July and August.

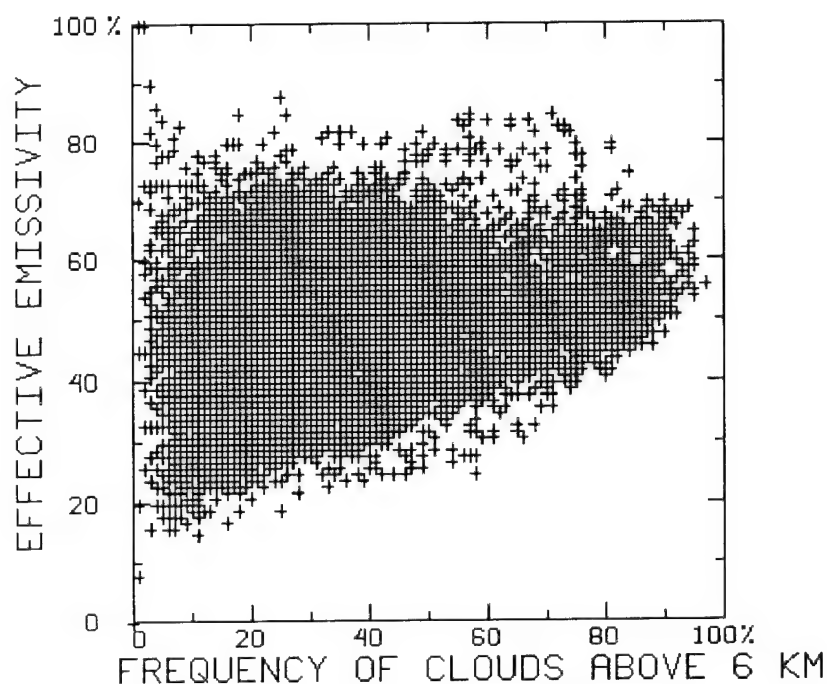


Figure 2: The effective emissivities of clouds above 6 km averaged over 2° latitude by 3° longitude boxes vs. the frequency of clouds in the same boxes. The study area is from 85° south to 85° north. The effective emissivity considers the density of the clouds and their infrared radiative attenuation.

4. References

- Jin, Y., W. B. Rossow, and D. P. Wylie, 1996: Comparison of the climatologies of high-level clouds from HIRS and ISCCP., *J. Climate*, **9**, 2850-2879.
- Rossow, W. B., and R. A. Schiffer, 1991: ISCCP cloud data products., *Bull. A.M.S.*, **72**, 2-20.
- Wylie, D. P., W. P. Menzel, H. M. Woolf, and K. I. Strabala, 1994: Four Years of Global Cirrus Cloud Statistics using HIRS. *J. Climate*, **7**, 1972-1986
- Wylie, D. P. and P. Wang, 1997: Comparison of Cloud Frequency Data from HIRS and SAGE II. submitted to *J. Geographical Research* for publication.
- _____, and W. P. Menzel, 1997: Eight years of global high cloud statistics using HIRS., submitted to the *J. Climate*.

GLOBAL HIGH-RESOLUTION LAYERED CLOUD DATABASE - RESEARCH AND DEVELOPMENT
AT THE COOPERATIVE INSTITUTE FOR RESEARCH IN THE ATMOSPHERE,
COLORADO STATE UNIVERSITY
1997 CONFERENCE (CIDOS-97)¹

Donald L. Reinke, John M. Forsythe, and Thomas H. Vonder Haar
Colorado State University
Fort Collins CO 80523
Phone: (970) 491-8397
Fax: (970) 491-8241
E-Mail: reinke@cira.colostate.edu

¹ This work is sponsored by the DoD Center for Geosciences - Phase II at the Cooperative Institute for Research in the Atmosphere, CSU under grant DAAH04-94-G-0420.

ABSTRACT

Ongoing research under "Task 10" of the DoD Center for Geosciences at CIRA has continued to focus on the use of meteorological satellite data to produce an improved global analysis of complex layered clouds. The emphasis of Task 10 is to improve the analysis of cloud base and cloud type as determined from both geostationary and polar orbiter imagery.

A special spinoff of the layered cloud research at CIRA is the production of a prototype global layered cloud product. The Climatological and Historical ANALysis of Clouds for Environmental Simulations (CHANCES) database was used, with additional supportive data, to produce an multi-layer cloud database (CLVL) for an initial 30-day period (selected from within the CHANCES database period of February 1994–January 1995 inclusive). The database consists of eight 1.5-km vertical resolution layers, on a 5-km, 1-hr space and time grid for the entire globe.

An overview of complex layered cloud research at the Center and a description of the new prototype global layered cloud product is presented. A new technique is also presented that uses a combination of bi-spectral clustering technique to produce an improved layered cloud product.

1. INTRODUCTION

The purpose of the Complex Layered Cloud Systems (Task 10) research at CIRA is to develop algorithms to produce cloud base and layer estimates from satellite data. Geostationary and polar orbiter visible and infrared imagery are used to produce global layered cloud products at a 5-km and 1-hr space and time resolution. Surface observations and rawinsonde soundings are used to add cloud base and layer information to the satellite derived cloud tops. The global cloud model, called CLVL for CHANCES Levels (Forsythe, et al., 1996), was built as a testbed for future layered cloud research efforts that will move toward a satellite-only layered cloud product.

After construction of the CLVL database, it was clear that improvements were necessary in the technique that was being used to assign cloud bases. A new technique was developed and tested in which satellite imagery was used to define cloud classes. These classes are then "calibrated" with cloud base observations found within (under) each class, as opposed to relying on one of the objective analysis techniques that are widely used in layered cloud models.

2. DATA

The data used in the Complex Layered Cloud research task are shown in figure 1. That diagram shows both the individual input data, and the interaction between the various intermediate products.

3. DATA PROCESSING

a. CLVL Layered Cloud Database

The CHANCES database was used along with global surface observations, relative humidity analyses, DMSP SSM/I, and the Navy ETOPO5 topography database to build a prototype global, 8-layer, 5-km, 1-hr, cloud product for the month of July, 1994. Details are given in Forsythe, *et al.* (1996). A summary follows:

CHANCES cloud/no cloud data and infrared radiance images were used along with USAF HIRAS upper air temperature profiles to assign cloud top heights where clouds were present in the cloud/no cloud analysis.

HIRAS relative humidity analyses were used to assign cloud layers below the satellite cloud tops where clouds were present in the CHANCES cloud/no cloud analysis. ($RH > 84\%$ and RH gradient analysis after Wang and Rossow [1995]).

The 85 GHz channel from SSM/I was used to identify precipitation. Data points under the precipitation were marked as cloudy from the infrared-derived cloud top to the surface layer.

Another separate product was constructed from surface observations. This product is the result of an objective analysis of observed cloud base height and cloud type information that is taken from the USAF DATSAV2 surface observation database.

b. Cloud Classification Study

Infrared and visible imagery from the GOES satellite was used to classify cloudy regions. A two-dimensional histogram of radiances was constructed, and a classifier was employed which finds clusters of radiances by minimizing a similarity function to arrive at the classification. This classification scheme requires no physical significance be attached to a class, they are simply "class 1, class 2, etc." This is sufficient for our purposes, since we only want to determine if a pixel in a class is similar to other pixels in the same class. In most instances, the classes do correspond to features which an analyst would classify, for instance clear land, stratus, or thunderstorms.

It should be noted that any good classification scheme can be used to identify the cloud classes used in this study. One example is a new neural network based technique that is being developed by Tian, *et al.* (1996) at the CIRA DoD Center for Geosciences.

c. Improved Cloud-Base Assignment

The problem we considered here is how to estimate cloud base at a location where surface observations are not available. Cloud base estimation using only surface observations, hereafter referred to as the NOSAT method, is often based on some rule where distance is a weighting factor. Gaussian, Barnes, and nearest neighbor interpolation methods are examples of this type of scheme, which is commonly used with smooth meteorological fields such as temperature and pressure. Since clouds often occur in distinct layers with sharp

edges, we expect better performance using a method which preserves the roughness of the cloud field. In our test, we use a cloud classification from satellite data (SAT method) to serve as a "mask" which preserves the discontinuous cloud structure, and then compare the results to those obtained from a nearest neighbor (NOSAT) approach.

4. COMPARISON OF THE SAT AND NOSAT METHODS

A one-month satellite data set was analyzed to produce layered cloud products from both the SAT and NOSAT techniques. Each surface observing point in the data set was used as a test point to make a comparison as follows:

- a. The bi-spectral classification analysis was performed on the satellite imagery for a given hour.
- b. Each surface observation that was available for that hour was then used as a test point.
- c. A cloud base was assigned to that test point based on a nearest-neighbor analysis of the other surface observations that were available for that hour (NOSAT).
- d. A second cloud base was assigned based on the same nearest-neighbor analysis. However in this case, a constraint was put on the surface data so that the nearest-neighbor must be found under the same satellite cloud classification.
- e. The resultant SAT and NOSAT cloud bases were compared with the actual observation at the test point.

The SAT and NOSAT results were gathered and compared for 235 cases. The results showed a significant improvement in the ability of the SAT technique to estimate cloud bases (figure 2).

5. REFERENCES

- Forsythe, J.M., Reinke, D.L., Randel, D.L., Eis, K.E., and C.L. Combs, 1996: CLVL - A global high-resolution layered-cloud database. *Proceedings of the 1996 Battlespace Atmospherics Conference*, Naval Command, Control and Ocean Surveillance Center, RTD & E Division, San Diego, California.
- Tian, B., M. A. Shaikh, M. R. Azimi-Sadjadi, T.H. Vonder Haar and D. L. Reinke, 1996: "Neural Network-Based Cloud Classification Using Textural Features" submitted to IEEE Transactions on Neural Networks
- Wang, J., and W.B. Rossow, 1995: Determination of Cloud Vertical Structure From Upper-Air Observations. *J. Appl. Meteor.*, **34**, 2243-2258.

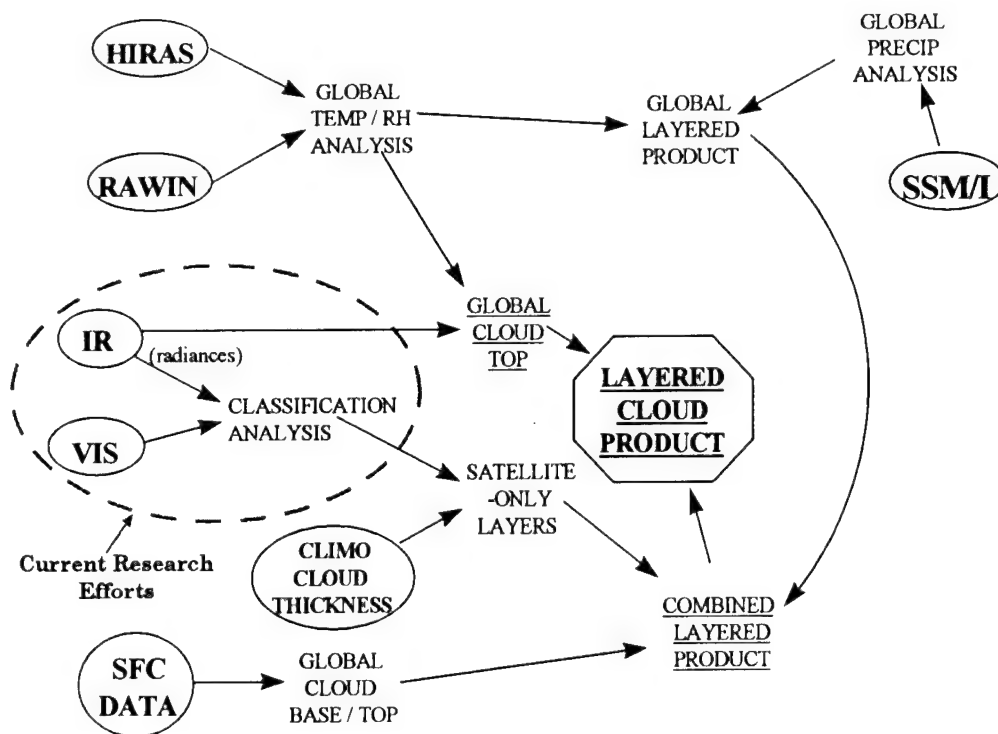


Figure 1. Task 10 Complex Layered Cloud Model data flow diagram.

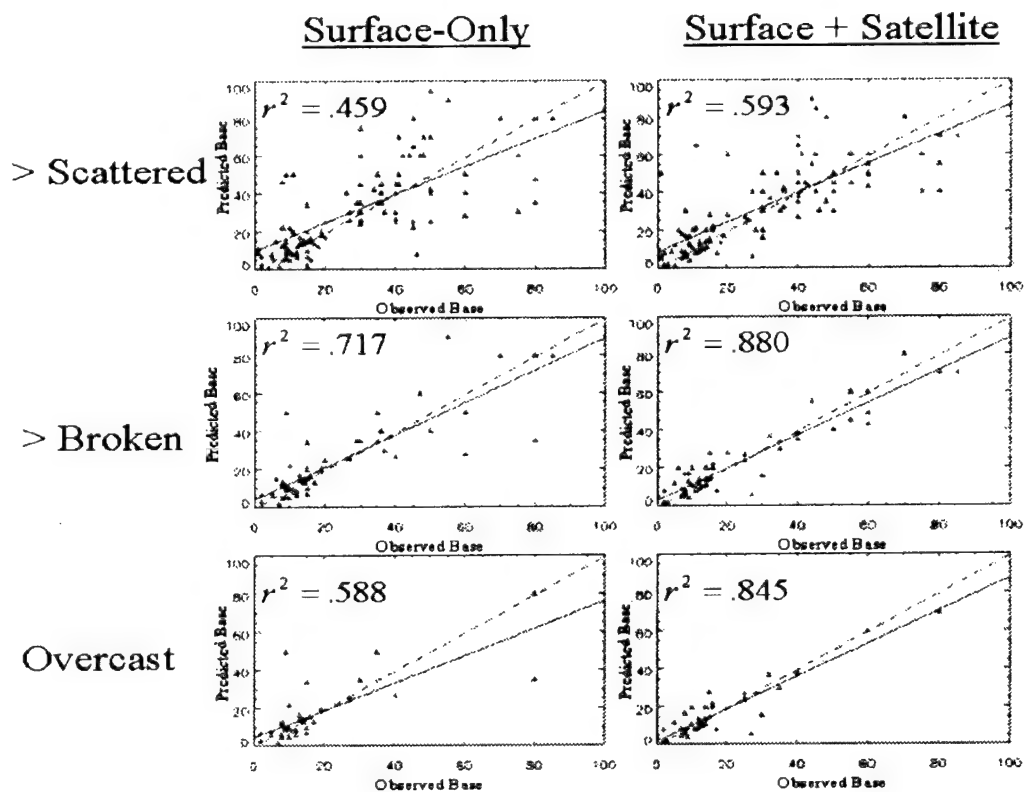


Figure 2. Comparison of SAT and NOSAT technique for cloud base determination.

OVERVIEW AND OBJECTIVES OF THE DOD CENTER FOR GEOSCIENCES SPONSORED
"COMPLEX LAYERED CLOUD EXPERIMENT" (CLEX)
1997 CONFERENCE (CIDOS-97)¹

Thomas H. Vonder Haar, Stephen K. Cox, Greame L. Stephens, John M. Davis, Timothy L. Schneider,
Walter A. Petersen, Arlie C. Huffman, Kenneth E. Eis, Donald L. Reinke, and John M. Forsythe

Colorado State University

Fort Collins CO 80523

Phone: (970) 491-8397

Fax: (970) 491-8241

E-Mail: reinke@cira.colostate.edu

Fuk K. Li

NASA Jet Propulsion Laboratory
Pasadena CA

Gregory A. Sadowy

University of Massachusetts
Boston MA

¹ This work is sponsored by the DoD Center for Geosciences - Phase II at the Cooperative Institute for Research in the Atmosphere, CSU under grant DAAH04-94-G-0420.

ABSTRACT

The DoD Center for Geosciences at the Cooperative Institute for Research in the Atmosphere (CIRA), Colorado State University, CO is sponsoring an ongoing field experiment called the Complex Layered Cloud Experiment (CLEX). The CLEX addresses a better physical understanding of the morphology of extensive layers of non-precipitating clouds in the middle and upper troposphere. A coordinated land, air, and space-based data collection produced a unique research data set during June, 1996. Data were collected from the NASA DC-8 airborne 95-GHz cloud radar, the U. Wyoming King Air *in-situ* microphysical collection systems, GOES, DMSP, and AVHRR meteorological satellites, Penn State Univ. 94-GHz cloud radar, and the Desert Research Inst. Mobile Microwave Radiometer, and a wide range of ground based systems at the Oklahoma ARM-CART site.

An overview of the CLEX objectives and a summary of data collected and analyzed during CLEX-1 in June-July of 1996 are presented.

1. INTRODUCTION

The CLEX experiment addresses a better physical understanding of the morphology of extensive layers of non-precipitating clouds in the middle and upper troposphere. These are in a sense the "forgotten" clouds on Earth. National weather services do not forecast these clouds and with a few exceptions, the civilian community generally ignores them.

Within the climate research community, only a subset of "CLEX clouds" – layers of "radiatively significant" cirrus – have been identified as a high-priority for study and understanding regarding their role in the climate system. However, in the last five years three realizations have caused us to greatly elevate the scientific priority of understanding the origin and duration of complex single and multi-layer cloud systems; Desert Storm, increased emphasis on the assimilation of satellite imagery into models, and new insights into the role of clouds in the radiation balance and atmospheric dynamics. Specifically:

1. Mid-level clouds had a significant effect on several key DoD operations during Desert Shield and Desert Storm. Various post-campaign reports and publications have documented the importance of understanding and forecasting such cloud layers and their details will not be repeated here.

2. The advent of new 3-D and 4-D variational assimilation of satellite radiance data into operational forecast models – and the improved forecast skill that resulted (Burridge, ECMWF, 1996) – focus special attention on proper model representation of these clouds (Tiedke, 1993) and forward radiances from them.

3. Third is a realization from the climate research community that the layer-to-layer and layer-to-surface radiative effects of extended cloud layers not only may play a key role in their morphology but may also strongly impact regional atmospheric dynamics. Additional details and background may be found in Vonder Haar et al. (1994) and (1996).

The first phase of CLEX, called CLEX-1, covered the period of 19 June - 3 July 1996 over the Central Great Plains of CONUS. Subsequent CLEX tests will be developed as needed. During CLEX the DoD Center of Geosciences will operate in collaboration with JPL and NASA as they concurrently test their new Airborne Cloud Radar for cloud layer profiling. Several other university and government groups are participating and assisting with CLEX. All data will be collected and organized into a central database for use by a wide group of scientists.

2. SCIENCE OBJECTIVES

CLEX will provide data to answer questions surrounding our understanding of "Complex Layered Clouds". These can generally be viewed as non-precipitating mid-level clouds that are of sub-tropical origin or not associated with large convective complexes. Preliminary results and a further discussion of these clouds are given in Vonder Haar et al. (1996). Specific questions that are being addressed are:

1. Can cloud bases and layers be estimated using satellite-only techniques?
2. Can existing layer cloud conditions be detected and serve as input to atmospheric models?
3. How does cloud layer-induced radiative heating/cooling impact the layer cloud lifetime?

3. FIELD MEASUREMENT SYSTEMS

Satellite - Satellite data include *GOES-8* and *9* geostationary data (all channels, 1-minute rapid scan when possible), *DMSP* overpasses including *SSM/I* and *SSM/T2* data, and *AVHRR* data aboard the *NOAA 11* and *12*.

Aircraft Systems -

The *University of Wyoming King Air* was flown to collect *in-situ* cloud microphysical data measurements. Instrumentation on the King Air included: a) cloud-droplet spectra/particle imaging probes such as Particle Measurements Systems (PMS) FSSP (.5 - 45 μm), 1D-C (12.5-186 μm), and 2D-C (25- 800 μm); b) for precipitation the PMS 2D-P (200-6000 μm) probe; and c) for liquid water content, both in-house and Johnson-Williams (J-W) hot-wire probes (accuracy 0.2 g m^{-3}). The King Air team also visually identified cloud layer tops and bases during the collection operation and captured the forward-looking view on video tape.

The *NASA DC-8* and *JPL Airborne Cloud-Profiling Radar* (ACR) was flown above the cloud layers to provide measurements of cloud bases, tops, and structure including estimates of cloud liquid water and ice content. The ACR is a scanning, Doppler, cloud-radar that operates at a frequency of 95 GHz. The minimum detectable signal of the radar for cloud-heights of 200 m (approximately 11 km from aircraft cruising altitude) is \sim -30 dBZ. The beamwidth of the radar is 0.56°, providing cross-track and along-track resolutions of approximately 120 m at aircraft cruising speeds. Vertical resolution (pulse length dependent) of \sim 90 m. (See example of cloud radar imagery in figure 1)

Ground-Based Systems -

The *Desert Research Institute (DRI) Dual Freq. Mobile Microwave Radiometer* is a van-mounted, scanning, dual-frequency (20.6 and 31.65 GHz) passive microwave sensor that is used to estimate column integrated water vapor and cloud liquid water. The instrument was operated in both mobile and stationary mode. When in scanning mode the radiometer can scan a full 360 degrees ($\pm 1^\circ$ accuracy), at a fixed elevation angle ($\pm 0.1^\circ$ accuracy). Temporal resolution in the scanning mode is approximately 3 minutes. The beam sampling angle is 2.6° . The instrument has an accuracy of 5-10%, and will measure values of water vapor and liquid water over ranges of 0-5 cm for vapor and 0-5 mm for liquid water.

The *Pennsylvania State University Cloud Radar* provided measurements of cloud bases, tops and liquid water content. The Doppler radar operates at a frequency of 94 GHz. The radar was operated at the Oklahoma ARM site in vertically pointing mode only. Data were collected for altitudes between 200 m and 15 km at a temporal resolution of 2 seconds and a vertical resolution of 50 m at a Nyquist velocity of 1.2 m s^{-1} . The beamwidth of the radar is approximately 0.3° , providing a horizontal resolution of approximately 30m at 10 km altitude.

A full compliment of *Surface Observations* including *Automated Surface Observing System (ASOS) Data* and *Rawinsonde Soundings* were collected and archived. ASOS data at 5 minute temporal resolution were collected from locations in the general area of operations for CLEX-1. These data consist of all meteorological information collected by the ASOS suite of sensors including laser ceilometer measurement of cloud bases (to 12,000 ft AGL) and sky cover. Special soundings were released at the ARM CART site, combined with radio theodolite soundings.

Table 1 provides a breakdown by operations day of observational platform participation during CLEX-1. Ground-based instrumentation at the ARM-CART site are collectively grouped into a single category "CART-ARM" in Table 1.

Table 1. Dates of data collection by platform

PLATFORM	6/10-6/15	6/21	6/22	6/23	6/24	6/25	6/26	6/27	6/28	6/29	7/1-7/2
King Air	-	X	\$	*	*	*	*	-	*	*	-
DC08	X	-	\$	-	*	X	*	X	-	-	X
DRI Radiometer	-	-	#	#	*	#	*	#	-	-	-
PSU Radar	-	#	#	#	#	#	#	#	*	#	-
CART-ARM	-	#	#	#	#	#	#	#	*	#	-
SSM/I	X	X	\$	X	X	*	*	X	X	X	X
SSM/T2	X	X	X	*	*	*	*	X	X	*	X
GOES 1-min.	-	-	-	-	*	-	-	-	-	-	-
GOES 7.5-min.	-	-	\$	-	*	-	-	-	-	-	-
GOES 15-min.	X	X	\$	*	*	*	*	X	X	X	X
ASOS 5-min.	-	X	\$	*	*	*	*	X	X	X	-

\$ = Coordinated/collocated data collection between TWO aircraft and other platforms

* = Coordinated/collocated data collection between SINGLE aircraft and other platforms

= Collocated data collection without aircraft;

X = Independent collection

- = Platform down or no data collected for CLEX

4. DATA ARCHIVE

CLEX data are archived at CIRA. For further information including case study examples, view the CLEX web site at: <http://www.cira.colostate.edu/geosci/clex/overview.htm> . For additional questions contact Mr. Don Reinke, e-mail: reinke@cira.colostate.edu phone: (970) 491-8465.

ACKNOWLEDGEMENTS

Many scientists and groups have contributed to CLEX discussions and planning. Dr. Fuk Li and colleagues at JPL developed the Airborne Cloud Radar (ACR) segment along with Professor Graeme Stephens of CSU. The ACR planning has paralleled and stimulated our CLEX science concepts. Dr. Bob Curran and Dr. Ramesh Kakar of NASA have been helpful with their discussions and questions as have Dr. Walter Bach, Jr. and other members of the DoD Center for Geosciences, Phase II Advisory Panel. Mr. Greg Sadowy at UMASS provided pre-processing of radar imagery from the airborne radar.

References

- Burrige, D., 1996: (personal communication of 1994 forecast model operations and results at the ECMWF).
- Tiedke, M., (1993): Representation of Clouds in Large-Scale Models. *Mon. Wea. Rev.*, **121**, 3040-3061.
- Vonder Haar, T.H., et al., 1994: Technical Proposal and Briefings submitted to the DoD Advisory Panel for the Center for Geosciences Research at CSU.
- Vonder Haar, T.H. et al., 1996: DoD Center for Geosciences - Phase II, Annual Report (1994-1995), 138 pp.

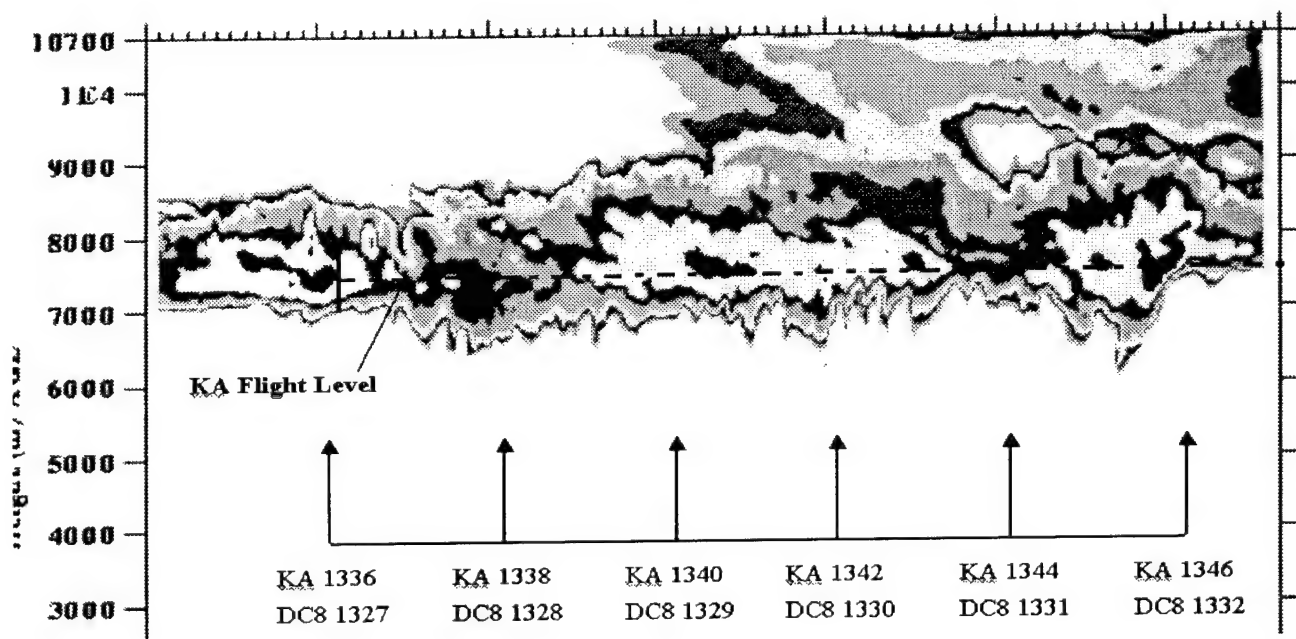


Figure 1. Sample of imagery from the 95GHz airborne cloud radar showing coincident sampling times of the King Air (flight level shown as dashed line at 7.3 km elevation) on 22 June, 1996 flight during CLEX-1.

Ground-based Digital Cloud Imagery Analysis and Applications

Robert P. Wright, Stanley H. Grigsby, Robert M. Holt
Planning Systems Incorporated
7923 Jones Branch Drive
McLean, VA 22102-3304

ABSTRACT

The visualization of clouds and the representation of their physical properties within simulations has presented many interesting problems. This is especially true in the "live play" case. Clouds form and dissipate in a non-linear, chaotic response to the local atmospheric state. The resulting cloud structures exhibit fractal characteristics. This has been demonstrated in analyses of cloud imagery obtained from space-based platforms. This paper describes results of the application of objective fractal image processing techniques to high-resolution digital cloud imagery obtained from an automated, ground-based imagery system. Objective estimates of image fractal dimension and fractal signature are obtained from Whole Sky Imager (WSI) data collected at the White Sands Missile Range. The WSI, developed by the Marine Physical Laboratory at the Scripps Institution of Oceanography, digitally processes and records sky and cloud radiance data. The purpose of this research is to continuously couple, in near real time, high-resolution cloud imagery and associated atmospheric properties from a live play exercise or operation with virtual simulations for Modeling and Simulation (M&S) support of war gaming, training and mission rehearsal. This paper also describes the application of this analysis to the real time environmental support of M&S programs; (1) correlation of cloud image fractal measurements with local atmospheric properties to enable high resolution atmospheric data retrieval, and (2) recreation of high fidelity virtual cloud images. Potential operational applications are also described.

1. INTRODUCTION

This work was motivated by interest in providing realistic environmental information to simulations that included a live play component. The resolution in space and time of observations and models of the environment is coarse compared to the effects experienced in the field. The ability of numerical models to accurately depict the state and dynamics of the atmosphere has become very good. These models provide an effective means to define or interpolate the state of the atmosphere at times and locations for which observations are unavailable. Therefore the use of models to provide data for live play is appropriate. The amount of data required to define the condition of a live play area is large. The purpose of this paper is to describe a cloud image data set and analysis method. The data set and analysis are relevant to the definition of the small scale behavior of the atmosphere.

1.1 The problem

A limitation in the high resolution scale, one hundred meters or less, is that it lies in the domain of turbulent eddies. The lifetime of these eddies is on the order of minutes. This falls below most meteorological measurement capabilities. The limiting factor in the ability of numerical models to describe the condition of the atmosphere is therefore defined by how well the model depicts these eddies. This requires observations that are of sufficient resolution in time and space that the models can include their existence and their demise. It is necessary, therefore, to develop a method by which the state of the atmosphere can be determined, at very high resolutions in time and space.

Analysis of cloud data, including fractal analysis, will provide a means of measuring the fine scale nature of the atmosphere in this region. Clouds were chosen to provide fine scale "tracers" because they are one of the most visible manifestation of the environment available.

1.2 Whole Sky Imager data

The Whole Sky Imager (WSI) data set provides a high resolution view of the atmosphere in the region of interest. The initial use of it here is to define qualitatively the state of the atmosphere. During this analysis there has been no attempt to relate the raw image data to a calibrated radiance value. The assumption is made that the "brightness" value variations from the raw image data contain information regarding the structure of the clouds. This data was collected only during the daylight hours. This data set has been described in a number of other works. Briefly the data was collected by a system developed by the Marine Physical Laboratory at the Scripps Institute of Oceanography. This system has evolved since the data described here was taken.

The system consisted of a charged-injection device camera behind a fisheye optical lens pointed in the vertical. The imaging grid was a 512 by 512 array. The angular resolution is 1/3 degree giving a spatial resolution of about 6 meters at a range of 1 kilometer. The data of interest were collected every ten minutes. It was collected through two color filters; blue, centered at 450 nm and; red, centered at 650nm. Additional images were created using a neutral density filter with the color filters, this served to increase the dynamic range. Therefore, four images existed at each ten minute collection time. Each raw image consists of a 512 by 512 array of values that range from 0 to 255.

The collection period of interest was at the White Sands Missile Range, New Mexico from August 5 through 10, 1989. The analysis will be based on this and other data collected at that time. Figure 1 is a filtered, 650 nm image acquired on 5 August 1989. The square object is the sun occulter that shields the lens from direct sunlight.

1.3 Fractal Analysis of WSI cloud data

The purpose of the work is to define small scale structure in the atmosphere. We chose to use the fractal dimension as a means to quantify the structure of the clouds in these images. The choice of the fractal dimension to define structure in clouds was based on reviewing the work of Cahalan (1988), Detweiler (1990), and, Eis et. al. (1996) who have investigated this approach. Cahalan and Eis have used satellite data while Detweiler used images obtained from balloon flights.

The KHOROS image analysis system was used to perform the following analysis steps. However a separate fractal dimension routine was developed for this analysis. Several frames of WSI data have been analyzed for fractal dimension. Our purpose was to develop a process to define a measure of the structure in the cloud images using fractal techniques. While there are many ways to estimate fractal dimension, we incorporated a box counting method intended to best define the structure of the edges of clouds. This method consists of several steps as described in the following paragraphs.

A series of non-overlapping equal width brightness bands was defined that, collectively, covered the entire range of brightness observed in the raw images. The images were processed for each band to create a series of band passed, or "thresholded" images. Figure 2 is the 5 August 1989 image after application of a brightness band pass. Our assumption was that narrow bands of equal brightness would define collocated points delineating the edges of clouds. Therefore, an analysis of the structure of these edges would provide information concerning the nature of the cloud.

The box counting method was applied to each band passed image (Figure 2) to generate fractal dimensions for each non-zero pixel as represented in Figure 3. The technique for each pixel was as follows: A region of size 15x15 pixels was defined, centered on the target pixel. The region was initially broken into

four windows by dividing each region edge into two equal segments. The number of windows that contain at least one non-zero pixel, i.e., a pixel within the same band as the target pixel, was captured. The process was repeated using incrementally finer divisions of the region edges from three to 15 segments, in steps of one. This yielded a table of populated window counts as a function of region side segments. The fractal dimension of the target pixel was calculated as the slope of a least squares fit to a plot of the natural log of the counts versus the natural log of the number of segments. Alternate approaches for evaluating cloud fractal dimension are also used.

By sequentially processing the bands, a composite fractal dimension image was created and is shown in Figure 4. This image was used to visualize the structure of the atmosphere as depicted by the cloud images.

1.4 Data Visualization and Analysis

The amount of information generated by this analysis scheme is large. Therefore a method was needed to display the data so that correlations could be determined. Vis5D was chosen. Vis5D was written by the Visualization Project at the University of Wisconsin-Madison Space Science and Engineering Center.

Using Vis5D the relevant data sets are compared for fine scale structure. The WSI data is mapped onto "flat" surfaces corresponding to a number of altitudes. Conventional observations are used to assist in placing the cloud elements at the correct altitude. In the first stage of the analysis there will be a qualitative assessment of the cloud character and motion.

2. CONCLUSIONS

This is a report of work in progress. The tools and data described in the report are assembled and the analysis is being performed. Preliminary results indicate that small scale variations in the atmosphere can be detected and quantified using the image data and the analysis techniques described. It can in turn be ingested into a small scale numerical model to provide a high resolution description of the condition of the atmosphere on a local scale. Whether or not this or similar techniques are sufficient to reproduce the dynamics of the atmosphere on a scale necessary to support a live play simulation is not known as of the writing of this report.

3. ACKNOWLEDGEMENTS

This project is sponsored by PEO-TAD under NAVSEA contract (97-C-4134). NRL 7604 provides technical management.

4. REFERENCES

- Cahalan, R.F., 1987: Overview of Fractal Clouds. *Advances in Remote Sensing Retrieval Methods*, A. Deepak Publishing.
- Cahalan, R.G., and J.H. Joseph, 1989: Fractal Statistics of Cloud Fields. *Monthly Weather Review*, 117, 261-272.
- Mandelbrot, B.B., 1983: *The Fractal Geometry of Nature*. W.H. Freeman and Co.
- Hastings, H.M. and G.Sugihara, 1993: *Fractals, A Users's Guide for the Natural Sciences*. Oxford Science Publications.
- Detwiler, A., 1990: Analysis of cloud imagery using box counting. *International Journal of Remote Sensing*, Volume 11, no. 5, 887-898.
- Eis, K.E., J. Forsythe, and D. Reinke, 1996: The Fractal Behavior of Cloud Systems. *Proceedings of the 1996 Battlespace Atmospherics conference, NCCOSC RDTE DIV Technical Document 2983, December 1996.*

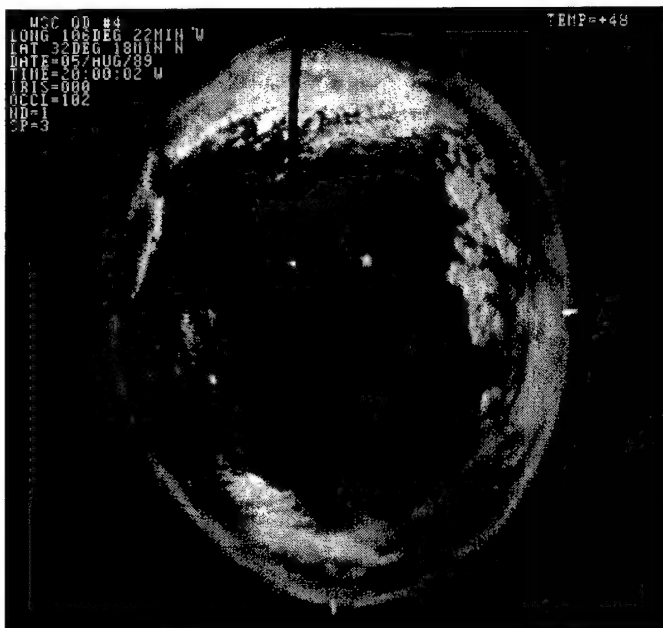
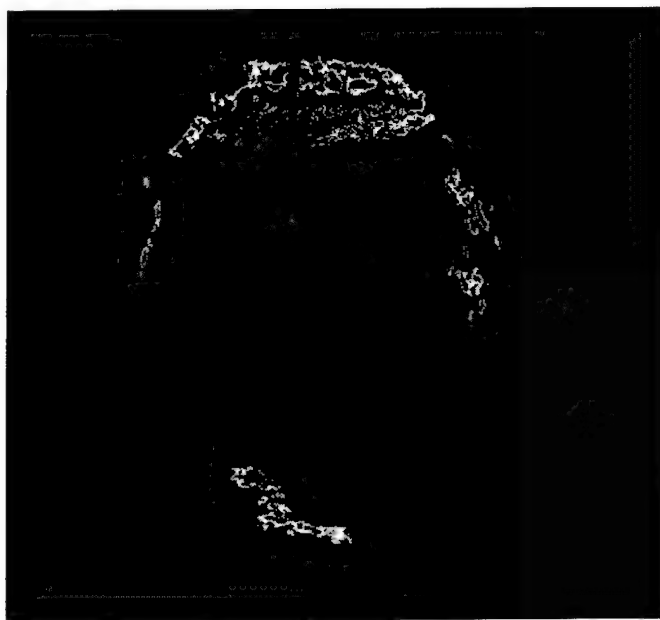


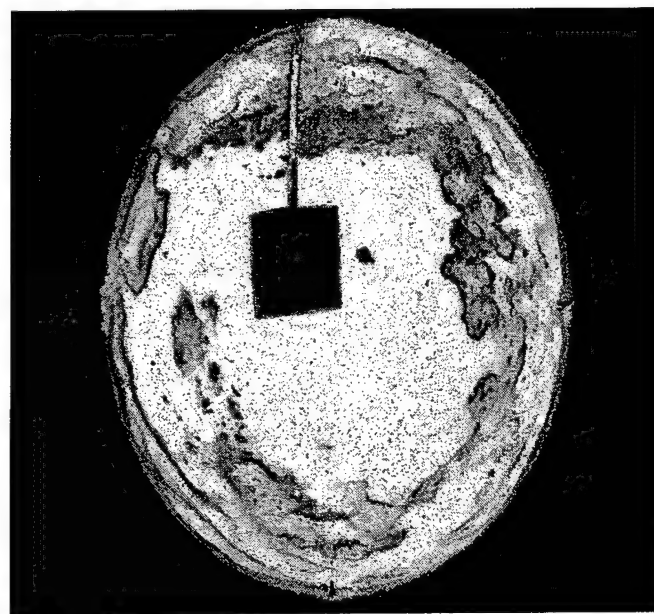
Figure 1: Cloud Image



Figure 2: Band Passed Image



**Figure 3: Fractal Dimensions
of Band**



**Figure 4: Composite
Fractal Dimensions**

CLOUD DATA GENERATION SYSTEM

Jeffrey S. Morrison, Steven L. Rubin

TASC

Reading, Massachusetts, 01867, USA

ABSTRACT

The Cloud Data Generation System (CDGS) is a stand-alone, user-friendly system serving to support simulation analyses requiring realistic high resolution cloud cover data. The CDGS can generate yearly, statistically correct and meteorologically coherent, cloud amount fields at user selected resolutions down to 3x3 nautical miles and at user-selected time steps as fine as 15 minutes. The CDGS generates both assessment (ground truth) and forecast cloud cover data. The forecast data are influenced by user-selected skill parameters.

1. INTRODUCTION

Developed to meet specific Government requirements, the CDGS provides a self-contained system for generating, packaging, reviewing, and managing cloud cover data sets. Simulators ingest these data to analyze systems which are sensitive to cloud cover and cloud cover forecasts. Key features of the system and its products include:

- high data quality,
- user-specified spatial and temporal resolution,
- year-long and global extents
- ground truth and forecast output fields, and
- tunable cloud forecast skill.

To capture the natural characteristics of cloud cover, the CDGS incorporates real cloud cover data derived from surface based or satellite observations during the data generation process. These real data are spatially coarse and temporally sparse. The CDGS uses sophisticated fractal-based algorithms to ensure the continuity of coverage in both spatial and temporal domains; no missing data are contained in the output field products.

2. SYSTEM OVERVIEW

The CDGS generates synthetic assessment (ground truth) and forecast cloud cover data on the Air Force's nephanalysis family of grids and WAC/ATC/WTM (World Aeronautical Chart/Air Target Chart/World Target Mosaic) family of grids, at user-selected resolutions down to the smallest grid size in each family--64th mesh (~4x4 nm) and 3x3 nm, respectively--and at user-selected time steps as fine as 15 minutes. The CDGS employs a fractal-based model to generate regional or worldwide high resolution fields which are spatially and temporally consistent with the underlying Real-Time Nephanalysis (RTNEPH) total cloud cover archived at the U.S. Air Force Combat Climatology Center (AFCCC). Forecast accuracy is consistent with a user-defined weather support architecture. To account for current or future cloud forecast (production system) quality, the CDGS

emulates weather support configurations (geostationary and polar-orbiting constellations, surface observations, data timelines, forecast process characteristics, etc.).

The CDGS employs a set of component application programs, described below, on a stand-alone platform running the OPENSTEP™ operating system. The CDGS displays its cloud depictions and statistical summaries using integrated map and graphics tools. Graphical user interfaces ensure intuitive, user-friendly operation of cloud data generation and statistical analysis components without the need to review detailed manuals. The system uses 8mm tape drives to access the input AFCCC cloud cover data and to prepare output tapes containing gridded cloud cover data and associated statistics.

3. CDGS COMPONENTS

The Preprocessor operates only once for each data year. It ingests a specially-processed year-long data set, acquired from AFCCC on twelve monthly 8mm tapes, from which it creates global, hourly cloud amount and cloud type fields, at both UTC and local time (LT). The CDGS eliminates artificial (persisted) data and fills all resulting data voids using a robust spatial/temporal procedure that ensures the existence of realistic cloud amount and type data at each gridpoint (see Figure 1 below). The Preprocessor also produces corresponding cloud cover statistics files needed by other CDGS components. The Synthetic Cloud Generator (see below) directly reads all data files produced by the Preprocessor.

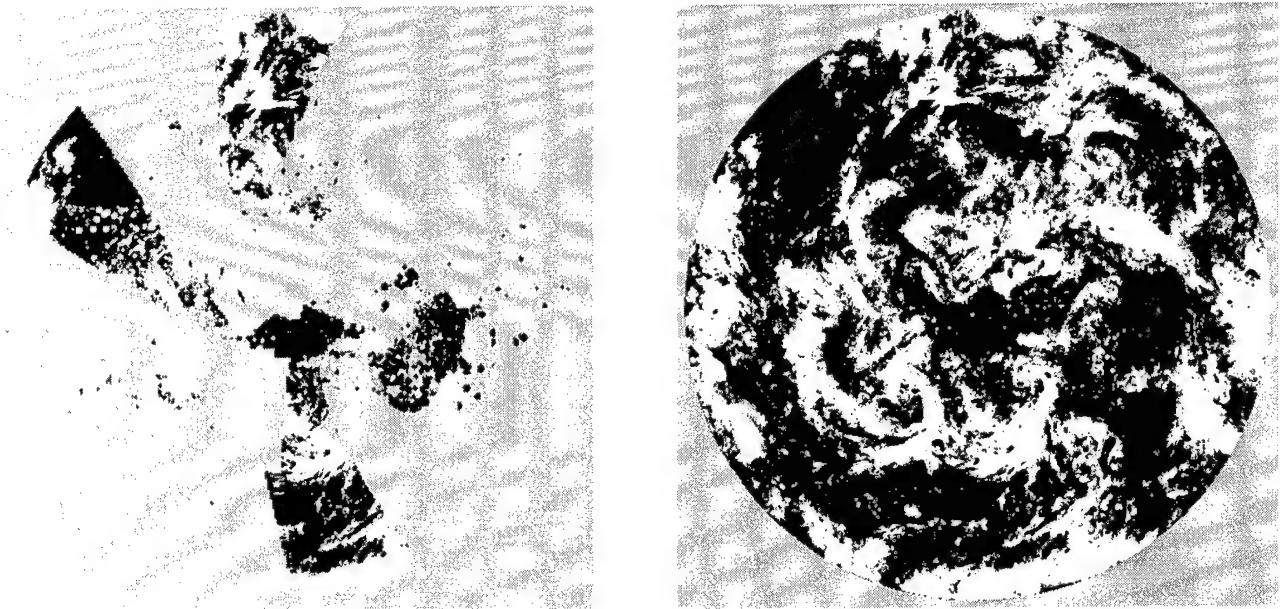


Figure 1. Preprocessed data. Original hourly, hemispheric cloud amount data (left) and cloud amount data after the spatial/temporal fill by the Preprocessor.

The Preprocessor performs time-consuming manipulations on the cloud data that, as indicated above, need only be done once per year-long AFCCC data set. As it completes each one-year run, it records this fact in such a way that the year of data for UTC or LT automatically becomes a selectable option during the scenario definition phase of cloud data generation. The user chooses whether to make local time data or UTC data during scenario definition (see below).

The Forecast Skill Generator (FSG), a separate program component, allows the user to specify weather support and forecast system characteristics, and creates a corresponding forecast skill file which is directly accessed by the Synthetic Cloud Generator. As the user creates various user-defined weather support scenarios,

they automatically become selectable options during scenario definition. The FSG is functionally independent of other CDGS components and is executed only when the user needs new forecast skill specifications.

The Synthetic Cloud Generator (SCG) is the core data generation component of the CDGS. The SCG allows the user to specify a collection of parameters (e.g., input year, geographic regions, forecast skill scenario, time-of-day selections, output resolution and grid) that determine the characteristics and scope of a particular output synthetic cloud data set. The user's scenario definition determines which cloud data file, cloud statistics file, and forecast skill file to read. The SCG then uses the data in these files, in a manner consistent with the remaining scenario parameters, to generate a synthetic cloud data set for simulator use. The SCG stores statistical parameters characterizing goal and achieved forecast quality as well as distribution characteristics of the assessment and forecast cloud cover fields for use by the Scenario Review Tool.

The Scenario Review Tool (SRT) reads the synthetic cloud data and corresponding assessment vs. forecast contingency table parameters associated with a particular scenario, and allows the user to examine and analyze these data to determine the extent to which scenario goals were achieved. For example, the user may view particular cloud fields (see Figure 2 below) and/or generate graphs depicting forecast accuracy and skill.

Supporting the SCG and the SRT is an ancillary application, the MapApp. This tool provides a powerful graphical map capability for conveniently selecting geographical regions for data generation and for displaying and zooming in on generated cloud scenes.

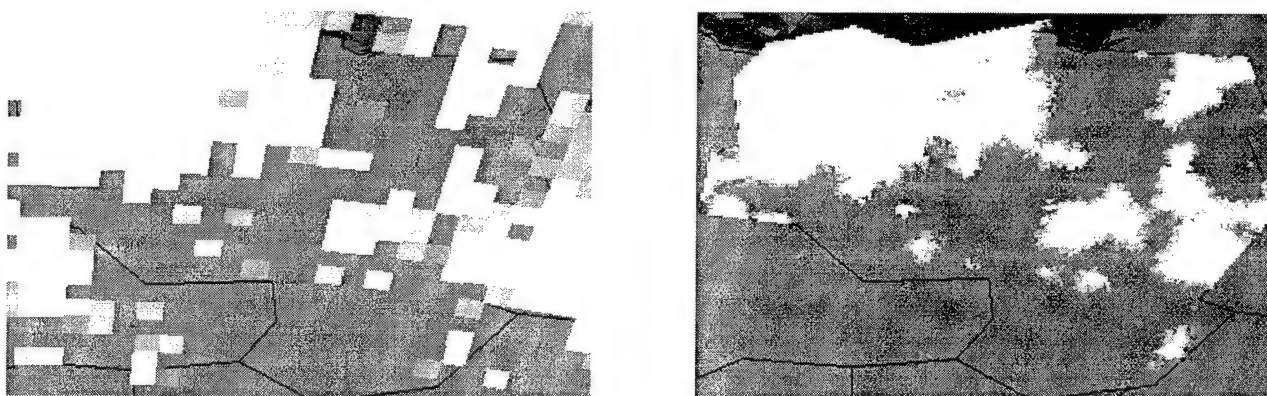


Figure 2. Cloud amount data. A 25 nm cloud field (left, input resolution) and the corresponding 3 nm cloud field generated by the SCG for a chosen subregion.

4. CONCLUSIONS

The primary use of the CDGS is to define a data generation scenario through the Synthetic Cloud Generator graphical user interface and to execute the scenario, generating the needed data for use in a particular simulation study. The CDGS can generate yearly, statistically correct and meteorologically coherent, cloud-amount fields down to 3x3 nautical mile resolution at 15 minute time steps. The user employs the Scenario Review Tool following data generation to inspect and evaluate, from a statistical viewpoint, the characteristics of the fields produced. The user can also revisit the results from past scenarios with the SRT. The user only operates the Preprocessor and the Forecast Skill Generator as needed to develop data files required by the SCG. Future plans include enhancing the system to generate cloud fields which deviate from climatology according to user specifications, and to generate layered cloud fields.

POSTER/PC/VIDEO PRESENTATIONS

References in some of the preprints had to be deleted by the editor because they referred the reader to papers with limited distribution that were not available to the public.

**WWW-BASED
CLOUD INFORMATION REFERENCE LIBRARY
AND ARCHIVE (CIRLA)**

John C. Burgeson
Paul D. Try
Science and Technology Corporation
Hampton, Virginia

Donald D. Grantham
Phillips Laboratory Geophysics Division
Hanscom AFB, Massachusetts

ABSTRACT

This paper reviews the Cloud Information Reference Library Archive (CIRLA) and updates its status. CIRLA is now available on the World Wide Web (WWW or Web). The Web pages are logically structured into brief descriptions of cloud information and related meteorological information on simulations/models, databases, algorithms, summaries, and references. CIRLA also includes information on recent additions, notices of upcoming events, meetings of interest to the cloud community, and an easy opportunity to provide comments. The purpose of CIRLA is to provide a rapid, user-friendly communication between those who need cloud information and those who can provide it. As its name suggests, CIRLA does not contain the actual cloud information itself; rather CIRLA contains entries that describe the information, its format, how it can be obtained and applied, and its status. CIRLA is easily accessible now, only a click away on your Web browser at <http://www.cais.com/stc/cirla>.

1. INTRODUCTION

The CIRLA is sponsored by the Geophysics Directorate of the Phillips Laboratory (PL/GP). The Science and Technology Corporation (STC) developed and manages CIRLA, which has about 100 entries. Each entry provides sufficient detail for users to determine if the available information (for example, on a database, model, or code) suits their purpose. CIRLA's objective is to provide a rapid, user-friendly communication between users of cloud information and its providers. CIRLA is now readily accessible to anyone who uses the Internet.

The purpose of this article is to motivate the reader to use CIRLA again, now readily available on the Web. The authors hope to reach a wide audience that includes former users, and potential users. First, to bring this audience together, CIRLA's background is briefly discussed. The discussion leads into a description of CIRLA and its access.

2. BACKGROUND

The concept of CIRLA originated at the Cloud Impacts on DoD Operations and Systems—1989/90 Conference (CIDOS—89/90), which formally recommended the development of CIRLA. The consensus at the conference was that the process of development and employment of increasingly sophisticated weapon systems, many of which rely on sensors that are adversely affected by clouds, could be improved with a better way for systems analysts and engineers to gain knowledge of and access to complete cloud information. As envisioned, CIRLA would offer rapid, user-friendly access to an efficiently managed database targeted to DoD applications.

2.1 INITIAL DEVELOPMENT OF CIRLA

STC developed the CIRLA database by preparing entries from more than 100 responses to questionnaires, sent to those who attended CIDOS 89/90 and to others with an interest in clouds. The CIRLA became operational in mid 1990, when the program entered a maintenance phase during which STC sought feedback from users. The database was accessible on a electronic bulletin board via E-mail to Omnet, a communications system management company.

The original database design was a database of databases. Data were placed into one or more of five categories: models/simulations, databases, algorithms, summaries, and reference information. Each of these were divided into cloud databases (low, middle, high, stratospheric/noctilucent, structures, CFLOS, or other), meteorological databases (temperature, water vapor, precipitation, liquid water content, visibility, optical depth, microphysics, or other), or other. Finally, databases contained recent additions, notices, meetings of interest, and comments about CIRLA.

By 1992 the original widespread interest in CIRLA was difficult to sustain. While some users were concerned that the information was not current; many users could not conveniently access CIRLA because they didn't have a PC with a modem, required to connect to the electronic bulletin board. The Phillips Laboratory Geophysics Directorate tasked STC to arrange for CIRLA to be accessible through the Internet. In addition, the authors had concluded that CIRLA should be revitalized. The CIDOS-93 Conference provided further motivation to make CIRLA better.

2.2 CIRLA UPDATE

In early 1993 STC launched a major campaign to update the entries in CIRLA and expand their information content. Anyone who contributed more than one CIRLA entry was contacted by telephone and telefax. Those who contributed a single entry to CIRLA received a letter and then follow-up telephone calls if necessary to establish contact. STC sent to all contributors copies of their entries, a reminder of what CIRLA is, instructions for logging on, an explanation of the update process, and a request for new cloud information and for their comments about CIRLA. The results yielded 13 new, 16 substantially modified, 73 slightly changed, and 14 deleted entries. In general, however, the information contained in CIRLA had aged well.

The updated CIRLA was ready for cloud community exploitation in late 1993; all entries included nearly all the detail provided by the contributor, who made full information available to requesters. Users took advantage of this unique data set.

2.3 RECENT HISTORY

Users maintained a high level of interest in CIRLA following the CIDOS-93 Conference. Unfortunately, less than a year later the electronic bulletin board system (BBS) hosting CIRLA became increasingly unreliable, causing user interest to decline. When the BBS went out of business and the CIRLA became unavailable, user interest was insufficient to lift CIRLA's priority to the level where funding would be provided for rehosting.

Recently, the Geophysical Directorate detected interest in CIRLA and funded its basing on the World Wide Web. STC designed and developed the CIRLA Web site, transferring CIRLA's structure from the BBS to Web pages. Users who accessed the CIRLA BBS will feel at home while visiting the CIRLA Web site.

3. CIRLA TODAY

CIRLA hasn't changed, but its access is easier today than ever before. A brief explanation of the Web pages is provided below along with an example of a CIRLA entry.

3.1 VISITING THE CIRLA WEB SITE

When you visit the CIRLA Home Page, please register in the Guest Book. The Guest Book allows comments, so you may prefer to register just before leaving the CIRLA Web site. It is important to register because user interest, which may lead to improvements of CIRLA, will be measured by the number of registrants and their comments—not merely hits on the site.

The site is organized into eight primary pages with menus that connect the user to related entries. The main CIRLA pages are: models/simulations, databases, algorithms, summaries, and reference information. Each of these five categories has three sub-categories: **cloud data**, which include low, middle, high, stratospheric/noctilucent, structures (e.g., size, spacing, edge effects, etc.), cloud-free line-of-sight (CFLOS), and other (e.g., total coverage, contrails, etc.); **meteorological data**, which include temperature, water vapor, precipitation, liquid water content (LWC), visibility, optical depth, microphysics, and other; and **other cloud-related information**. In addition, there are pages on recent additions, notices of upcoming events, and meetings of interest to the cloud community (e.g., abstracts from CIDOS-95 papers).

This structure maintains CIRLA's original design, which focused on a highly discriminating organization. In practice, most of the CIRLA entries overlap into other categories, for example, a cloud database may contain information on all types of clouds, a numerical weather prediction model generates a database with several types of meteorological parameters, and so on. Consequently, users should browse the "other" categories whenever they can't locate the desired information from their seemingly obvious choice of page.

Links are provided at the bottom of all pages to move users conveniently through the Web site. You can always return to the Home Page from any other page, or you can send e-mail with your comments from any page. The authors encourage comments, recommendations, and updates or new entries. Enjoy your visit.

3.2 A SAMPLE CIRLA ENTRY

This example illustrates the details provided by a CIRLA entry. The authors strongly encourage contributors to provide as much detail as necessary to describe their entry clearly and completely.

Title:	LOWTRAN/MODTRAN/FASCODE Cloud Models
Description:	Models the radiative properties of clouds within the LOWTRAN, MODTRAN, and FASCODE atmospheric transmission/radiance models. The cloud models include cumulus, stratus, stratocumulus, nimbo-stratus, altostratus, and cirrus clouds (standard, sub-visual, and the NOAA cirrus model from LOWTRAN 6). The radiative properties include the attenuation coefficients and asymmetry parameters as a function of wavelength from the UV through the microwave regions (wavelengths longer than 0.2 microns).
Format:	Fortran code.
Access:	Models are distributed by the National Climatic Data Center (NCDC) in Asheville, NC.
Application:	Basic research and theoretical investigations.
Status:	Operational
CIRLA Updated:	2/24/93
POC Name:	Ms. Gail Anderson
Phone Number:	(617) 377-2337
Address:	Phillips Laboratory, PL/GPOS, Hanscom AFB MA 01731-5000
Co-Contributor:	E. P. Shettle and V. J. Falcone
Remarks:	For further information, reference "Models of Aerosols, Clouds, and Precipitation for Atmospheric Propagation Studies", E. P. Shettle (1989), in "Atmospheric Propagation in the UV, Visible, IR & MM-Wave Region and Related System Aspects", AGARD Conference Proceedings No. 454, Proceedings of the AGARD Electromagnetic Wave Propagation Panel Symposium, Copenhagen, Denmark, 9-13 October 1989.

4. CONCLUSIONS

The Cloud Information Reference Library Archive can help to close the gap between the weapon system developers who need unique cloud information and those researchers who have that information. Basically, CIRLA should be serving as a facilitator for information transfer. Members of the cloud community can easily access CIRLA and should do so whenever they need, for example, to consider environmental effects on system and sensor development as well as tactical war gaming and mission planning.

CIRLA has been unavailable to most users for two years; consequently, its potential has been unrealized. To revitalize user interest in CIRLA, it has been made readily accessible over the World Wide Web. Try CIRLA, either again or for the first time, at <http://www.cais.com/stc/cirla>.

CLOUD DETECTION/EDITING EXPERIMENTS ON THE *LEWIS* AND *CLARK* SATELLITES

Richard E. Davis, R. Gale Wilson, and Robert L. Jones
NASA Langley Research Center
Hampton, VA 23681-0001

ABSTRACT

Algorithms for prototype cloud-detection/editing systems will be tested in technology demonstration experiments on the two missions--*Lewis* and *Clark*--in NASA's Small Spacecraft Technology Initiative (SSTI) program, with launches in 1997-98. This paper presents the system development approach and describes two algorithms currently under evaluation.

1. INTRODUCTION

Fifty percent or more of the Earth is covered by clouds, on average; consequently, much "useless" data is collected by Earth Resources (ER)-dedicated satellites. The data volume from present satellites is already large, straining data reduction and archival resources. This problem will worsen as hyperspectral imagers come into use, with more spectral channels and finer spatial resolution. Therefore, there is a need for autonomous, onboard cloud-sensing systems that can be tailored to interface with ER satellite instrumentation, detect cloud-obscured frames of imagery during the data collection process, and bypass (edit) them out in subsequent image storage, transmission, and ground processing operations. The advent of small satellites (smallsats) for commercial remote sensing provides further motivation for the development of simple, real-time cloud discrimination methods, to improve the time and cost efficiency of commercial operations. The SSTI program, a NASA-Industry partnership with two satellite launches (*Lewis* and *Clark*) planned for 1997-1998, provides an opportunity to conduct technology demonstration experiments which address this onboard cloud detection/editing goal for ER sensors aboard small commercial satellites. Prototype cloud-detection-algorithm experiments are being developed to support the ER sensors on *Lewis* and *Clark*. This paper presents our approach, and describes two such experiments.

2. APPROACH

For this investigation, clouds are regarded as "contaminants" to be detected and bypassed in the data reduction/archival process, and not as objects of investigation themselves as, e.g., in SERCAA¹ or CERES.² These are our arbitrary constraints on the onboard systems: (1) they should be autonomous, using only a smallsat's onboard ER sensor channel set, i.e., they should use no ancillary data (as, e.g., data fusion from MetSat IR channel data or surface-feature data bases); and (2) they should operate in real time. Our approach includes these steps: (1) assess what can be done using existing technology, choosing as baseline concepts the simplest algorithms providing acceptable levels of performance, and testing them on the SSTI missions; (2) assess the cloud detection/editing impact (e.g., the reduction in data volume) of applying the baseline concepts to the SSTI mission; (3) iterate steps 1-2, augmenting the baseline concepts by, e.g., adding additional spectral channels /new logic elements; and (4) iterate steps 1-3, investigating alternate concepts.

3. SSTI MISSIONS AND SUPPORTED ER SENSORS

The SSTI missions will be launched (*Clark*, January, 1998; *Lewis*, August, 1997) from Vandenberg AFB on Lockheed Launch Vehicles (LLV) into nominal 500- km , 97- degree inclination sun-synchronous orbits. *Clark* carries one ER sensor--the EarthWatch, Inc. Imager (EWI), having three spectral channels (0.55, 0.65, and 0.84 μ m) with a 15-m pixel spatial resolution at nadir, and a panchromatic channel with a 3-m ground

resolution. *Lewis* carries the TRW, Inc. Hyperspectral Imager (HSI), having two spectrometers spanning the 0.4- to 2.5- μm spectral range in 384 channels with a 30-m ground resolution in a pushbroom-type scan pattern, and a 5-m resolution panchromatic channel.³

4. CLOUD ALGORITHMS FOR SSTI

Clark: Using only the onboard channel sets means that the algorithms must operate in the visible and near-infrared. Only one algorithm--our baseline concept--is currently implemented on *Clark*. It is based on the NASA - Langley/ Martin Marietta Feature Identification and Location Experiment (FILE),^{4,6} which was operated aboard aircraft and the Space Shuttle during the 1980s, with good results. The *Clark* experiment is based on signal magnitudes in the 0.66- and 0.86- μm channels of the EWI, their ratio, and signal thresholds that depend on solar zenith angle (SZA). These parameters are used in a two-channel approach, with linear decision boundaries as shown in Figure 1. A four-way classification (i.e., four possible outcomes) is provided for each pixel: bare land, vegetation, water, and the combined class cloud/snow/ice. The classifier operates on raw radiometer signal levels, rather than derived apparent reflectances. The approximate SZA at the pixel is the only parameter needing external specification. Presently, only two levels of signal threshold are used, depending on whether SZA exceeds 45 degrees. Due to the simplicity of this approach, and the automatic spatial registration of the pixels in the three spectral channels, the *Clark* /FILE algorithm is implemented easily in spacecraft software, and will provide on-board real-time classification.

Lewis: Having 384 HSI spectral channels available across a wide spectral range--0.4 to 2.5 μm --affords many possibilities for algorithm experimentation. However, the HSI pixel spatial registration is performed in non-real-time ground processing. Also, several concepts require the computation of a pixel's apparent reflectance, which requires precise knowledge of the SZA and modeling of the exoatmospheric solar irradiance. Because of these added complexities, none of the present *Lewis* algorithm concepts is implemented in real-time on the spacecraft. Instead, the concepts will be evaluated in non-real-time ground processing of the HSI data, to simulate real-time application. Several cloud algorithm concepts for *Lewis* may be evaluated in parallel, using this ground-processing approach. Due to space considerations, only the simplest is described here.

Lewis algorithm 1 ("enhanced FILE") 6 channels: 0.66, 0.86, 1.25, 1.38, 1.55, 1.88 μm : This algorithm adds four channels to the baseline (*Clark*/FILE) concept. Strong water vapor absorption channels at 1.38 and 1.88 μm are added as a two-channel preprocessor for detecting high altitude clouds (HAC).⁷ Low signal values imply absence of HAC; exceeding a threshold means that HAC are present. The 1.38- μm channel is used equatorward of 50 degrees latitude. The 1.88- μm channel, with stronger absorption, performs the same function in the drier atmosphere poleward of 50 degrees. The ratio of the 0.65 and 1.55- μm signals decides between "cloud" and "snow/ice" classification, while the ratio of the 0.65 and 1.25- μm signals decides between snow and ice.⁸ This algorithm is the least complex in the *Lewis* suite, because it does not require apparent-reflectance calculations. It provides seven outcomes: HAC, bare soil, vegetation, cloud, snow, water, ice, as shown by the logic flow in Figure 2. Its performance will be compared to that of the baseline algorithm; the degree of performance enhancement provided by the four additional channels can then be evaluated.

5. ALGORITHM SIMULATIONS

Preliminary logic for the algorithms described above was developed in C code, tested and debugged on a set of synthetic input signal (total radiance) data generated using the *MODTRAN3* atmospheric radiative transfer program.⁹ A variety of spectral reflectance backgrounds from *MODTRAN3* and reference 10 was combined with "clear" (23-km visible range) or "hazy" (5-km visible range) aerosol contents, to model the pixel scenes. The simulation set comprised twenty-three backgrounds/aerosol haze model scenes, ten of which contained clouds. The tests pointed out that bare land is often misclassified as cloud; therefore, further algorithm refinement is needed. Otherwise, the algorithms performed well.

6. ALGORITHM COMPLEXITY

Beyond its accuracy, an algorithm must be assessed for its suitability for ultimate real-time, autonomous implementation aboard a satellite. This assessment requires determining its computational complexity, storage requirements, and execution times. To determine its complexity, we determined the maximum number of independent computational operations--such as additions, multiplications, channel signal ratios, exponentiations, etc.--that would be required to classify a pixel, as well as the storage space requirement, for an image of m by n pixels. Then, we simulated the time required to classify a 512-by-512-pixel image, using a 60MHz Sun SPARC20 computer. Preliminary results show that all the algorithms evaluated to date are efficient, in that the space requirement is only linearly proportional to the number of pixels. Algorithm 1 required approximately 1.2 seconds per image.

7. PLANS AND CONCLUDING REMARKS

Several cloud detection/editing algorithm approaches will be evaluated on the SSTI *Lewis and Clark* missions; two have been described here. The on-ground evaluation-in-parallel approach described above is flexible, allowing for evolutionary refinement of the present approaches, and the inclusion of new algorithm concepts as, e.g., may be suggested by SERCAA¹ or CERES.² Shadow-and sun-glnt detection are examples of refinements which could be included. Evaluation of algorithms will include an assessment of their complexity. It is planned to use RTNEPH¹¹ cloud analyses, as well as surface observations, in the validation process. While the current approach assumes autonomous algorithms that use only the onboard ER sensor channel sets, sensor fusion of data from other satellites or surface data bases remains a challenging possibility for the future.

8. REFERENCES

1. Gustafson, G.B., et al.: Support of Environmental Requirements for Cloud Analysis and Archive(SERCAA): Algorithm Descriptions. Phillips Laboratory Scientific Report No. 2, PL-TR-94-2114, Directorate of Geophysics, Air Force Materiel Command, Hanscom AFB, 28 March 1994. ADA283240
2. Baum, B.A., et al.: Clouds and the Earth's Radiant Energy System (CERES) Algorithm Theoretical Basis Document. CERES-ATBD Subsystem 4.1, Release 2.2, June 2, 1997.
3. Marmo, J., et al.: The Lewis Hyperspectral Imager Payload Development. *Proc.: Imaging Spectrometry II*, SPIE Vol. 2819, pp. 80-90, Aug. 7-8, 1996.
4. Sivertson, W.E., et al.: Use of the Space Shuttle for Remote Sensing Research: Recent Results and Future Prospects - Feature Identification and Location Experiment. *Science*, Vol. 218, No. 4576, pp. 993-1033, December 2, 1982.
5. Sivertson, W.E., Jr.: Space Shuttle Cloud Detection and Earth Feature Classification Experiment. *Sensors Expo Paper Technical Session 302*, O'Hare Exposition Center, Chicago, September 16-19, 1986.
6. Wilson, R.G., et al.: Radiometric Responsivity Determination for Feature Identification and Location Experiment (FILE) Flown on Space Shuttle Mission 41-G, NASA TM 89017, December, 1986.
7. Gao, B.C.; Goetz, A.F.H.; and Wiscombe, W.J.: Cirrus Cloud Detection from Airborne Imaging Spectrometer Data Using the 1.38 - μ m Water Vapor Band. *Geophys. Res. Ltr.*, Vol. 20, No. 4, pp. 301-304, Feb. 19, 1993.
8. Valovcin, F.R.: Spectral Radiance of Snow and Clouds in the Near Infrared Spectral Region. AFGL-TR-78-0289, AFGL-AFSG-403, Nov. 17, 1978. ADA063761
9. Berk, A.; Bernstein, L.S.; and Robertson, D.C.: MODTRAN: A Moderate Resolution Model for LOWTRAN7, GL-TR-89-0122, 1989. ADA214337
10. Bowker, D.E. et al.: Spectral Reflectance of Natural Targets for Use in Remote Sensing Studies. NASA RP-1139, June, 1985.
11. Hammill, T.M.; d'Entremont, R.P.; and Bunting, J.T.: A Description of the Air Force Real-Time Nephanalysis Model. *Wea. Forecasting*, Vol. 7, pp. 288-306, 1992.

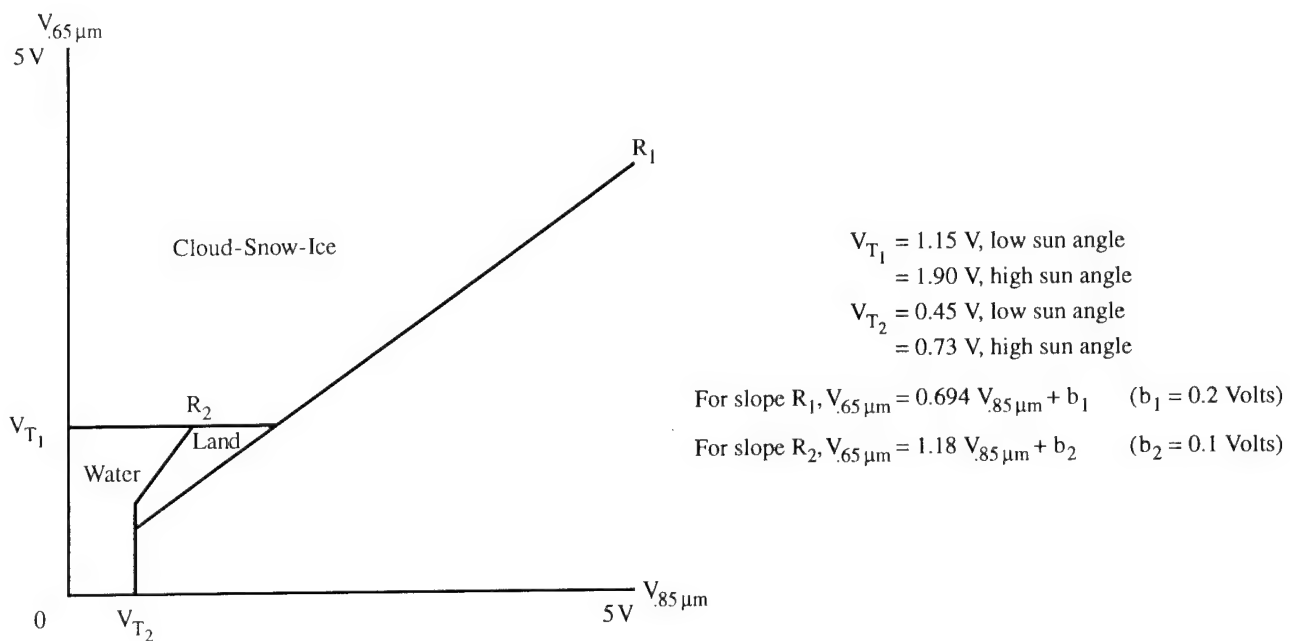


Figure 1. Clark Algorithm Studies (preliminary decision boundaries)

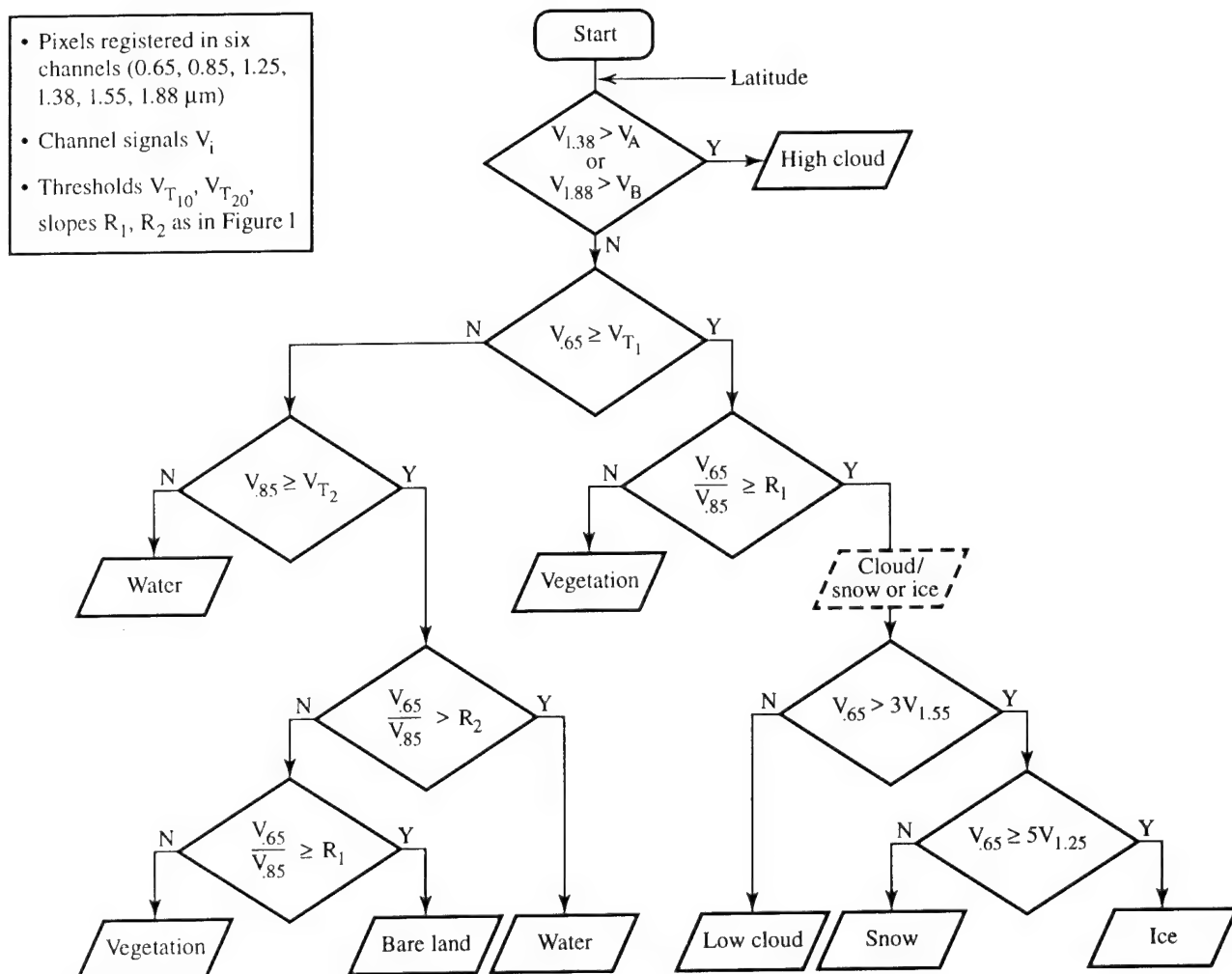


Figure 2. Cloud/Feature Detection Logic – Lewis Algorithm 1

Single-Channel Cloud Detection Using Land-Surface Bidirectional Reflectance Distribution Functions

Robert P. d'Entremont
Satellite Meteorology Group
Atmospheric and Environmental Research, Inc.
840 Memorial Drive, Cambridge, MA 02139-3794

1. Introduction

Bidirectional reflectance distribution functions (BRDFs) are of value in single-channel threshold cloud detection algorithms that discriminate cloudy pixels from cloud-free pixels. Cloud detection thresholds are typically specified as constant or are allowed to vary temporally based on time series analysis of recent cloud-free reflectance observations. Most single-channel cloud detection algorithms utilize satellite sensor data in the visible spectral region ($0.55\ \mu\text{m}$). In this portion of the spectrum vegetated surfaces have low reflectances and hence contrast well with most clouds. This allows for easy specification of regionally constant cloud/no-cloud reflectance thresholds since the underlying surface is very dark and has little reflectance variation.

However, DMSP OLS "visible" data are broadband data measured in the visible and near-infrared ($0.4\text{--}1.1\ \mu\text{m}$) spectrum, so that the background land surface is brighter. Land surfaces are also brighter in AVHRR near-IR data. Consequently there is more variation in the land-surface reflectance in both a spatial and view/illumination geometry sense, and clouds do not contrast as well with adjacent clear pixels.

BRDFs were used to model the spatial variation and view/illumination geometry dependence of NOAA/TIROS AVHRR $0.86\text{-}\mu\text{m}$ near-IR land-surface reflectances over New England during a four-day period in September 1995. Satellite sensor observations were then compared to the BRDF model reflectances; if observation exceeded the BRDF land-surface reflectance threshold, cloud was detected and vice versa. Results were then compared quantitatively to manually generated cloud-truth masks.

2. Land-Surface BRDFs

Radiation reflected from the surface changes as a function of time of day and the direction from which that surface is being viewed, even though energy exchange and transfer surface attributes remain unchanged. The manner in which a particular type of surface reflects incident solar energy (as a function of solar position and the direction from which that surface is viewed) is a fundamental response property of the surface. This property is quantified by means of the BRDF, which is a mathematical description of the angular variation of a surface's ability to reflect illuminating radiation (Nicodemus, 1977).

Knowing the BRDF for a particular location on the earth's surface allows for prediction of a satellite-observed reflectance prior to actual measurement of the reflectance itself. Such predictions are useful to global cloud detection models in that any reflectance observations that do not match those expected of the cloud-free surface are indicative of cloud.

The BRDF models tested during this research are "kernel-driven" in nature; each

model has the general form (after Wanner et al., 1995)

$$r = f_{\text{iso}} + f_{\text{geo}} K_{\text{geo}} + f_{\text{vol}} K_{\text{vol}}, \quad (1)$$

where r is the directionally dependent land-surface reflectance (sr^{-1}). The f_x s are coefficients called *model parameters* whose values are influenced by the sub-pixel morphologic and spectral reflectance attributes of the vegetated surface. Model parameters have explicit theoretical dependencies on vegetation canopy attributes such as leaf reflectance, underlying soil reflectance, leaf area index (LAI), leaf angle distribution (LAD), canopy number distributions, and vegetation crown shapes and sizes. The kernels K_x are deterministic predictors that carry information pertaining to the basic shape of the BRDF given the vegetation structural properties, but are simple analytic functions only of the illumination and viewing geometries. Kernels are independent of wavelength and of the parameters f_{iso} , f_{geo} , and f_{vol} (after d'Entremont, 1997).

3. BRDFs and Automated Cloud Detection

The BRDF models described by Wanner et al. (1995) were used to assign single-channel thresholds to a simple cloud detection algorithm in order to discriminate cloudy pixels from cloud-free pixels over New England. Typically, single-channel cloud-detection reflectance thresholds are specified as constant or are allowed to vary temporally based on time series analysis of recent cloud-free reflectance observations. The most versatile automated satellite cloud detection technology, called Support of Environmental Requirements for Cloud Analysis and Archive (SERCAA), uses such dynamic visible reflectance thresholding (after Gustafson et al., 1994). However, BRDFs provide expected clear-scene reflectances that subsequently can be used as location-dependent single-channel cloud detection thresholds.

Many single-channel cloud detection algorithms utilize satellite sensor data in the visible spectral region ($0.55 \mu\text{m}$), where vegetated surfaces have low reflectances and hence contrast well with most clouds. For example, the SERCAA cloud analysis algorithm uses only $0.63\text{-}\mu\text{m}$ visible AVHRR data in its single-channel threshold algorithm (Gustafson et al., 1994).

In this study it was decided to test the BRDF threshold algorithm under more stressing conditions using AVHRR near-infrared BRDFs. Near-IR vegetation reflectances are higher than those in the visible, and are therefore closer in magnitude to cloud reflectances. Consequently, clouds do not contrast as well with adjacent clear pixels in $0.86\text{-}\mu\text{m}$ imagery. Thus the near-IR data provide for a more challenging test of BRDF model ability to "predict" a spatially varying clear-scene land-surface reflectance that, with the addition of atmospheric scattering effects, can be applied accurately as a cloud detection threshold.

Once computed, the TOA reflectance is then compared directly with AVHRR observation on a pixel-by-pixel basis (i.e., at 1-km nominal resolution). Any pixels whose TOA reflectances exceed the BRDF clear-scene threshold are classified as cloud-filled; otherwise, they are clear. AVHRR data from 28-30 August and 1 September 1995 were collected, mapped, and interactively cloud-masked to provide a source of cloud truth for validation. The four images span the range of meteorological conditions from mostly clear to mostly cloudy, and the view and illumination geometries are representative of both backscatter and forward scatter azimuth angles. Consequently, this set of four images represents well the extent of conditions under which a BRDF might be expected to perform for cloud detection purposes.

Date	n	Accuracy			Relative Azimuth	Total Cloud Cover
		0%	5%	10%		
28 Aug	53720	51	82	95	Backscatter	5%
29 Aug	48197	85	90	91	Backscatter	54%
30 Aug	53687	66	88	96	Forward-Scatter	5%
1 Sept	43428	71	81	87	Forward-Scatter	76%

Table 1. BRDF-6S Cloud/No-Cloud Classification Accuracies. A Total of 199,032 Pixels Were Analyzed Over a Four-Day (Four-Scene) Period

Table 1 has seven columns. Columns 3-5 contain the cloud detection accuracies for near-IR cloud/no-cloud reflectance thresholds that are "+n" percent of the BRDF-6S predicted values. Assume for a moment that the BRDF-6S combination generates precisely correct predictions of clear-scene AVHRR TOA reflectances. When observations are compared directly to the cloud/no-cloud threshold predictions, a 100 percent accuracy would be obtained. However it is unrealistic to expect exact matches between BRDF-predicted and AVHRR-observed TOA reflectances, primarily due to AVHRR sensitivity to random and systematic noise, atmospheric radiative transfer model approximations, sensor calibration errors, and the limiting accuracy of the BRDF semiempirical kernel linearizations. As can be seen from the results in the zero-percent column of Table 1, BRDF-6S predictions in a "precise" sense are fairly inaccurate. Many pixels were falsely identified as cloudy because the single-channel threshold was "slightly" lower than actual observation.

Such uncertainties can be handled algorithmically by allowing for some appropriate flexibility in the threshold-setting process. Table 1 results indicate that by increasing the cloud detection threshold to 1.05 and 1.10 times higher than its absolute, BRDF-predicted value, cloud/no-cloud classification accuracies as high as 96 percent are achieved. Such a flexibility in setting single-channel cloud thresholds is consistent with the approaches of other operational cloud analysis algorithms such as SERCAA (after Gustafson et al., 1994; 1996) and the U.S. Air Force Real-Time Nephanalysis (Hamill et al., 1992). Overall pixel classification accuracies in the "10%" column are high.

4. Significance of Results

The Real-Time Nephanalysis (RTNEPH) is the operational cloud detection and analysis model of the United States Air Force (Hamill et al., 1992). The majority of data analyzed by the RTNEPH is observed by DMSP satellites, although conventional cloud observations and some NOAA/TIROS data are also used. The visible satellite data processor of the RTNEPH uses DMSP broadband (0.4-1.1- μ m) data and a corresponding database of earth-surface background reflectances. RTNEPH is primarily a single-channel threshold technique that compares satellite reflectance observations with expected "background brightnesses." Background brightness is the expected clear-column reflectance as previously and recently measured by the DMSP OLS visible sensor under cloud-free conditions. This is a dynamic background reflectance database that is updated in real time to track short-term and seasonal changes in snow and ice cover, and vegetation health. Observations that are higher than the background (plus an "uncertainty" factor) are classified as cloud-filled, analogous to the BRDF-based cloud detection tests performed in this study.

Key to the overall performance and reliability of the RTNEPH visible cloud detection algorithm is an accurate specification of the expected clear-scene reflectance. The current RTNEPH background brightness database supplies a single reflectance threshold for each 48-km grid location on the earth's surface. It does not explicitly account for BRDF effects, especially at very localized (i.e., pixel-resolution) scales. To compound the problem, DMSP satellites are typically launched into early-morning, near-terminator polar orbits. They observe the earth's surface under a wide variety of stressing illumination and view geometries that range from dawn to dusk, specular to backscatter. Consequently, the variation of bidirectional reflectance from the eastern edge of the satellite pass to the western edge is highly pronounced. Due to bidirectional effects the background reflectance for a particular earth location is not constant from one overpass to the next. The RTNEPH background brightness database does not have sufficient flexibility to account for these effects.

Consequently as much as 75 percent of the available OLS visible sensor data are not processed. Even when they are, the "threshold-plus-uncertainty" approach adopted by the RTNEPH is sometimes forced to choose rather large uncertainties, again due in substantial part to land surface bidirectional reflectance effects. Adoption of BRDF retrievals into the background surface reflectance database has the potential to increase both the accuracy of the RTNEPH visible cloud detections and, perhaps more significantly, the quantity of visible data that are processed.

The application of BRDF theory to the specification of expected (predicted) clear-scene reflectances would help minimize any uncertainty in the accuracy of the background reflectance database itself. Use of increased amounts of visible data would be especially valuable for detection of boundary-layer low clouds whose LWIR detection is problematic because their brightness temperatures are often close to that of the underlying surface.

5. References

- d'Entremont, R. P., 1997: **Meteorological Applications of Surface Bidirectional Reflectance Distribution Functions Retrieved from Satellite Data**. Ph.D. Thesis, Center for Remote Sensing, Boston University, 170 pp.
- Gustafson, G. B., R. G. Isaacs, R. P. d'Entremont, J. M. Sparrow, T. M. Hamill, C. Grassotti, D. W. Johnson, C. P. Sarkesian, D. C. Peduzzi, B. T. Pearson, V. D. Jakabhazy, J. S. Belfiore, and A. S. Lisa, 1994: **Support of Environmental Requirements for Cloud Analysis and Archive (SERCAA): Algorithm Descriptions**. USAF Phillips Laboratory Technical Report PL-TR-94-2114, Hanscom AFB, MA 01731-3010, 100 pp. ADA283240
- Gustafson, G. B., R. P. d'Entremont, and R. G. Isaacs, 1996: **Support of Environmental Requirements for Cloud Analysis and Archive (SERCAA): Final Report**. USAF Phillips Laboratory Technical Report PL-TR-96-2224, Hanscom AFB, MA 01731-3010, 71 pp. ADA32201
- Hamill, T. M., R. P. d'Entremont, and J. T. Bunting, 1988: **A Description of the Air Force Real-Time Nephanalysis Model**. *Weather and Forecasting*, 7, 288-306.
- Nicodemus, F. E., J. C. Richmond, J. J. Hsia, I. W. Ginsberg, and T. Limperis, 1977: **Geometrical Considerations and Nomenclature for Reflectance**. National Bureau of Standards Monograph 160, *Inst. for Basic Standards*, Washington D. C., 52 pp.
- Wanner, W., X. Li, and A. H. Strahler, 1995: **On the Derivation of Kernels for Kernel-Driven Models of Bidirectional Reflectance**. *Journ. Geophys. Res.*, 100, No. D10, 21077-21089.

**A FUSED METHOD OF DETERMINING SOIL MOISTURE USING
HIGH RESOLUTION GEOSTATIONARY IMAGERY¹
1997 CIDOS CONFERENCE**

**Kenneth E. Eis and Andrew S. Jones
Cooperative Institute for Research in the Atmosphere (CIRA)
Colorado State University, Foothills Campus
Fort Collins, CO 80523**

ABSTRACT

Vastly improved analysis products to determine soil moisture are needed for DOD simulations and operational use. An accurate, timely, and high resolution soil moisture product could be used for trafficability, fog, thunderstorm forecasting, and to improve IR background analysis. Agromet and other analysis simulations could also benefit from an improved soil moisture product.

This paper describes new remote sensing soil moisture research that uses geostationary satellite data and meso-model analysis tools in a fused process. The result is a high-resolution (5-km) soil moisture index that represents a significant theoretical improvement over the current experimental product, which is based on DMSP/SSM/I channel subtraction techniques.

INTRODUCTION

Soil moisture is currently measured in just a few locations across the globe. Lysimeters, which measure soil moisture by weight, are usually located at agricultural research stations. Their data are not reported in real-time, and are highly dependent on soil type and terrain, and are never used in operational forecasting. Clearly a satellite based technique is needed to fill in this sparse data set. Three satellite-based methods are available. The first is based on DMSP SSM/I radiometric measurements and the second on IR surface heating rate measurements. Both measure effects on the surface to a depth of less than a centimeter. The SSM/I radiometer method indirectly measures the emissivity changes due to the presence of water, but unfortunately, the vegetation overlying the soil also adds to the emissivity that is not easily removed from the classified signal. This same problem occurs when the thermal mass of the soil is measured from satellite with IR sensors to provide a soil moisture index. Fortunately this problem is minimized using a coupled approach where the thermal mass measurements are compared iteratively with a meso-model's surface temperature output.

Another method that is often considered for determining soil moisture is that of using rain rate estimates from the SSM/I instrument. This method assumes that an SSM/I measurement of a few milliseconds a day is as accurate as using a few milliseconds of rain gage data. Since rain rates fluctuate wildly, and the beginning and end of a rain event are not measured during the overpass, the accumulated rain of the event, which is the primary parameter required to calculate soil moisture, is totally unknown. It is much better to measure the accumulated soil moisture directly.

¹ This work is sponsored by the Center for Geosciences Phase II under grant DAAH04-94-G-0420.

METHODOLOGY

Soil temperature change (dT) is dependent upon soil type, overlaying vegetation, soil moisture content, sub-surface heat flux, and radiative heating (and cooling). IR images from the GOES satellite are taken 15 minutes apart (dt). The surface temperature heating rate is functionally dependent upon soil moisture content. The best sensitivity is obtained from images taken during morning periods of maximum solar heating rate. It should be noted that this method will not work well with current polar orbiting satellites. First, the over flight times of polar orbiting satellites, even given a three satellite configuration, do not give desirable time intervals at the appropriate times of day. Second, the two consecutive temperature measurements would be taken with two different IR instruments on two different satellites. This precipitates cross calibration problems that do not occur when a single IR instrument is used. Since we are using the difference between two IR radiance temperatures, the problem of requiring highly accurate calibrated surface temperatures for the model coupling is minimized.

Given a measure of dT/dt from the satellite, we now turn to the model. Most mesoscale forecast models such as RAMS and MM5 contain soil moisture as an explicit input or output variable and in the prediction mode predict the surface temperature and moisture values. The models also incorporate soil type databases as well as vegetation and moisture percolation to some extent. If these models are run in their diagnostic (instead of their prognostic) mode, then the surface temperature fields can be used as input variables and the moisture as output variables.

A schematic of the method is shown in Fig. 1. Bare soil and vegetation components of the land surface parameterization are solved sequentially, such that the fractional coverage of the components appropriately contributes to the surface energy dynamics. In Fig. 1, the subscripts l and v denote land and vegetation components, where T is the surface skin temperature, η , is the volumetric soil moisture, d is the stomatal conductance of the vegetation, Ψ is the root zone soil moisture potential, and f denotes the various functional dependencies within the surface parameterization scheme.

Figure 2 shows the output of the RAMS model for a specific case. Panel a is the output without the satellite IR data to initialize the diagnostic run. The isopleths are in one percent increments of soil moisture saturation. Panel b is the diagnostic output when the dT/dt values (at 5-km resolution) are used to initialize the model run. The large dark gray area represents an area of dry soil and the smaller dark gray areas in eastern Kansas and north central Oklahoma are areas of saturated soil. A thunderstorm had passed from the Texas panhandle through eastern Kansas. The isopleths are the same increment in both panels, 1 percent increments. Clearly the satellite data improves the resolution.

This method has several significant advantages over other methods:

- Corrections for soil moisture and vegetation are in the model.
- Improvements in meso-model treatments of soil type, vegetation, and hydrology are automatically incorporated into the method.
- Any geostationary IR image set: GOES, METEOSAT, or GMS are capable of generating moisture values including the new Chinese geostationary satellite.

FORECAST CONSIDERATIONS

As numerical weather forecasting methods improve, their dependence upon moisture and sensible heat fluxes at the surface becomes more important to their accuracy. Large storms with strong synoptic scale forcing are treated well without significant sensitivity to the surface fluxes, but many features like radiation fog, air mass thunderstorms, and convection are affected by the heterogeneous nature of surface albedo, heating, and moisture. With improved antecedent moisture measurements, forecast models will predict thunderstorm development and locations and fog boundaries more accurately.

FUTURE CONSIDERATIONS

Currently the soil moisture index has not been quantitatively validated. It needs to be coupled to soil type databases and engineering data to be used as a trafficability product.

For more information and references please go to

<http://www.cira.colostate.edu/GeoSci/yr2/S2/T6/Task6.html>

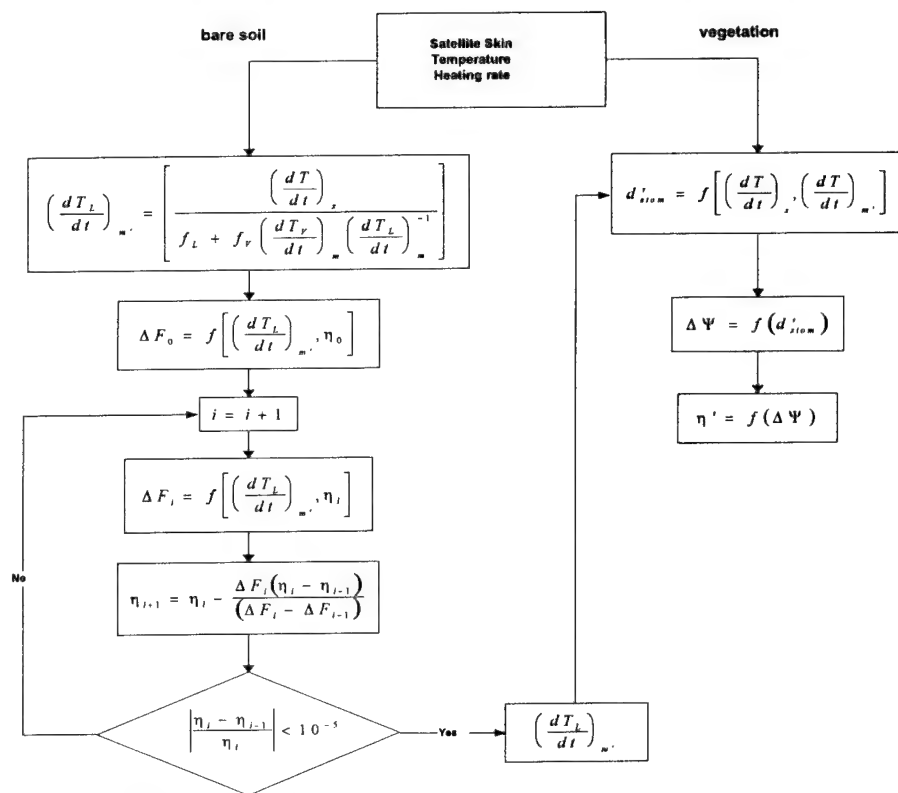


Fig. 1: IR fused model/satellite soil moisture analysis method.

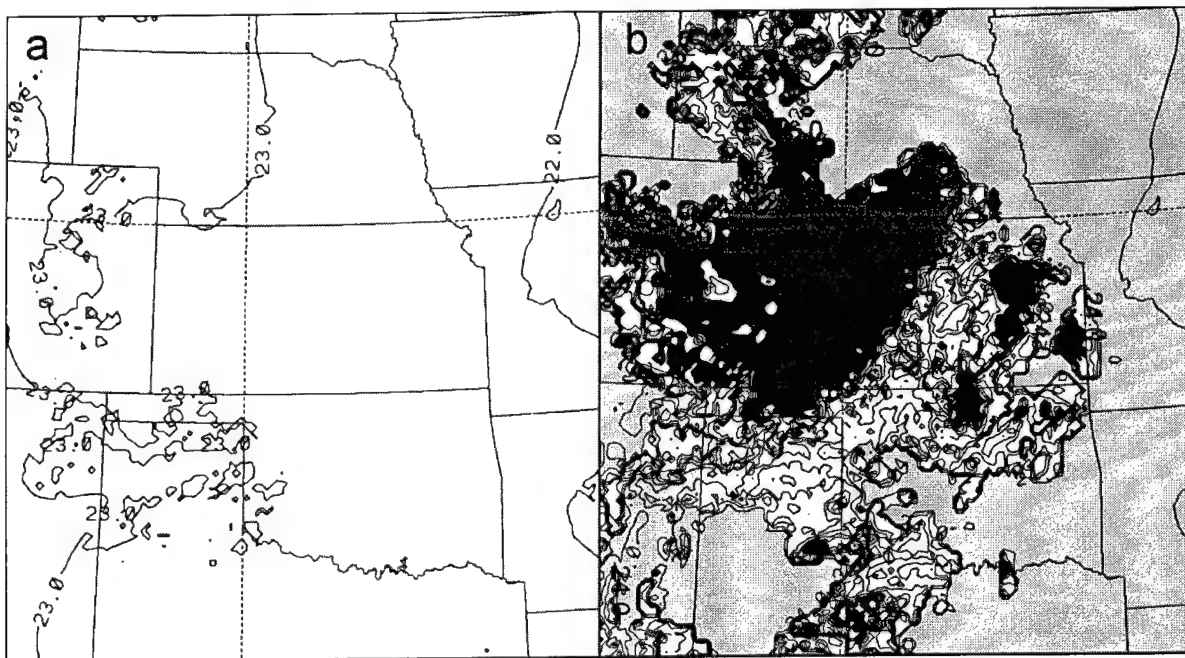


Fig. 2: Surface soil moisture (%) model output results from model runs a) without satellite data, and b) results using the fused model/satellite data analysis method.

THE OPTICAL PROPERTIES OF SUB-TROPICAL CIRRUS CLOUDS DERIVED FROM THE UNIVERSITY OF WISCONSIN HIGH SPECTRAL RESOLUTION LIDAR

E. W. Eloranta

University of Wisconsin

1225 W. Dayton St., Madison, WI 53706, USA

1. Abstract

The University of Wisconsin High Spectral Resolution Lidar was operated from a site in Everglades City, Florida, to observe tropical cirrus clouds. Statistics describing the optical properties of clouds observed between September 5 and September 23 of 1996 are presented. These show the presence of many very tenuous cirrus cloud elements which make it difficult to define cloud edges uniquely and make cloud masks and cloud fraction determinations highly sensitive to the cloudy/clear threshold definition.

2. Introduction

Optical systems viewing the earth from space or viewing high altitude targets from the earth's surface are affected by the presence of cirrus clouds. Even though the clouds are often tenuous, they attenuate optical signals and provide a source of clutter signals which may complicate the identification of targets. These problems are even more severe for systems which must look horizontally in cirrus clouds. In addition, cirrus clouds scatter incoming sunlight and trap outgoing infrared radiation. As a result they have a strong influence on the earth's climate and must be included in models of the earth's radiation budget. For these reasons, it is important to acquire information on the optical properties and spatial distribution of cirrus clouds.

Ultimately, the global mapping of cirrus clouds must be done from satellite borne sensors. However, they are difficult targets for the current generation of passive satellite sensors. Nadir viewing instruments must view the clouds against the earth background while limb sensing instruments are blocked by all except the most tenuous clouds. The CO₂ slicing algorithm provides one of the best current means of producing global cirrus climatologies.¹ However, even this approach has difficulty with the thinnest clouds and it is important to test the observational limits of the technique.

Lidar measurements would seem to provide an ideal way to verify the satellite measurements and to provide quantitative information on the optical properties of cirrus. However, traditional lidars provide insufficient information to separate variations in backscatter cross section from variations in the two-way attenuation to the target. The University of Wisconsin High Spectral Resolution Lidar (HSRL) eliminates this difficulty by dividing the lidar return into separate molecular and aerosol backscatter signals.²⁻⁴ This separation, which is based on the spectral differences in molecular and aerosol scattering, allows us to use the molecular scattering to calibrate the aerosol backscatter signals.

3. Experiment

Between Sept 5 and Sept 23, 1996, both University of Wisconsin Lidars were employed to observe sub-tropical cirrus clouds from a site located in Everglades City, Florida. This experiment included observations by the University of Massachusetts millimeter wave radar, multi-spectral radiometers carried on the NASA WB-57 aircraft, satellite observations, special local radiosonde launches, and the Aeromet Lear jet aircraft. The experiment site was selected to allow observations of cold, high altitude cirrus clouds typical of the tropics without incurring the expense of transporting systems to an off-shore location. The site provided excellent weather conditions. Initial inspection of the data showed that cirrus clouds were observed in 20 of 24 data collection periods scheduled during 19 days of the experiment.

Tropopause temperatures are typically much lower in the tropics than at mid-latitude locations. Ice crystal habit and particle size distribution are sensitive to temperature. Thus, high altitude tropical cirrus are likely to differ from

mid-latitude clouds. The experiment was successful in observing low temperature clouds. Tropopause temperatures of less than -70°C were measured in all cases with one case of -78°C . Cirrus top altitudes up to 16.2 km were measured. Figure 1 presents a comparison of a temperature sounding measured during the experiment with the mean-annual sounding from a site in the deep tropics. Clearly, the Florida sounding on this day provides tropopause temperatures similar to those found in the tropics.

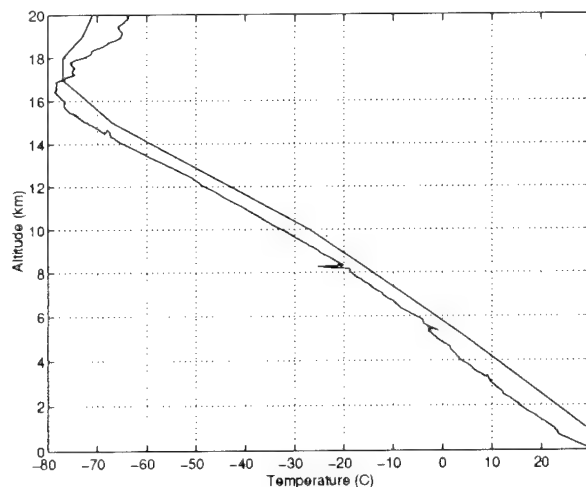


Figure 1. The temperature profile measured above Everglades City, Florida on 5 September 1996 (jagged line) compared with the annual-mean temperature profile measured at Diego Garcia (smooth line). Diego Garcia is located in the tropics near the center of the Indian Ocean.

4. Results

The Florida cirrus clouds were observed at higher altitudes than those measured in Wisconsin. Figure 2 presents cirrus cloud top altitudes plotted as a function of cloud base altitude derived by visual inspection of lidar images. Values of cloud top versus cloud base measured in a year long lidar climatology compiled in Madison, Wisconsin occurred in the shaded area. Except for higher altitudes the Florida and Madison results are similar. (The Florida points with bases below 5 km and tops above 13 km consisted of multi-layer clouds which were not separated into layers in the visual analysis. If separated, these points would fall in the shaded area.)

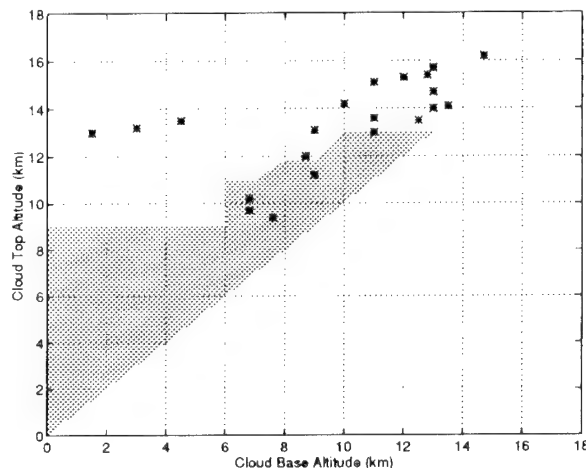


Figure 2. Cloud-top vs. cloud base altitudes for measured by lidar during the Florida experiment (data points) and in 1994 Wisconsin lidar climatology. (shaded area)

The HSRL identifies cirrus clouds by measuring depolarization. A contour plot showing the depolarization and temperature of data points measured in the Florida experiment is presented in the left panel of figure 3. Contours for frequency of occurrence have been drawn on a scatter plot constructed from 23549 data points where each point represents a 315 m altitude range and a ~ 3 min time average. This includes all data points with a signal-to-noise ratio greater than 6 at altitudes between 4 km and 15 km. The right panel of this figure shows a frequency of

occurrence plot constructed from the same data set as a function of depolarization and backscatter cross section. These plots are used to set thresholds to differentiate cirrus clouds from liquid water and aerosol clouds. Below -40°C water freezes by homogeneous nucleation, thus clouds on the left half of the depolarization versus temperature plot must be comprised of ice. Clearly, the maxima in both plots at a depolarization of 42% is produced by cirrus cloud parcels. The very strong peaks which occur at a backscatter cross-section $10^{-7} (\text{m str})^{-1}$ and a temperature of 0°C are produced by spherical haze particles. These plots are similar to those derived from a year-long climatology of lidar measurements acquired in Madison, Wisconsin, during 1994. The 1994 results were used to set depolarization and backscatter cross-section thresholds to differentiate cirrus parcels from water and aerosol cloud parcels. Parcels with depolarization greater than 17% and backscatter cross-section greater than $10^{-6} (\text{m str})^{-1}$ were identified as cirrus.

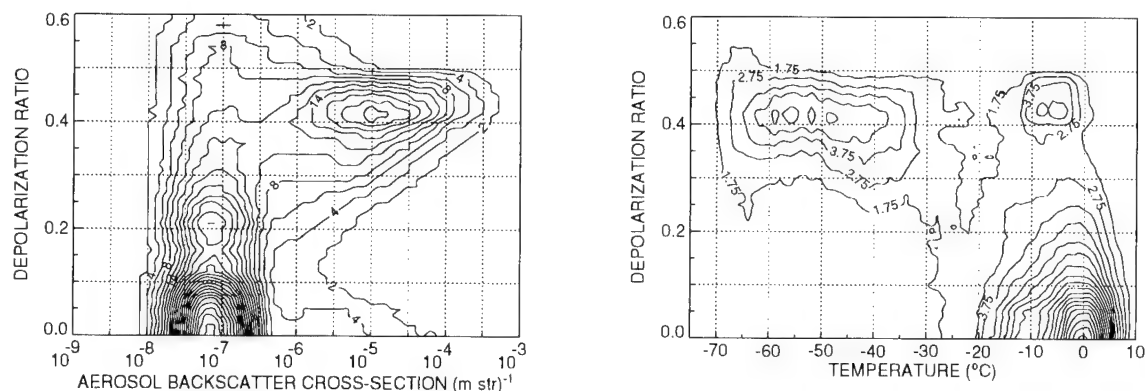


Figure 3. The occurrences of depolarization as a function of temperature and backscatter cross-section measured for the Florida HSRL data. All data points between altitudes of 4 and 15 km with a signal to noise ratio greater than 6 are included.

It appears as if the depolarization threshold could be increased slightly to $\sim 20\%$ for the Florida data. However, it is very close to the 17% value derived from the 1994 Wisconsin climatology and the difference may be due to the fact that the fewer days are included in the Florida data set.

As with the Wisconsin data set, the scattering cross-section threshold definition is rather arbitrary. The left panel of figure 4 shows the probability of observing a given backscatter cross-section as a function of the backscatter cross-section. This plot provides separate curves for water and ice clouds. Data has been averaged over 315 m in altitude and ~ 3 min. All data points at altitudes between 500 m and 15 km with signal-to-noise ratios over six are plotted.

The heavy concentration of low altitude aerosol is clearly evident in the water curve shown in the left panel of figure 4. It shows large contributions from spherical particles at low scattering backscatter cross-sections. This low altitude aerosol and the associated water vapor impacted satellite retrievals of cloud parameters by making it impossible to find clear pixels anywhere near the experiment site. All apparently clear pixels in the 11 micron GOES and HIRS radiometers provided surface temperatures at least 7 K below the sea surface temperature.

The ice curve (Fig. 4) provides little evidence to support the backscatter threshold, $10^{-6} (\text{m str})^{-1}$, used to define the presence of cirrus clouds in the 1994 data set. This is not surprising because the 1994 data show a similar distribution; the threshold was chosen because it provided qualitatively reasonable cloud boundaries.

The right panel of figure 4 shows the same probability curves for altitudes between 4 and 15 km. This eliminates the low altitude aerosol and the water curve is dominated by parcels with very small backscatter cross-sections. Most of the scattering in this layer is due to cirrus. Notice that only a few parcels of the ice at backscattering cross-sections below $10^{-6} (\text{m str})^{-1}$ are eliminated by removing the lowest 4 km. These must consist of irregularly shaped aerosols or be the result of noise contributions which caused spherical aerosols to be misclassified. An examination of the points rejected because the signal-to-noise ratio was less than six indicates that most of these points have a backscatter cross-section less than $10^{-7} (\text{m str})^{-1}$. These data and the 1994 Wisconsin data indicate the existence of many very tenuous cirrus cloud elements. It appears that cloud masks and the concept of cloud fraction are highly sensitive to threshold definitions and may be inappropriate for use with cirrus clouds.

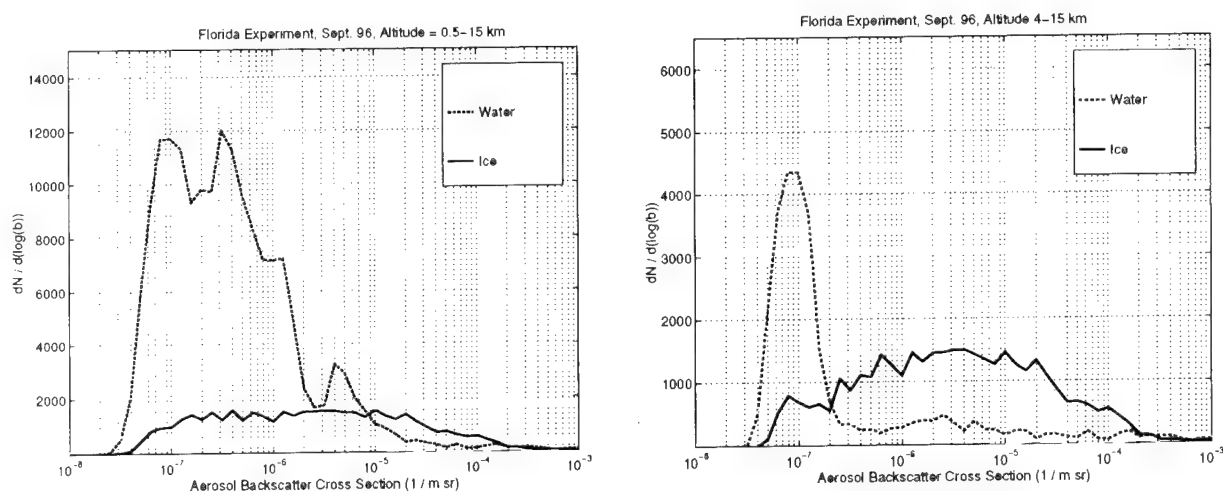


Figure 4. The probability of observing a given backscatter cross-section as a function of backscatter cross-section derived from the Florida data set for water and ice clouds. All data between the surface and 15 km are plotted in the left panel and data from between 4 and 15 km plotted in the right panel. Data points derived from parcels where the lidar signal-to-noise ratio was less than six have been removed prior to plotting.

Additional results, including optical depth, backscatter phase function statistics, and more detailed comparisons with the 1994 climatology, are included in the poster presentation.

5. Acknowledgements

Funding for this research was provided by Air Force contract F19628-96-C-0097, National Science Foundation Grant ATM-9321330, and by Lockheed Missiles and Space Company contract SK30G4160F. Data was acquired and processed with the assistance of D. DeSolver, D. K. Forrest, R. Holtz, R. Kuehn, S. Mayor, P. Piironen, A. Piironen, and W. Wolf.

6. References

1. Wylie, D. P., W. P. Menzel, H. M. Woolf and K. I. Strabala, "Four Years of Global Cirrus Cloud Statistics Using HIRS", *J. of Climate*, **7**, 1971-1986 (1994).
2. S. T. Shipley, D. H. Tracy, E. W. Eloranta, J. T. Trauger, J. T. Sroga, F. L. Roesler, and J. A. Weinman, "High resolution lidar to measure optical scattering properties of atmospheric aerosols. 1: Theory and instrumentation," *Appl. Opt.* **22**, 3716-3724 (1983).
3. P. K. Piironen, and E. W. Eloranta, "Demonstration of a high-spectral resolution lidar based on an iodine absorption filter," *Opt. Lett.* **19**, 234-236 (1994).
1. C. J. Grund, and E. W. Eloranta, "University of Wisconsin High Spectral Resolution Lidar," *Optical Engineering* **30**, 6-12 (1991).

PARTICLE MEASUREMENT AND ANALYSIS CRITERIA FOR INTERCOMPARISON WITH NUMERICAL MODELS OF CLOUD RADIATIVE PROPERTIES

W. Patrick Arnott, John Hallett and Matthew Meyers
Desert Research Institute
Reno, Nevada 89506-0220

ABSTRACT

Measurement of size/shape distributions of cloud and aerosol particles in order to assess transfer of radiation from visible to thermal infrared to radar wavelengths requires the simultaneous deployment of several instruments to cover a wide dynamic range. In general, small particles are more numerous, although on occasion spectra are near monodisperse or bimodal. Specific instruments are designed to give sensitivity for different sizes, depending on the moment (N ; ND ; ND^2 ; ND^3 ; ND^6) required. Of particular interest is the sample volume required to give a statistically significant concentration for the maxima of the above moments. We address the issue of the occurrence and detection of 'hot' or 'cold' spots depending on the geometry of the sample volume and the sampling time required both in reality and in the statistics of the spectrum derivation.

1. INTRODUCTION

Direct measurement of atmospheric particulates for assessing the utility of remote sensing technologies at different wavelengths of electromagnetic radiation poses a challenge both in methodology and in instrumentation. The atmosphere is a turbulent medium, giving irregularities of all properties from the scale of the atmosphere itself down to below the viscous dissipation eddy limit of 1 mm or so. Particles exist from size of large 10 cm hailstones to the smallest cloud nucleus (CN) size some few nm; equilibrium concentrations range from a few per 1000 m³ to beyond 10⁶ per cm³. Particles significantly interact with radiation (qualified in terms of the scatter parameter ($\pi D/\lambda$)) from UV to radio transmission wavelengths giving both scatter and absorption of radiation (Pueschel et al., 1997). From a practical viewpoint, one is concerned both with transmission characteristics (as from a changing temperature source to a distant detector) and with scattering characteristics (as of a lidar/radar pulse to, from and by a volume of particulates). From the viewpoint of theoretical prediction of scatter, standard Mie theory is of help for spherical particles when the complex refractive index is known; for non-spherical particles (ice, some smokes and mineral dusts) severe uncertainties may arise both in scatter and absorption, only to be resolved by laboratory measurement.

In reality, even for spherical particles, variability in spectral distribution of particles in the distribution of sizes leads to uncertainty of the inversion of sensed signals (Arnott, et al., 1997). Uniform conditions never exist in the idealized atmosphere; approach to uniformity varies depending on the nature of the turbulence and the specific fluid processes in which the particulates are embedded. It follows that any attempt to characterize a particle cloud needs to assess two quite different criteria: first, the variability of measurement of each particle size in a specified volume (Poisson statistics in a volume with mean properties) and the known (or assumed) spatial limitations of the volume considered. This may be determined by physical conditions, as is the case for a cumulus cloud tower or by the measurement volume - m³ for a lidar pulse, 1000 m³ for a radar pulse, or 1000 km³ for a satellite footprint *in situ* sampling necessarily implies severe limitations on what can be accomplished: There is an intrinsic sample volume for any instrument, an integration time for each set of data, and a protocol which sets the sampling geometry over the selected time. A stationary site samples particles carried by the wind through a monitored region; a balloon borne instrument samples a vertical profile, displaced by ambient wind at each level; an aircraft a long, thin sample which may be wrapped in an ascending/descending spiral, advected with the wind, if appropriate. We here address issues related to instrument design and use in making such measurements, and the intrinsic limitations of this approach.

2. INSTRUMENT CHARACTERISTICS

We may characterize various instruments for particle characterization (i) by the dynamic range, here defined as the minimum size particle detected such that requiring an acceptable correction (for example collection efficiency $> 10\%$) and the maximum size detected with a sufficient probability say ($\pm 10\%$) over a selected sampling interval. Since the overall tendency is for particle number to increase with decrease of size, we may further characterize instruments (ii) through a sample volume per unit time (s) and the dynamic range established by (i) above. Some available and proposed instruments are shown in Fig. 1. Note that, in general, the lowest size limit of an instrument is determined by inlet collection efficiency and or diffusion loss along the passage to the detection or collection site. It is noted that an aircraft, the sampling rate depends directly on aircraft speed. The largest size is determined by the entrance geometry, together with the concentration itself; a measure of 10 in a given time interval/sample volume is liable to a statistical uncertainty of $\pm \sqrt{10}$ i.e. 7 to 13.

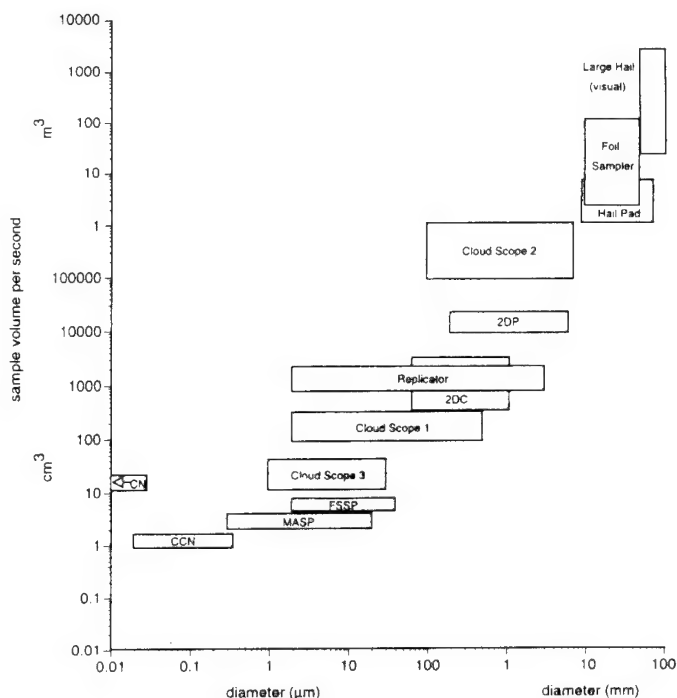


Figure 1. Comparison of instruments for measurement of particle concentration and spectra.

Notes: Foil sample for aircraft use with impaction at leading edge.

Hail pad - hail at ground.

Cloudscope II: new DRI instrument for low resolution high sample volume.

2DP - Standard PMS probe with 100 μm pixel.

2DC - Standard PMS probe with 2, 0 μm pixel.

Replicator - DRI/U.S. Airforce/NASA instrument.

Cloudscope I - Standard DRI cloudscape as used in recent missions.

FSSP - Standard PMS instrument

Cloudscope III - High resolution DRI

MA SP - NCAR instrument

CCN - Hudson spectrometer

CN - Commercial instrument.

Boxes represent range of collection conditions (aircraft speed) and spectra size for significant collection efficiency. Poisson statistics make the box edges fuzzy toward larger size and lower concentration.

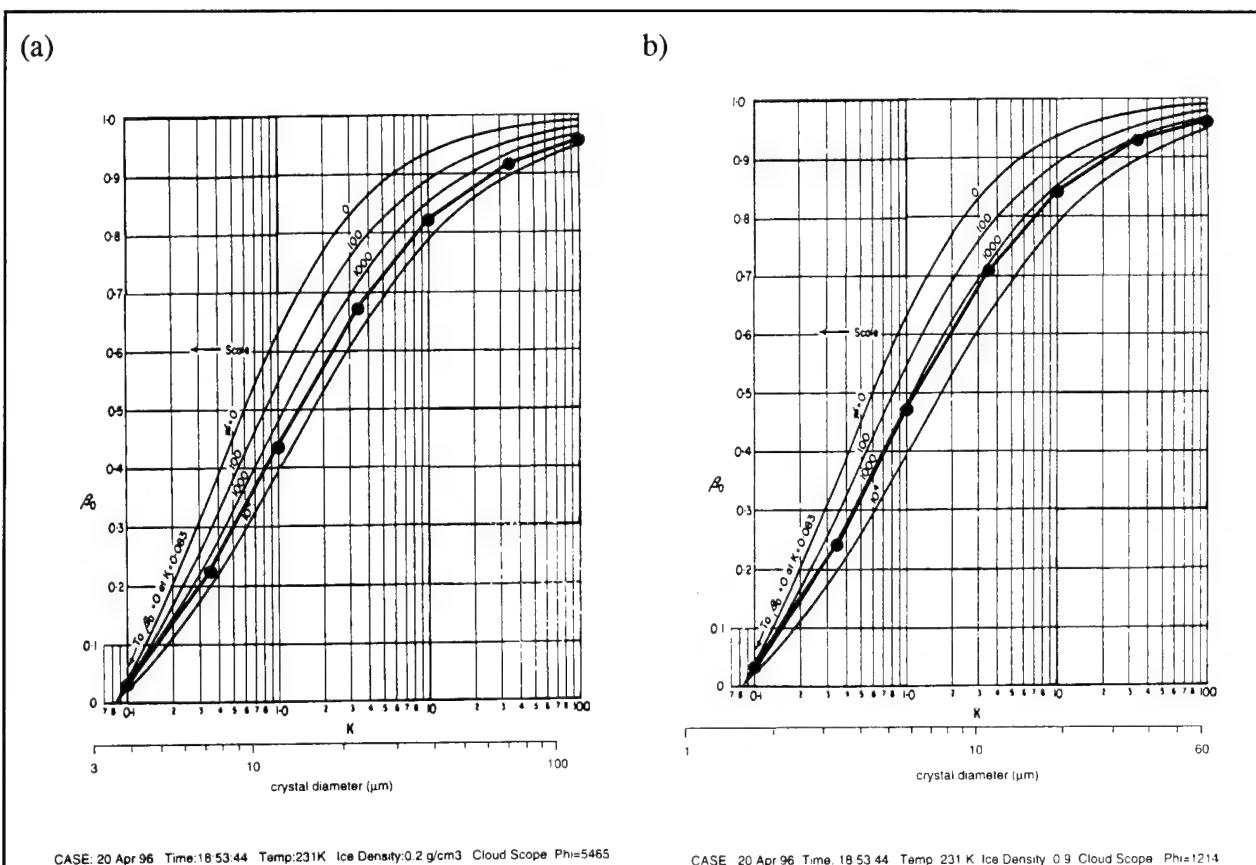
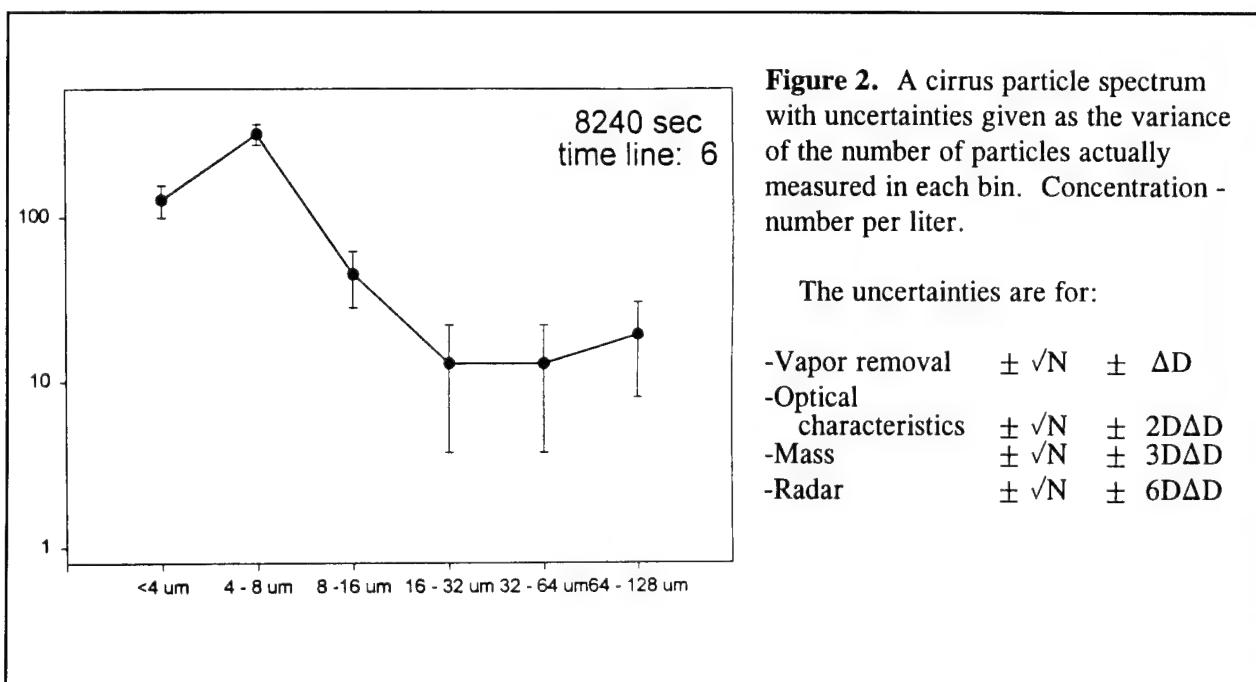


Figure 3: Stagnation collection efficiency for cloudscope mark I for different density particles. Extrapolated from the early work of Langmuir and Blodgett.
 ϕ — dimensionless parameter, characterizing air velocity/air density.

The choice of sampling time is of interest. A simplistic approach suggests that the sampling time needs to approach that required to cover the remote sensing volume. In practice, however, other considerations may dominate. Purely physical considerations suggest that measurements be made over a distance (time) when dynamic considerations suggest some uniformity - for example along the leading edge of a lenticular cloud, or parallel to an advancing frontal system. Any alternative approach may be to attempt measurements of as many spectra as possible (assuming each observed spectrum is but one of a subset) where the most likely spectrum, resulting from a juxtaposition of random events, gives a believable relationship when averaged over a very large set of data (Liu & Hallett 1997 a, b). Any single given measurement may depart dramatically from this relation. Hence, probability of deducing R (rate of precipitation) from Z (radar reflectivity) is a highly uncertain business for a single measurement. It is a challenge to establish criteria for a data set to be large enough to give a convergence of the particle spectrum from statistical considerations alone; it is no doubt related to the overall turbulence level but the physical processes cannot be ignored.

3. COLLECTION INSTRUMENTS DESIGN AND CONSTRUCTION

As an example of an application of the above concepts, we describe an aircraft instrument, the cloudscope (Arnott et al. 1994) suitable for collection and analysis of ice cloud particles as might occur in cirrus clouds, which even a cursory observation show is to be variable over distances of at least a few tens of meters. Fig. 1 shows the design sizes and ranges selected for different designs of this instrument, compared with other instruments. The principle of operation is to collect particles at a forward facing stagnation point, where they evaporate at stagnation conditions. Rate of change of particle area gives particle density; time for evaporation (at constant particle density) gives particle mass, from aerosol to ice particle. Cloudscope sample volumes per second over 10, 100 cm³ and about ½ cm³ for more larger particles, of particular importance in assessing radar scatter. Fig. 2 shows distributions with anticipated errors based on number of particles measured in each size bin for the cloudscope mark I.

4. CONCLUSION

It is to be concluded from these considerations that local concentrations of particle size distribution may depart significantly from any long term relationship, used to give algorithms for the properties to be used for observational decisions on cloud structure, and composition. Instruments having appropriate dimensions range to adequately cover the spectrum are far from satisfactory for particle assessment in some sizes and for some wavelengths. The implications for variances from selected algorithms in specific situations are important in operational procedures and require much more detailed analysis. A concurrent approach is to design a learning procedure as more spectra are collected, to be updated in a way guided by inferred physical processes.

5. ACKNOWLEDGMENTS

Research supported by DEPSCoR Grant F49620-96-1-0470, AFOSR. The software development for the cloudscope was supported by a NASA Grant NAG 2-1104.

6. REFERENCES AND FOOTNOTES

- Arnott, W.P., C. Schmitt, Y. Liu, and J. Hallett, 1997: Droplet size spectra and water vapor concentration of laboratory water clouds: Inversion of FTIR (500-5000 cm⁻¹) optical-depth measurement. *Appl. Opt.*, **36**, 5205-5216.
- Arnott, W.P., Y. Dong, R. Purcell and J. Hallett, 1995: Direct Airborne Sampling of Small Ice Crystals and the Concentration and Phase of Haze Particles. Ninth Symposium on Meteorological Observations and Instrumentation. Charlotte, North Carolina, 27-31 March, 415-420.
- Pueschel, R. F., J. Hallett, A. W. Strawa, S. D. Howard, G. V. Ferry, T. Foster, and W. P. Arnott, 1997: Aerosol and Cloud Particles in Tropical Cirrus Anvil: Importance to radiation balance [In press, *J. Aerosol Sci.*].
- Liu, Y. and J. Hallett, 1997a: On Size Distributions of Cloud Droplets Growing by Condensation: A New Conceptual Model. [Accepted for publication in *J. Atmos. Science*].
- Liu, Y. and J. Hallett, 1997b: A Note on "1/3" Power-law between Effective Radius and Liquid Water Content. [In press, *Q. J. Roy. Meteorol. Soc.*].

POST-ENGAGEMENT GROUND EFFECTS MODEL

Kevin W. Bruening and Jason A. Wampler
MEVATEC Corporation
1525 Perimeter Parkway, Suite 500
Huntsville, AL 35806-3575

Sponsoring Agency:
Dr. Julius Lilly
United States Army Space and Strategic Defense Command

ABSTRACT

The Post-Engagement Ground Effects Model (PEGEM) is a comprehensive simulation tool that provides ground hazard assessment for chemical/biological agent release and high explosive (HE) weapons. Model output includes chemical/biological agent ground contamination and cloud representation or HE blast zones, data for unit effectiveness or many-on-many models, as well as estimated casualties at user-specified times-of-interest. PEGEM encompasses a number of modeling areas in order to assess ground effects from unitary (bulk) and submunition (canister or bomblet) payload intercepts and offensive deployments (Figure 1). Continuing proliferation of theater ballistic missiles (TBM) to Third World Nations causes concern for both military and civilian populations. Potential threats may arise either from direct attacks (offensive deployment) or from collateral effects following intercepts of chemical/biological weapon (CBW) and conventional weapon payloads.

INTRODUCTION

The Office of the Secretary of Defense has mandated that PEGEM be used by the tri-services for Operational Test and Evaluation (OT&E) activities which support milestone acquisition decisions. This requires verification, validation, and accreditation of PEGEM. The accreditation activity was initiated in December 1996. PEGEM has already been used in the Capstone Cost and Operational Effectiveness Assessment (COEA), Army COEA, and Navy COEA studies. Theater missile and possibly strategic missile defense will require sensitivity analysis for collateral damage minimization (Reference 3). PEGEM has been used in test planning for lethality sled tests (pre-test predictions) and in post-test analysis of flight test data. Additionally, it can be used to extend the synthetic battlefield environment through its distributed interactive simulation (DIS) compliance.

PEGEM

PEGEM is an integration of several previously existing models, as well as models developed for this application. Payload and agent type require specific algorithms to accurately model ground effects. These algorithms are tailored to each type and are not necessarily employed in every scenario. In a typical case, the analyst specifies a chemical, biological, or high explosive weapon event scenario including all threat details and the locations and times of the various events on the user defined grid. Intercept lethality information can be provided through the output of an endgame lethality model. The lethality model provides PEGEM with a prediction of the fraction of payload surviving following an intercept event. For canister submunition payloads, the location of surviving submunitions within the target payload are given. This information is used by PEGEM to propagate the potential residual threat(s) to the ground.

PEGEM Architecture and External Interfaces

Given endgame data for submunition payloads, PEGEM determines the ejection velocity vectors of surviving submunitions using a semi-empirical methodology. This methodology is derived from relationships between endgame characteristics and ejection velocities established through extensive review of data from high speed impact sled tests, quarter-scale light-gas gun tests, and hydrocode analysis. Once initial velocity vectors are determined, submunitions are propagated to the ground using a three degree-of-freedom (3-DOF) model with averaged tumbling munition drag data. Certain munitions with more complex flight characteristics require use of a six degree-of-freedom (6-DOF) model. With either flyout approach, wind effects on submunition propagation are included. Meteorological (MET) data are provided to PEGEM through a stratified atmosphere model that provides wind velocity as a function of altitude along with the basic atmospheric parameters as a function of time. A MET profile can be specified at multiple times to help simulate operational environments, which can be linearly interpolated by PEGEM in flyout calculations. MET profiles for various cities of interest world wide are included in a PEGEM database. These specific profiles cover a range of weather over the different sites that have been stressed as areas of CBW concern.

In contrast to submunition payloads, unitary (bulk) chemical payload analyses require the PEGEM Aerodynamic Breakup Model (ABM) to characterize the initial chemical agent source cloud that results when a unitary threat is intercepted, or when it is operationally dispensed into the atmosphere. This model determines chemical agent line source length, lateral dimension, removes in situ losses, aerosolization (losses due to atmospheric interaction), and agent droplet size distribution as a function of release conditions. This empirically based approach is derived from extensive agent simulant testing results.

Once the initial source cloud is described, the Vapor, Liquid, and Solid Tracking (VLSTRACK) model, an atmospheric transport and hazard assessment model (Reference 4), determines ground deposition, dosage, and concentration from a unitary chemical release. This model calculates the transport, evaporation, and diffusion of tri-variate Gaussian puff clouds of liquid, vapor, and in some cases, solids. Since casualty calculations will be based on short-term cumulative contamination levels, the atmospheric transport model is normally run in a cumulative mode. As with the previously described flyout models, the atmospheric transport model uses interpolated MET data in performing transport calculations. Atmospheric transport model output is in the form of deposition, dosage, cloud size sigmas at user-specified intervals, and concentrations. Deposition is a measure of contamination area coverage typically measured in milligrams of agent per square meter. Concentration is a volumetric measure of agent contamination measured in milligrams per cubic meter, usually at a specified height above the ground (~2 m for personnel effects) throughout an area. Dosage is the time integral of concentration, taking into account not just level of exposure, but time exposure as well. Dosage is typically given in units of milligram-minutes per cubic meter. Cloud size sigmas are expressed in terms of horizontal, vertical, and lateral sigmas. When biological agents are involved the unit of mass in the above measurements typically changes from milligrams to micrograms.

Once ground deposition, dosage, and concentration for all threats are determined, the final steps in the simulation are to produce contamination grids and calculate casualties. The PEGEM Effects Integrator Model (EIM) convolves atmospheric transport model contamination grids, discrete population data, and probit methodologies for assessing toxicity effects to produce casualty estimates. The approach for estimating casualties is a standard probit-based approach originally proposed by D. J. Finney (Reference 5) for probabilistically determining response to a pathogen. This approach requires that response data be available in order to determine a median lethal effective dosage or deposition value for the agent in question, along with the probit-response slope which describes the rate of change of effectiveness as dosage or deposition level changes. This toxicity data is often derived from extensive tests on mammals including, in some cases, humans. Chemical agent toxicity data employed by PEGEM are derived from a recent toxicity standard report (Reference 6). Similar standards are currently being compiled for agents of biological origin (ABO).

Chemical/biological submunition payloads also require the use of the atmospheric transport and hazard assessment models. Once the ground impact points of submunitions have been determined using the appropriate flyout model, munitions are assumed to undergo normal (usually ground level) detonation. The initial source cloud from the detonation is provided and the resulting deposition, dosage, and concentration

are determined. Cloud size sigmas are not furnished for submunition generated agent clouds because they begin as a point source.

Conventional payloads are handled in a similar manner to chemical and biological payloads. Offensively deployed unitary HE payloads impact on or near the ground while those unitary HE payloads that are successfully intercepted are destroyed. However, HE submunitions may survive an intercept. Surviving HE submunitions are handled similarly to chemical/biological submunitions. The location of surviving submunitions within the target payload must be provided by a lethality model. This information is used by PEGEM to propagate the potential residual submunitions to the ground using either a 3-DOF or 6-DOF model. Under investigation is a model to impart momentum to the residual submunitions due to the HE initiation of the destroyed submunitions. Conventional munitions require the use of a blast model upon impact with or just above the ground (Reference 7). Blast zones are then determined.

Once the ground blast zones are determined, the final steps in the simulation are to produce blast grids and calculate casualties similar to the chemical and biological agent methodology. Blast grids, discrete population data, and probit methodologies for assessing blast effects are convolved to produce casualty estimates. The approach for estimating casualties is a standard probit-based methodology (Reference 8) for probabilistically determining response to a pressure wave. This approach requires that response data be available in order to determine a median lethal effective pressure value for the HE agent in question, along with the probit-response slope which describes the rate of change of effectiveness as pressure changes.

Population data for casualty estimations are currently drawn from a database compiled by the Department of Commerce, Bureau of Census. This data is provided for many non-U.S. urban areas in seventy-eight countries (Reference 9). As an alternative to the existing population database supplied with PEGEM, users may specify their own population area. An important asset of PEGEM is the ability to specify population data to any desired level of fidelity. Often, sensitivity studies are performed where intercept or chemical agent properties are varied. In these cases, only the relative effect of changing a parameter is needed, hence, the fidelity of the population is not of great concern. In these cases, a uniform population density can be employed. In other cases, very specific predictions might be desired where the locations of certain individuals or assets becomes important.

PEGEM is capable of modeling multiple theater missile attacks over a user-specified period of time; hence, output produced can be voluminous. Post-processors provided with PEGEM can be very beneficial for interpreting these results. Users can quickly assess the effected area and extents of ground contamination relative to ground assets or populations. Recently a seamless interface between PEGEM and the Army Unit Resiliency Analysis (AURA) code was developed. Coupled with AURA, PEGEM can help evaluate the effects of CBW attacks on military unit effectiveness.

Distributed Interactive Simulation (DIS)

PEGEM, a DIS compliant model, is capable of operating in real time or non-real time. Models, such as the many-on-many simulations Extended Air Defense Test Bed (EADTB) and Extended Air Defense Simulation (EADSIM), have been connected via DIS to PEGEM. These models provide data on the interceptors, threats, and ground assets to which PEGEM responds whenever an intercept occurs or the threat payload is offensively deployed. PEGEM returns information identifying assets that were effected by the chemical/biological agents or conventional munitions, ground sensor warning messages, and contamination cloud locations. In the future, PEGEM will pass its environmental effects data to other models and become compliant with the emerging High Level Architecture (HLA).

Test and Evaluation

PEGEM not only uses flight test, sled test, quarter-scale light-gas gun test, and hydrocode data to validate its models, but it also has been used in making pre-test predictions, test planning, and post-test analysis for high speed sled tests and flight tests. These efforts have allowed for identification of regions where submunitions are most likely to land along with the expected submunition distribution, and agent contamination zones. This can be most helpful in assessing the overall system vulnerability/lethality associated with live fire tests.

CONCLUSIONS

In the past, interceptor effectiveness was measured in terms of hitting or missing the threat, or more recently, in terms of damage to the threat. PEGEM extends these approaches by providing answers to questions concerning what happens to the payload that survives the engagement. CBW intercept lethality and HE submunition lethality can now be measured in terms of the effects which ultimately reach the ground. Ground effects measures of effectiveness may include casualties, aimpoint short fall, or casualty area. This permits evaluating defended areas and keepout zones by minimizing ground effects or setting keepout altitudes. The next step is to expand this PEGEM capability to include effects from other payload types and additional collateral effects. To this end, future efforts will include integration of an existing debris model along with conventional weapon fragmentation effects, HLA compliance, and eventually nuclear weapon effects models.

PEGEM is an important tool for assessing the ground effects hazard from chemical/biological agents and convention weapons by simulating battlefield operational environments. Future enhancements will expand its capabilities to other threat types and effects, producing a complete theater missile defense ground effects tool. It may be used alone or to enhance the synthetic battlefield by helping to simulate battlefield operational environments.

References

1. *Post-Engagement Ground Effects Model Version 2.0 User's Manual*, MEVATEC Corporation, December 1996.
2. *Post-Engagement Ground Effects Model Version 2.0 Technical Manual*, MEVATEC Corporation, December 1996.
3. *Capstone Operational Requirements*, 3 December 1993.
4. Bauer, T., *Software User's Manual for the Chemical/Biological Agent Vapor, Liquid, and Solid Tracking (VLSTRACK) Computer Model Version 1.6*, Naval Surface Warfare Center, February 1995.
5. Finney, D. J., *Probit Analysis*, Cambridge GB, Cambridge University Press, 1971.
6. Reutter, S., and Wade, J. LTC, *Review of Existing Toxicity Data and Human Estimates for Selected Chemical Agents & Recommended Human Toxicity Estimates Appropriate for Defending the Soldier (U)*, Edgewood Research Development & Engineering Center, 1994.
7. Church, H., "Catalog of Atmospheric Acoustic Prediction Models," Report No. RCC 383-95, June 1995.
8. Richmond, D.R., et. al., *The Relationship Between Selected Blast-Wave Parameters and the Response of Mammals Exposed to Air Blast*.
9. Pitman, S., and Scollard, J., *Urban Population (P95) Volume 1 - Middle East*, Science Application International Corporation, July 1991.

Time Series Cloud Forcing Study of Cloud Scene Simulation Model

Guy P. Seeley, Joel B. Mozer and Erol Emre
USAF Phillips Laboratory, GPOF
29 Randolph Road
Hanscom Air Force Base, Massachusetts 01731-3010

Abstract

Several DoD target modeling applications require knowledge of the total radiant energy delivered to a target area over many hours. To address this need synthetic cloud fields are required. The Air Force Cloud Scene Simulation Model (CSSM) is capable of producing 4D cloud fields that can be used as a starting point for these types of calculations. Comparison of CSSM liquid water content fields with experimental data is needed. Inexpensive pyranometer measurements are capable of probing some aspects of cloud structure. Spatial characteristics of the clouds are evaluated by comparing derived obscuration time series with pyranometer, radar and satellite data for a site located at Hanscom AFB, MA. The object is not to perform detailed radiative transfer, but rather to compare the spatial characteristics of the CSSM generated cloud fields with actual cloud fields.

1. Introduction

The Cloud Scene Simulation Model, CSSM [1] is a fractal cloud model that can generate 3 dimensional cloud liquid water content fields and evolve these fields in time. The model does not perform detailed physics calculations, as first principles cloud field generation requires extraordinary amounts of computation. The model's fractal algorithms have been tuned via visual inspection of resulting clouds and from analysis of aircraft based liquid water content data. The fields generated from CSSM can be used as input to radiative transfer schemes and scene rendering software to visualize specific cloud scenes. In order to have confidence in the generated scenes comparison with field data is necessary.

Many studies of cloud spatial structure try to access the smallest spatial scales that their instrumentation will permit. Many of these instruments are flown aboard aircraft, an expensive process that severely limits the number of cloud fields that can be probed. Satellite imagery provides another means to measure high altitude structure. Overhead views do not provide a direct means of quantifying the surface situation, especially in overcast conditions. This study will attempt to measure cloud structure over length scales of about 3 to 30km using inexpensive and simple pyranometer measurements.

Analysis of pyranometer time series can reveal a considerable amount about cloud cover. Assuming relatively constant wind speed and optically thick clouds the signal observed at a pyranometer should closely reflect the spatial characteristics of the clouds passing between the instrument and the sun.

2. Approach

Spectral analysis of the pyranometer data is one way to characterize this complex time domain signal. Spectral analysis has several shortcomings, the most disturbing of which is very different time domain signals can have similar frequency spectra [2]. On the other hand spectral analysis of the pyranometer signal is straightforward to perform and provides a quantitative if limited way to compare synthetic and real spatial structure. It is unlikely that two processes whose spatial power spectra are significantly different are substantially similar.

Spectral analysis has been used on several different sources of cloud data, ranging from satellite imagery to in-situ hot-wire probe measurements. [3]. A result confirmed in several studies shows power law decay of spatial fluctuations in Fourier space as:

$$E(k) \propto k^{\beta}$$

These studies have observed a power law spectrum over length scales of 0.5 to about 20km. At either end of this range the spectrum is no longer a power law. Both in-situ aircraft and satellite measurements report β to be in the range from -1.4 to -2.0. The well known theoretical Kolmogorov result for 3 dimensional turbulent flow gives β a value of -5/3. This universal result provides a benchmark value to compare our results to.

3. Results

The Air Combat Targeting Electro Optical Simulation experiment site at Hanscom AFB has collected approximately week long pyranometer time series for several years at one minute resolution. This data set covers all four seasons and many weather conditions. We use this dataset which includes radar and other measurements as our primary source. Figure 1 shows raw pyranometer data for one diurnal cycle. Cloud signatures are clearly visible in the data. Subtraction of the characteristic cosine of solar elevation angle curve for the given day and location yields a cloud forcing signal at the surface. Figure 2 shows a spectral analysis of the cloud forcing signal with a β of -1.64. The pyranometer power spectrum appears to be a reasonable power law for most of its length. Our measurements can access time scales from 10^{-3} to 0.5 cy/minute. This translates into length scales of 3.6km to 500km assuming a 30 m/s wind speed at cloud height.

During the experiment there was an upward looking 35Ghz TPQ-11 cloud radar located 0.25km away from the pyranometer. This radar is capable of showing cloud structure up to 60,000 feet or so. By vertically integrating the raw reflectivity from the radar we are able to get another indicator of the time and space variation of the cloud structure moving over the site. Figure 3 shows a spectral analysis of the radar signal for the same time period as the previous pyranometer plot. The radar β is -1.52, very close to the pyranometer and not too far from the Kolmogorov result.

As an additional probe of cloud structure we retrieved visible AVHRR imagery for the New England area during the same experimental time period. The lower curve in figure 4 shows a spectral analysis of this imagery with a β of -1.73. The upper curve shows a spectral analysis of a stratocumulus cloud scene generated using the CSSM. The CSSM spectrum shows a β of -1.48, fairly close to the observed spectra. This CSSM run was not tuned to the specific atmospheric state for the observed day. It is possible that this could change the spectral exponent slightly.

After examining the pyranometer data for several experiments we find spectral exponents that fall in the range of about -1.4 to -2.4. These results show a generally steeper falloff than those quoted in [3] who observe exponents of about -1.4 in their analysis of marine stratocumulus during FIRE and ASTEX. The pyranometer dataset used is much larger and encompasses many more cloud types than the 5 airplane flights used by Davis, therefore it is not too surprising that our results show more variability.

4. Conclusions

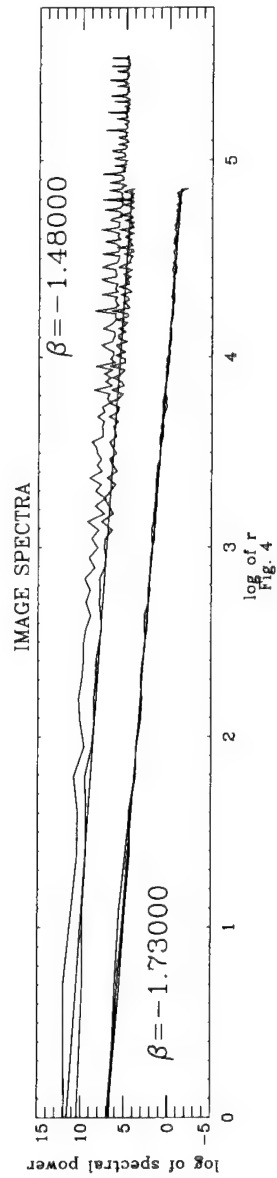
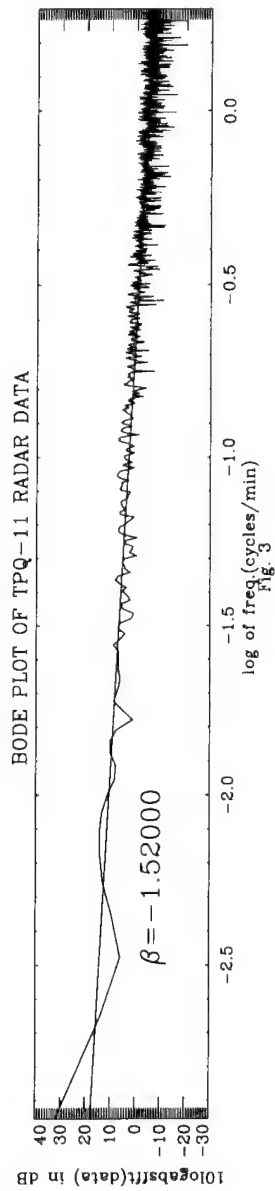
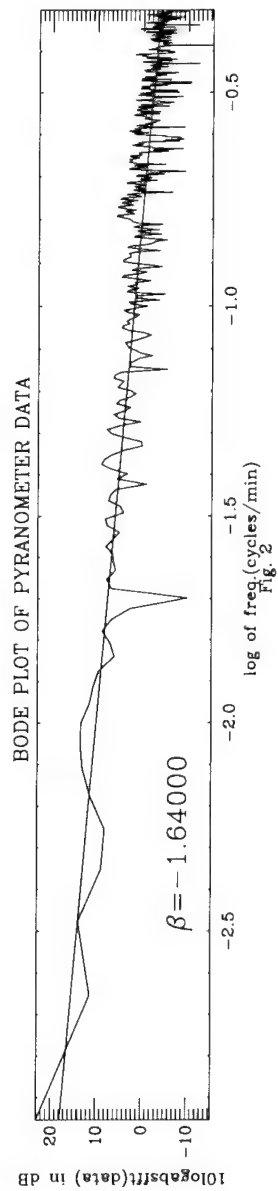
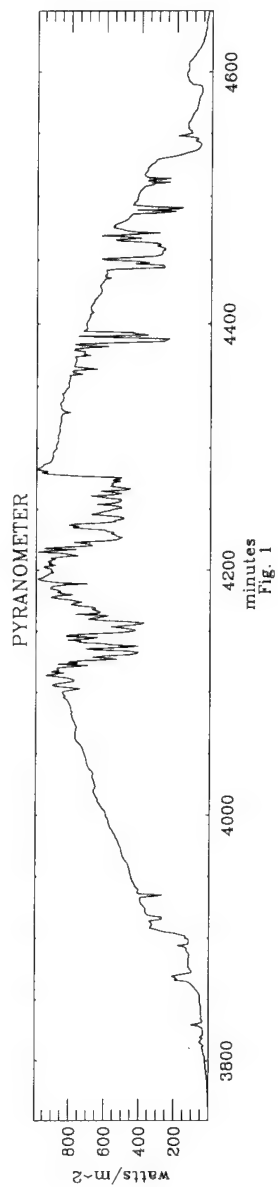
Simple ground based pyranometer measurements can provide information on cloud field spatial structure. This is confirmed by both ground and space based sources. Clearly the analysis presented here ignores much radiative transfer physics. However when cloud cover is broken and wind reasonably steady the pyranometer can access spatial cloud information. Spectral exponents are only one metric to compare spatial structure, however the nearly identical values from three different remote sensing methods are quite interesting. Investigation of how the method performs in overcast conditions are needed. It is expected that significant differences between radar and pyranometer measurements will be observed. More detailed comparison with CSSM generated cloud fields are underway at our laboratory.

Acknowledgements

The authors would like to thank: Dr. Stanley J. Heckman for valuable discussions and criticism of this work, Mr. Dave Smalley for his assistance with some of the spectra, and Mr. Tim Hiett for his extraordinary data acquisition and design efforts. This work was supported at Phillips Laboratory, Hanscom AFB, MA through contract F19628-95-C-0106.

References

- [1] Ciancilo, M.E., M.E. Raffensberger, E.O. Schmidt, J.R. Stearns, 1996: Atmospheric scene simulation modeling and visualization. PL-TR-96-2079, USAF Phillips Laboratory, Hanscom AFB, MA, 110 pp.
- [2] Marshak, Davis et. al, "Scale Invariance in Liquid Water Distributions in Marine Stratocumulus Part II: Multifractal Properties and Intermittency Issues", Journal of Atmospheric Science, Volume 54 Number 11, 1997
- [3] Marshak, Davis et. al, "Scale Invariance in Liquid Water Distributions in Marine Stratocumulus Part I: Spectral Properties and Stationarity Issues", Journal of Atmospheric Science, Volume 53 Number 11, 1996



STATE OF THE BATTLESPACE: CLOUD AND WEATHER EFFECTS VISUALIZATION FOR THE TACTICAL BATTLEFIELD

Donald W. Hoock Jr.
David H. Tofsted
Richard Shirkey
Jon Martin
U.S. Army Research Laboratory
Information Science and Technology Directorate
Battlefield Environment Division
White Sands Missile Range, NM and Adelphi, MD

John C. Giever
Physical Science Laboratory
New Mexico State University
Las Cruces, NM

ABSTRACT

In the future, battlefield commanders and staff weather officers will routinely immerse themselves in virtual battlefields. There they will tap into intuitive, multi-dimensional, seamlessly-distributed digital databases. They will be aided by "smart software" to help them assess the threat, plan the mission, and gain situational awareness. This will exploit knowledge of the current state of the battlespace, including forecast effects and impacts on weapons, tactics, and operations of dynamic weather, clouds, terrain, illumination, and battle-induced environments. This paper shows how existing technology can be easily adapted to advance the visualization of meteorological information, such as clouds, weather effects, and weather impacts. We demonstrate how meteorological forecast outputs can be interfaced to the University of Wisconsin's Vis5D and extended to include other data and derived effects parameters. We contrast the performance of the product on different computers to highlight the need for future tactical computer hardware standards to include graphics hardware that can run under "open" graphics languages.

1. INTRODUCTION

Technology demonstrations indicate that the Tactical Operations Centers (TOC's) of the future will be highly automated and interoperable, sharing many digital information products. Battlefield commanders and staff will be able to routinely immerse themselves in "virtual battlefields". There they will tap into intuitive, multidimensional, seamlessly-distributed digital information databases. They will be aided by "smart software" to help them easily extract and synthesize critical information to assess the threat, plan the mission and gain situation awareness.

Realization of this vision may be several years away, however. Currently text messages, paper maps and overlays are still evolving into digital maps and 2-D graphic screen overlays, with analysis information shared via data tables and images downloaded by direct file transfers. Data exchange interfaces may soon evolve to include distributed "push-pull" database access and "client-server" architectures, perhaps within some form of a "web-page and browser" environment.

In the spirit of this information evolution, we describe in this paper a current effort to adapt a 3-dimensional weather and effects data-visualization tool to support weather forecast analysis and displays: the Battlescale

Forecast Model (BFM) has been chosen as our test bed. BFM is part of the tactical Integrated Meteorological System (IMETS). The existing 3-D weather data display software being adapted is Vis5D¹.

2. INTEGRATED METEOROLOGICAL SYSTEM AND BATTLESIZE FORECAST MODELS

The U. S. Army's IMETS supports the warfighter in the TOCs on the battlefield. IMETS runs on Army Common Hardware/Software (ACHS); currently the ACHS is a SUN Sparc 20. Included in IMETS is the BFM². BFM is a hydrostatic forecast model that is sufficiently compact to run on the ACHS Sparc 20 desktop while delivering the high spatial resolutions needed for predicting terrain-coupled effects at tactical scales. BFM produces high resolution, 24 hour forecasts on the ACHS battlefield system at a horizontal spacing of typically 10 km or 5 km over regions from 500x500 km to 100x100 km, and at 16 unevenly spaced vertical levels from the ground surface up to 7 km above ground level (AGL). BFM currently uses DTED terrain elevation data. BFM is initialized using coarser-grid forecast data, for example from the Air Force Global Spectral Model (GSM) and the Navy Operational Global Atmospheric Prediction System (NOGAPS), which are global-scale models, plus observations and soundings in the battle area

Figure 1 shows one example of a tactical display of BFM output on IMETS. The data here are wind speed streamlines forecast for a region of Bosnia and displayed over a 2-D map provided by a map server. Using IMETS, many other types of 2-D "overlays" and 1-D vertical profile displays of meteorological forecast data can be generated in the field.

Another mesoscale model currently used by the Battlefield Environment Division for special studies requiring high resolution, time dependent meteorological data (e.g. atmospheric transport and diffusion of hazardous materials, acoustic propagation in complex terrain), for the support of special projects is based on the University of Wisconsin's Non-Hydrostatic Modeling System (UW-NMS)³. This mesoscale forecasting model is used to provide time dependent 3-D meteorological parameters (e.g., winds, temperature, moisture, cloud, turbulence parameters, etc.) over complex terrain. The model has been tailored to address domains and scales of importance to the US Army at the Meso-g⁴ (2km/1hr) and higher resolutions.

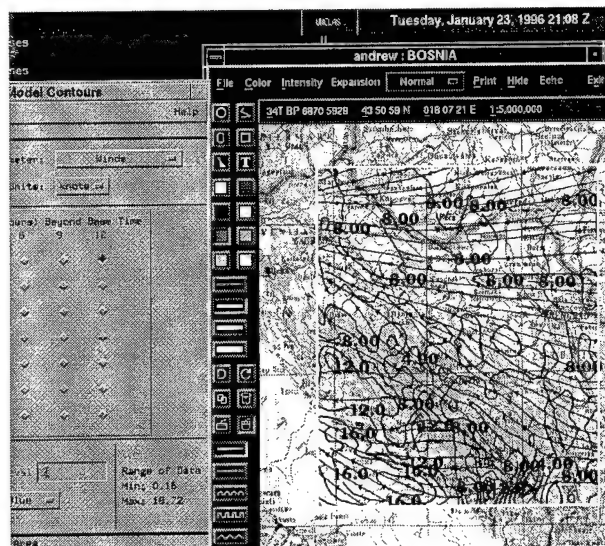


Figure 1. IMETS BFM Display

For small domains this model provides adequate predictability when initialized with a single atmospheric sounding; for other applications the model can be initialized with gridded model data, or with a 3-D analytic meteorological field. The modeling system permits nesting of grids, with variable positioning, movement and sizing of the inner grids. This model is being adapted to replace the current operational (hydrostatic) IMETS BFM.

ARL is currently extending the IMETS basic weather data visualization capability to three dimensions and time by using the University of Wisconsin's Vis5D. Vis5D is a system for interactive visualization of large 5-D gridded data sets such as those made by numeric weather models (e.g. BFM). Isosurfaces, contour line slices, colored slices, volume renderings, etc. of 3-D gridded data may be rotated and animated in real time. Vis5D also allows for wind/trajectory tracing. Vis5D software is publicly available from the University of Wisconsin under the terms of a GNU General Public License; it runs on the ACHS desktop systems and on many other computers. Only minimal changes to the Vis5D graphics library have been required to adapt contouring algorithms to the specific terrain-coupled vertical data layer spacing used by BFM.

3. WEATHER DISPLAYS

3.1 MESOSCALE MODELS

Figure 2 is a composite of examples of BFM forecast data from the Joint Warfighter Interoperability Demonstration as displayed in Vis5D. It shows forecast wind streams at two levels, liquid water content contours and isosurfaces, and near-surface pressure contours. These data are displayed over the default pseudo-colored topographic elevation data of the South and North Carolina regions, with the Appalachian mountains in the northwest corner.

Figure 3 shows an example from a Vis5D visualization of the UW-NMS model's predictive capability at the Micro-a (250 meter/15 minute) and Meso-g scales. The actual thunderstorm occurred within 30 minutes and 2 kilometers of the location predicted by the model. This particular case study should not be used as an

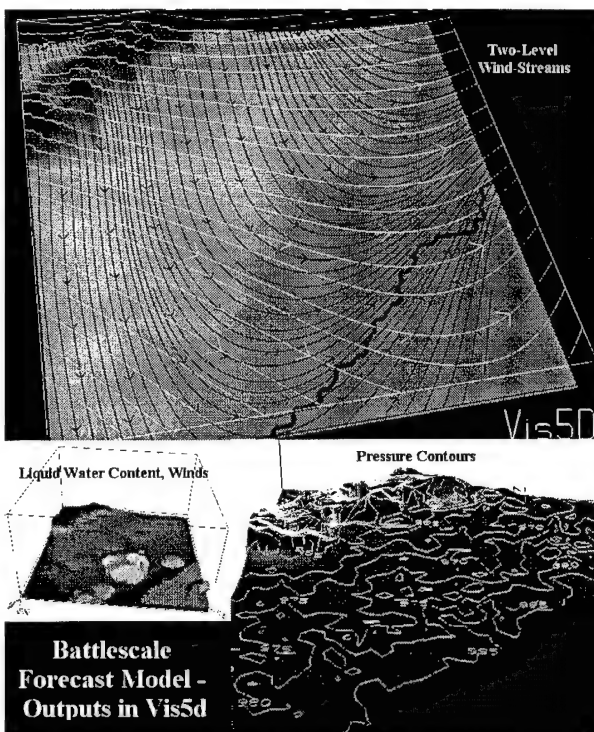


Figure 2. BFM in Vis5D Viewer

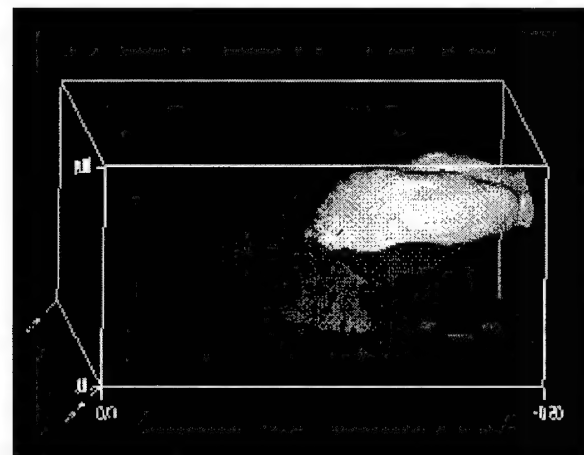


Figure 3. UW-NMS in Vis5D Viewer

indication of the overall accuracy of the predictive capability of the model but rather as a demonstration of the model's potential for providing atmospheric related data on scales important to military maneuver units.

3.2 FUTURE DERIVED EFFECTS

A new Army Science and Technology Objective (STO), Weather Effects and Battlescale Forecasts for Combat Simulation and Training, has the objective of making the IMETS capabilities an asset for use in mission planning, training and simulations. Currently IMETS has been "isolated" to the tactical operations centers on the battlefield and to ACHS hardware and software. Under this STO ARL will not only make the IMETS assets available to the outside simulation communities, but will also use models and simulations to make new derived environmental effects parameters and weather impacts available to IMETS.

An example of a future capability is to display natural clouds along with various properties such as concentration, transmission and radiance. Figure 4 shows modeled clouds based on their transmission and

radiance⁵ on the top, and Vis5D display of cloud liquid water content (concentration) contours below. In future such data may also be derived from satellite imagery and forecast liquid water content.

4. Vis5D PERFORMANCE CONSIDERATIONS

Vis5D executes extremely well on computers with dedicated graphics hardware. On Silicon Graphics (SGI) machines, the screen update is approximately 3 to 20 frames/sec depending on the amount of displayed data. On the Sun Sparc 20 ACHS the corresponding rates using the Mesa graphics library in the main cpu are about 1/10 the SGI rate (visualizations are virtually identical on both systems).

5. CONCLUSIONS

We have detailed here the use of the Vis5D graphics software for the real-time, interactive 3-D visualization of forecast data from the BFM and UW-NMS models. Vis5D is being integrated into IMETS in 1997 for evaluation. If evaluations go well, then Vis5D is expected to become available on the tactical battlefield for the display and analysis of weather. In the future, the data and tactical weather forecast capabilities of IMETS will be made available by ARL to the mission planning, simulation and training communities through an Army Science and Technology Objective. In turn, various weather effects models and simulations will be adapted and evaluated for their use in tactical forecasting of effects and to upgrade current tactical battlefield software for the display of impacts on systems and operations.

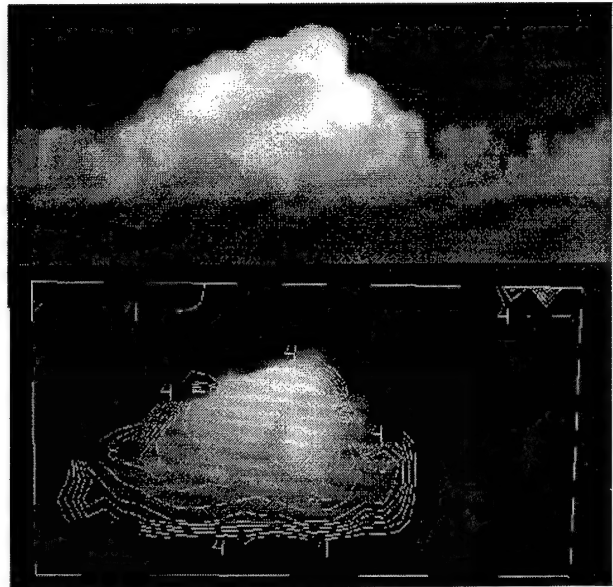


Figure 4. Modeled Clouds from the Side

REFERENCES

1. Hibbard, Bill and Paul, Brian, 1996, Overview of Vis5D, Version 4.2, available on-line at <http://www.ssec.wisc.edu/~billh/vis5d.html>, or <ftp://iris.ssec.wisc.edu/pub/vis5d>, Space Science and Engineering Center, University of Wisconsin - Madison, 1225 West Dayton Street, Madison, WI.
2. Lee, Martin, et. al., 1994, U.S. Army Battlescale Forecast Model, in Proceedings of the 1994 Battlefield Atmospherics Conference, 1 Dec 94, Army Research Laboratory, White Sands Missile Range, NM.
3. Tripoli, G. J., 1992, A Nonhydrostatic Numerical Model Designed to Simulate Scale Interaction, Mon. Wea. Rev., **120**, 1342-1359.
4. Orlanski, I., 1975, A Rational Subdivision of Scales for Atmospheric Processes, Bull. Amer. Meteor. Soc., **56**, 529-530.
5. Tofsted, David and O'Brien, Sean, 1996, Application of the WAVES Modeling Suite to the Visualization of Natural Cloud Fields, in Proceedings of the 1996 Battlescale Atmospherics Conference, Dec 1996, San Diego, CA, NRAd-TD-2938.

MOBILE AIRCRAFT ICING FORECAST SYSTEM

Steven J. Walter, Philip I. Moynihan
Jet Propulsion Laboratory, California Institute of Technology
Pasadena, CA 91109

ABSTRACT

An integrated mobile field system for forecasting ground and in-flight aviation icing hazards would be a vital asset for winter operations. Improved icing forecasts are critical to managing aviation icing hazards. Forecast accuracy, currently limited by existing weather observational systems, do not benefit from technology that has been shown to improve icing forecasts. Advanced ground-based and airborne sensors with state-of-the-art retrieval algorithms will improve the accuracy of regional forecast models. It is feasible to package these sensors with appropriate communication and information systems into a mobile forecast system that would increase aircraft reliability and safety.

INTRODUCTION

Aircraft icing presents a serious hazard for military aviation. An integrated mobile field system for forecasting ground and in-flight aviation icing hazards would provide important tactical and strategic advantages during mid-latitude winter and year-round polar operations. Freezing precipitation and supercooled cloud liquid will cause an aircraft to accrete ice, potentially compromising its performance and safety. Improved forecasting capability reduces risk by identifying and characterizing icing conditions that endanger military aviators, restrict surveillance opportunities, and impact combat effectiveness.

Effective management of icing hazards requires a systems approach. Hazard reduction needs to be information-driven starting with meteorological measurements that are sensitive to impending and existing icing hazards. Expert systems must integrate the meteorological data stream into regional forecast models to ensure timely analysis and accurate, reliable forecasts. The pilot, air traffic control, and the airfield controllers must possess appropriate tools and training to evaluate the impact of the impending forecast on specific air operations. The successful integration of these components will allow pilots and controllers to make informed decisions that will decrease the impact of weather on air operations. A conceptual system design is depicted in Figure 1.

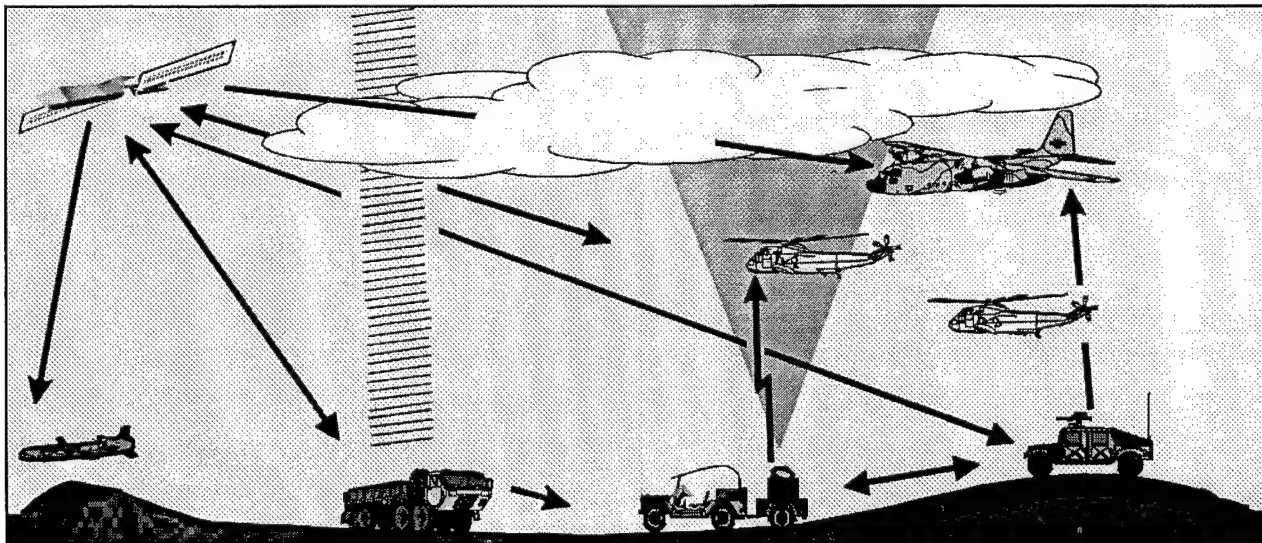


Figure 1. Mobile Aircraft Icing Forecast System. An integrated mobile field system for forecasting ground and in-flight aviation icing hazards enhances combat effectiveness by providing timely, accurate information to aviators, air traffic controllers, and field commanders during winter operations.

2. ICING METEOROLOGY

Ground and in-flight aircraft icing is usually associated with freezing precipitation. Non-precipitating clouds also present in-flight hazards when they contain appreciable amounts of supercooled liquid. An aircraft encountering sub-freezing liquid acts as a nucleation site for liquid to freeze. Large areas of freezing precipitation are commonly associated with regional winter storms that dump snow in the North and rain in the South. The boundary between the rain and snow exhibits freezing rain and drizzle and usually contains an abundance of supercooled cloud liquid.

The severity of hazard associated with supercooled cloud liquid or freezing precipitation depends on the local meteorology. Important microphysical parameters include liquid water content, temperature, and drop-size. Statistics on liquid contents and drop-size distributions are limited, leading many studies to rely on "typical" values. The vast majority of clouds and rainfall events have liquid contents ranging from 0.01 g/m³ to 1.0 g/m³ with isolated occurrences of clouds and precipitation exceeding 1.0 g/m³ [1]. High liquid water contents pose significant hazards because they induce rapid ice accretion rates. Although standard terminology has not been developed to classify drop sizes, reference to "cloud droplets" usually includes particle sizes ranging from 10 µm to 100 µm, "drizzle drops" generally range from 50 µm to 500 µm, and "rain drops" are usually defined to be larger than 500 µm [2]. The larger drops present a greater hazard because they also induce rapid accretion rates.

3. AVIATION HAZARDS

Icing compromises aircraft performance by changing the aerodynamics of the wings and propellers, decreasing lift. Icing also increases weight and drag and can disable control surfaces. Ice shed from the airframe occasionally impacts and damages adjacent aircraft structures. The rate at which ice accumulates depends on meteorological conditions and aircraft-specific characteristics such as velocity and airfoil shape. Exposure time is critical because prolonged exposure increases the amount of ice that will accumulate.

Helicopters, piston-engine, and turboprop aircraft are most susceptible to icing. Not only do they fly at lower altitudes where icing occurs most often, but they also operate close to their performance margins and are less able to tolerate a loss of lift, and are therefore less able to climb to avoid icing. Since they fly slower than jets, they require additional time to exit hazardous areas, prolonging exposure. Smaller aircraft and helicopters are often not certified to fly in icing conditions and are not equipped with deicing systems. Ryerson [1] provides a brief review of how icing affects military air operations.

4. SENSOR TECHNOLOGY FOR DETECTING ICING HAZARDS

4.1 OVERVIEW

A system-level analysis should drive the choice of sensors. In general, the combination of several types of sensors will provide a clearer picture of the local weather than a network of identical sensors [3]. Issues affecting a sensor's selection include its contribution to the existing meteorological network, technological maturity, suitability for the intended platform, and the potential to compromise security. In-situ sensors directly sample local meteorology, while remote sensors probe meteorological properties at a distance. Microwave remote sensors usually have an advantage over optical sensors in detecting icing conditions because they can "penetrate" clouds. Remote sensors can be divided into two categories: active systems which emit signals and then measure their interaction with the environment and passive systems that measure natural radiation emitted by the environment. Although active systems usually provide the best portrait of the meteorological environment, they also tend to require more power, are harder to conceal, are more expensive, and are more likely to interfere with other C³I systems. The choice of sensors requires optimizing system needs, cost, and logistical requirements.

Sensors for improving icing forecasts have already been developed and many are commercially available. However, there are two areas where targeted research and development would yield significant benefit.

Considerable value could be derived from re-engineering research instrumentation. Scientific sensors developed with a design emphasis that maximized capability, accuracy, and operational flexibility can be redesigned with a focus on developing an application-specific design, increasing reliability, improving automation and reducing cost. R&D is also needed to develop advanced airborne sensors to detect and forecast icing. Commercial airborne sensors currently detect ice formation with acoustic, optical, and impedance probes. The next generation of sensors will likely measure meteorological parameters and estimate the icing rate prior to ice forming on the aircraft. This approach will give pilots extra time to develop effective avoidance and mitigation strategies.

4.2 CLOUD AND PRECIPITATION TEMPERATURE MEASUREMENT

There are several methods used to measure cloud temperature. In-situ temperature probes measure cloud temperature directly. In-situ probes require an aircraft or balloon to transport the sensor. In CONUS, temperature probes are currently carried on some commercial airplanes and are used to measure the temperature profile near major airports. IR radiometers are often used to retrieve cloud base temperature. They measure the infrared brightness of the cloud base and derive cloud base temperature from the measured radiance.

Atmospheric temperature profiles can be measured in the presence of clouds with microwave radiometry radio-acoustic sounding, and in-situ measurements. A microwave radiometric temperature profiler is a sensitive radio receiver tuned to the 60 GHz emissions of molecular oxygen. The radiance of oxygen emissions depends on temperature. Measurements made at several frequencies and elevation angles will yield the temperature profile. Radio acoustic sounding systems (RASS) are active sensors that transmit a powerful acoustic pulse and track its upward propagation with a VHF radar. Since the acoustic velocity is a sensitive function of temperature, the temperature profile is retrieved from the acoustic pulse propagation velocity. RASS provides higher resolution than microwave temperature profilers, although they are much more expensive and require orders of magnitude more power and area to operate. RASS are not adaptable to airborne platforms, whereas airborne radiometers are routinely used on NASA aircraft to profile temperature.

Cloud temperature is retrieved from the temperature profile with a simultaneous determination of cloud altitude using a Ka-band radar, lidar, ceilometer, or in-situ sensor. While a lidar is a laser radar, a ceilometer is a simple lidar designed to measure only cloud base altitude. High-power lidars can penetrate multiple cloud layers. However, Ka-band radars are often preferred because they can penetrate much thicker clouds with comparable signal power. In-situ balloon-borne, capacitive and resistive humidity sensors are regularly used to identify cloud height, but are limited in their temporal coverage.

4.3 MACRO- AND MICROPHYSICAL PROPERTIES OF CLOUDS AND PRECIPITATION

Dual-polarization radars, lidars, and microwave radiometers can determine cloud phase (ice or liquid). Polarization sensitive measurements discriminate between ice and liquid hydrometeors by providing sensitivity to the scattering particle height-to-width aspect ratio. As an ice crystal melts, its aspect ratio changes, altering the ratio of reflection cross-sections at each orthogonal polarization. Since radar reflectivity depends on both drop size and total water content, radars, alone, are unable to independently determine liquid content. Lidars are limited in range due to hydrometeor-induced attenuation. Liquid-sensing microwave radiometers are sensitive radio receivers tuned to continuum emissions of liquid water in the 30 GHz and 90 GHz atmospheric windows. The radiance of a cloud is proportional to the columnar liquid content. Microwave radiometers can discriminate between ice and water because the dielectric constant of ice is two orders of magnitude smaller than that of liquid and is therefore "transparent" to the radiometer. Thus, clouds or precipitation that emit significant amounts of microwave radiation must contain liquid. Although radiometers do not provide distance information, they have an advantage in some applications because they are passive and less expensive than radars and lidars. Combining radars and radiometers can be a very powerful strategy because it allows cloud liquid to be profiled [3].

In-situ sensors are very effective at determining the phase of precipitation and cloud water. For ground-based applications, rain gauges can differentiate between snow and rain. Supercooled liquid precipitation can

be detected with a vibrating wire or rod. Supercooled liquid freezes to the wire or rod, thereby changing the vibrating mass. The associated shift in resonant frequency signals the presence of supercooled liquid. Vibrating wires and rods are used in ground-based stations and have been flown on radiosondes.

Characteristics such as drop size and liquid water content can be inferred by combining microwave radiometers with radars. Drop size and liquid water content can also be retrieved using lidars. In-situ instruments are able to resolve the drop-size spectrum and liquid content by measuring the intensity and angular distribution of light scattered by an atmospheric sample [4]. Ground-based systems that record light scattering along a short atmospheric path can be used to constrain drop size and phase by determining the precipitation rate of descent.

5. FORECASTING AND THE NEED FOR A SYSTEMS APPROACH

Generating a detailed picture of icing-hazards on a regional scale requires a systems approach. Advanced warning of icing hazards requires enhanced surveillance using a variety of measurement techniques from multiple locations. These data need to be rapidly integrated into a regional forecast model which includes advanced algorithms for predicting icing conditions [5]. The forecasts, in turn, need to be promptly disseminated to users in a format that highlights possible impacts to air systems, operations, and maneuvers. It is the combination of enhanced surveillance, improved modeling, integrated information systems, and reliable communications that can extend the time available to effectively mitigate the hazard, or avoid it altogether.

CONCLUSIONS

An integrated mobile field system for forecasting ground and in-flight aviation icing hazards is feasible and would provide a significant tactical advantage during winter. Advanced warning of freezing precipitation and supercooled cloud liquid is needed to improve the safety, reliability, and effectiveness of air operations. While standard meteorological sensors are relatively insensitive to critical parameters needed to accurately forecast icing, technology exists that can provide these data such as short-wavelength radars, microwave radiometers, and in-situ meteorological probes. These measurement systems can be quite compact, reducing logistical requirements and enhancing mobility. Ground-based and airborne sensors with state-of-the-art retrieval algorithms will improve the capability of regional forecast models to provide accurate, timely forecasts of hazards. Packaging these components into a mobile forecast system with appropriate communication and information system interfaces is feasible. Advanced sensors that determine the ambient and approaching meteorological conditions could predict the impending rate of ice deposition, thereby increasing warning time. Autonomous and networked sensors would be an essential component in an integrated field system for forecasting aviation icing hazards. A systems-level analysis extending from meteorological sensors to the cockpit will identify effective strategies for increasing aircraft reliability and safety, given the improved forecasts. For example, tailoring hazard forecasts to specific aircraft can maximize the value of enhanced prediction capability.

ACKNOWLEDGMENTS

The authors would like to thank Charles Ryerson at CRREL for his helpful suggestions. The research described in this paper was carried out by the Jet Propulsion Laboratory, California Institute of Technology, under a contract with National Aeronautics and Space Administration.

REFERENCES

1. Ryerson, C., *Proc. FAA Int. Conf. on Aircraft In-Flight Icing, Vol. II* (Tech Rep. **DOT/FAA/AR-96/81,II**), p. 179, (1996)
2. Jeck, R., *Proc. FAA Int. Conf. on Aircraft In-Flight Icing, Vol. II*, (Tech Rep. **DOT/FAA/AR-96/81,II**), p. 57, (1996)
3. Stankov, B., B. Martner, M. Politovich, *Jour. Of Atmos. and Oceanic Tech.*, **12**, p. 488, (1994)
4. Lawson, R. P., R. H. Cormack, *Atmos. Res.*, **35**, p. 315, (1995)
5. Thompson G., R. Buintjes B. Brown, F. Hage, *Wea. and Fore.*, (In Press - to appear in vol. **36**, 1997)

ONE YEAR OF WORLD WIDE CLOUD COVER

Arnold A. Barnes, Jr.
Optical Effects Division
Phillips Laboratory
Air Force Research Laboratory
Hanscom AFB, MA 01731-3010
Phone: 617-377-2939
Fax: 617-377-8892
barnes@plh.af.mil

ABSTRACT

STC-METSAT produced for the Air Force world wide cloud cover data for each hour of the period from 1 February 1994 through 31 January 1995. These data are on 365 exabyte tapes, one day to a tape. For each hour there are three maps: an IR map of the cloud cover, a Cloud/No-Cloud map for each 5 km square, and a map of the quality of the data at each data point. Examples of the data are shown. Methods of construction and some of the limitations of the data set are discussed.

1. INTRODUCTION

Under a Phase I and a Phase II Small Business Innovative Research (SBIR) contract with the Air Force STC-METSAT developed the methods to process and combine the imagery from eight of the then operational meteorological satellites. These included GOES, GMS and two each of the Meteosat, NOAA and DMSP satellites. The project was named "Climatological and Historical Analysis of Clouds for Environmental Simulation" (CHANCES).

2. DATA DESCRIPTION

Both visible and IR data from the satellites were used to provide world wide cloud data. Global cloud cover was obtained for ~5 km square grid for every hour from 0000Z on 1 February 1994 to 2400Z on 31 January 1995. IR data were used to obtain cloud cover over the areas not in sunlight, and the polar satellites filled in most of the areas not covered by the geostationary satellites.

2.1 DATA PROCESSING

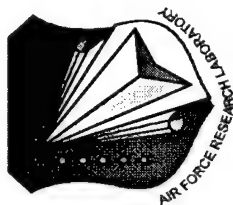
In order to conserve area the mollweide projection was used. First the data within plus or minus 30 minutes of the hour taken from the polar orbiting satellites was put down. Then the data from the geostationary satellites was put down and replaced any data from the polar satellites. For those areas where there were no data within plus or minus 30 minutes, linear interpolation was used. This caused some sharp cloud boundaries in areas where geostationary coverage was lacking, such as over parts of the Indian Ocean. For each hour three mollweide map were produced. For each ~5 km square grid the first map gave a cloud/no-cloud (binary) value; the second map gave an IR gray shade value; and the third map gave information on the quality of the data.

2.2 DATA AVAILABILITY

The processed data exists on 365 Exabyte tapes, one for each day, with 2.4 Gb on each tape. Detailed description of the data and processing methods is given in the STC Technical Report 2932 (PL-TR-95-2101) CLIMATOLOGICAL AND HISTORICAL ANALYSIS OF CLOUDS FOR ENVIRONMENTAL SIMULATIONS (CHANCES) DATABASE - FINAL REPORT. The tapes and the report may be obtained from Science and Technology Corp., 101 Research Drive, Hampton, VA 23666-1340.



CHANCES IR DATA 23 APR 1994, 2000 UTC



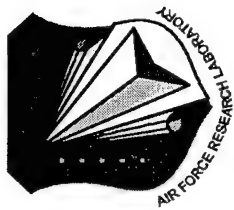
STC-METSAT

IR Temperatures Indicate Cloud Top Heights

PL/GPA/AAB/7600/TIS97/970604 97/08/26 11



GLOBAL CLOUD COVER 23 APR 1994, 2000 UTC



STC-METSAT

~70% of the Earth Covered With Clouds

PL/GPA/AAB/7600/TIS97/970604 97/08/26 7

THE CFLOSA (CLOUD-FREE line-OF-SIGHT ALOFT) PC PROGRAM

Albert R. Boehm
Hughes STX Corporation
2501 Ermine Drive
Huntsville, AL 35810

ABSTRACT

The CFLOSA (Cloud-Free Line-Of-Sight) PC Program provides the climatological probability of a cloud-free line-of-sight between any two altitudes for any location, season, or time of day. The CFLOSA PC program presents these statistics in a variety of ways including graph, maps, and output to monitor, file or printer. Data for CFLOSA is from a blending of satellite, surface, radar, and aircraft observations. From these observations the point probability of an opaque cloud is modeled. Also the correlation structure is modeled in the vertical and horizontal. Given the point probabilities along a line and the correlation structure, the CUB algorithm is used to calculate the frequency that the line-of-sight will have no opaque clouds.

1. INTRODUCTION

Here a cloud-free line-of-sight is defined as having no natural cloud (liquid or frozen water) obscuration to viewing by the human eye. All observations are adjusted to this definition. Other sensors would, in general, differ in defining what is an obscuration.

Data is stored in CFLOSA as point probabilities and correlation structure. The point probability, P_0 , is the probability of an opaque cloud at a point (zero volume). Given the point probability and correlation structure, the CUB algorithm (described below) calculates the probability of obscuration for the entire line.

2. THE COVERAGE ALGORITHM - CUB

The CUB (Coverage Using the Boehm distribution) algorithm was originally developed for areal coverage of clouds. However, its underlying theory is applicable to any domain - volumes, hyper-volumes, or in this case, lines. Details of the CUB algorithm are found in Boehm¹.

Coverage is defined as the fraction of a domain that has a specified event, in this case, opaque clouds. Each point in the domain has a probability, P_0 , that the event will occur there.

In general, there is a correlation between events at pairs of points, particularly points that are close. The overall effect of correlation is taken into account by calculating the mean correlation over the domain. This mean correlation is the arithmetic mean from all possible pairs of points in the domain. For a continuous field, a double integral over the domain is used to calculate all possible pairs of points. This mean correlation is a measure of how continuous the event is in the domain: Is it many small areas or just one or two large areas? For example, a tropical sky dome with fair weather cumulus may have a correlation of 0.1 while a winter mid-latitude sky dome with stratus may have a mean correlation of 0.9.

If the correlation between pairs of points for a continuum is set up in a matrix, that matrix will have an effective rank. The rank of this matrix is called the degrees of freedom in CUB. These degrees of freedom are the effective number of independent things that change in the domain. The degrees of freedom is equivalent to the effective number of eigenvalues of the matrix.

Given the point probability, mean correlation, and degrees of freedom, CUB quickly calculates the probability of a given domain coverage, for this application, all clear of opaque clouds along a line-of-sight.

3. DISTRIBUTION OF CLOUDS IN THE VERTICAL

There are many models but few climatological measurements of cloud or not at a given altitude. These few studies include: deBarry and Moller², Matveev³, and Willand and Boehm⁴. Most cloud measurements are actually CFLOS either from space to the top of the cloud (satellite) or from the ground to the base of the cloud (ceiling data). CUB is used to convert these CFLOS measurements into probability of cloud at an altitude.

Since a CFLOS at any altitude is needed, a piecewise model was chosen. At the base is clouds at the surface (fog), segments are fitted to the mean base of the lower clouds, to the mean tropopause (as determined by cloud probabilities not temperature), and a small segment above the mean tropopause. The piecewise model gives a reasonably good fit to the observed probabilities and yet its simplicity is needed to transform the satellite and ceiling CFLOS into point probabilities. To say more study is needed in this area is an understatement. Nevertheless, the resulting model of the vertical distribution of clouds is deemed satisfactory.

4. CORRELATION STRUCTURE OF CLOUDS

The vertical correlation structure of clouds including thickness, between layers, and obscuration of further layers due to nearer layers has many models, some case studies, but few climatological measurements. Thus the vertical structure was derived from references 2 and 3 which are based on a planned series of aircraft accents and 4 which is based on vertical radar.

The horizontal correlation structure of total clouds is rather well known due to the fascinating ability of coverage theory to convert a coverage distribution into a correlation (See 1). Also the horizontal correlation structure of cirrus was measured in the GASP⁵ program.

5. THE GLOBAL MODEL

In CFLOSA the parameters of the vertical segments and correlation structure are stored as spherical harmonics over the earth. A triangular 18 set of spectral harmonics is used. Higher sets of harmonics were tested with little additional accuracy. Thus, the parameters needed by CUB can be calculated for any latitude and longitude and used to calculate the probability of CFLOS along any given path.

6. ACKNOWLEDGMENTS

This work was supported by the Geophysics Directorate of the Phillips Laboratory with Mr. Donald D. Grantham and Dr. Joel Moser as contract monitors under contract number F19628-93-C-0051. Mr. Jim Willand performed most of the data base calculations. Mr. Marc Periera produced several applicable sub-studies. Also thanks are given to Prof. Humi Meyer for calculating the inverse CUB results for GASP data.

7. REFERENCES

1. Boehm, A., 1992: CUB A general purpose coverage algorithm, *Preprints of the Fifth International Meeting On Statistical Climatology*, Toronto, Canada, American Meteorological Society, Boston, MA.
2. deBarry, E., and Moller, F., 1963: The vertical distribution of clouds, *J. Appl. Meteorol.*, 2, 806-808.
3. Matveev, L.T., 1984: *Cloud Dynamics*, D.Reidel Publishing Co. Boston, MA, p235-239.
4. Willand, J. and Boehm, A., 1995: Vertical Cloud Layer Statistics derived from echo intensities received by a 35-GHz Radar, **PL-TR-95-2034**, Phillips Lab., Hanscom AFB. AD A294 826.
5. Jasperson, W. H., Nastrom, G. D., Davis, R. E., and Holdeman, J.D., 1985: Variability of cloudiness at airline cruise altitudes from GASP measurements, *J. of Climate and App. Met.* 24, 74-82.

Building an Improved Cirrus Model in the CSSM

Maureen E. Cianciolo, Mark E. Raffensberger, and Ryan B. Turkington

TASC

Reading, Massachusetts USA 01867

ABSTRACT

This paper describes planned improvements to the cirriform cloud model within the Cloud Scene Simulation Model (CSSM). A recent survey of research uncovered a fair amount of useful information concerning the average ice water content, vertical structure, and general characteristics of a variety of cirrus cloud types. Our design incorporates this information in improvements to the existing CSSM models for non-precipitating cirrus layer cloud types (cirrus, cirrostratus, and cirrocumulus) as well as the development of a new precipitating cirrus cloud model (cirrus uncinus). Aircraft-based observations of ice water content will be used to estimate model parameters that control the statistical characteristics of the resulting water content fields. Software implementation of the improvements outlined above is currently underway. An outline of the overall design is described in this paper.

1. INTRODUCTION

The CSSM includes models for stratiform, cirriform, and cumulus cloud types. It generates high-resolution cloud scenes for use in a wide variety of simulation applications including mission rehearsal, sensor test and evaluation, and scene visualization.

The CSSM builds four-dimensional (space and time) cloud scenes consistent with user-supplied coarse-resolution cloud and meteorological input fields. The primary output variable of the model is water content (g/m^3) at every gridpoint in a user-defined simulation domain. Typical scenes, with output resolutions of 10-100 meters, take only seconds to build on a standard workstation.

The CSSM is a parametric model that relies on stochastic field generation algorithms (the Rescale and Add fractal algorithm)¹ to build external cloud structures and their internal water density perturbation fields. For stratiform and cirriform cloud types, the resulting perturbation fields are converted to absolute water content using computed field statistics and a mean water content (WC) profile given by the Feddes model². A simple convection model is also employed when simulating cumulus cloud structures and water content values. (Note: the model does not attempt to model the exact cloud structures present at a given date/time/location, rather, it generates cloud fields that are statistically consistent with the observed cloud conditions.)

Previous efforts have focused on evaluating the CSSM's stratiform and cumulus cloud models^{3,4}. As part of an ongoing effort, we are now working to improve and validate the cirriform model. This effort consists of three primary tasks: first, we will evaluate the overall cloud generation methodology and identify areas for improvement, as necessary, to better replicate the structure of cirrus clouds; second, we will analyze cirrus observations to extract quantitative measures which can be related to internal model parameters controlling the character of the cirrus clouds; third, we will validate the improved cirrus model by comparing model water content fields to observed cirrus data. More detailed descriptions of our plans and preliminary results from this effort are described in the following sections.

2. CONCEPTUAL DESIGN FOR NEW CIRRUS MODEL

A recent survey of research uncovered a fair amount of information concerning the average ice water content, vertical structure, and general characteristics of a variety of cirrus cloud types. Qualitative comparisons of model-generated and observed cirrus clouds show that the fractal-based field generation methodology employed in the CSSM reproduces the types of structures observed in a variety of thin cirrus cloud types,

including cirrus fibratus. (Of course, this methodology also satisfies the computational speed requirements set by the user simulation applications.) However, the highly parametric fractal-based model is not appropriate for simulating the more complex, vertically-developed cirrus cloud types, such as cirrus incinus.

Therefore, our model development effort will focus both on improving the existing thin cirrus model, and developing a new model to handle the vertically-developed cirrus cloud types. We refer to these two cirrus cloud categories as *non-precipitating* and *precipitating*, respectively, although clearly there are no such simple categories in nature. Non-precipitating clouds in the CSSM include: cirrus, cirrostratus, and cirrocumulus. Precipitating cirrus clouds will be limited to the cirrus incinus type.

Our planned improvements to the *non-precipitating* cirrus cloud model will include: the introduction of a generating head embedded within the upper parts of the cirrus layers; modifications to the vertical distribution of ice water content to account for ice production, growth, and sublimation regions; updates to the horizontal spatial characteristics of the cloud types (e.g., distance between bands, length of bands, angle of bands with respect to large-scale wind features); introduction of more cellular structure within the cirrocumulus model produced by generating regions within the cloud layer; and improved estimates for several parameters used within the fractal field generation algorithms (see the next section for discussion of the parameter estimation task).

The *precipitating* cirrus cloud model will reproduce the characteristic cirrus precipitation trails consisting of generating head and particle fallout regions. Typical dimensions, average ice water contents, variations of microphysical properties with temperature and altitude will be taken primarily from literature⁵⁻⁸. Development efforts will include the following: model generating head with upshear and downshear regions and "hole" separating the two regions where ice concentrations are at a minimum; build model of horizontal dimensions of generating head elements; model horizontal distribution of generating heads; estimate terminal velocities of single bullet and rosette crystals created in generating head; calculate particle trajectories based on local scale advection and a simplified trajectory model; and model temperature dependence of ice water content for vertically extended cirrus precipitation trails.

Efforts are underway on some of the tasks listed above. Initial efforts are focused on improving the non-precipitating cirrus cloud model by identifying the best values for several internal model parameters which control the horizontal character of the output cloud fields. A description of our effort and preliminary results is presented in the next section.

3. PARAMETER ESTIMATION

A number of parameters within the CSSM control the statistical characteristics of the resulting WC fields. Previous modeling efforts^{3,4} relied on literature reviews and on visual inspection of model-produced and observed cloud fields to estimate the model parameters for cirriform clouds. The current effort will employ aircraft-based observations spanning a variety of climatological and seasonal conditions to estimate and tune the model parameters for the existing cirriform cloud types as well as for the new cirriform type described above. This section briefly describes the model parameters to be tuned and the methodology we will follow.

The WC at each gridpoint is represented as the sum of an average WC and a perturbation WC. Currently, the average WC is calculated as a function of cloud type, cloud temperature, and vertical position within the cloud layer following Feddes². As noted above, efforts are underway to modify the calculation of the average WC for cirriform clouds. The RSA algorithm is used to build a perturbation field within the cloud boundaries. The RSA model uses two tunable parameters: the Hurst parameter (H) and the lattice resolution (LR). The RSA field values are transformed to WC perturbations by scaling the RSA field distribution by the ratio of the standard deviations of the RSA field and an assumed standard deviation (SD) of the water content.

Table 1 shows the current values for the CSSM parameters that control the internal structure of the simulated water content fields. For the remainder of this discussion, these values will be referred to as the "baseline" values. Figure 1 shows the effect of varying these parameters from the baseline values (denoted by "B") for the cirrus cloud type. In the figures, LR(x) and LR(y) are the lattice resolutions along and perpendicular to the mean wind, respectively.

Table 1 CSSM Parameters Used in Internal Water Content Generation

CLOUD TYPE	HURST PARAMETER	LATTICE RESOLUTION	STANDARD DEVIATION
cirrus	0.3	2, 10	0.5
cirrocumulus	0.3	0.5, 5	0.5
cirrostratus	0.3	2, 15	0.5

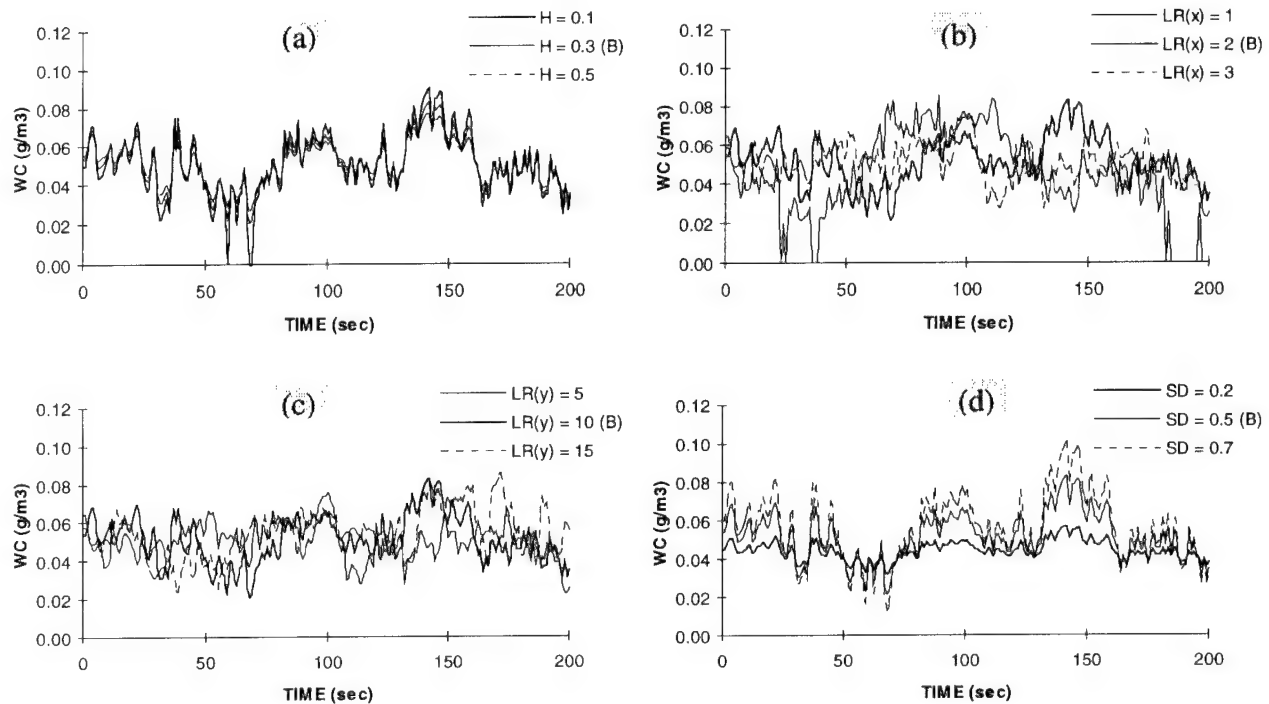


Figure 1 - CSSM internal water content parameters. Each panel shows a sample simulated path extracted from model output generated with varying model parameters. The plots show variations due to changes in (a) Hurst parameter, (b) lattice resolution along wind (x), (c) lattice resolution perpendicular to wind (y), and (d) assumed standard deviation.

Aircraft measurements of ice water content and other microphysical variables will be used in this effort to estimate the model parameters described above. For example: the Hurst parameter within the model can be directly related to the fractal dimension of the ice water content sampled along the aircraft paths; lattice resolution parameters used in the RSA algorithm can be related to the autocorrelation function computed from the cirrus observations; means and standard deviations can also be employed to tune the model to produce realistic water content distributions.

At this time, we have obtained a limited set of microphysical measurements collected by the University of North Dakota Citation aircraft during FIRE II (First ISCCP Regional Experiment II). Measurements of ice water content were taken using PMS 2D-C and 2D-P particle measuring probes. Figure 2a shows a sample path of 5-second average ice water content data taken from a cirrus cloud centered over Tulsa, Oklahoma on 25 November 1991. Figure 2b shows the autocorrelation function for this path. Comparable plots can be made from CSSM output fields (generated with similar temperature and cloud cover conditions) for comparison with the observed data to guide parameter estimation in the CSSM.

The limited cirrus measurements gathered to date will be used to build first estimates for model parameters. Final analyses will require higher resolution data in order to match the most typical user-specified resolutions. For accurate estimation of the CSSM cirrus parameters, the resolution of the aircraft ice water

content data should be at least one second (with average aircraft speeds of 100 m/s), resulting in approximately 100 meter data resolution.

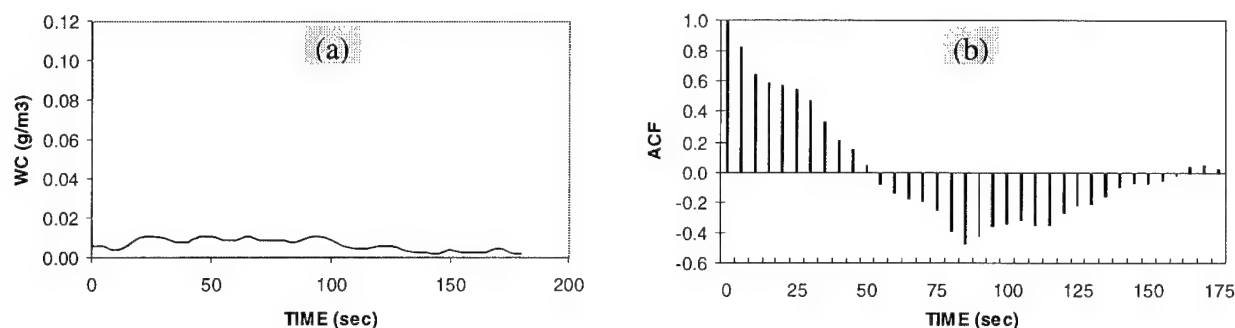


Figure 2. Sample water content time series and corresponding autocorrelation function from aircraft data.

4. SUMMARY

The CSSM includes models for stratiform, cirriform, and cumulus cloud types. Planned improvements to the cirriform cloud model incorporate recent information gathered from the literature concerning several important characteristics of cirrus clouds. Our design includes changes to the existing CSSM models for non-precipitating cirrus layer cloud types (cirrus, cirrostratus, and cirrocumulus) as well as the development of a new precipitating cirrus cloud model (cirrus uncinus). Aircraft-based observations of ice water content will be used to estimate model parameters that control the statistical characteristics of the resulting water content fields. Implementation of the improved cirrus model and parameter estimation tasks are newly underway.

5. ACKNOWLEDGMENTS

The authors would like to acknowledge the U.S. Air Force Geophysics Directorate as sponsors of this simulation model development effort under contract F19628-96-C-0113.

6. REFERENCES

1. Saupe, D., Point evaluation of multi-variable random fractals, *Visualisierung in Mathematik und Naturwissenschaft*, H. Jurgens and D. Saupe, Eds., Springer-Verlag, Heidelberg, 1989, pp. 117-129.
2. Feddes, R. G., A synoptic-scale model for simulating condensed atmospheric moisture, USAFETAC-TN-74-4, 1974.
3. Cianciolo, M. E., M. E. Raffensberger, E. O. Schmidt, and J. R. Stearns, Atmospheric scene simulation modeling and visualization, PL-TR-96-2079, April 1996. [NTIS AD-A312 179].
4. Cianciolo, M. E., Hersh, J. S., and M. P. Ramos-Johnson, Cloud Scene Simulation Modeling - interim technical report, PL-TR-91-2295, November 1991. [NTIS AD-A256 689].
5. Heymsfield, A. J., and L. J. Donner, A scheme for parameterizing ice-cloud water content in general circulation models, *J. of the Atmos. Sciences*, vol. 47, no. 15, pp. 1865-1877, 1 August 1990.
6. Heymsfield, A. J., and C. M. R. Platt, An empirical model of the physical structure of upper-layer clouds, *Atmos. Research*, vol. 26, pp. 213-228, 1991.
7. Sassen, K., D. O'C Starr, T. Uttal, Mesoscale and microscale structure of cirrus clouds: three case studies, *J. of the Atmos. Sciences*, vol. 46, no. 3, pp. 371-396, February 1989.
8. Varley, D. J., et al., Cirrus particle distribution study - Parts 1-8, Air Force Surveys in Geophysics, AFGL-TR-#, various dates. Pt 1: AFGL-TR-78-0192, ADA061485; Pt 2: AFGL-TR-78-0248, ADA063807; Pt 3: AFGL-TR-78-0305, ADA066975; Pt 4: AFGL-TR-79-0134, ADA074763; Pt 7: AFGL-TR-80-0324, ADA100269

CLOUDSCAPE® VR: RADIOMETRIC VISUALIZATION OF CLOUDS FOR INTERACTIVE TRAINING AND SIMULATION

John G. DeVore and James H. Thompson
Visidyne, Inc.
Goleta, CA, 93117, USA

Ken W. Sartor, Timothy L. Stephens, and Ross J. Thornburg
Visidyne, Inc.
Huntsville, AL, 35801, USA

ABSTRACT

This paper describes CloudScape® VR, a COTS tool for adding weather clouds, munitions dust clouds, and other atmospheric obscurants to interactive simulations. It employs efficient, physics-based models of radiative transfer to produce radiometrically realistic simulations at wavelengths in both the visible and infrared. Partial transparency is rendered where appropriate. Cloud lighting includes solar or lunar, skyshine, earthshine, thermal and self shadowing. CloudScape® VR utilizes facetized descriptions of cloud surfaces based on three-dimensional particulate density databases to achieve real-time frame rates on Silicon Graphics workstations.

CloudScape® VR is derived from Phase I and Phase II SBIR development efforts with the Geophysics Directorate of the U.S. Air Force Phillips Laboratory. CloudScape® VR works in conjunction with Paradigm Simulation's Vega™ visual simulation software and Photon Simulations' SensorVision™ radiometric image-rendering tool to provide a complete modeling suite for interactive simulation development. An overview of CloudScape® VR modeling, validation, and applications is presented. Sample images are also shown.

1. INTRODUCTION

CloudScape® VR is a product of Phase I and II SBIR development efforts with the Phillips Laboratory to demonstrate a physics-based approach to the quantitative modeling of the reflectivity, emissivity, and transmissivity of natural clouds. CloudScape® VR has been integrated with Paradigm Simulation's Vega™ 3-dimensional visual simulation software. It is compatible with Photon Simulations' SensorVision™ module, which renders backgrounds in real-time in any user-selected waveband from the ultraviolet through the infrared. Together they form an integrated, real-time, simulation environment for Silicon Graphics workstations as diagrammed in Figure 1.

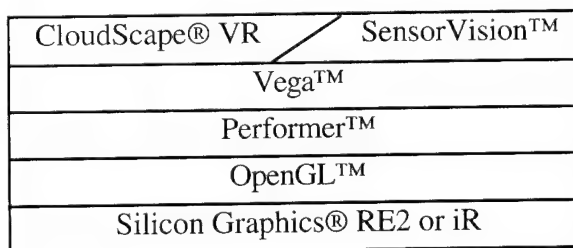


Figure 1. CloudScape® VR is part of an integrated simulation environment.

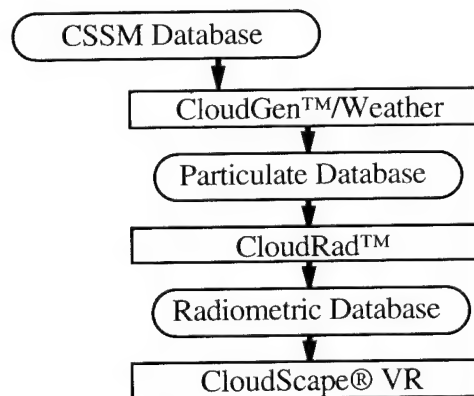


Figure 2. CloudScape® VR is supported by CloudRad™ and the CloudGen™ family.

CloudScape® VR visualizations start with a facetted description of cloud radiative properties (see Figure 2). These radiometric databases are prepared with the CloudRad™ tool from 3-dimensional

descriptions of cloud condensed-water or dust-particulate content. The particulate databases are generated with members of the CloudGen™ family of tools or are translated from output of the U.S. Air Force Phillips Laboratory's Cloud Scene Simulation Model (CSSM)².

2. MODELING

The primary function of the particulate database is to provide a macroscopic description of the distribution of cloud particles. This takes the form of a 3-dimensional grid of mass densities. There is also a microphysical description, which consists in the specification of particle composition, e.g., water, ice, or dust, and particle size distribution parameters. CloudGen™/Weather associates typical particle size parameters with cloud types, e.g., St, Sc, Cu, etc, using a modified version of the LOWTRAN distributions³.

CloudRad™ converts the cloud mass density distribution $L_s(x,y,z)$ from a 3-dimensional (x,y,z) particulate database into an effective incremental extinction distribution $k_e(x,y,z)$ for user-specified wavebands. The complex index of refraction depends upon the particle composition. Currently CloudRad™ employs the robust Thompson Mie scattering code⁴ to calculate the mass extinction coefficient μ , the single scattering albedo ω_o , the scattering pattern and f_d , the fraction of the scattering pattern concentrated in the forward peak. The effective incremental extinction is then given by:

$$k_e(x,y,z) = L_s(x,y,z) \mu [1 - \omega_o, f_d] .$$

By putting the narrow angle forward scattered radiation back into the direct beam, the time required to calculate multiple scatter effects is greatly reduced.

CloudRad™ selects a threshold value of k_e based on the grid spacing to define a cloud surface. The Marching Cubes⁵ algorithm is applied to facetize the surface. At each cloud vertex, CloudRad™ solves the integral form of the radiative transfer equation; single scatter is solved exactly and multiple scatter is approximated using a validated technique developed by Visidyne staff⁶. Atmospheric path attenuation, scattering, and emission are factored in using parametric databases generated with the Phillips Laboratory's MOSART code⁷.

CloudScape® VR processes the radiometric databases and applies an appropriate grayscale for weather clouds or a brownscale for dust clouds in Vega™ simulations. In quantitative applications CloudScape® VR uses the same grayscale or greenscale as SensorVision™ so that radiances can be derived from the calibrated images using SAOimage⁸.

3. SAMPLE CLOUD IMAGES

A sample image produced with CloudScape® VR is presented in Figure 3. For this example CloudGen™/Weather was used to prepare a database for broken stratocumulus clouds. CloudRad™ performed the radiative transfer calculations for this database. CloudScape® VR was run in Vega™ to visualize the clouds with the fighter over Onyx Town.

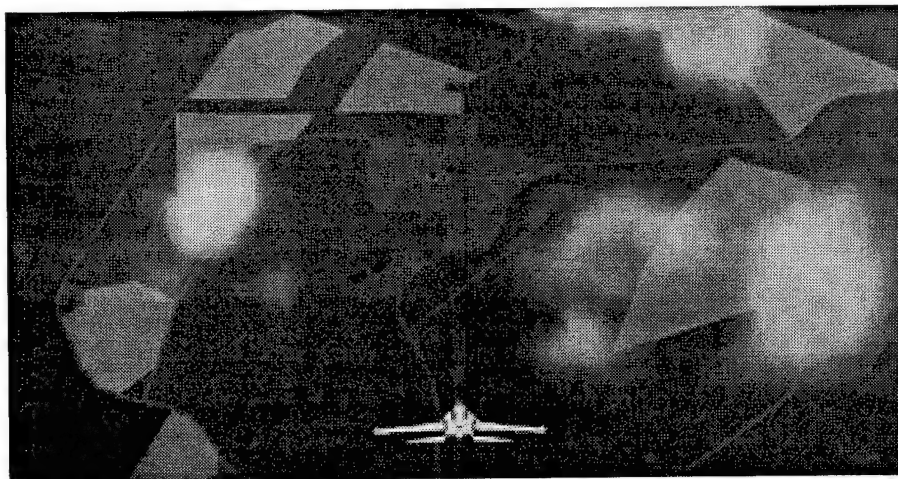


Figure 3. CloudScape® VR - Vega™ visualization of broken stratocumulus.

Databases from the Phillips Laboratory's CSSM can be visualized with CloudScape® VR. Figure 4 shows views looking to the east of a CSSM-generated stratus layer over Onyx Town.

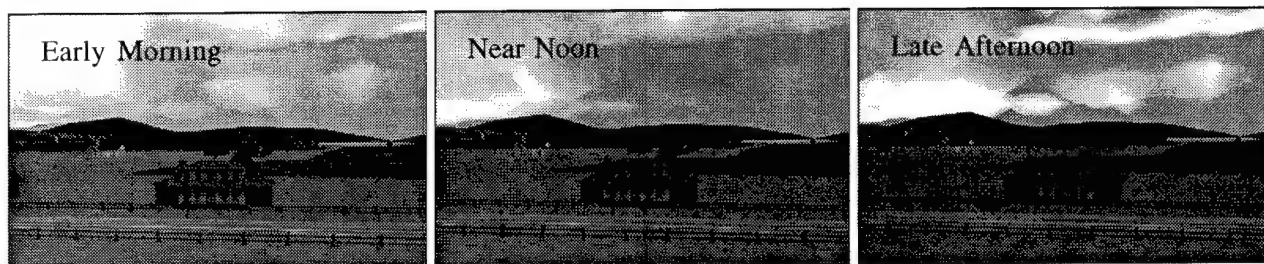


Figure 4. CloudScape® VR - Vega™ views to the east of a CSSM-modeled stratus layer over Onyx Town.

The CloudScape® VR approach to visualizing weather clouds works equally well for rendering other volumetric phenomena, whether they are essentially opaque or transparent, or vary between the two extremes. Figure 5 shows a visualization of the dust cloud from a 1000-lb munition two minutes after detonation in Onyx Town. For this example CloudScape® VR was run together with SensorVision™ in Vega™. The image shows the view in a night vision sensor band. Figure 6 is the SAOimage display of the quantitative radiance values from the image in Figure 5.



Figure 5. CloudScape® VR - SensorVision™ visualization in a night vision sensor band of a dust cloud two minutes after detonation of a 1000-lb munition in Onyx Town.

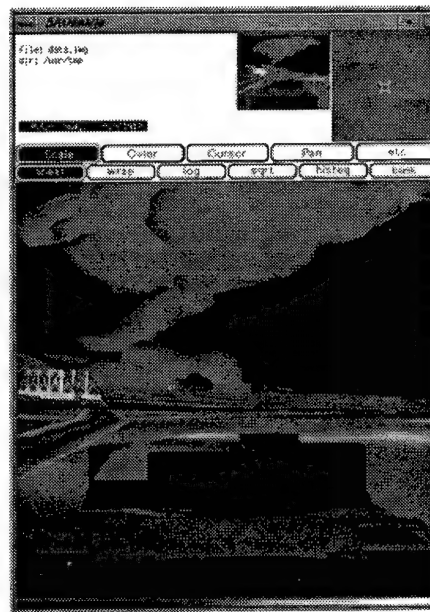


Figure 6. SAOimage display of the quantitative radiance values from the image in Figure 5.

4. UPGRADE PLANS

There are several upgrades planned for CloudScape® VR. Most important for visualizing weather clouds will be the application of texture. This upgrade will improve the rendering of small-scale cloud structure and also allow cloud databases to be constructed using fewer facets. A decrease in the number of facets improves rendering performance. For dynamically changing clouds, such as munitions dust clouds, the utilization of vertex morphing will result in smoother cloud evolution.

5. ACKNOWLEDGEMENTS

The authors are pleased to acknowledge the kind support and encouragement of Dr. William Blumberg and Dr. Laila Jeong who monitored the CloudScape® SBIR development effort. CloudScape® VR development and commercialization also benefitted from the contributions of Mr. David Anding of Photon Simulations, Inc., and Mr. Alex Szabo of Szabo Software, Inc., who were subcontractors on the Phase II SBIR effort.

6. REFERENCES AND FOOTNOTES

- ² Ciancolo, M.E., and M.E. Raffensberger, Atmospheric Scene Simulation Modeling and Visualization (AMV): Cloud Scene Simulation Model User's Guide, TIM-07169-2, TASC, Reading, MA, April 1996.
- ³ Thomas, M.E., and D.D. Duncan, "Atmospheric Transmission," in Atmospheric Propagation of Radiation, The IR/EO Systems Handbook, Volume 2, Smith, F.G., ed., ERIM, 1993.
- ⁴ Ewing, L.E., et al., The ROSCOE Manual, Volume 31, Sight Path Integration, DNA-001-76-C-0237, Defense Nuclear Agency, Alexandria, VA, 1978., 1978.
- ⁵ Lorenson, W.E., and H.E. Cline, "Marching Cubes: A High-Resolution 3-D Surface Construction Algorithm", Computer Graphics (ACM SIGGRAPH '87 Conference Proceedings), 1987.
- ⁶ DeVore, J. G., J. H. Thompson, and R. J. Thornburg, "Physics-Based Background Visualization from Volumetric Cloud Descriptions Using CloudScape™", Proceedings of the IRIS Specialty Group Meeting on Targets, Backgrounds, and Discrimination, Sandia National Laboratory, Albuquerque, NM, 1996.
- ⁷ Cornette, W.M., P.K. Acharya, D.C. Robertson, and G.P. Anderson, Moderate Spectral Atmospheric Radiance and Transmittance Code (MOSART), Version 1, (4 volumes), Phillips Laboratory, Geophysics Directorate, Hanscom AFB, MA, 1994.
- ⁸ VanHilst, M., "SAOimage", Bulletin of the American Astronomical Society, 22, p. 935, 1990.

CLOUD GENERATION USING RENDERWORLD

Karl Garrison, Harry Bishop, and David A. Wasson
Areté Associates

Manuscript not available at time of printing. Please contact author for further information.

Visualization Of Cloud Effects In Battle-scene Modeling And Simulation

Steven M. Ayer, Joel B. Mozer
USAF Phillips Laboratory, GPOF
29 Randolph Road
Hanscom Air Force Base, Massachusetts 01731-3010

Abstract

DoD modeling and simulation applications are increasingly seeking fast methods for visualization of realistic clouds as a method for gauging atmospheric effects on missions during planning, rehearsal and training. A three-dimensional cloud field, however, does not lend itself easily to conventional visualization techniques, which involve the description of scene objects with polygon shapes. These fast algorithms tend to produce flat, blocky cloud pictures, characteristics that are aggravated by camera motion through the volume. Physically realistic modeling typically requires radiative transfer calculations that reveal the complex shape and light scattering effects of clouds, but the time necessary to produce a single image is prohibitive for real-time rendering requirements.

We present a technique that uses three-dimensional texture-mapping to render clouds realistically in near real-time. Clouds are easily integrated into scene rendering software written employing OpenGL libraries and SGI's specialized texture-mapping hardware. The cloud data visualized by this software are produced using USAF Phillips Laboratory's Cloud Scene Simulation Model (CSSM), which uses fractal and physics-based techniques to produce synthetic fields of liquid water content corresponding to atmospheric clouds.

1. Introduction

The cloud visualization technique presented in this work grew from a desire to meld the benefits of fast, hardware-based volume rendering with the physically accurate images obtained by radiative transfer calculations performed on a cloud field; a process too slow for real-time simulations.

Since clouds are characteristically form-less objects, they are not amenable to traditional polygon rendering methods. Some cloud rendering techniques utilize a 2D texture, where the image of a cloud is draped as a translucent decal over a polygon. One common method uses a single polygon representing a plane transecting a cloud field, appropriately known as "billboarding," because as the viewer moves close to the clouds, they appear as if drawn on a billboard. Another method attempts to mimic the shapes of clouds using polygons, which typically produces tent-like objects. These techniques offer a fair visual representation when viewed from great distance, but suffer from a lack of depth and no fine detail, making this method unattractive for fly-through simulations.

Three-dimensional texture-mapping is a natural fit with the cloud visualization problem because this texture is also a form-less structure. The cloud model used as data input to the visualization technique presented here is the Phillips Laboratory Cloud Scene Simulation Model (CSSM). Using extensions to Silicon Graphics (SGI) OpenGL libraries, CSSM cloud fields are visualized realistically with sufficient frame rate and close detail for fly-through simulations.

2. Data Input

The CSSM produces a gridded field of cloud liquid water content. The model is fractal and physics-based and takes inputs of meteorological, topographical, and cloud parameter data. More detailed information regarding the CSSM is given in Cianciolo et al [1] as well as several companion papers in

this pre-print volume. [2] The spatial and temporal resolution of the output field is user-specified. The cloud field used during development of this technique measured $6.4 \times 6.4 \times 6.4$ km, with cell resolution of 100 m. The cloud parameters specified an 80 percent cumulus field with cloud bottom at 700m.

An optical properties tool called Fastmap was used to derive optical depth information from the CSSM output. [1] Fastmap uses lookup tables – constructed by a radiative transfer model – of optical and radiative properties to map CSSM liquid water content to particle-size distribution information and graphical quantities such as extinction optical depth in both infrared and visible spectra.

3. Rendering Environment

We used the Phillips Laboratory Weather Impact Decision Aids (WIDA) program's Infra-Red Target Scene Simulation Software (IRTSS) software as a visualization environment in which to develop this cloud rendering capability. IRTSS renders radiometrically-correct target high-resolution terrain scenes in both the IR and visible spectra at a high frame rate using OpenGL, hardware polygon rendering and texture-mapping. The IRTSS rendered visible spectrum scenes for this project.

4. Technique

The format of the CSSM/Fastmap output was well-suited to the 3D texture supported by an SGI OpenGL library extension. The software developed in the work converts the liquid water content grid of a CSSM output file directly into a rasterized texture image. At present, cloud rendering is in the visible spectrum, where liquid water content modulates opacity of the texture.

The cloud texture is visible only where a polygon provides a surface upon which to map the texture volume; the texture is drawn on the intersecting plane of the polygon. To provide detail and depth to the scene, a method was created to draw a series of polygons that transect the texture volume parallel to one another and perpendicular to the frame view-vector.

Recognizing that the cloud field is bounded by the data domain, each polygon shares these boundaries, and therefore has a variable number of vertices depending upon the view angle and number of boundaries the polygon intersects. Since these polygons are drawn only to reveal the cloud texture, only the texture's color and opacity contribute to the rendered scene. The method of drawing perpendicular to the viewing angle eliminates most polygon artifacts when viewing the volume from an oblique angle or near the cloud volume borders.

In keeping with a physics-based visualization, we determine the radiance field through a Beer's law attenuation calculation [3] for setting cloud brightness values. Simply, we wanted to preserve the facts that 1) clouds are darker on the bottom, and 2) there is less ambient light beneath a cloud deck than above it.

The software ray-traces the Fastmap extinction coefficient grid produced from the input CSSM clouds, from each grid cell toward a hypothetical distant light source above the cloud field once while collecting cloud data. The software then integrates extinction optical depth along this path, then uses the value to estimate cloud brightness for each grid cell.

5. Implementation and Performance

Implementation is in C using OpenGL for rendering and the SGI graphics extension for 3D texture manipulation. Rendering is performed on an SGI Indigo2 High Impact workstation, with 192M core memory and 4M texture memory. The texture format is four-channel red-green-blue-alpha bytes. The IRTSS loaded a terrain grid of approximately 24×24 km.

Four different CSSM cloud fields were loaded during performance testing, ranging from 4K to 1M grid cells. For each cloud grid, the number of sampling polygons varied from approximately 400 down to

1. This last case produced no usable images, but exhibited the limiting factor in rendering speed. Also, two different image sizes were rendered in order to establish the relationship between texture memory saturation, the number of polygons drawn, and the number of pixels rendered.

As illustrated by the left graph in Figure 1, the number of polygons sampling the texture dominates other governing parameters in rendering speed. Interestingly, varying the texture size affected rendering speed proportionally little, and increasing the number of image pixels by more than 2.5 times typically affected rendering speed by less than a factor of 2.

The number of grid cells represented in the texture and the number of sampling polygons affect the realism of the images most dramatically. The right graph illustrates a breakpoint in scaled rendering speed at about 130 polygons. Coincidentally, as the number of polygon samples decreases from that point, the image quality degrades very rapidly.

Optimally, the ratio of polygon samples to the number of grid cells in any direction should be 2:1 or higher to render high-quality images. For example, approximately 130 polygon samples of a 64x64x64 gridded texture produces good results. Also, a terrain size to cloud data ratio of 4:1 or lower gives good results. For example, using 100m cloud resolution as a benchmark, the 6.4km³ cloud grid used with the 24km² terrain grid during development is minimal by this standard. The hardware-implemented interpolation routines failed to provide useful detail fewer cloud data.

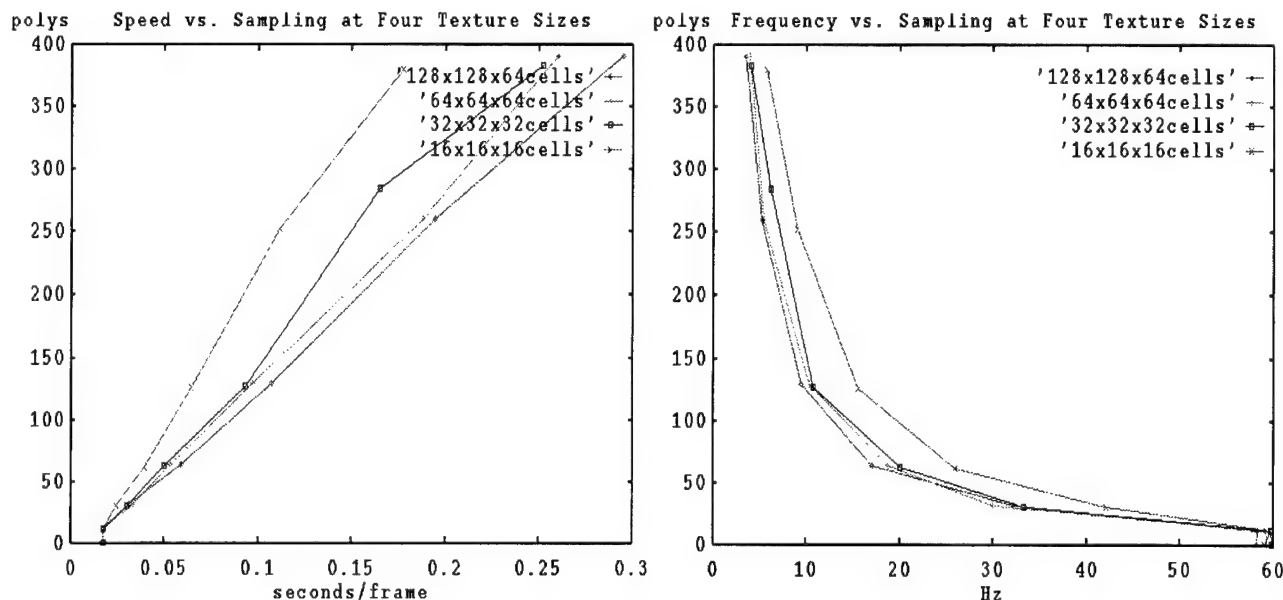


Figure 1: Left graph: Rendering speed vs. the number of texture sampling polygons. Note linearity and how little effect size of texture has on speed. Right graph: Rendering frequency vs. sampling polygons. Note breakpoint (in box) where slope flattens but image quality degrades rapidly.

6. Future Directions

We have two short-term goals for enhancing this cloud-rendering technique, both addressing needs of the WIDA program and the DoD modeling and simulation community at large. The first is to render clouds in the IR so that IRTSS can generate a complete atmospheric effects suite to its weather-impact simulations. The second meshes with the first, which is to add more elaborate radiative transfer calculations to the cloud rendering framework. This improvement will add radiometric correctness to

the clouds, a requirement if this cloud visualization technique becomes a part of the production IRTSS, which simulates target scenes from the perspective of a weapons sensor. Clouds create probably the single most profound and unpredictable adversity in any given airborne mission, so this will constitute a critical addition to a physically-validated modeling and simulation application.

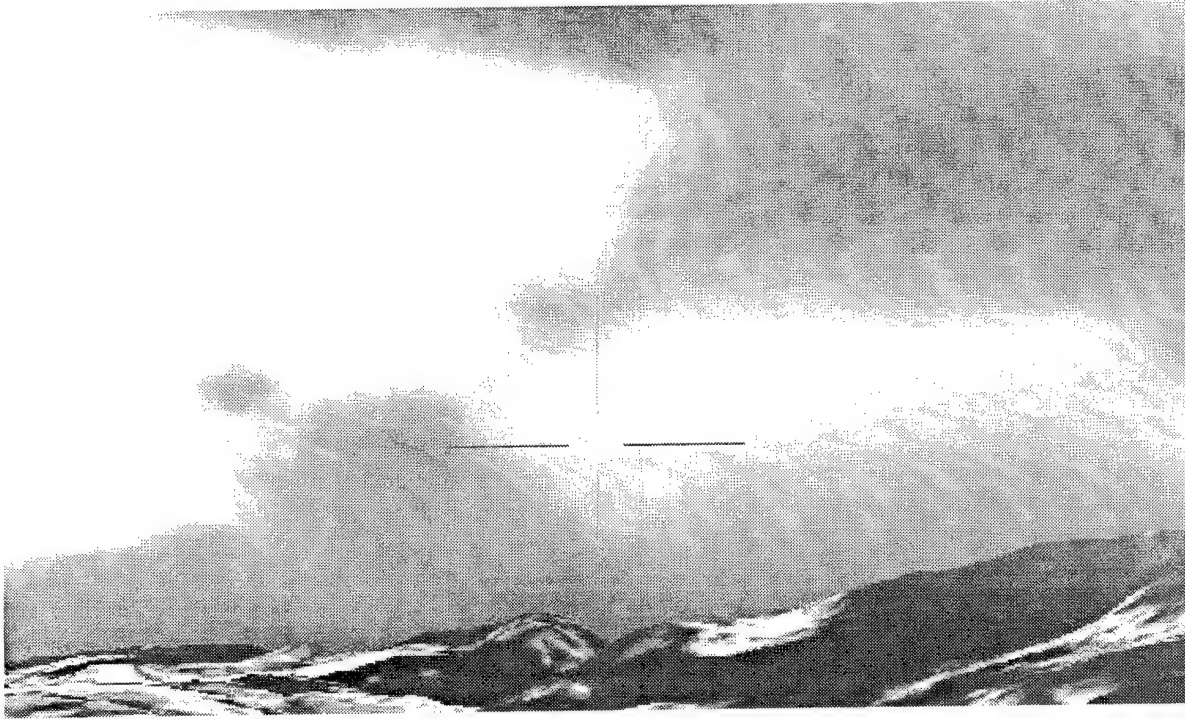


Figure 2: Low altitude stratocumulus rendered over a mountainous region.

7. Conclusions

Through the use of 3D texture-mapping, realistic cloud scenes can be visualized at a relatively high frame rate with sufficient fine detail for use in fly-through simulations. Furthermore, clouds can be introduced into DoD modeling and simulation packages to ameliorate mission planning efforts by adding visually accurate atmospheric effects to a battlescene.

Acknowledgments

We thank Stan Heckman, who was instrumental to the development of the sampling polygon scheme, and Guy Seeley, the author of IRTSS, who kept us sane while we juggled coordinate systems.

References

- [1] Cianciolo, M.E., M.E. Raffensberger, E.O. Schmidt, J.R. Stearns, 1996: Atmospheric scene simulation modeling and visualization. PL-TR-96-2079, USAF Phillips Laboratory, Hanscom AFB, MA. ADA312179
- [2] Mozer, J.B., Ayer, S.M., Seeley, G.P., Cianciolo, M.E., "Cloud Transmission Effects in Distributed Simulation," *CIDOS 97*, September 1997.
- [3] Max, Nelson, "Optical Model for Direct Volume Rendering," *IEEE Transactions on Visualization and Computer Graphics*, Volume 1 Number 2, June 1995.

AIRBORNE CLOUD CHARACTERIZATION FOR RADIOMETRIC SENSORS

Brian J. Morrison, James Jung, and R. Lynn Rose
Aeromet, Inc.
Tulsa, OK 74037

ABSTRACT

Accurate knowledge of the macro- and micro-physical cloud environment during target viewing can be essential for defining uncertainties involved in making radiometric measurements with remote sensors. The High Altitude Reconnaissance Platform (HARP), a Learjet 36A, carries an instrument suite comprising a measurement system specially suited and cost-effective for cloud characterization. This paper illustrates how data from the HARP were analyzed to characterize the cloud environment for two recent DoD programs concerned with optical discrimination of target signatures. The application of these results to radiometric measurements is discussed.

1. INTRODUCTION

Radiometric sensors are becoming ever more sensitive with higher resolutions. This can make them more susceptible to noise introduced by the cloud environment, particularly over visible and infrared wavelengths. Quantification of the cloud macro- and micro-physical environment during viewing events can be essential to reducing the uncertainties in radiometric measurements of targets. When these measurements are conducted through large atmospheric volumes with multiple sensors at different locations, obtaining a meaningful cloud characterization can be difficult.

A high-performance airborne platform capable of in-situ and remote cloud observations can obtain temporally and spatially coherent data to accurately characterize the cloud environment. Aeromet's High Altitude Reconnaissance Platform (HARP), a Learjet 36A, is well suited for this purpose and carries a unique suite of in-situ and remote sensors for conducting cloud characterization. The HARP recently participated in two DoD operations for this purpose. Examples of the data collected and analyses performed for these programs will be presented. Additionally, the utility of this information for reducing the error in radiometric observations will be discussed.

2. THE HARP: AN AIRBORNE MEASUREMENT SYSTEM FOR CLOUD CHARACTERIZATION

The HARP is a Learjet 36A that can be configured with a wide variety of instruments for atmospheric characterization. Its relatively high speed (0.8 Mach), rate of climb, and service ceiling (45 kft) make it possible to conduct sampling through a large region in a relatively short period of time. Additionally, the HARP can easily change flight profiles to rapidly adapt to dynamically changing environmental conditions or mission configurations. The conventional business jet origins of the aircraft permit relatively low cost operation and maintenance.

The instrument suite utilized for cloud characterization consists of three main components: A dual wavelength lidar, a K_a -band radar, and a set of Particle Measuring Systems (PMS) cloud particle probes. The lidar is typically used for detecting and measuring high altitude cirrus. It is especially useful for sub-visual cirrus and during night missions when thin high clouds are not easily observed. The radar provides a detailed two-dimensional cross-section of reflectivity measurements below the aircraft's flight path. The cloud particle probes provide in-situ measurements of particle sizes and concentrations and information on particle habits (shapes). In addition to the information obtained independently from these sensors, the in-situ measurements can be correlated with the remote sensing data from the lidar and radar to derive vertical and horizontal

profiles of microphysical quantities within the sampled atmospheric volumes. These results can then be used to analyze the radiative environment or customize atmospheres in radiative transfer models. In this way, the contributions of the cloud environment to radiometric observations can be quantified.

3. CLOUD CHARACTERIZATION FOR SBIRS

In 1995 and 1996 the HARP participated in several missions for the U.S. Air Force's Space-Based Infrared Systems (SBIRS) phenomenology program (Morrison, *et. al.*, 1997). Field tests were conducted to collect detailed cloud scene data to evaluate potential satellite surveillance systems' response to background signals generated by clouds. The HARP's role was to collect data on the microphysical characteristics of the observed clouds and obtain measurements of their vertical and horizontal dimensions. These observations were conducted in conjunction with ground-based lidars and radars, meteorological satellites, and multispectral imaging from satellite and airborne platforms. This engendered a *synoptic* approach to cloud characterization to provide observations that were co-located in space and time with the other sensors. The HARP generally flew a pattern that would repeatedly take it over the ground-based sensors. The flight altitude was systematically varied to sample the cloud layers of greatest interest.

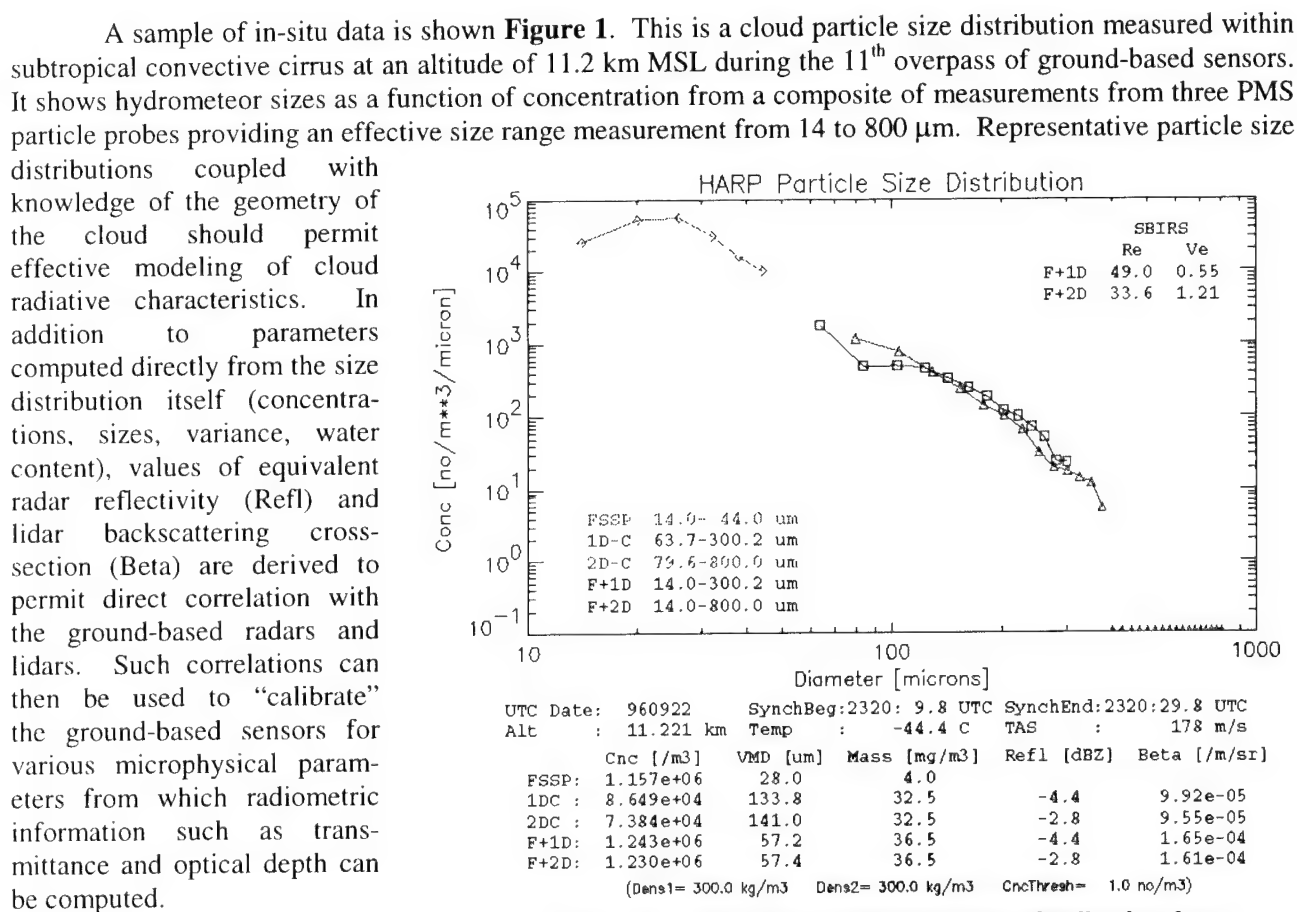


Figure 1 – Example of a particle size distribution from convective cirrus over Everglades City, Florida.

Macro-physical data were collected on cloud layers, thicknesses, horizontal dimensions, and structure using the K_a-band radar and lidar. Data from the radar were processed and displayed as vertical cross-sections of equivalent radar reflectivity along the flight track below the aircraft (**Figure 2**). The data are color-coded according to equivalent reflectivity in dBZ. For positional reference the HARP flight track and altitude profiles are shown to the left of the radar image and any ground based sensor overpasses are indicated on the radar image. In addition to groups of radar images, animations in the same display format were built from sequential radar images stepping forward in 15 second intervals over an entire flight. This permits easy

viewing of an entire flight's data allowing for a better grasp of continuity and the ability to select any time interval of interest from a single file. Lidar data were displayed in a similar format, but as vertical depictions of backscattering cross-section (Beta) above the aircraft.

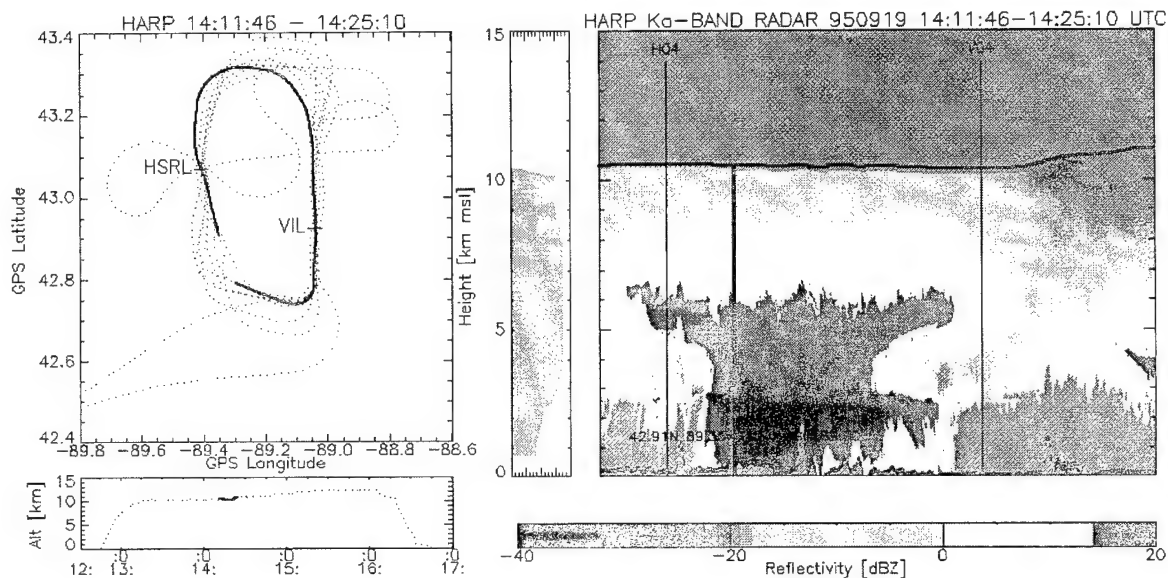


Figure 2 – Example of combined K_a-band radar image and flight track plot during a mission flight over deep convection near Madison, WI. H04 and V04 designate ground-based lidar overpasses.

4. TROPICAL CENTRAL PACIFIC: A STATISTICAL APPROACH TO CLOUD CHARACTERIZATION FOR OPTICAL SENSORS

Cloud characterization for multiple mobile optical sensors observing a single short time period ballistic event over the central tropical Pacific required a different approach to cloud characterization. In this case there were no other cloud sensors and the viewing geometries of the optical sensors differed through large volumes of the atmosphere. The sampling strategy was to obtain as much 3-dimensional high cloud data as possible through the viewing volumes using the airborne lidar. Microphysical parameters were then computed from the lidar measurements utilizing relationships derived from in-situ data sampling runs; a technique referred to as *sensor fusion*. A *statistical* methodology was then employed to derive average, best-case, and worst-case vertical profiles of selected microphysical parameters relative to each mobile sensor.

An example of the application of this technique to obtain water content profiles from the data collected during one mission flight is illustrated in **Figures 3 and 4**. The relationship between backscattering cross-section (Beta) and equivalent liquid water content (LWC) that was derived from in-situ measurements is shown in **Figure 3**. By applying this relationship to values of backscattering cross-section from the lidar collected through one of the mobile sensors sampling volumes, a vertical profile of liquid water is obtained (**Figure 4**). Note that an average profile is displayed with values plus and minus one standard deviation shown to each side, suggesting average, best, and worst-case conditions.

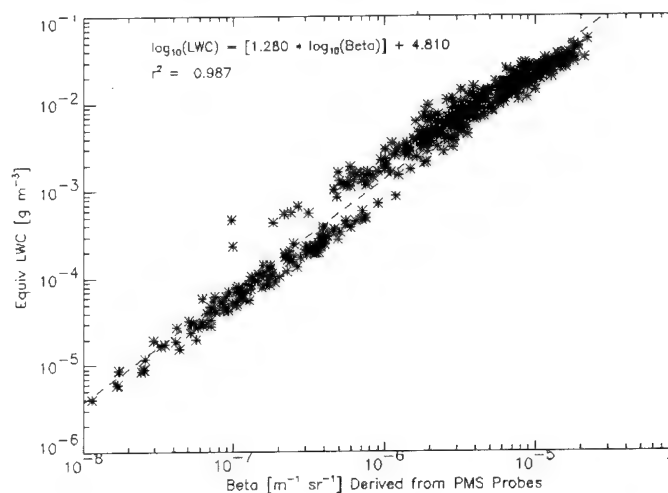


Figure 3 - Relationship between backscattering cross-section (Beta) and liquid water content (LWC) for in-situ cloud measurements above 10.5 km.

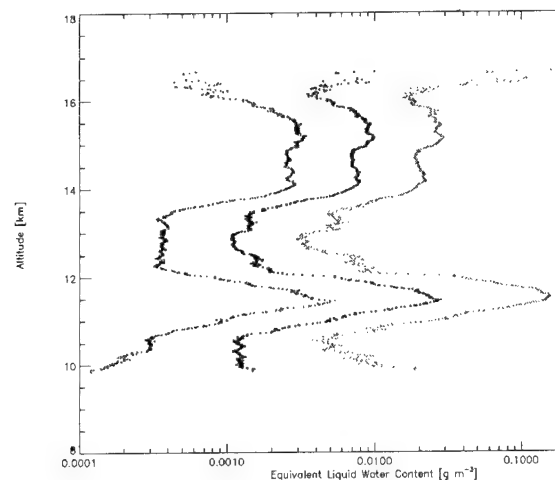


Figure 4 - Mean and standard deviations of vertical profiles of liquid water content obtained from the sensor fusion technique.

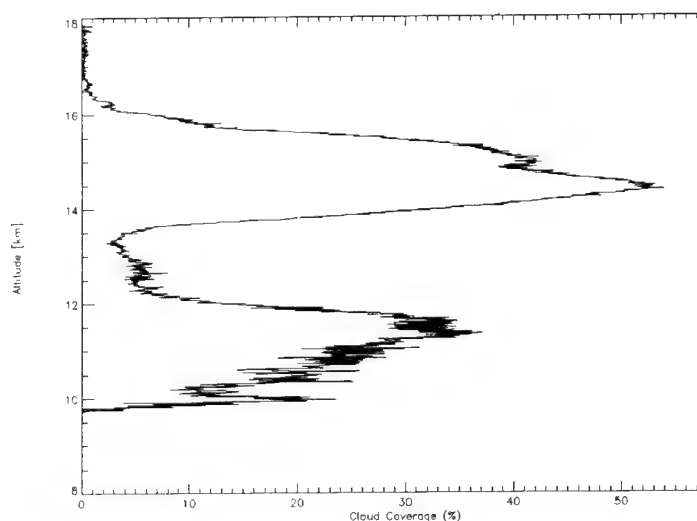


Figure 5- Lidar derived percent cloud coverage vs. altitude.

provide sufficient information to calculate radiative properties of clouds in the radiometric sensors' fields of view. The impact of clouds on critical measurements can be assessed, reducing the uncertainties in radiometric measurements.

5. ACKNOWLEDGEMENTS

This study was funded under contract number LMSC SHAGJO501F for work being done under contract to Lockheed for the U.S. Air Force.

6. REFERENCES

Morrison, B.J., R. Hobbs, D. Rusk, J. Jung, and R.L. Rose, 1997: The High Altitude Reconnaissance Platform (HARP) SBIRS Final Report.

AN ANIMATED VIEW OF GLOBAL WATER VAPOR, 1988–1994

Thomas H. Vonder Haar, Mark A. Ringerud, David L. Randel,
Graeme L. Stephens, and Donald L. Reinke
Science and Technology Corporation – METSAT

Manuscript not available at time of printing. Please contact author for further information.

APPENDIX A
AGENDA

CLOUD IMPACTS ON DOD OPERATIONS AND SYSTEMS 1997 CONFERENCE

Naval War College, Sims Building, Nott Auditorium
Newport, Rhode Island
23–25 September 1997

Theme

“CLOUD EFFECTS IN WAR GAMING, MODELING, AND SIMULATION”

TUESDAY, 23 SEPTEMBER 1997

0800 – 0900 REGISTRATION

Naval War College, Sims Building Lobby

SESSION I. INTRODUCTION

Conference Chair: **Paul Tattelman**, Phillips Laboratory, Geophysics Directorate

0900 – 0910 Administrative Remarks

Paul Tattelman, Phillips Laboratory, Geophysics Directorate

LCDR Bruce Kitchen, Naval Training for Meteorology and Oceanography
Detachment Newport

0910 – 0920 Welcome

Captain Fred G. Orchard, Director, Naval War College War Gaming Department

0920 – 0945 Introductory Address

Colonel Alan R. Shaffer, U.S. Air Force Assistant for Battlespace Environment, Office of
Defense Research and Engineering

0945 – 1020 Keynote Address

Rear Admiral Paul E. Tobin, Jr., U.S. Navy, Oceanographer of the Navy

1020 – 1050 BREAK

SESSION II. PROGRAM REVIEWS

Chair: **CDR Timothy Cummings**, Office of Executive Agent for Air and Space Natural Environment

1050 – 1110 Modeling and Simulating Clouds and Visibility: The MSEA Perspective

Gary B. McWilliams, Office of Executive Agent for Air and Space Natural Environment

1110 – 1130 National Polar Orbiting Environmental Satellite System (NPOESS)

Col John A. Goyette, U.S. Air Force National Polar Orbiting Environmental Satellite
System/IPA Deputy Director

1130 – 1150 Integrating Weather Exploitation into Air and Space Power Doctrine Using Modeling and Simulation
Lt Col John M. Lanicci, Headquarters, U.S. Air Force, Directorate of Command and Control

1150 – 1315 **LUNCH BREAK**

1315 – 1335 THE MASTER ENVIRONMENTAL LIBRARY: An Environmental Data Source for DoD Applications
Richard A. Siquig, Naval Research Laboratory; Steven J. Lowe, SAIC

1335 – 1355 TAOS and High-Fidelity Virtual Environments for STOW
David Whitney, Robert Reynolds, Steve Olson, Peter Dailey, Dana Sherer, and Mavis Driscoll, TASC

1355 – 1415 Environmental Representation and the Role of Clouds in Studies and Analysis Models
John R. Hummel and A. Peter Campbell, Argonne National Laboratory

**SESSION III: CLOUD M&S APPLICATIONS TO WAR GAMING
STUDIES, AND ANALYSES**

Co-Chairs: **CDR George Davis**, Naval War College
LCDR Bruce Kitchen, Naval Training for Meteorology and Oceanography Detachment Newport

1415 – 1435 The Impact of Clouds on an Engagement-Level Simulation
Capt Mark M. Edwards, Capt Edward E. Hume, and Lt Col Frank A. Zawada, Phillips Laboratory, Geophysics Directorate

1435 – 1455 Cloud Transmission Effects in a Distributed Simulation
Joel B. Mozer, Steven M. Ayer, and Guy P. Seeley, Phillips Laboratory, Geophysics Directorate; Maureen Cianciolo, TASC

1455 – 1525 **BREAK**

1525 – 1545 Cloud Simulation for a Flight Mission Rehearsal System
Louis Hembree, Naval Research Laboratory

1545 – 1605 Simulating Thin-Cloud Effects on Multi-Spectral Target Detection
Joseph G. Shanks and Frederick C. Mertz, Photon Research Associates, Inc.; William A.M. Blumberg, Phillips Laboratory, Geophysics Directorate

1605 – 1625 Cloud Modeling and Infrared Spatial Structure
Robert A. McClatchey, Robert J. Jordano, and A.T. Stair, Jr., Visidyne, Inc.; Col William Smith, BMDO/TOS

1625 – 1700 3-minute overview of poster presentations

1650 **End of Day 1**

1800 – 2100 **SOCIAL and Poster Session**
Commissioned Officer's Club

WEDNESDAY, 24 SEPTEMBER 1997

0800 REGISTRATION
Naval War College, Sims Building Lobby

SESSION IV: CLOUD AND CLOUD EFFECTS MODELING
Co-Chairs: **Raymond Godin**, Office of the Oceanographer of the Navy
George Koenig, Cold Region Research Engineering Laboratory

- 0830 – 0850 MODTRAN4: Simulating Atmospheric Radiation Budgets for Clouded Atmospheres**
Gail P. Anderson and J.H. Chetwynd, Phillips Laboratory, Geophysics Directorate; A. Berk, L.S. Bernstein, and P.K. Acharya, Spectral Sciences, Inc.; H.E. Snell, Atmospheric and Environmental Research, Inc.; E.P. Shettle, Naval Research Laboratory
- 0850 – 0910 Radiometric Validation of CSSM**
Joel B. Mozer and Guy P. Seeley, Phillips Laboratory, Geophysics Directorate; Alan Wetmore, Patti Gillespie, David Ligon, and Samuel Crow, Army Research Laboratory
- 0910 – 0930 Validation of Cloudscape® AF with Aircraft Data**
Ross J. Thornburg, John G. DeVore, James H. Thompson, Robert J. Jordano, and Timothy L. Stephens, Visidyne, Inc.
- 0930 – 0950 Cloud Phenomenology Relevant to Space Based Infrared Systems**
Hsiao-hua K. Burke and J. William Snow, MIT Lincoln Laboratory; Capt David O'Donnell, United States Air Force
- 0950 – 1020 BREAK**
- 1020 – 1040 Atmospheric Correction Through Transmissive Clouds**
J. William Snow, Hsiao-hua K. Burke, Michael P. Jordan, Daniel C. Peduzzi, and Kristine E. Rhoades, MIT Lincoln Laboratory
- 1040 – 1100 The Fractal Behavior of Cloud Systems**
Kenneth E. Eis, John M. Forsythe, and Donald L. Reinke, Cooperative Institute for Research in the Atmosphere, Colorado State University
- 1100 – 1120 A Method for Calculation of Near-Horizontal Cloud Free Line of Sight Probabilities**
Eric L. Strobel and Dwayne Pribik, Schafer Corporation
- 1120 – 1140 A Relocatable Climate Window for Generating Cloud Scenarios Including Structure and Physical Attributes**
Albert R. Boehm, Hughes STX Corporation
- 1140 – 1200 Dense Cloud Radiative Transfer Scenarios and Model Validation**
David H. Tofsted, Army Research Laboratory; Sean G. O'Brien, Physical Science Laboratory
- 1200 – 1215 3-minute overview of PC/Video poster presentations**

1215 – 1315 **LUNCH BREAK**

1315 – 1400 PC/Video Poster Session in Nott Auditorium

1400 – 1420 Lattice Boltzmann Equation Models: A New Approach for Microscopic Simulation of Cloud Physics

Xiaowen Shan and Joel B. Mozer, Phillips Laboratory, Geophysics Directorate

1420 – 1440 A Lattice Boltzmann Cloud Model with Moisture Parameterization

Susan Triantafyllou, Xiaowen Shan, and Joel B. Mozer, Phillips Laboratory, Geophysics Directorate

1440 – 1510 **BREAK**

SESSION V: CLOUD PREDICTION

Chair: **Maj Paul Bellaire**, Air Force Office of Scientific Research

1510 – 1530 Diagnosis of Cloud Variables from Mesoscale Numerical Weather Prediction Model Forecasts
Donald C. Norquist, Phillips Laboratory, Geophysics Directorate

1530 – 1550 Statistical Contrail Forecasting

Artie Jackson, Brian Newton, Doug Hahn, and Allan Bussey, Phillips Laboratory, Geophysics Directorate

1550 – 1610 ADVCLD: Air Force Global Weather Center's Updated Cloud Forecast Model

Thomas J. Kopp, Margaret M. Wonsick, Louis E. Cantrell, and Francis D. Bieker, Headquarters, U.S. Air Force Global Weather Central

1610 – 1630 Cloudy Regions Below the Marine Stratus Deck

James W. Telford, Atmospheric Concepts

1630 – 1650 Ensemble Cloud Modeling for Mesoscale Forecast

Ted Yamada, Yamada Science & Art Corporation

1650 – 1710 The Cloud Depiction and Forecast System II Nephanalysis Model

Gary B. Gustafson and Ronald G. Isaacs, Atmospheric and Environmental Research, Inc.; Bonnie McDonald, Sterling Software, Inc.

1710 **End of Day 2**

THURSDAY, 25 SEPTEMBER 1997

SESSION VI: MEASUREMENT SYSTEMS AND SENSORS

Co-Chairs: **William Denig**, Phillips Laboratory

Richard Shirkey, Army Research Laboratory

0800 REGISTRATION

Naval War College, Sims Building Lobby

0830 – 0850 Optimal Visualization of Multispectral and Multisensor Environmental Satellite Data
Robert P. d'Entremont, Joanne Zhou, and Karen Cady-Pereira, Atmospheric and Environmental Research, Inc.; James T. Bunting, Phillips Laboratory, Geophysics Directorate

0850 – 0910 CloudSat: A Spacecraft to Measure the Vertical Structure of Clouds
Steven J. Walter, Deborah G. Vane, and Fuk K. Li, Jet Propulsion Laboratory, California Institute of Technology; Graeme L. Stephens, Colorado State University

0910 – 0930 Cloud Analysis During the NPOESS ERA
Gary B. Gustafson, Robert P. d'Entremont, David P. Hogan, and Ronald G. Isaacs, Atmospheric and Environmental Research, Inc.

0930 – 0950 Use of Reconnaissance Assets in Support of Theater Weather
Maj Michael S. Kapel, Capt John F. Polander, and Steven P. Weaver, 88th Weather Squadron; Jeffrey Pesler, Aeronautical Systems Center, Reconnaissance Program Office

0950 – 1020 BREAK

1020 – 1040 NASA DC-8 Airborne Scanning Lidar Cloud and Contrail Observations
Edward E. Uthe, Terje E. Oseberg, and Norman B. Nielsen, SRI International

1040 – 1100 Cloud Database Collected in Support of the Space-Based Infrared System (SBIRS) Phenomenology Exploitation Program
Thomas R. Caudill, William A.M. Blumberg, and Alan Griffin, and John Wise, Phillips Laboratory; Geophysics Directorate; Capt David J. O'Donnell, Space and Missile Systems Center

1100 – 1120 Lidar Observations Provide Information on the 3-Dimensional Structure and Optical Properties of Clouds Required for Scene Generation
Edwin W. Eloranta, University of Wisconsin-Madison

1120 – 1140 Comparison of Satellite-Based Cirrus Retrievals with Coincident Ground-Based Radar and Lidar Observations
Robert P. d'Entremont and Gary B. Gustafson, Atmospheric and Environmental Research, Inc.; Thomas R. Caudill, Phillips Laboratory, Geophysics Directorate

1140 – 1155 3-minute overview of PC/Video poster presentations

1155 – 1315 LUNCH BREAK

1315 – 1400 PC/Video Poster Session in Nott Auditorium

- 1400 – 1420 Airborne Retrieval of Cirrus Cloud Temperature and Composition Using ARES 5.1-5.3 μm and 3.7 μm Radiance Data
Steve C. Ou, K.N. Liou, P. Yang, and P. Polland, University of Utah; Thomas R. Caudill, Phillips Laboratory, Geophysics Directorate; J. Lisowski, SCITEC;
Brian J. Morrison, Aeromet, Inc.

SESSION VII: CLOUD DATASETS

Chair: **LTC Lauraleen O'Connor**, National Polar Orbiting Environmental Satellite System

- 1420 – 1440 Global Cloud Data for System Design and Simulation
Donald Wylie, University of Wisconsin-Madison; W. Paul Menzel, NOAA/NESDIS
- 1440 – 1500 Global High-Resolution Layered Cloud Database—Research and Development at the Cooperative Institute for Research in the Atmosphere, Colorado State University
Donald L. Reinke, John M. Forsythe, and Thomas H. Vonder Haar, Colorado State University
- 1500 – 1530 **BREAK**
- 1530 – 1550 Overview and Objectives of the DoD Center for Geosciences Sponsored “Complex Layered Cloud Experiment” (CLEX)
Thomas H. Vonder Haar, Stephen K. Cox, Graeme L. Stephens, John M. Davis, Timothy L. Schneider, Walter A. Petersen, Arlie C. Huffman, Kenneth E. Eis, **Donald L. Reinke**, and John M. Forsythe, Colorado State University; Fuk K. Li, NASA Jet Propulsion Laboratory; Gregory A. Sadowy, University of Massachusetts
- 1550 – 1610 Ground-Based Digital Cloud Imagery Analysis and Applications
Robert P. Wright, **Stanley H. Grigsby**, and Robert M. Holt, Planning Systems, Inc.
- 1610 – 1630 Cloud Data Generation System
Jeffrey S. Morrison and Steven L. Rubin, TASC
- 1630 **End of Day 3**
- CIDOS-97 Adjournment**

POSTER/PC/VIDEO PRESENTATIONS

TUESDAY, 23 SEPTEMBER 1997

1800 – 2100 SOCIAL and Poster Session, Commissioned Officer's Club

WWW-Based Cloud Information Reference Library and Archive (CIRLA)

John C. Burgeson and Paul D. Try, Science and Technology Corporation;
Donald D. Grantham, Phillips Laboratory, Geophysics Directorate

Cloud Detection/Editing Experiments on the *Lewis* and *Clark* Satellites

Richard E. Davis, R. Gale Wilson, and Robert L. Jones, NASA Langley Research Center

Single-Channel Cloud Detection Using Land-Surface Bidirectional Reflectance Distribution Functions

Robert P. d'Entremont, Atmospheric and Environmental Research, Inc.

A Fused Method of Determining Soil Moisture Using High Resolution Geostationary Imagery

Kenneth E. Eis, and Andrew S. Jones, Cooperative Institute for Research in the Atmosphere,
Colorado State University

The Optical Properties of Sub-Tropical Cirrus Clouds Derived from the University of Wisconsin High Spectral Resolution Lidar

Edwin W. Eloranta, University of Wisconsin-Madison

Particle Measurement and Analysis Criteria for Intercomparison with Numerical Models of Radiative Cloud Properties

W. Patrick Arnott, **John Hallett**, and Matthew Meyers, Desert Research Institute

Post Engagement Ground Effects Model

Kevin W. Bruening and Jason A. Wampler, MEVATEC Corporation;
Julius Q. Lilly, U.S. Army Space and Strategic Defense Command

Time Series Cloud Forcing Study of Cloud Scene Simulation Model

Guy P. Seeley, Joel B. Mozer, and Erol Emre, Phillips Laboratory, Geophysics Directorate

State of the Battlespace: Cloud and Weather Effects Visualization for the Tactical Battlefield

Donald Hooch, **David H. Tofsted**, Richard Shirkey, and Jon Martin, Army Research Laboratory; John C. Giever, Physical Science Laboratory, New Mexico State University

Mobile Aircraft Icing Forecast System

Steven J. Walter and Philip I. Moyniha, Jet Propulsion Laboratory, California Institute of Technology

WEDNESDAY, 24 SEPTEMBER 1997

1315 – 1400 PC/Video Poster Session in Nott Auditorium

One Year of World Wide Cloud Cover

Arnold A. Barnes, Jr., Phillips Laboratory, Geophysics Directorate

The Cloud-Free Line-of-Sight Aloft (CFLOSA) PC Program

Albert R. Boehm, Hughes STX Corporation

Building an Improved Cirrus Model in the CSSM

Maureen E. Cianciolo, Mark E. Raffensberger, and Ryan B. Turkington, TASC

Cloudscape® VR: Radiometric Visualization of Clouds for Interactive Training and Simulation

John G. DeVore, James H. Thompson, Ken W. Sartor, Timothy L. Stephens, and
Ross J. Thornburg, Visidyne, Inc.

Cloud Generation Using RenderWorld

Karl Garrison, Harry Bishop, and David A. Wasson, Areté Associates

MEL Demo

Steve Lowe, Naval Research Laboratory

THURSDAY, 25 SEPTEMBER 1997

1315 – 1400 PC/Video Poster Session in Nott Auditorium

Visualization of Cloud Effects in Battlescene Modeling and Simulation

Steven M. Ayer and Joel B. Mozer, Phillips Laboratory, Geophysics Directorate

Airborne Cloud Characterization for Radiometric Sensors

Brian J. Morrison, James Jung, and **R. Lynn Rose**, Aeromet, Inc.

An Animated View of Global Water Vapor, 1988–1994

Thomas H. Vonder Haar, Mark A. Ringerud, David L. Randel, Graeme L. Stephens,
and Donald L. Reinke, Science and Technology Corporation – METSAT

APPENDIX B
List of Registered Attendees

CIDOS-97 LIST OF REGISTERED ATTENDEES

A

Dr. Michael D. Abel
Ball Aerospace & Technologies Corp
Systems Engineering Operations
2875 Presidential Drive, Suite 180
Fairborn, OH 45324
Tel: 937/320-4161
Fax: 937/429-1687
E-Mail: mabel@ball.com

Ms. Karen Allen
Mevatec Corporation
1525 Perimeter Parkway, Suite 500
Huntville, AL 35806
Tel: 205/890-8066
Fax: 205/890-8055
E-Mail: karen_allen@mevatec.com

Ms. Gail P. Anderson
PL/GD/GPOC
29 Randolph Road
Hanscom AFB, MA 01731
Tel: 617/377-2335
Fax: 617/377-8900
E-Mail: ganderson@plh.af.mil

Mr. Rodney L. Arndt
PL/GPBF
29 Randolph Road
Hanscom AFB, MA 01731-3010
Tel: 617/377-7881
Fax: 617/377-5974
E-Mail: arndt@plh.af.mil

Dr. Steven M. Ayer
Phillips Laboratory/GPOF
29 Randolph Road
Hanscom AFB, MA 01731-3010
Tel: 617/377-2959
Fax: 617/377-2984
E-Mail: ayer@meltemi.plh.af.mil

B

Dr. Arnold A. Barnes, Jr.
Phillips Laboratory/GPO
29 Randolph Road
Hanscom AFB, MA 01731-3010
Tel: 617/377-2939
Fax: 617/377-8892
E-Mail: barnes@plh.af.mil

Ms. Cindy Beeler
Visidyne, Inc.
10 Corporate Place
South Bedford Street
Burlington, MA 01803
Tel: 617/273-2820
Fax: 617/272-1068
E-Mail: beeler@visidyne.com

Major Paul J. Bellaire, Jr.
Air Force Office of Scientific Research
AFOSR/NM
Bolling AFB, DC 20331-8050
Tel: 202/767-7900
Fax: 202/404-7496
E-Mail: paul.bellaire@afosr.af.mil

Mr. Harold R. Bishop
Arete Associates
1725 Jefferson Davis Hwy
Crystal Square 2, Suite 703
Arlington, VA 22202
Tel: 703/413-0290
Fax: 703/413-0295
E-Mail: bishop@arete-dc.com

Mr. Albert R. Boehm
Hughes STX
2501 Ermine Drive
Huntsville, AL 35810
Tel: 205/859-8051
Fax: 205/890-2299
E-Mail: boehm@ziplink.net

CIDOS-97 LIST OF REGISTERED ATTENDEES
--

Mr. Sam Brand
 Naval Research Laboratory
 7 Grace Hopper Avenue
 Monterey, CA 93943-5502
 Tel: 408/647-4748
 Fax: 408/656-4769
 E-Mail: brand@nylmry.navy.mil

Mr. Kevin Bruening
 Mevatec Corporation
 1525 Perimeter Parkway, Suite 500
 Huntsville, AL 35806
 Tel: 205/890-8023
 Fax: 205/890-0000
 E-Mail: kevin_bruening@mevatec.com

Mr. John C. Burgeson
 Science and Technology Corporation
 23 Decatur Drive
 Nashua, NH 03062
 Tel: 603/891-4813
 Fax: 603/891-4813
 E-Mail: burgeson@tiac.net

Dr. Hsiao-hua K. Burke
 MIT Lincoln Laboratory
 244 Wood Street
 Lexington, MA 02173
 Tel: 617/981-7999
 Fax: 617/981-4603
 E-Mail: burke@ll.mit.edu

C

Mr. A. Peter Campbell
 Argonne National Laboratory
 9700 South Cass Avenue/DIS-900
 Argonne, IL 60439-4832
 Tel: 630/252-0270
 Fax: 630/252-5217
 E-Mail: campbell@dis.anl.gov

Dr. Thomas R. Caudill
 PL/GROP
 29 Randolph Road
 Hanscom AFB, MA 01731-3010
 Tel: 617/377-2943
 Fax: 617/377-8892
 E-Mail: caudill@plh.af.mil

Ms. Maureen E. Cianciolo
 TASC
 427 Sweetgum Drive
 Knoxville, TN 37922
 Tel: 423/671-0460
 Fax: 423/671-0460
 E-Mail: mecianciolo@tasc.com

CAPT Robert L. Clark
 U.S. Naval Observatory
 3450 Massachusetts Avenue, NW
 Washington, DC 20392-5421
 Tel: 202/762-1042
 Fax: 202/762-1018
 E-Mail: 961@ocean.usno.navy.mil

Mr. Rene Cormier
 Dynamics Research Corporation
 PL/GPOF
 29 Randolph Road
 Hanscom AFB, MA 01731-3010
 Tel: 617/377-4871
 Fax: 617/377-2984
 E-Mail: cormier@plh.af.mil

CDR Timothy Cummings
 M&S Executive Agent for Air and Space
 859 Buchanan Street
 Scot AFB, IL 62225-5116
 Tel: 618/256-3902
 Fax: 618/256-3964
 E-Mail: cummingt@thunder.safb.af.mil

CIDOS-97 LIST OF REGISTERED ATTENDEES

D

CDR George Davis
Naval War College
Newport, RI 02841-1207

Mr. Richard E. Davis
Aerospace Electronic Systems Division
NASA Langley Research Center
MS 474

Hampton, VA 23681-0001
Tel: 804/864-1647
Fax: 804/864-8809
E-Mail: r.e.davis@larc.nasa.gov

Mr. Robert P. d'Entremont
Atmospheric & Environmental Research, Inc.
840 Memorial Drive
Cambridge, MA 02139
Tel: 617/547-6207
Fax: 617/661-6479
E-Mail: bob@arcuni.plh.af.mil

Dr. Adarsh Deepak
Science and Technology Corp
101 Research Drive
Hampton, VA 23666
Tel: 804/865-1894
Fax: 804/865-1294
E-Mail: adeepak@stcnet.com

Dr. William Denig
AFRL/PL (NPOESS/IPO Liaison)
Centre Bldg, Suite 1450
8455 Colesville Road
Silver Spring, MD 20910
Tel: 301/427-2084
Fax: 301/427-2164
E-Mail: wdenig@ipo.noaa.gov

Dr. John DeVore
Visidyne, Inc.
5951 Encina Road, Suite 208
Goleta, CA 93117-2211
Tel: 805/683-4277
Fax: 805/683-5377
E-Mail: devore@visidyne.com

E

Capt Mark M. Edwards
PL/GP-M
29 Randolph Road
Hanscom AFB, MA 01731-3010
Tel: 617/377-4008
Fax: 617/377-5688
E-Mail: medwards@plh.af.mil

Mr. Kenneth E. Eis
CIRA, Colorado State University
Foothills Campus
Fort Collins, CO 80523-1375
Tel: 970/491-8397
Fax: 970/491-8241
E-Mail: eis@cira.colostate.edu

Dr. Edwin W. Eloranta
Department of Atmospheric Sciences
University of Wisconsin
1225 W. Dayton Street
Madison, WI 53706
Tel: 608/262-7327
Fax: 608/262-5974
E-Mail: eloranta@lidar.ssec.wisc.edu

Mr. John R. Elrick
HQ AFOTEC
8500 Gibson Boulevard SE
Kirtland AFB, NM 87117-5558
Tel: 505/846-2644
Fax: 505/846-5235
E-Mail: elrickj@afotec.af.mil

CIDOS-97 LIST OF REGISTERED ATTENDEES

F

Mr. John W. Formento
Argonne National Laboratory
9700 S. Cass Avenue
Argonne, IL 60439
Tel: 630/252-5757

Mr. Gary B. Gustafson
Atmospheric & Environmental Research, Inc.
840 Memorial Drive
Cambridge, MA 02139
Tel: 617/547-6207
Fax: 617/661-6479
E-Mail: garyg@aer.com

G

Dr. Karl Garrison
Arete Associates
1725 Jefferson Davis Highway, Suite 703
Arlington, VA 22202
Tel: 703/413-0290
Fax: 703/413-0295
E-Mail: garrison@arete-dc.com

Mr. Raymond H. Godin
U.S. Naval Observatory
3450 Massachusetts Avenue, NW
Washington, DC 20392-5421
Tel: 202/762-0255
Fax: 202/762-1018
E-Mail: 961b@ocean.usno.navy.mil

Col John A. Goyette
NPOESS/IPO
Centre Bldg, Suite 1450
8455 Colesville Road
Silver Spring, MD 20910
Tel: 301/427-2070
Fax: 301/427-2164
E-Mail: jgoyette@ipo.noaa.gov

Mr. Stanley H. Grigsby
Planning Systems Incorporated
7923 Jones Branch Road
McLean, VA 22102-3304
Tel: 703/734-3400
Fax: 703/734-3456
E-Mail: grigsby@bdcmail.nrl.navy.mil

H

Dr. John Hallett
Desert Research Institute
Atmospheric Sciences Center
P.O. Box 60220
Reno, NV 89506-0220
Tel: 702/677-3117
Fax: 702/677-3157
E-Mail: hallett@rigel.physics.unr.edu

Mr. Louis Hembree
Naval Research Laboratory
7 Grace Hopper Avenue
Monterey, CA 93943-5502
Tel: 408/656-4787
Fax: 408/656-4769
E-Mail: hembree@nrlmry.navy.mil

Dr. John R. Hummel
Argonne National Laboratory
9700 South Cass Avenue
DIS-900
Argonne, IL 60439-4832
Tel: 708/252-7189
Fax: 708/252-5128
E-Mail: hummel@athens.dis.anl.gov

I

Mr. Robert E. Introne
TASC
55 Walkers Brook Drive
Reading, MA 01867
Tel: 617/942-2000, x 2331
Fax: 617/942-7100
E-Mail: reintrone@tasc.com

CIDOS-97 LIST OF REGISTERED ATTENDEES

J

Mr. Artie Jackson
Phillips Laboratory
29 Randolph Road
Hanscom AFB, MA 01731
Tel: 617/377-2958
Fax: 617/377-8892
E-Mail: jackson@plh.af.mil

Mr. Robert J. Jordano
Visidyne, Inc.
10 Corporate Place
South Bedford Street
Burlington, MA 01803
Tel: 617/273-2820
Fax: 617/272-1068
E-Mail: jordano@visidyne.com

K

Major Michael S. Kapel
88th Weather Squadron
2049 Monahan Way, Bldg 91
WPAFB, OH 45433-7204
Tel: 937/255-2207
Fax: 937/255-1158
E-Mail: kapelms@88abw.wpafb.af.mil

LCDR Bruce Kitchen
NTMOD
686 Cushing Drive
Newport, RI 02841-1207
Tel: 401/841-4390
Fax: 401/948-3257
E-Mail: kitchenb@usnwe.edu

Dr. George G. Koenig
U.S. Army Cold Region Research
Engineering Laboratory
72 Lyme Road
Hanover, NH 03755-1290
Tel: 603/646-4130
Fax: 603/646-4693
E-Mail:
u2sw9gk@crrel41.crrel.usace.army.mil

Dr. Thomas J. Kopp
HQ, AFGWC
106 Peacekeeper Drive, Suite 2N3
Offutt AFB, NE 68113-4039
Tel: 402/294-3395
Fax: 402/294-3505
E-Mail: koppt@afgwc.offutt.af.mil

Major James T. Kroll
AF/XOWP
1400 Key Bridge, Suite 301
Arlington, VA 22209
Tel: 202/696-5062
Fax: 202/696-3682
E-Mail: kroll@af.pentagon.mil

L

Lt Col John M. Lanicci
HQ USAF/XOCP
1510 Air Force Pentagon
Washington, DC 20030-1510
Tel: 202/761-5341, x 139
Fax: 202/761-5352
E-Mail: laniccij@af.pentagon.mil

Dr. Julius Lilly
USASSDC
ATTN: CSSD-TC-WL
PO Box 1500
Huntsville, AL 35807-3801
Tel: 205/955-3059
Fax: 205/955-3641
E-Mail: lillyj@ssdch-usassdc.army.mil

Mr. James J. Lisowski
SciTec, Inc.
100 Wall Street
Princeton, NJ 08540
Tel: 609/921-3892, x 253
Fax: 609/921-1926
E-Mail: jlisowski@scitec.com

CIDOS-97 LIST OF REGISTERED ATTENDEES

Mr. Steven J. Lowe
SAIC / NRL
550 Camino El Estero, Suite 205
Monterey, CA 93940
Tel: 408/649-5242
Fax: 408/649-8048
E-Mail: steven.j.lowe@cpmx.saic.com

M

Dr. Robert A. McClatchey
McClatchey Associates
3 Gould Road
Bedford, MA 01730
Tel: 617/271-1480
Fax: 617/271-1480
E-Mail: rmccclatchey@msn.com

Mr. Gary B. McWilliams
MSEA A&SNE
859 Buchanan Street
Scott AFB, IL 62225-5116
Tel: 618/256-4107
Fax: 618/256-3964
E-Mail: mcwillig@thunder.safb.af.mil

Mr. William K. Moore
MEVATEC Corporation
1525 Perimeter Parkway, Suite 500
Huntsville, AL 35806
Tel: 205/890-8000
Fax: 205/890-0000
E-Mail:

Mr. Jeffrey S. Morrison
TASC
55 Walkers Brook Drive
Reading, MA 01867
Tel: 617/942-2000, x2479
Fax: 617/942-7100
E-Mail: js Morrison@tasc.com

Mr. Philip I. Moynihan
Jet Propulsion Laboratory
Mail Stop 306-4130
4800 Oak Grove Drive
Pasadena, CA 91109
Tel: 818/354-4130

Dr. Joel B. Mozer
USAF Phillips Laboratory, GPOF
29 Randolph Road
Hanscom AFB, MA 01731-3010
Tel: 617/377-2945
Fax: 617/377-2984
E-Mail: mozer@plh.af.mil

N

Ms. Michelle A. Najarian
SciTec, Inc.
100 Wall Street
Princeton, NJ 08540
Tel: 609/921-3892, x 255
Fax: 609/921-1926
E-Mail: mnajarian@scitec.com

Mr. Donald C. Norquist
PL/GPOF
29 Randolph Road
Hanscom AFB, MA 01731-3010
Tel: 617/377-2962
Fax: 617/377-8892
E-Mail: norquist@plh.af.mil

O

LTC Lauraleen O'Connor
NPOESS/IPO
Centre Bldg, Suite 1450
8455 Colesville Road
Silver Springs, MD 20910
Tel: 301/427-2079, x 178
Fax: 301/427-2164
E-Mail: oconnorl@ipo.noaa.gov

CIDOS-97 LIST OF REGISTERED ATTENDEES

Capt Fred Orchard
Director
Naval War College War Gaming Department
Newport, RI 02841-1207

Dr. S.C. Ou
Department of Meteorology/CARSS
University of Utah
819WBB
Salt Lake City, UT 84112
Tel: 801/581-6136
Fax: 801/581-4065
E-Mail: ssou@climate.met.utah.edu

Mr. Steve O. Ouzts
TASC
55 Walkers Brook Drive
Reading, MA 01867-3297
Tel: 617/942-2000
Fax: 617/941-7100
E-Mail: soouzs@tasc.com

R

Dr. Lawrence F. Radke
National Center for Atmospheric Research
P.O. Box 3000
Boulder, CO 80307-3000
Tel: 303/497-8778
Fax: 303/497-8770
E-Mail: radke@ucar.edu

Mr. Mark E. Raffensberger
TASC
55 Walkers Brook Drive
Reading, MA 01867
Tel: 617/942-2000, x 2438
Fax: 617/942-7100
E-Mail: meraffensberger@tasc.com

Mr. Donald L. Reinke
CIRA, Colorado State University
Foothills Campus
Fort Collins, CO 80523
Tel: 970/491-8465
Fax: 970/491-8241
E-Mail: reinke@cira.colostate.edu

Mr. R. Lynn Rose
Aeromet, Inc.
P.O. Box 701767
Tulsa, OK 74170-1767
Tel: 918/299-2621
Fax: 918/299-8211
E-Mail: lynnr@aeromet.com

S

Dr. Guy P. Seeley
Radex, Inc.
c/o Phillips Laboratory
29 Randolph Road
Hanscom AFB, MA 01731-3010
Tel: 617/377-6069
Fax: 617/377-2984
E-Mail: seeley@hurricane.plh.af.mil

COL Alan R. Shaffer
ODDR&E(SE&BE)
3080 Defense Pentagon
Washington, DC 20301-3080
Tel: 703/614-0205
E-Mail: shaffer@acq.osd.mil

Dr. Xiaowen Shan
PL/GPOF
29 Randolph Road
Hanscom AFB, MA 01731-3010
Tel: 617/377-2959
Fax: 617/377-2984
E-Mail: xiaowen@plh.af.mil

CIDOS-97 LIST OF REGISTERED ATTENDEES

Dr. Joseph G. Shanks
Photon Research Associates, Inc.
5720 Oberlin Drive
San Diego, CA 92121
Tel: 619/455-9741
Fax: 619/455-0658
E-Mail: jgs@photon.com

Dr. Richard Shirkey
Army Research Laboratory
ATTN: AMSRL-IS-EW
WSMR, NM 88002-5501
Tel: 505/678-5470
Fax: 505/678-4449
E-Mail: rshirkey@arl.mil

Dr. Richard A. Siquig
Naval Research Laboratory
7 Grace Hopper Avenue
MS 2
Monterey, CA 93943-5502
Tel: 408/647-4732
Fax: 408/656-4769
E-Mail: siquig@nrlmry.navy.mil

Dr. J. William Snow
MIT Lincoln Laboratory
24 Wood Street
Lexington, MA 02173
Tel: 617/981-3025
Fax: 617/981-7271
E-Mail: snow@ll.mit.edu

Dr. Eric L. Strobel
W.J. Schafer Associates, Inc.
1901 N. Fort Myer Drive, Suite 800
Arlington, VA 22209
Tel: 703/558-7900
Fax: 703/525-2691
E-Mail: estrobel@wjasa.com

T

Mr. Paul Tattelman
PL/GPOF
29 Randolph Road
Hanscom AFB, MA 01731-3010
Tel: 617/377-2982
Fax: 617/377-2984
E-Mail: tattelman@plh.af.mil

Dr. James W. Telford
Atmospheric Concepts, Inc.
1975 Fallen Leaf Court
Reno, NV 89509
Tel: 702/825-7515
Fax: 702/829-0658
E-Mail: telford@clouds.sage.dri.edu

Dr. Ross J. Thornburg
Visidyne, Inc.
3322 South Memorial Parkway, Suite 223
Huntsville, AL 35801-5368
Tel: 205/880-3411
Fax: 205/880-3284
E-Mail: thornbrg@visidyne.com

RADM Paul E. Tobin, Jr.
U.S. Naval Observatory
3450 Massachusetts Avenue, NW
Washington, DC 20392-5421

Mr. David H. Tofsted
US Army Research Laboratory
ATTN: AMSRL-IS-EW
WSMR, NM 88002-5501
Tel: 505/678-3039
Fax: 505/678-3385
E-Mail: dtofsted@arl.mil

Ms. Susan Triantafillou
PL/GPOF
29 Randolph Road
Hanscom AFB, MA 01731-3010
Tel: 617/377-2971
Fax: 617/377-2984
E-Mail: susan@hurricane.plh.af.mil

CIDOS-97 LIST OF REGISTERED ATTENDEES

Dr. Paul D. Try
Science and Technology Corp
409 Third Street SW, Suite 203
Washington, DC 20024
Tel: 202/863-0012
Fax: 202/488-5364
E-Mail: try@stcnet.com

Mr. Ryan Turkington
TASC
55 Walkers Brook Drive
Reading, MA 01867-3297
Tel: 617/942-2000, x 3128
Fax: 617/941-7100
E-Mail: rbtkurkington@tasc.com

Dr. Paul Twitchell
Science and Technology Corp
409 Third Street SW, Suite 203
Washington, DC 20024
Tel: 202/863-0012
Fax: 202/488-5364
E-Mail: twitchell@stcnet.com

U

Dr. Edward E. Uthe
SRI International
333 Ravenswood Avenue
Menlo Park, CA 94025-3493
Tel: 415/859-4667
Fax: 415/859-5036
E-Mail: edward_uthe@qm.sri.com

V

Ms. Deborah Vane
Jet Propulsion Laboratory
Mail Stop 264-648
4800 Oak Grove Drive
Pasadena, CA 91109
Tel: 818/354-3708
Fax: 818/393-4508
E-Mail: deborahg.vand@jpl.nasa.gov

Dr. Thomas H. Vonder Haar
Science and Technology Corporation-METSAT
515 South Howes
Fort Collins, CO 80521
Tel: 970/221-5420
Fax: 970/493-3410
E-Mail: metsat@stcnet.com

W

Dr. Steven J. Walter
Jet Propulsion Laboratory
California Institute of Technology
Mail Stop 246-101
4800 Oak Grove Drive
Pasadena, CA 91109
Tel: 818/354-1626
Fax: 818/354-4341
E-Mail: steven.j.walter@jpl.nasa.gov

Mr. Jason Wampler
Mevatec Corporation
1525 Perimeter Parkway, Suite 500
Huntville, AL 35806
Tel: 205/890-8132
Fax: 205/890-0000
E-Mail: jason_wampler@mevatec.com

Dr. David A. Wasson
Arete Associates
P.O. Box 57294
Sherman Oaks, CA 91413
Tel: 818/501-2880
Fax: 818/501-1196
E-Mail: wasson@arete.com

Mr. Steven P. Weaver
88th Weather Squadron
2049 Monahan Way, Bldg 91
WPAFB, OH 45433-7204
Tel: 513/255-2207
Fax: 513/255-1158
E-Mail: weavers@88abw.wpafb.af.mil

CIDOS-97 LIST OF REGISTERED ATTENDEES
--

Mr. David A. Whitney
TASC
55 Walkers Brook Drive
Reading, MA 01867
Tel: 617/942-710
Fax: 617/942-7100
E-Mail: dawhitney@tasc.com

Dr. Donald P. Wylie
University of Wisconsin-Madison
1225 W. Dayton Street
Madison, WI 53706
Tel: 608/263-7458
Fax: 608/262-5974
E-Mail: don.wylie@ssec.wisc.edu

Y

Mr. Tetsuji Yamada
Yamada Science & Art Corporation
Rt. 4, Box 81-A
Santa Fe, NM 87501
Tel: 505/989-7351
Fax: 505/989-7965
E-Mail: ysa@ysasoft.com

APPENDIX C
Author Index

CIDOS-97 AUTHOR INDEX

A

Acharya, P.K., 55
 Anderson, Gail P., 55
 Arnott, W. Patrick, 197
 Ayer, Steven M., 35, 231

B

Barnes, Jr., Arnold A., 217
 Berk, A., 55
 Bernstein, L.S., 55
 Bieker, Francis D., 107
 Bishop, Harry, 230
 Blumberg, William A.M., 43, 140
 Boehm, Albert R., 83, 220
 Bruening, Kevin W., 201
 Bunting, James T., 123
 Burgeson, John C., 177
 Burke, Hsiao-hua K., 67, 71
 Bussey, Allan, 103

C

Cady-Pereira, Karen, 123
 Campbell, A. Peter, 24
 Cantrell, Louis E., 107
 Caudill, Thomas R., 140, 145, 149
 Chetwynd, J.H., 55
 Cianciolo, Maureen E., 35, 222
 Cox, Stephen K., 163
 Crow, Samuel, 59

D

Dailey, Peter, 20
 Davis, John M., 163
 Davis, Richard E., 181
 d'Entremont, Robert P., 123, 131, 145, 185
 DeVore, John G., 63, 226
 Driscoll, Mavis, 20

E

Edwards, Capt Mark M., 31
 Eis, Kenneth E., 75, 163, 189
 Eloranta, Edwin W., 144, 193
 Emre, Erol, 205

F

Forsythe, John M., 75, 159, 163

G

Garrison, Karl, 230
 Giever, John C., 209
 Gillespie, Patti, 59
 Goyette, Col John A., 14
 Grantham, Donald D., 177
 Griffin, Alan, 140
 Grigsby, Stanley H., 167
 Gustafson, Gary B., 119, 131, 145

H

Hahn, Doug, 103
 Hallett, John, 197
 Hembree, Louis, 39
 Hogan, David P., 131
 Holt, Robert M., 167
 Hoock, Jr., Donald W., 209
 Huffman, Arlie C., 163
 Hume, Capt Edward E., 31
 Hummel, John R., 24

I

Isaacs, Ronald G., 119, 131

J

Jackson, Artie, 103
 Jones, Robert L., 181
 Jones, Andrew S., 189
 Jordan, Michael P., 71
 Jordano, Robert J., 47, 63
 Jung, James, 235

K

Kapel, MAJ Michael S., 132
 Kopp, Thomas J., 107

CIDOS-97 AUTHOR INDEX

L

Lanicci, Lt Col John M., 15
 Li, Fuk K., 127, 163
 Ligon, David, 59
 Lilly, Julius Q., 201
 Liou, K.N., 149
 Lisowski, J., 149
 Lowe, Steven J., 16

M

Martin, Jon, 209
 McClatchey, Robert A., 47
 McDonald, Bonnie, 119
 McWilliams, Gary, 9
 Menzel, W. Paul, 155
 Mertz, Frederick C., 43
 Meyers, Matthew, 197
 Morrison, Brian J., 149, 235
 Morrison, Jeffrey S., 171
 Moynihan, Philip I., 213
 Mozer, Joel B., 35, 59, 89, 93, 205, 231

N

Newton, Brian, 103
 Nielsen, Norman B., 136
 Norquist, Donald C., 99

O

O'Brien, Sean G., 85
 O'Donnell, Capt David J., 67, 140
 Olson, Steve, 20
 Orchard, Captain Fred Gregg, 3
 Oseberg, Terje E., 136
 Ou, Steve C., 149

P

Peduzzi, Daniel C., 71
 Pesler, Jeffrey, 132
 Petersen, Walter A., 163
 Polander, Capt John F., 132
 Polland, P., 149
 Pribik, Dwayne, 79

R

Raffensberger, Mark E., 2, 222
 Randel, David L., 239
 Reinke, Donald L., 75, 159, 163, 239
 Reynolds, Robert, 20
 Rhoades, Kristine E., 71
 Ringerud, Mark A., 239
 Rose, R. Lynn, 235
 Rubin, Steven L., 171

S

Sadowy, Gregory A., 163
 Sartor, Ken W., 226
 Schneider, Timothy L., 163
 Seeley, Guy P., 35, 59, 205
 Shaffer, Colonel Alan R., 4
 Shan, Xiaowen, 89, 93
 Shanks, Joseph G., 43
 Sherer, Dana, 20
 Shettle, E.P., 55
 Shirkey, Richard, 209
 Siquig, Richard A., 16
 Smith, Col William, 47
 Snell, H.E., 55
 Snow, J. William, 67, 71
 Stair, Jr., A.T., 47
 Stephens, Graeme L., 127, 163, 239
 Stephens, Timothy L., 63, 226
 Strobel, Eric L., 79

T

Telford, James W., 111
 Thompson, James H., 63, 226
 Thornburg, Ross J., 63, 226
 Tobin, J., Rear Admiral Paul E., 5
 Tofsted, David H., 85, 209
 Triantafillou, Susan, 93
 Try, Paul D., 177
 Turkington, Ryan B., 222

U

Uthe, Edward E., 136

CIDOS-97 AUTHOR INDEX

V

Vane, Deborah, G., 127
Vonder Haar, Thomas H., 159, 163, 239

W

Walter, Steven J., 127, 213
Wampler, Jason A., 201
Wasson, David A., 230
Weaver, Steven P., 132
Wetmore, Alan, 59
Whitney, David, 20
Wilson, R. Gale, 181
Wise, John, 140
Wonsick, Margaret M., 107
Wright, Robert P., 167
Wylie, Donald, 155

Y

Yamada, Ted, 115
Yang, P., 149

Z

Zawada, Lt Col Frank A., 31
Zhou, Joanne, 123

CIDOS-97 NOTES

CIDOS-97 NOTES

CIDOS-97 NOTES

CIDOS-97 NOTES

CIDOS-97 NOTES

CIDOS-97 NOTES

CIDOS-97 NOTES

CIDOS-97 NOTES

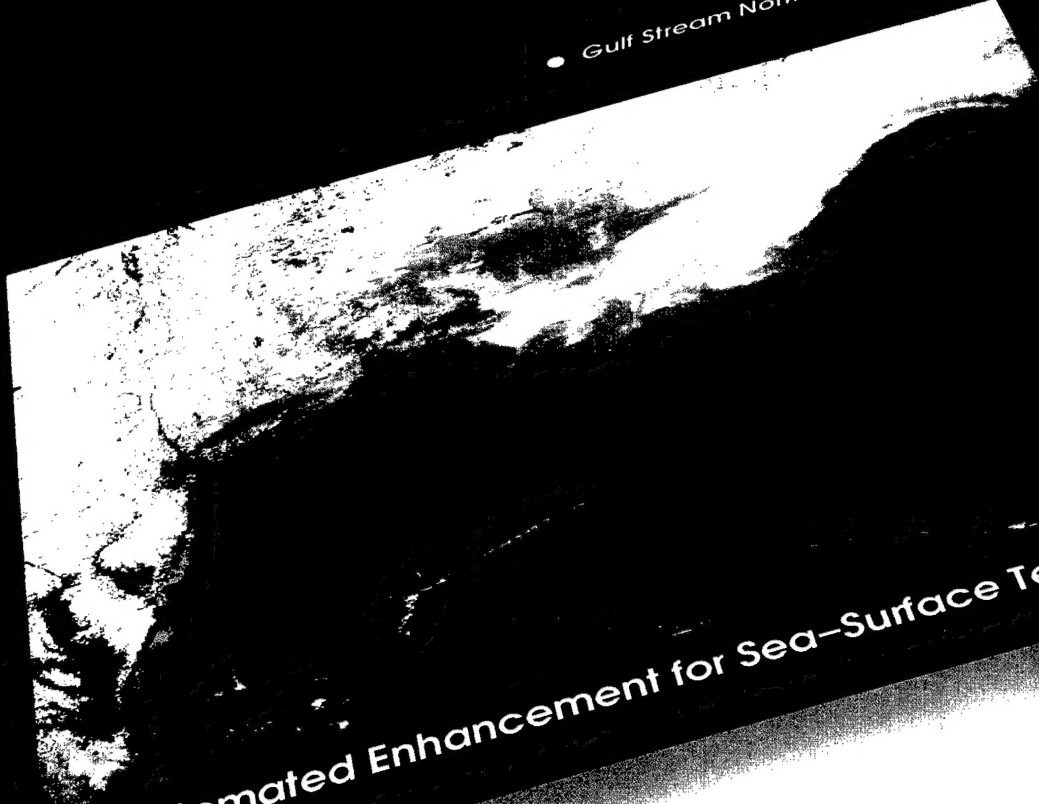
CIDOS-97 NOTES

CIDOS-97 NOTES

CIDOS-97 NOTES

NOAA-14 AVHRR
Raw Color Composite

● Gulf Stream North Wall



MSI Automated Enhancement for Sea-Surface Temperature